# Molecularly resolved studies of the reactions of amines with Cu(110) surfaces

Dyfan Edwards

Thesis submitted to Cardiff University
in candidature for the degree of Doctor of Philosophy

Department of Chemistry, Cardiff University, Cardiff, Wales, U.K.
September 2006


Supervisor:P.R. Davies





ProQuest LLC
789 East Eisenhower Parkway
P.O. Box 1346
Ann Arbor, MI 48106-1346

# *Declaration/Statements*

| | |
|---|---|
| **CANDIDATE'S ID NUMBER** | 99240697C |
| **CANDIDATE'S SURNAME** | **Please circle appropriate value** EDWARDS<br>**(Mr) Miss / Ms / Mrs / Rev / Dr / Other please specify** ..... |
| **CANDIDATE'S FULL FORENAMES** | DYFAN' |

**DECLARATION**

This work has not previously been accepted in substance for any degree and is not concurrently submitted in candidature for any degree.

Signed ...D Edwards..... (candidate)

Date...30.09.06.....

**STATEMENT 1**

This thesis is being submitted in partial fulfillment of the requirements for the degree of ...PhD.....(insert MCh, Md, MPhil, PhD etc, as appropriate)

Signed ...D Edwards..... (candidate)

Date ...30.09.06.....

**STATEMENT 2**

This thesis is the result of my own independent work/investigation, except where otherwise stated.
Other sources are acknowledged by footnotes giving explicit references.

Signed ...D Edwards..... (candidate)

Date ...30.09.06.....

**STATEMENT 3**

I hereby give consent for my thesis, if accepted, to be available for photocopying and for inter-library loan, and for the title and abstract to be made available to outside organisations.

Signed ...D Edwards..... (candidate)

Date ...30.09.06.....

# *Abstract*

The interaction of aniline with clean, partially oxidised and fully oxidised Cu(110) surfaces has been studied by XPS and STM at room temperature and is compared to the reactions of 2-tertbutylaniline. Limited dissociation occurs at clean Cu(110), but at a partially oxidised surface, a chemisorbed phenyl imide ($(C_6H_5N(a))$ product is formed, together with water which desorbs. The phenyl imide forms three different domains, described by $\begin{pmatrix} 4 & 0 \\ 2 & 2 \end{pmatrix}$, $\begin{pmatrix} 4 & 0 \\ -1 & 2 \end{pmatrix}$ and $\begin{pmatrix} 4 & 0 \\ 1 & 2 \end{pmatrix}$ unit meshes. A coadsorption of aniline and dioxygen in a 300:1 mixture results two structures, described by $\begin{pmatrix} 3 & 0 \\ -1 & 2 \end{pmatrix}$ and $\begin{pmatrix} 3 & 0 \\ 1 & 2 \end{pmatrix}$ unit meshes. In both cases, the maximum surface concentration predicted by STM is half that actually determined by quantification of the XPS peaks. Pi-stacking of the phenyl rings is proposed to account for this discrepancy. 2-tertbutylaniline adsorbs at partially oxidised Cu(110) surfaces, forming a moderately ordered p(2x2) structure. The maximum surface coverage predicted by STM is in agreement with the actual maximum surface concentration of $2.5 \times 10^{14}$ $cm^{-2}$.

The interaction of dimethylamine with clean, partially oxidised and fully oxidised Cu(110) surface at room temperature has been studied by STM and XPS. Reaction with partially oxidised Cu(110) causes reconstruction of the chemisorbed oxygen islands from the well know p(2x1)-O(a) structure to a (3x1) phase. The expanded oxygen islands desorb as water and structures orientated in the <110> direction, assigned to $(CH_3)_2N$, form in their place. The structures are stable for several minutes, after which they desorb, possibly as $CH_3NCH_{2(g)}$ via a β-elimination reaction. Reaction with a complete O(a) monolayer results in limited dimethylamine adsorption. Dimethylamine does not react with clean Cu(110) at room temperature.

The reaction of ethylamine with clean, partially oxidized and fully oxidized Cu(110) has been studied by STM and XPS at room temperature and is compared with the

reactions of diaminoethane and 2,2,2-trifluoroethylamine. Ethylamine reacts with partially oxidized Cu(110) causing expansion of the oxygen islands from p(2x1) to (3x1) structures. After a period of several minutes, the expanded oxygen islands desorb as water, leaving a clean surface. Ethylamine reacts with a full O(a) monolayer without any reconstruction, causing desorption of all surface oxygen and resulting in a clean surface. It is proposed that the ethylamine desorbs as $CH_3CHNH$ via a β-elimination reaction. Diaminoethane reacts with partially oxidized Cu(110) in the exact same manner as ethylamine. At partially oxidized Cu(110), 2,2,2-trifluorethylamine causes desorption of all chemisorbed oxygen without causing any reconstruction of the oxygen islands. A clean surface is left at the end of the reaction. A full O(a) monolayer is inert to 2,2,2-trifluorethylamine.

The interaction of 4,4-diaminobenzophenone, $(H_2NC_6H_4)_2CO$, with clean Cu(110) surfaces has been investigated by STM and XPS at room temperature. Sub-monolayer coverages give rise to three distinct, highly ordered structures. The first can be described using by a $\begin{pmatrix} 4 & 0 \\ 2 & 3 \end{pmatrix}$ unit mesh. The others are based around a pair of molecules, forming $\begin{pmatrix} 7 & 0 \\ -4 & 3 \end{pmatrix}$ and $\begin{pmatrix} 7 & 0 \\ -2 & 3 \end{pmatrix}$ lattices. Above a monolayer, order breaks down.

**To my parents**

# *Acknowledgements*

I would like to take this opportunity to sincerely thank the following people.

Dr Phil Davies for first of all allowing me to undertake this project and work under him, and for the help and enthusiasm throughout the duration of the course.

Dr David Morgan for offering a helping hand and technical know-how whenever I needed it. It would have been impossible without you.

Dr Albert Carley, especially for his XPS expertise.

Darran , Paul, Martin, Matt and everyone else in the surface science labs for the fun times and help with the bake-out covers.

To Alun and the rest of the support staff.

# Contents

# *Glossary*

All gas exposures are expressed in Langmuirs, L, defined as $10^{-6}$ torr s.

A chemisorbed oxygen monolayer at Cu(110) surfaces is defined as 5.5 x$10^{14}$ atoms $cm^{-2}$ i.e. the coverage at which the surface is saturated.

AES . . . . . Auger Electron Spectroscopy
ARUPS . . . . . Angle Resolved Ultraviolet Photoelectron Spectroscopy
ARXPS . . . . . Angle Resolved X-ray Photoelectron Spectroscopy
EELS . . . . . Electron Energy Loss Spectroscopy
HREELS . . . . . High Resolution Electron Energy Loss Spectroscopy
IR . . . . . Infrared
LEED . . . . . Low Energy Electron Diffraction
RAIRS . . . . . Reflection Absorption Infrared Spectroscopy
SES . . . . . Secondary Electron Spectroscopy
SEXAFS . . . . . Surface Extended X-ray Absorption Fine Structure
SPM . . . . . Scanning Probe Microscopy
STM . . . . . Scanning Tunnelling Microscopy
STS . . . . . Scanning Tunnelling Spectroscopy
TPD . . . . . Temperature Programmed Desorption
VEELS . . . . . Vibrational Electron Energy Loss Spectroscopy
XPS . . . . . X-ray Photoelectron Spectroscopy
UHV . . . . . Ultra-High Vacuum*
UPS . . . . . Ultraviolet Photoelectron Spectroscopy

* UHV conditions are in the range $10^{-9}$ to $10^{-11}$ mbar.

# *Introduction*

This thesis presents the results of a series of experiments investigating the reactions of amines with Cu(110) surfaces using STM and XPS. The combination of STM and XPS in the same system is a powerful tool in the study of reaction mechanisms at single crystal surfaces. XPS can give qualitative and quantitative analysis of adsorbed molecules, while STM can give structural information at a molecularly resolved level regarding the same species, as well as following surface reactions in real time.

To date, the majority of surface science investigations into amine chemistry have utilised TPD and vibrational spectroscopic techniques. It is hoped that the combination of STM and XPS will lead to a better understanding of the reaction mechanisms that simple amine species undergo at metal surfaces.

Most previous surface science investigations into amine chemistry have focussed only on adsorption at clean metal surfaces. Previously, the group has investigated the reactions of ammonia[1-7] and pyridine[8] with copper surfaces. The results show how the presence of chemisorbed oxygen can acutely affect the reactions occurring. A large focus of this thesis, therefore, is concerned with the interaction of amines with oxidised Cu(110) surfaces. Study of this kind may also help characterise the reactions that occur at oxidised sites in real catalytic systems. For example, the enantioselective hydrogenation of α-functionalised ketones and olefins over a platinum catalyst require a basic N atom in the presence of oxygen[9].

The study and characterisation of the reactions of amines with model systems such as copper and copper oxide single surface crystals can assist a great deal in clarifying the mechanistic details of a whole host of commercial processes.

Amines play an important role in catalysis and are commonly used to modify the selectivity and activity of catalytic reactions. As such, amine modification enhances palladium[10] and ruthenium[11] based hydrogenation catalysts.

Commercially, methylamines are produced by the amination of methanol over a solid acid catalyst, producing monomethylamine, dimethylamine and trimethylamine in a ratio of 17:21:61. However the industrial demand for these chemicals is in the ratio of approximately 30:60:10. It has recently been shown[12-15] that alkylamines can be synthesised in a ratio much closer to that required by industry through use of copper catalysts. This process uses carbon dioxide as the feedstock and therefore also has enviromental advantages over the current method.

Amines have important applications in the area of adhesion, as they are commonly used as curing agents in epoxy resins. Epoxy-copper adhesion is important to processes such as the manufacture of circuit boards and microelectronic packaging[16-17]. A better understanding of the interactions between amines and the copper surface can therefore help the development of such technologies.

Studies of organic semiconducting film materials that consist of small aromatic molecules show that the structure of the contact layer between the film and the substrate is very important in determining the electronic properties of the film[18]. Since aniline is the monomer of one of the most commonly used conducting polymers, investigation into its interaction with metal substrates may prove useful.

Research has also been conducted into the use of aniline and various derivatives to help inhibit copper corrosion in acidic solution[19-23]. A recent theoretical study[19] showed that the corrosion inhibition by aniline is associated mainly with the interaction of the molecule with surface defect sites which, due to their high reactivity to external agents, are prime sites for corrosion.

The interaction of amine moieties with surfaces is therefore an important subject. It is also important from a fundamental perspective, as the study of amines can show

the relative importance of CH, NH and CN bond scission mechanisms in determining the overall chemistry of a reaction.

## References

[1] Davies, P. R.; Keel, J. M. *Surf. Sci.* **2000**, *469*, 204.

[2] Carley, A. F.; Davies, P. R.; Roberts, M. W. *Catal. Lett.* **2002**, *80*, 25.

[3] Carley, A. F.; Davies, P. R.; Jones, R. V.; Harikumar, K. R.; Kulkarni, G. U.; Roberts, M. W. *Top. Catal.* **2000**, *11*, 299

[4] Carley, A. F.; Davies, P. R.; Roberts, M. W.; Vincent, D. *Top. Catal.* **1994**, *1*, 35.

[5] Afsin, B.; Davies, P. R.; Pashusky, A.; Roberts, M. W.; Vincent, D. *Surf. Sci.* **1993**, *284*, 109.

[6] Afsin, B.; Davies, P. R.; Pashuski, A.; Roberts, M. W. *Surf. Sci.* **1991**, *259*, L724.

[7] Carley, A. F.; Davies, P. R.; Harikumar, K. R.; Jones, R. V.; Kulkarni, G. U.; Roberts, M. W. *Top. Catal.* **2001**, *14*, 101

[8] Carley, A.F.; Davies, P.R,; Edwards, D.; Jones, R.V; Parsons, M. *Topics in Catalysis*, **2005**, *36*, 21

[9] Wells, P. B.; Wilkinson, A. G. *Top. Catal.* **1998**, *5*, 39

[10] Huntsman, W. D.; Madison, N. L.; Schlesinger, S. I. *J. Catal.* **1963,** *2*, 498

[11] Struijk, J.; Scholten, J. J. F. *Appl. Catal. A*, **1992**, *82*, 277.

[12] Gredig, S. V.; Maurer, R.; Koeppel, R. A.; Baiker, A. *J. Mol. Catal. A.* **1997**, *127*, 133.

[13] Gredig, S. V.; Koeppel, R. A.; Baiker, A. *App. Catal. A.* **1997**, *162*, 249.

[14] Gredig, S. V.; Koeppel, R. A.; Baiker, A. *Catal. Today*, **1996**, *29*, 339.

[15] Baiker, A. *Appl. Organomet. Chem.* **2000**, *14*, 751.

[16] Pignataro, S.; Tarrisi, A.; Ferla, G. *Surf. Interface Anal.* **1985**, *7*,12

[17] Miller, C. H. *J. Vac, Sci. Technol. A 1989*, *7*, 1818

[18] Schroder, P. G.; France, C. B.; Park, J. B.; Parkinson, B. A. *J.Appl. Phys.* **2002**, *91*, 3010

[19] Padilla-Campos, L.; Zagal, J. H.; Rangel, C. M.; Costamagna, J. *J. Molecular Structure: Theochem*, **2005**, *757*, 1

[20] Khaled, K. F.; Hackerman, N. *Electrochimica Acta*, **2004**, *49*, 485

[21] Lazarova, E.; Petkova, G.; Raicheff, R.; Neykov, G. *J. Appl. Electrochem.* **2002**, *32*, 1355.

[22] Du, T. B.; Chen, J. J.; Cao, D. Z. *J. Mater. Sci.* **2001**, *36*, 3903.

[23] Luo, H.; Guan, Y. C.; Han, K. N. *Corrosion* **1998**, *54*, 721

# *Chapter 1*

## *Instrumentation, theory and experimental*

### 1.1 General instrumentation

All experiments documented in this thesis were conducted on a combined XPS/STM instrument developed by Omicron Vakuumphysik GmbH, a simplified schematic of which is shown in figure 1.1. The instrument is comprised of two main chambers, one of which houses the scanning tunnelling microscope, whilst the other contains the x-ray source for XPS, together with an $Ar^+$ sputtering gun for sample cleaning, two leak valves for gas and vapour dosing, a Knudsen cell for the dosing of solids and a mass spectrometer.

The system is pumped with turbo and ion pumps. The combination of both pumps brings the pressure down to a typical $1 \times 10^{-11}$ mbar.

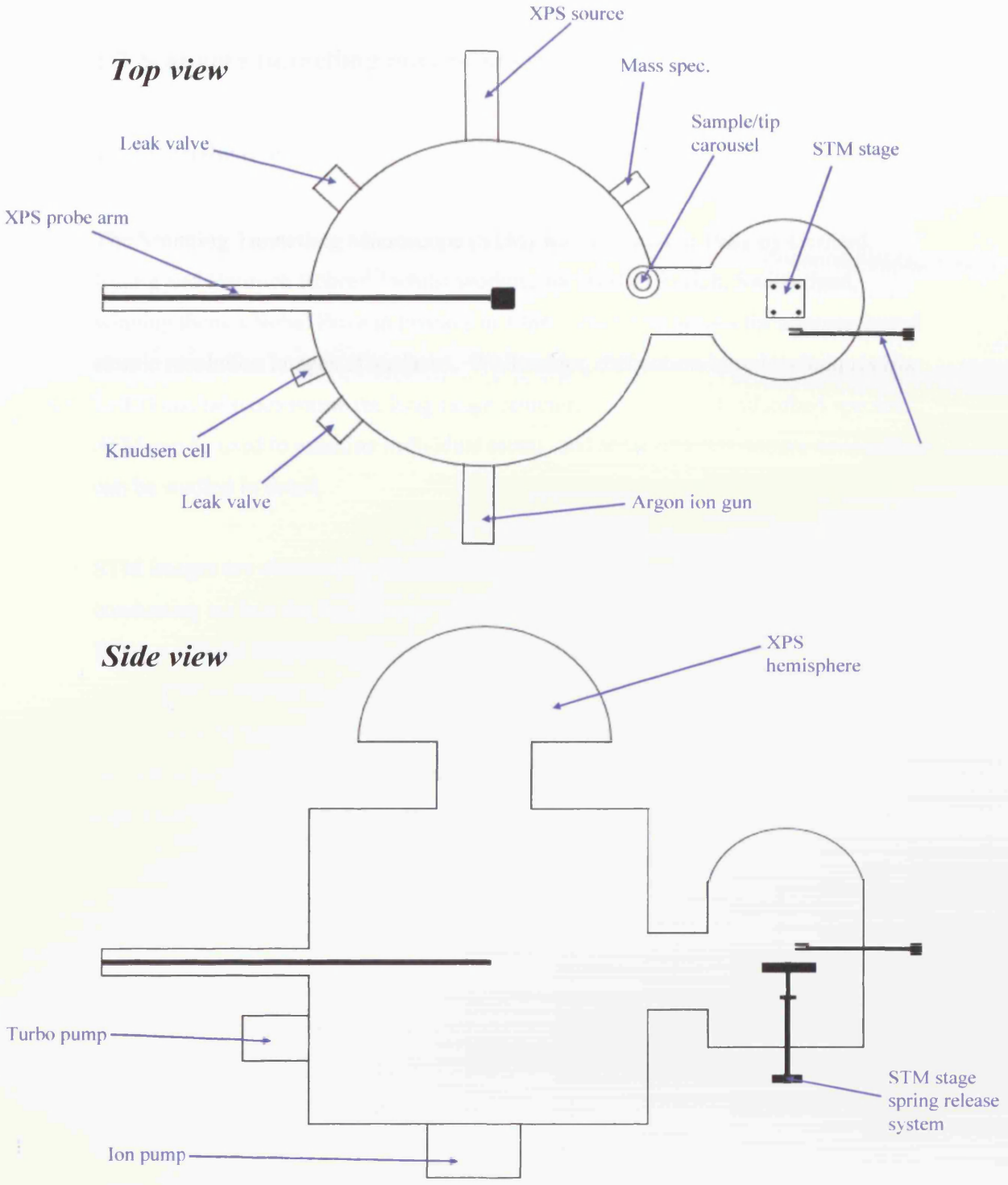


Figure 1.1: Simplified diagram of the XPS/STM system showing major components

## 1.2 Scanning tunnelling microscopy

### 1.2.1 Introduction

The Scanning Tunnelling Microscope (STM) was invented in 1981 by Gerhard Binnig and Heinrich Röhrer[1] whilst working for IBM in Zurich, Switzerland, winning them a Nobel Prize in Physics in 1986. The STM allows for unprecedented atomic resolution images of surfaces. While older, diffraction-based techniques like LEED can help determine the long-range structure of an ordered, adsorbed species, STM can be used to examine individual atoms, and areas of a few square nanometres can be studied in detail.

STM images are obtained by moving an atomically sharp metal tip close enough to a conducting surface for the electron clouds of the surface and the tip to overlap. When a voltage is applied, electrons can travel from the surface to the tip or vice versa. This is known as electron tunnelling. The current depends exponentially on the distance between the tip and the surface, and by scanning the tip across the surface, a picture of the electron density in that area is formed. If the resolution is high enough, atomic detail can be obtained.

### 1.2.2 Electron Tunnelling

Electron tunnelling is the flow of electrons through a classically forbidden barrier such as the vacuum between tip and sample in an STM instrument. It can only be explained by quantum mechanics. Classic mechanical theory states that the vacuum between the surface and the STM tip is a finite barrier, yet when the tip is brought to within a few nanometers of the surface and voltage is applied between the two, a current is formed. If the sample is positively biased, electrons will flow from the tip to the sample, and vice versa. This clearly contradicts the classic mechanics theory that in order to remove an electron, an amount of energy equal to the sample's work function must be supplied. The work function, $\phi$, is defined as the minimum energy

required to remove an electron from the highest occupied energy level (the fermi level) in the sample. There is not enough energy available at room temperature to overcome the work function of most conductors, yet if the tip is close enough to the sample, a current will indeed flow between the two.

Quantum mechanics can describe electrons as a wavefunction. This theory states that an electron has a finite probability of entering a classically forbidden region[2]. Essentially, this means that the electron density of the sample extends a short distance beyond the surface, into the vacuum. Similarly, the electron density of the STM tip also extends into this classically forbidden zone. When the tip and sample are brought close enough together, the two electron wavefunctions can overlap, allowing for the flow of electrons through such a space (figure 1.2).

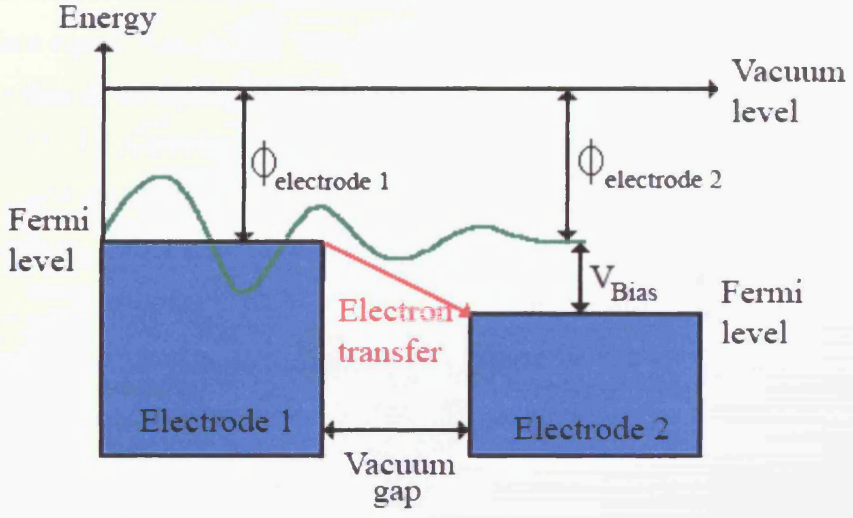


Figure 1.2: Energy level diagrams illustrating electron tunnelling between two electrodes in close proximity

STM is based on the fact that the tunnelling probability is exponentially dependent on the distance between the tip and the surface of the sample, with the maximum separation being approximately 0.2nm[3].

The tunnelling current can be described equation (1.1), where $I$ is the tunnelling current, $W$ is the tunnelling gap, $\phi$ is the sample work function and $C$ is a constant[4].

$$I(W) = C\exp\left(-W\sqrt{\phi}\right) \qquad (1.1)$$

### 1.2.3 Scanning

An STM image is obtained by rastering the tip over an area of the surface. A detailed image showing the distribution of electron density is then built up. Classically there are two methods of scanning the surface, constant current mode, and constant height mode.

Constant current mode (figure 1.3) involves keeping the current between the tip and the surface equal. Any surface features or adsorbed species will cause movement in the $z$-position of the tip (i.e. perpendicular to the surface). The voltage that needs to be applied to the piezoelectric drive in order to keep the tunnelling current constant is recorded, and the changes in this voltage are used to build up a topographical image of the surface.

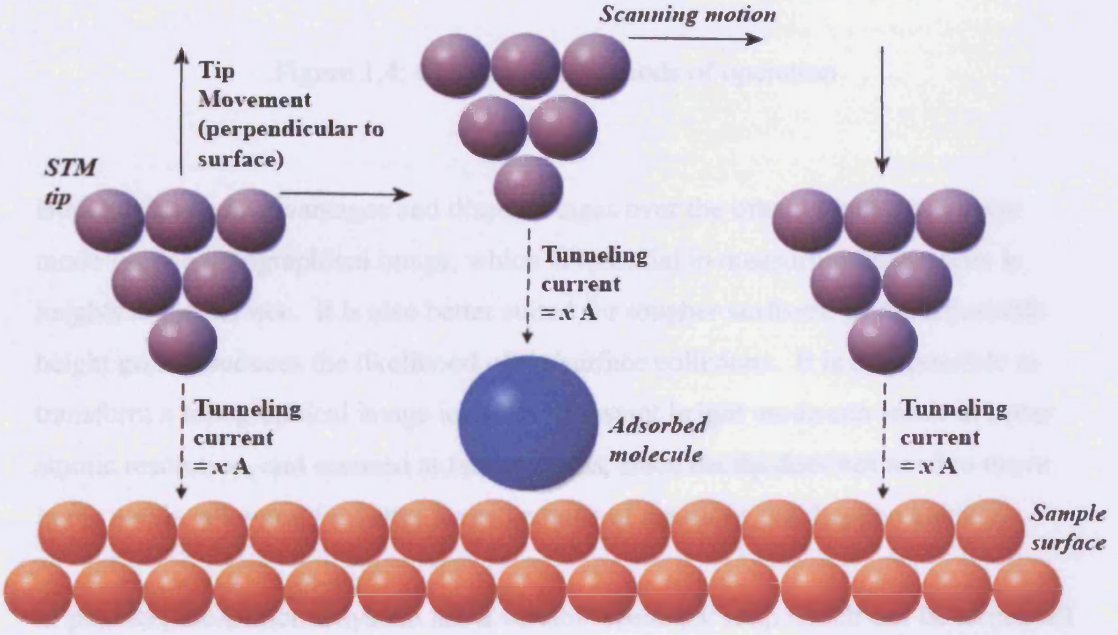


Figure 1.3: Constant current mode of operation

Constant height mode (figure 1.4) involves keeping the tip constant in the *z*-plane. As the tip is rastered across the surface, surface features or adsorbed species will cause a change in tunnelling current. A protrusion in the surface will result in a decrease in the distance between tip and surface, and therefore the tunnelling current will increase. A hole or a lower terrace will cause a decrease in tunnelling current. These changes in tunnelling current form an STM image.

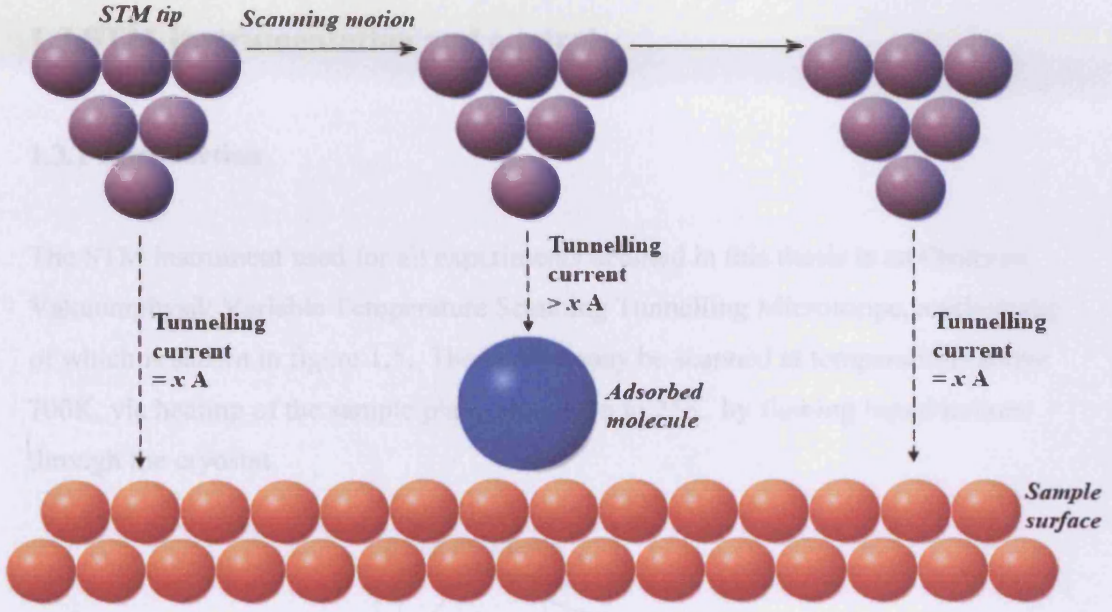


Figure 1.4: Constant height mode of operation

Both modes have advantages and disadvantages over the other. Constant current mode gives a topographical image, which is essential in measuring differences in heights at the surface. It is also better suited for rougher surfaces, as the adjustable height greatly reduces the likelihood of tip/surface collisions. It is also possible to transform a topographical image into 3D. Constant height mode can result in better atomic resolution, and scanned at faster speeds, since the tip does not need to move in the z-axis, allowing for better investigations of reactions that happen quickly.

In practice, the Omicron system has a variable feedback loop which can be turned off for constant height mode. For the experiments presented in this thesis, a mixture of

both scanning modes was used. Depending on the parameters used, image quality of the *z*-mode (constant current) or *I*-mode (constant height) would be superior to the other, the most important parameter being the feedback loop gain. For example, a low loop gain increases the constant current type mode of operation, resulting in better definition in the *z* image.

## 1.3 STM Instrumentation and control

### 1.3.1 Introduction

The STM instrument used for all experiments detailed in this thesis is an Omicron Vakuumphysik Variable Temperature Scanning Tunnelling Microscope, a schematic of which is shown in figure 1.5. The surface may be scanned at temperatures above 700K, via heating of the sample plate, and down to 25K, by flowing liquid helium through the cryostat.

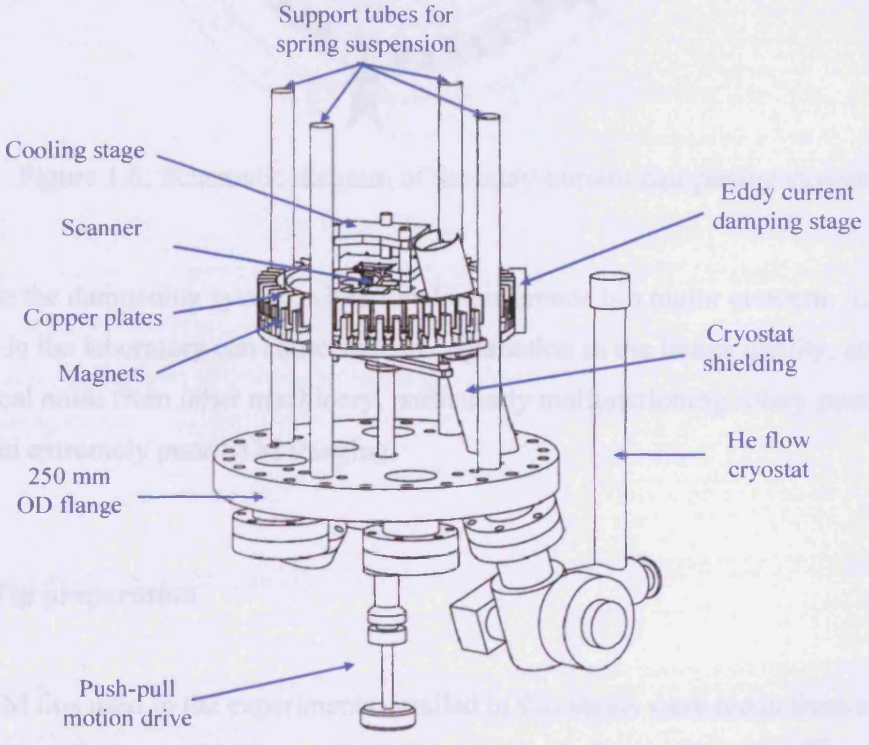


Figure 1.5: STM instrument.

### 1.3.2 Vibration dampening

There are two mechanisms by which external vibrations are prevented from affecting the tip; the STM stage is suspended by four soft springs and an eddy current dampening mechanism is used to intercept vibrations of this system. This is achieved by a ring of copper plates, which are mounted on the STM stage, and a ring of permanent magnets, which are fixed at the columns of the spring suspension. The dampening system is shown in figure 1.6.

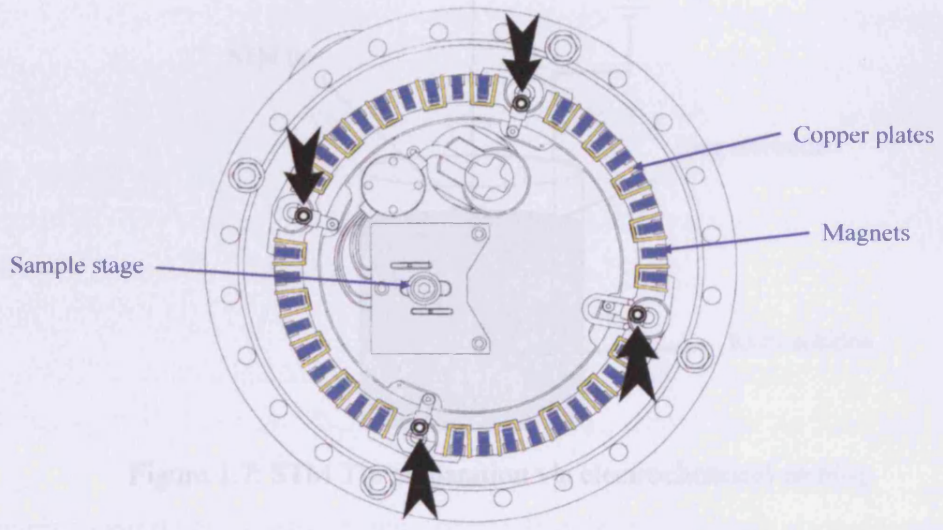


Figure 1.6: Schematic diagram of the eddy-current dampening system

Despite the dampening system, vibrational interference is a major concern. Loud noises in the laboratory can cause sudden degradation in the image quality, and electrical noise from other machinery, particularly malfunctioning rotary pumps, can result in extremely poor STM imaging.

### 1.3.3 Tip preparation

All STM tips used in the experiments detailed in this thesis were made from tungsten wire with a diameter of 0.38mm. Each tip was electrochemically etched[5] so that

they terminated in a sharp V-shape, ideally with a single atom at the apex. This was achieved using the apparatus detailed in figure 1.7. A ring shaped tungsten electrode is placed in a beaker containing a solution of 0.6 M KOH so that it is just submerged below the surface of the solution. The tip is connected to the electrode and lowered into the solution. A current is then applied between the electrodes, and any part of the tip that is submerged is etched away, resulting in a sharp termination to the tungsten wire. The tip is then washed with acetone and placed into the spectrometer.

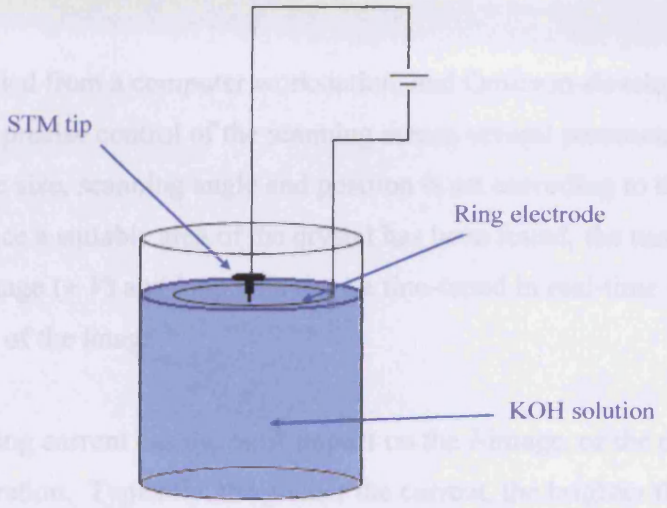


Figure 1.7: STM Tip preparation via electrochemical etching

The quality of a tip plays an integral role in the quality of the STM images, although it is not possible to fully discern a tip's quality without testing it. The STM chamber contains a carousel, onto which up to six tips can be mounted at a time, reducing the need to open the system to the atmosphere to change tips. The carousel can also house sample holders, allowing for several single surface crystals to be contained in the chamber at any one time.

### 1.3.4 Piezoelectric tube scanner

A piezoelectric drive is used in order to achieve the extremely precise control of the STM tip required for scanning. When a voltage is applied across a piezoelectric material, it will expand or contract, by typically 1Å per mV. The Omicron STM has

the tip mounted in a piezoelectric cylinder. When a voltage is applied between pairs of opposing electrodes on the outside walls of the cylinder, it will bend. This effect can be used to scan the tip in the $x$ and $y$ plane of the surface in a controllable manner. A voltage can also be applied between the inside and outside surface to expand and contract the cylinder and hence control movement in the $z$ direction.

### 1.3.5 Scanning parameters

The STM is controlled from a computer workstation, and Omicron-developed software allows for precise control of the scanning across several parameters. Typically, the frame size, scanning angle and position is set according to the needs of the experiment. Once a suitable area of the crystal has been found, the tunnelling current ($I$), bias voltage ($\pm V$) and loop gain can be fine-tuned in real-time in order to improve the quality of the image.

Varying the tunnelling current has the most impact on the $I$-image, or the constant height mode of operation. Typically, the greater the current, the brighter the image.

For the scanning of Cu(110), voltages in the range of 0.02V and 3V were typically used. The polarity of the voltage can be changed during a scan, reversing the flow of tunnelling electrons. Fine-tuning of the bias voltage is important in better defining atoms adsorbed onto the substrate.

The loop gain plays an integral part in the quality of the images from both constant height and constant current modes of operation. When scanning large areas (>400nm x 400nm), the loop gain is typically set at approximately 60%. It is generally a requirement that as the area being scanned gets smaller, so must the loop gain. For areas of 60nm x 60nm and smaller, values of >1% are used. In order to achieve atomic resolution in the $Z$-image (constant current mode), the loop gain is typically required to be approximately 0.1%.

## 1.4 X-ray photoelectron spectroscopy

### 1.4.1 Introduction

Photoelectron spectroscopy (PES) is one of the most widely used techniques for the study of surfaces. It relies on the photoelectric effect wherein photons of a defined energy, hν, impinge on a solid and, assuming the photon energy is greater than the work function of the solid, absorption of the photon causes the ejection of a photoelectron. The photoelectron possesses a discrete kinetic energy, dependent on the orbital from which it was ejected. This kinetic energy is given by the Einstein relationship[6] shown in equation (1.2), where $E_K$ = kinetic energy of the emitted photoelectrons/eV, hν = energy of the impinging photons,/eV, $E_B$ = binding (or ionisation) energy of the ejected photoelectrons/eV.

$$E_K = h\nu - E_B \qquad (1.2)$$

PES is generally divided into two techniques, which vary in the ionising source and hence the energy of the photons impinging on the surface. X-ray photoelectron spectroscopy (XPS) uses electron bombardment of Al or Mg to create X-rays with respective energies of 1486.6 and 1253.6 eV. The photons produced by such methods have energies great enough to probe the core orbitals of atoms. Since these levels are quantised, the photoelectrons have a kinetic energy distribution, n(E), made up of a series of discrete bands. Thus, plotting n(E) against $E_K$ gives the photoelectric spectrum and can give elemental information.

Although the X-rays used for XPS penetrate approximately $10^4$ Å, due to inelastic scattering of the photoemitted electrons, the measured photoelectrons originate from a depth of under 50Å from the surface. It is for this reason that XPS is a surface sensitive technique. The inelastic scattering of photoelectrons also means that XPS requires UHV.

Ultraviolet photoelectron spectroscopy (UPS) uses photons with lower energy, resulting in photoemission from the valence band.

### 1.4.2 Core-hole decay

Following the emission of an electron from a solid via the photoelectric effect, there are two pathways available for the decay of the core-hole formed; X-ray fluorescence and the Auger process[7,8] (figure 1.8).

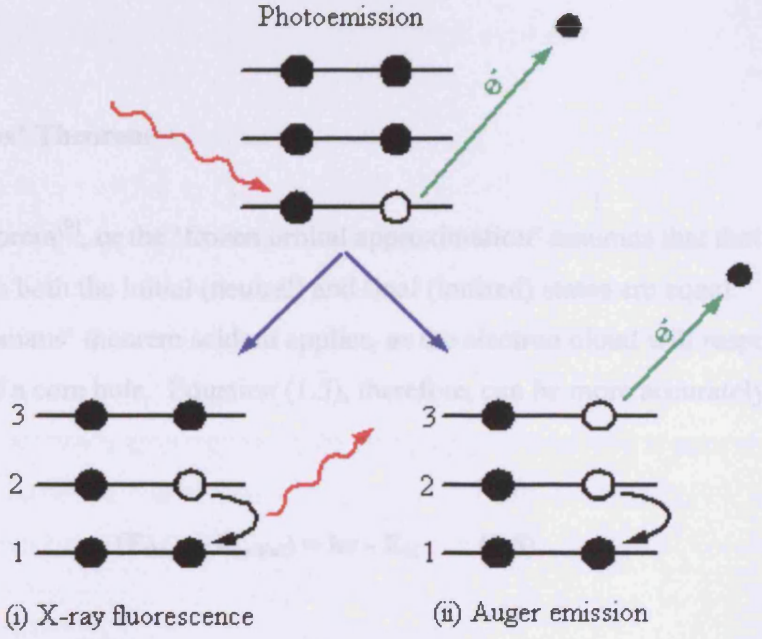


Figure 1.8: Core-hole decay mechanisms

During X-ray fluorescence, an electron falls from a higher energy orbital to fill the core-hole, releasing an X-ray photon as it does so, the energy of which is given by equation (1.3), Where Ea and Eb are the respective energy levels involved in the process.

$$h\nu = E_b - E_a \qquad (1.3)$$

The Auger process involves ionisation of a secondary outer electron, the Auger electron, resulting in a doubly ionised state. The electron is ejected by the energy released by filling the core-hole. Auger electron energies depend only on the difference between the levels concerned and not on the incident photon energy (equation (1.4)).

$$E_{auger} = E_1 - (E_2 + E_3) \qquad (1.4)$$

Auger electrons give rise to signals in the photoelectron spectrum as well as forming the basis of Auger Electron Spectroscopy (AES).

### 1.4.3 Koopmans' Theorem

Koopmans' theorem[9], or the 'frozen orbital approximation' assumes that that the orbital energy in both the initial (neutral) and final (ionised) states are equal. However, Koopmans' theorem seldom applies, as the electron cloud will respond to the formation of a core hole. Equation (1.5), therefore, can be more accurately expressed as:

$$(E_{final} - E_{initial}) = h\nu - E_K \qquad (1.5)$$

### 1.4.4 Final state effects

The formation of a positive core-hole due to photoemission affects the final state of the atom. In order to minimise the effect of the new positive charge, it can relax via the following mechanisms, all of which can affect the photoelectron spectrum.

#### 1.4.4.1 Intra atomic relaxation

Upon photoionisation, the occupied atomic orbitals of the excited atom relax by contracting towards the positive core-hole and lower the energy of the final state. The difference in energy is passed on to a photoelectron. In a photoelectron spectrum, this can result in a feature shifting to a slightly lower binding energy.

#### 1.4.4.2 Electron shake-up and shake-off processes

Shake-up and shake-off are terms given to the processes by which electrons other than the escaping photoelectron undergo simultaneous excitation.

During a shake-up process, a specific quantum of energy is used to promote a valence electron into a higher, unoccupied level. This reduces the amount of energy available to the escaping photoelectron and results in a discrete satellite peak in the corresponding photoelectron spectrum at a BE energy that is lower than the parent peak. Such satellites can provide extra information about an atom's chemical state.

During a shake-off process, energy from the escaping photoelectron is passed on to a valence electron, ejecting it to an unbound state and leaving vacancies in the core and valence levels, resulting in a doubly ionised state. Unlike the shake-up process, the energy involved here is not discrete and so discrete structure is not observed in the photoelectron spectrum.

#### 1.4.4.3 Spin-orbit coupling

Electrons orbiting a nucleus have an orbital angular momentum, $l$, and spin angular momentum, $s$. In a neutral state, these electrons exist in pairs with opposing spin, resulting in a net magnetic moment of zero. Upon photoionisation however, the atom will be left with an unpaired electron, the spin angular momentum of which

will interact with the orbital angular momentum. Depending on the electron left unpaired, the spin will either reinforce or oppose the angular momentum. This causes two non-degenerate states to be formed, and hence two different values for the total angular momentum, $j$ (where $j = l \pm s$). The opposing state has a higher energy than the parallel state.

These two different final states for the atom can affect the photoelectron spectrum, resulting in a splitting of the primary photoelectron peak into two of differing intensity. The ratio of the intensities of these peaks is related to $j$, and is given by equation (1.6).

$$\textbf{Intensity} = 2j + 1 \qquad \textbf{(1.6)}$$

Figure 1.9 shows the effects of spin-orbit coupling in the Ni(2p) spectrum. The peak is split in two, with an intensity ratio of 2:1.

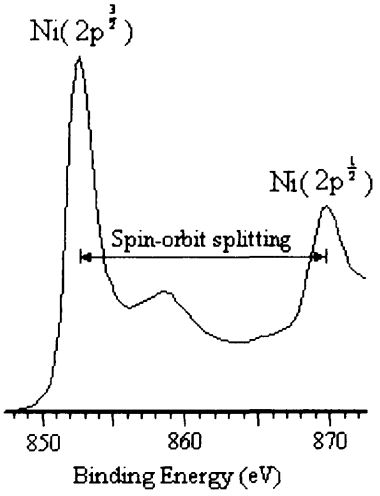


Figure 1.9: Spin-orbit splitting in the Ni(2p) XP spectrum.

### 1.4.4.4 Multiplet splitting

Multiplet splitting occurs when an unpaired core electron becomes coupled with an unpaired valence electron. Their spin vectors can align either parallel or antiparallel

resulting in two states. This manifests itself in the photoelectron spectrum as two peaks separated by the exchange interaction energy, ΔE.

### 1.4.4.5 Plasmon loss

When a photoelectron passes through a solid, it can induce collective oscillations within the conduction band of free electrons. This phenomenon is known as a plasmon. Plasmons have a fixed frequency (ω) depending on the solid, and occur at multiples of this frequency (2 ω, 3 ω, 4 ω etc.).

A photoelectron that induces a plasmon experiences a discrete energy loss. This 'plasmon loss' gives rise to a series of regularly spaced peaks of decreasing intensity in photoelectron spectra. The effect is most commonly observed for solids with *s*- or *p*-type valence density. Most transition metals, therefore, exhibit no plasmon losses, whereas alkaline earth metals can exhibit extensive plasmon loss. Figure 1.10 highlights such a case. It shows the plasmon loss peaks in the $Al^0$ (electronic configuration $3s^2 3p^1$) XP spectra[10,11]. Plasmons can occur in the bulk and at the surface. The localised oscillation at the surface appears on the spectrum as a lower intensity peak next to the higher intensity bulk plasmon loss peaks.

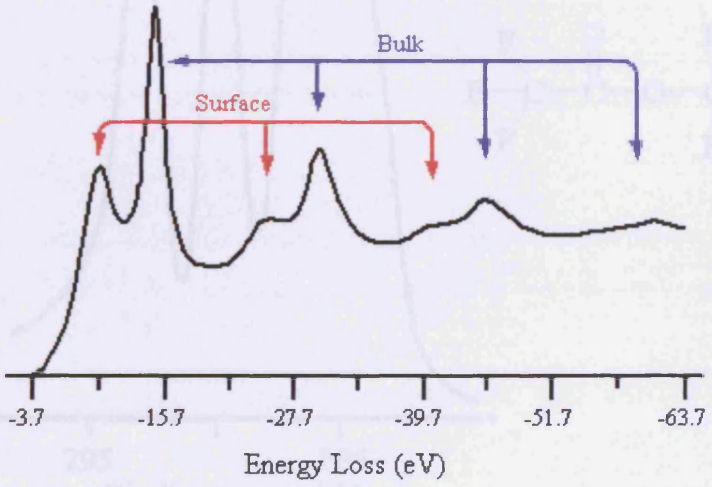


Figure 1.10: Plasmon loss peaks in the $Al^0$ spectrum

### 1.4.5 The chemical shift

The initial state of a molecule can also affect the photoelectron spectrum. The main initial state effect to be considered in XPS is the chemical shift. Chemical shifts are caused by a redistribution of charge occurring in atomic valence orbitals when a change in their chemical environment occurs, e.g. the formation of a chemical bond. The difference in charge alters the electrostatic fields around the core orbitals, resulting in small shifts in energies of the core orbitals, and hence the binding energy.

Figure 1.11 shows the C(1s) XP spectrum of ethyl-trifluoroacetate[12]. The different electronegativity of the substituent groups result in four chemically distinct peaks. Highly electronegative atoms, such as fluorine, attract electron density away from carbon atoms to which they are bonded, resulting in a small positive charge in the carbon atom and thus a higher ionisation energy, which manifests itself as a shift in binding energy in XP spectra.

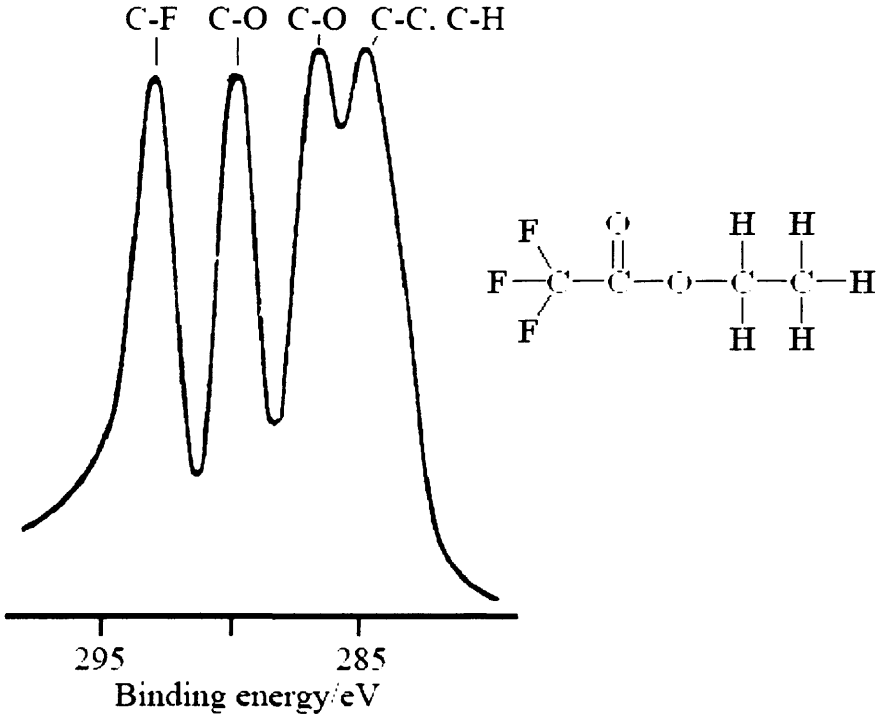


Figure 1.11: C(1s) XP spectrum of ethyl-trifluoroacetate

### 1.4.6 Inelastic scattering and surface sensitivity

Although X-rays used for XPS analysis can penetrate the bulk of a solid up to $10^4$ Å, due to the inelastic scattering of the emitted electrons, the measured photoelectron signal originated from a surface depth of less than 50 Å from the surface. The inelastic scattering, which is referred to as the inelastic mean free path (IMFP), escape depth or the attenuation length, may be quantified by the parameter λ, and is defined as the thickness of material that will attenuate an incident flux of electrons ($I_0$) by a factor of $1/e$. The resulting photoelectron flux is given by equation 1.7, and shown schematically in figure 1.12..

$$I' = I_0 \exp\left(\frac{-d}{\lambda}\right) \qquad \textbf{(1.7)}$$

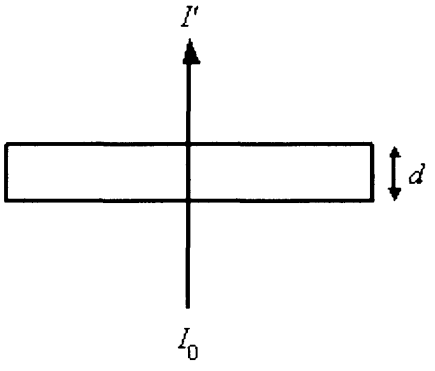


Figure 1.12: The detected photoelectron flux passing through a material of thickness $d$

The mean free path of electrons for inelastic scattering in solids depends on the kinetic energy of the emitted electrons and is shown graphically in figure 1.13, which is commonly known as the universal curve.

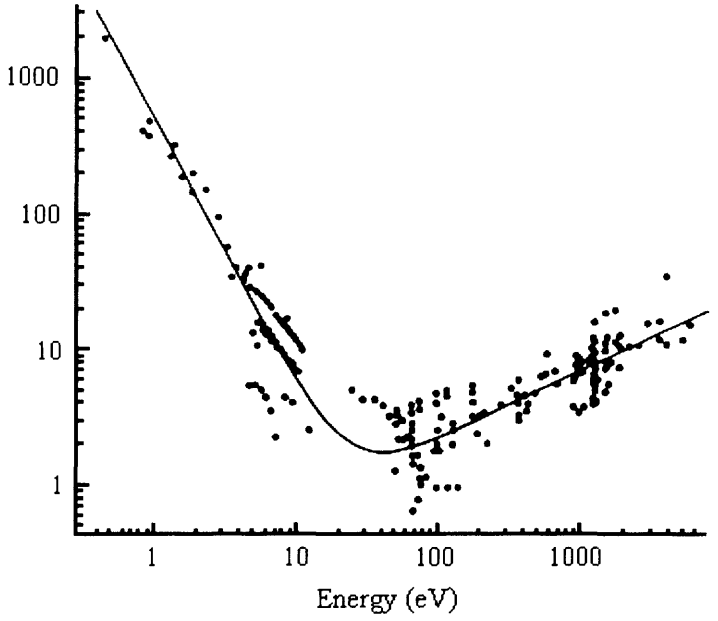


Figure 1.13: The universal curve measured from a range of elements[12]

Electrons that undergo energy loss due to inelastic scattering do not contribute to the photoelectron peaks, and instead make up most of the spectral background.

### 1.4.7 Instrumentation

A schematic diagram of the XPS function of the spectrometer is shown in figure 1.14.

The spectrometer contains a dual anode X-ray source, containing Al and Mg anodes. The anodes are bombarded with electrons from a hot filament and are ionised, forming core-holes. The core-holes are filled by electrons from outer levels and the excess energy is emitted as X-ray photons. Although the Mg anode was used on occasion (alternating between anodes can distinguish between XP and Auger peaks, as the kinetic energy of Auger electrons do not depend on the photon energy), the results presented here were all obtained through use of the Al anode.

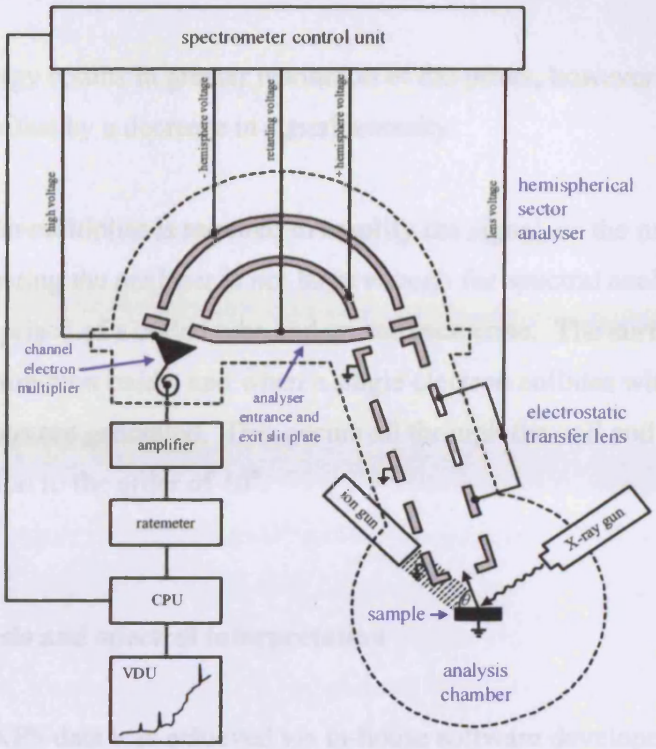


Figure 1.14: Schematic of the XPS system used

A concentric hemispherical analyser (figure 1.15) is used to analyse the photoemitted electrons. It is comprised of two concentric hemispherical surfaces of radii $R_1$ and $R_2$, which are positively and negatively charged, respectively. Equidistant between the two surfaces, there is a path of equipotential, $R_0$. As photoelectrons pass through the entrance slit, a retarding potential is applied, slowing the electrons to a constant pass energy. The retarding potential is then varied and photoelectron peaks appear in the spectrum according to the value of the retarding potential required to decelerate them to the fixed pass energy.

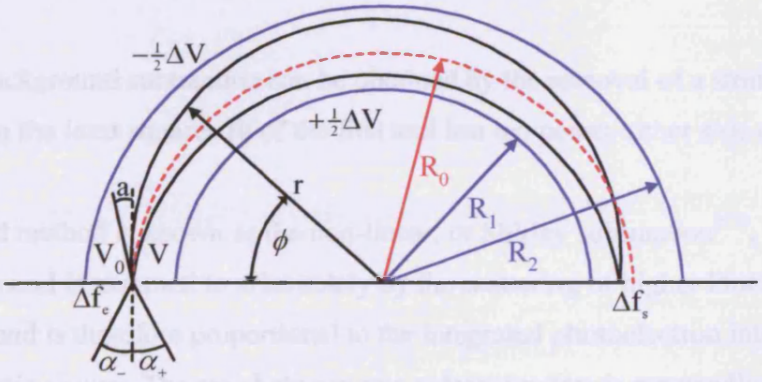


Figure 1.15: Schematic diagram of the CHA.

A lower pass energy results in greater resolution of the peaks, however this enhancement is offset by a decrease in signal intensity.

A channel electron multiplier is required to amplify the signal, as the number of photoelectrons exiting the analyser is not large enough for spectral analysis. The multiplier is comprised of a coiled tube and an entrance cone. The surface is coated with a low work function oxide, and when a single electron collides with the surface, secondary electrons are generated. This occurs all through the coil and results in signal amplification to the order of $10^8$.

### 1.4.8 Data analysis and spectral interpretation

Analysis of raw XPS data was achieved via in-house software developed by CarleyREF. The software was used mainly for background removal, spike removal, spectral subtraction, and peak area calculation.

#### 1.4.8.1 Background removal

Inelastically scattered electrons are responsible for the most of the underlying background intensity in XP spectra. This is usually observed as a sloping background rising towards high binding energy. There are two ways of removing this background, a step that must be taken in order to accurately measure peak areas.

A linear background subtraction can be obtained by the removal of a straight line drawn from the least squares fit of the first and last ten points either side of the peak.

The second method is known as the non-linear, or Shirley subtraction[13], whereby the background is assumed to arise solely by the scattering of higher kinetic energy electrons, and is therefore proportional to the integrated photoelectron intensity at higher kinetic energy. The area between two selected points is repeatedly integrated

until a converged background value is obtained, which can then be subtracted from the peak intensity.

In general, the linear method is used for adsorbate peaks, as there are very few inelastic electrons, whereas the Shirley method is used for bulk metal peaks.

### 1.4.8.2 Peak area calculation

Following background removal, the peak area can be calculated, and from that the surface concentration of the species giving rise to photoelectron peak can be deduced. This is done by the software by integrating the intensity above a baseline drawn between two points either side of the photoelectron peak (figure 1.16).

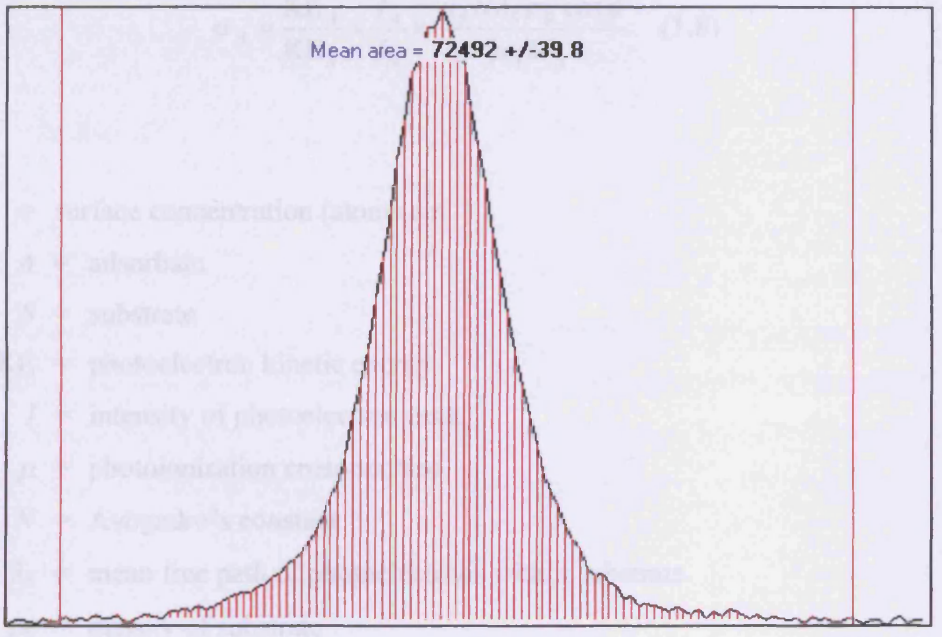


Figure 1.16: Peak area measurement

### 1.4.8.3 Quantification

XPS is a quantitative technique with the signal intensity directly related to the number of atoms sampled. Determination of the surface concentration of an element is achieved by integration of the area under a background-subtracted XP peak.

Equation (1.8), developed by Carley and Roberts[14], is used to relate the peak areas to surface concentrations. It is a modified version of an original equation derived by Madey[15], and now includes the photoionisation cross section to account for the probability that an electron is photoemitted from a particular orbital of a particular atom. This value is dependent on the size and shape of the orbital and the ionising photon energy. Values for the photoionisation cross sections of elements are obtained from data tabulated by Schofield[16].

$$\sigma_A = \frac{\mathrm{KE}_A}{\mathrm{KE}_S} \times \frac{I_A}{I_S} \times \frac{\mu_S N \lambda_S \rho_S \cos\phi}{\mu_A M_S} \qquad (1.8)$$

$\sigma_A$ = surface concentration (atoms $cm^{-2}$)
$A$ = adsorbate
$S$ = substrate
KE = photoelectron kinetic energy
$I$ = intensity of photoelectron peak
$\mu$ = photoionisation cross-section
$N$ = Avogadro's constant
$\lambda_S$ = mean free path of photoelectrons within substrate
$\rho_S$ = density of substrate
$\phi$ = angle of collection of photoelectrons with respect to the sample normal
$M_S$ = relative atomic mass of substrate

#### 1.4.8.4 Curve fitting

Occasionally, two XP peaks arising from different chemical states of a particular surface species overlap. Curve fitting can resolve each component of the composite peak.

The software used employs and iterative routine that optimizes the fit between a synthesized spectrum and the available raw data. Through the predefinition of the number of species present within the composite spectra, the user may then select initial values for the intensity energy and FWHM. These parameters form Gaussian peaks, which are summed to give an approximate fit. The result is passed through an iterative least-squares minimization to automatically yield a 'good' fit.

## 1.5 Miscellaneous equipment

### 1.5.1 The gas line

Two leak valves on the main chamber are connected to a stainless steel gas line, and can be used for the controlled exposure of gases and vapour over a range of approximately $1 \times 10^{-9}$ mbar to $1 \times 10^{-4}$ mbar. A schematic of the gas line is shown in figure 1.17. It is comprised of two sides, one for each leak valve, which can be isolated from each other, allowing for simultaneous dosing of two different gases. It is pumped by a diffusion pump to a typical pressure between $1 \times 10^{-6}$ and $1 \times 10^{-7}$ mbar.

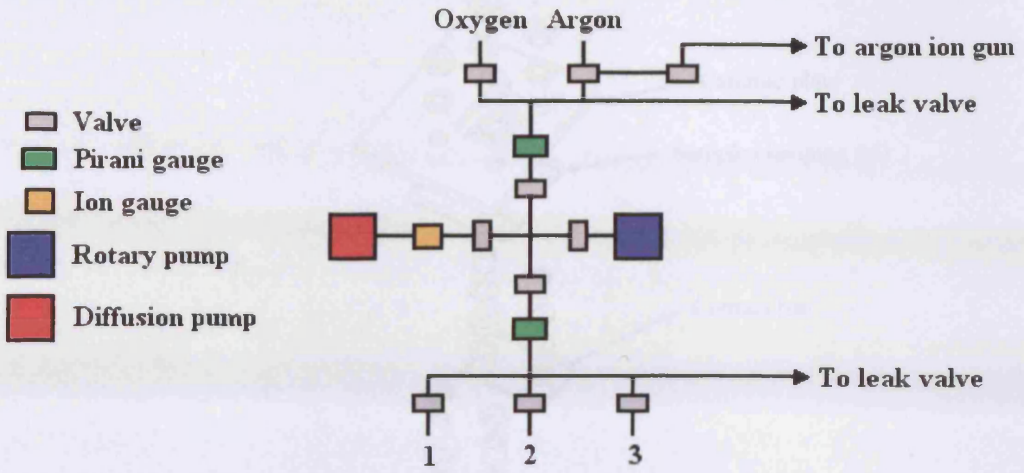


Figure 1.17: Schematic diagram of the gas line

### 1.5.2 The sample holder

Figure 1.18 shows an explosion diagram of the sample holder used to hold the single crystal surfaces in the STM/XPS instrument. The ceramic top plate allows the holder to be placed securely in the STM stage and the XPS probe, while the Mo base plate allows a manipulator arm to grasp the holder and move the sample between the STM stage, the XPS probe and the carousel.

The sample is heated by a PBN plate, which heats up when a current is passed through it.

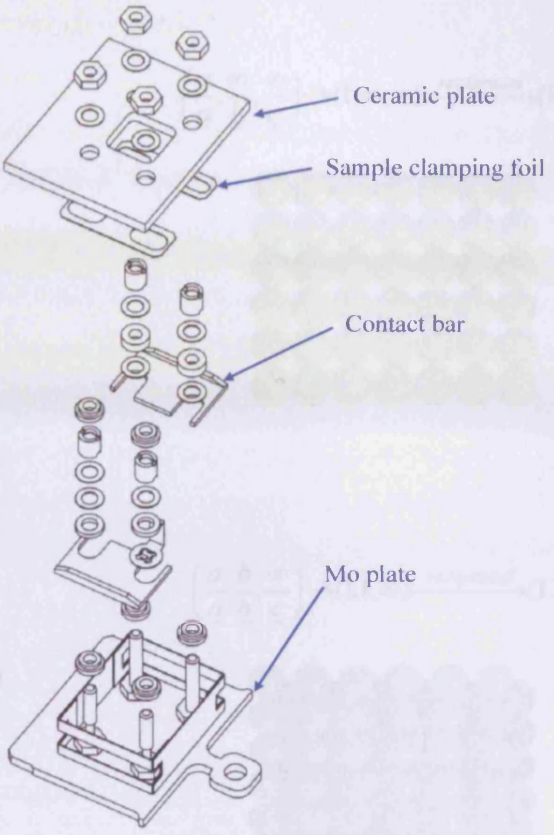


Figure 1.18: Sample holder diagram

## 1.6 Adsorbate and substrate classification

### 1.6.1 Miller Indices

Single crystals can be cut in different directions to expose different crystallographic planes. A Miller Index describes the way a crystal plane intersects the bulk unit cell of a crystalline solid. For the cubic structure of Cu(110), the surface studied in this thesis, there exist a set of axes (x, y, z) assigned to the cube vertex. The Miller Index of (110) can be defined as cutting the x-axis at a length x, cutting the y-axis in a similar manner at a length y, and never intersecting z (i.e. at $z = \infty$). The Miller Index is constructed from the reciprocal of those intersects ($x, y, \infty$), yielding (110). The low Miller Indices, (100), (110) and (111), for a face centred cubic packed system are shown in figure 1.19.

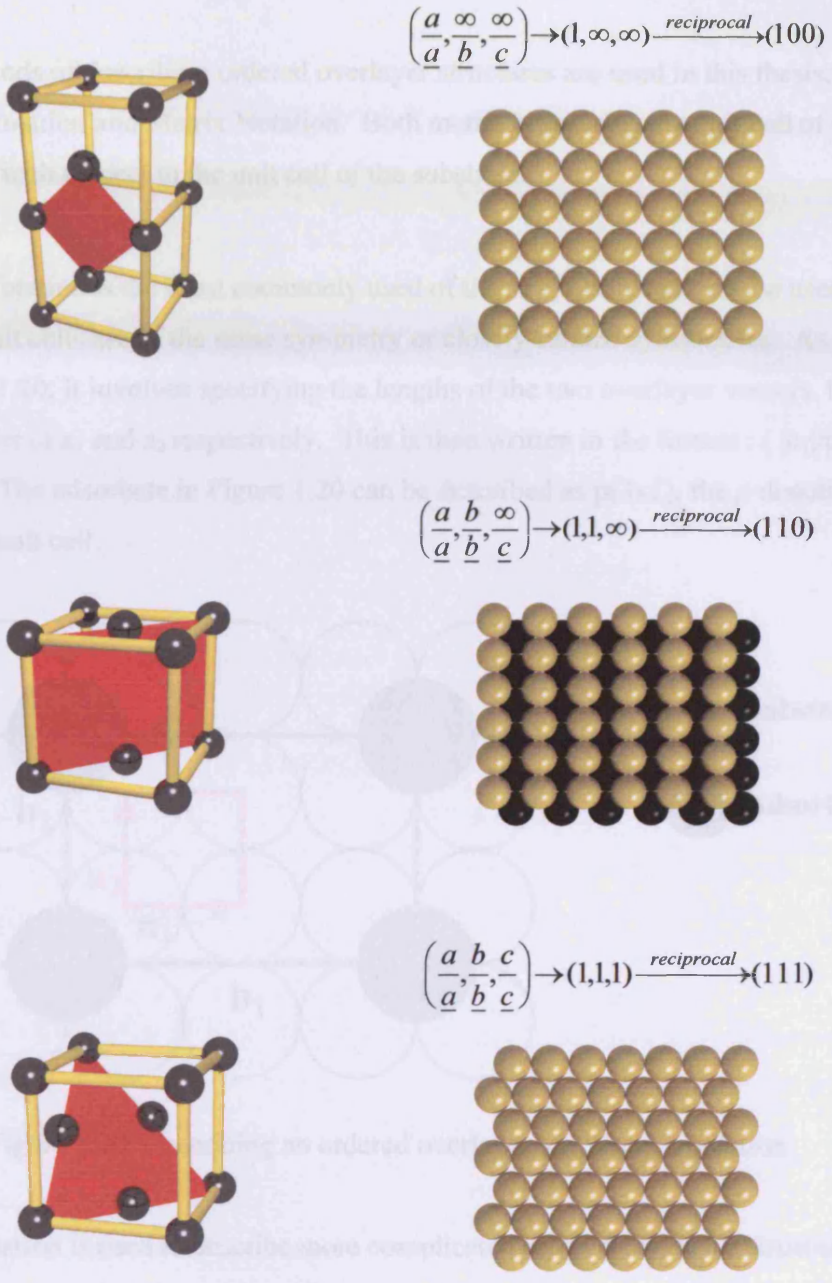


Figure 1.19: The low index crystal lattice planes

### 1.6.2 Classification of overlayer structures

Two methods of describing ordered overlayer structures are used in this thesis; Wood's Notation and Matrix Notation. Both methods describe the unit cell of the adsorbate with respect to the unit cell of the substrate.

Wood's Notation is the most commonly used of the two, but it can only be used if the two unit cells are of the same symmetry or closely-related symmetries. As shown in Figure 1.20, It involves specifying the lengths of the two overlayer vectors, $b_1$ and $b_2$, in terms of $a_1$ and $a_2$ respectively. This is then written in the format : ( $|b_1|/|a_1|$ x $|b_2|/|a_2|$ ). The adsorbate in Figure 1.20 can be described as p(3x1), the *p* denoting a primitive unit cell.

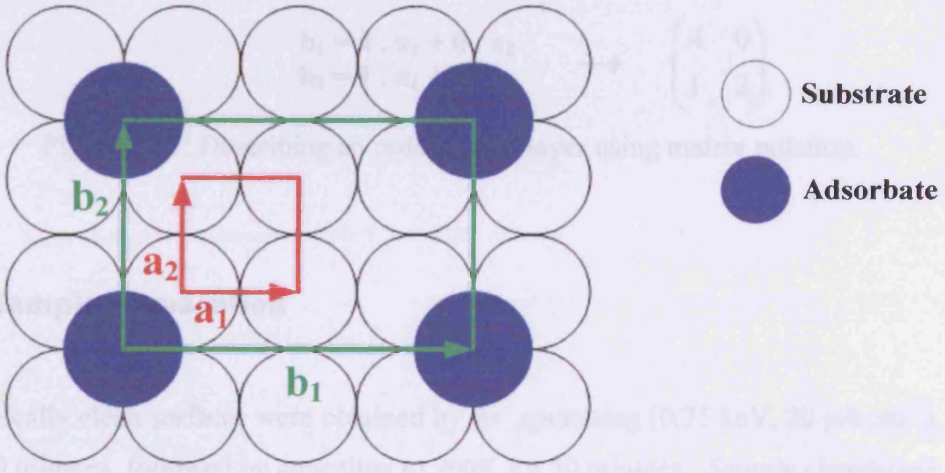


Figure 1.20: Describing an ordered overlayer via Wood's notation.

Matrix notation is used to describe more complicated ordered overlayer structures. it also relates the vectors $b_1$ and $b_2$ to the substrate vectors $a_1$ and $a_2$, this time using a simple matrix, i.e.

$$\begin{pmatrix} b1 \\ b2 \end{pmatrix} = \begin{pmatrix} * & * \\ * & * \end{pmatrix} \begin{pmatrix} a1 \\ a2 \end{pmatrix}$$

Figure 1.21 shows an adsorbate that can be described as $\begin{pmatrix} 4 & 0 \\ 1 & 2 \end{pmatrix}$ using matrix notation.

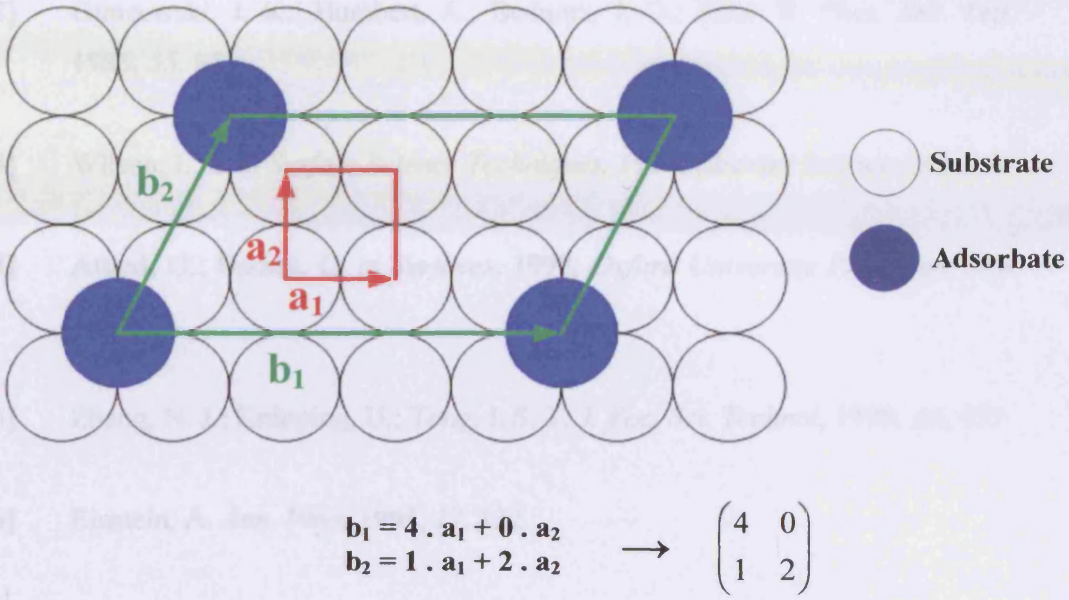


$$\begin{aligned} b_1 &= 4\,.\,a_1 + 0\,.\,a_2 \\ b_2 &= 1\,.\,a_1 + 2\,.\,a_2 \end{aligned} \quad \longrightarrow \quad \begin{pmatrix} 4 & 0 \\ 1 & 2 \end{pmatrix}$$

Figure 1.21: Describing an ordered overlayer using matrix notation.

## 1.7 Sample preparation

Atomically clean surfaces were obtained by $Ar^+$ sputtering (0.75 keV, 20 μA $cm^{-2}$) for 20 minutes, followed by annealing to 900K for 50 minutes. Sample cleanliness was checked by XPS.

## 1.8 References

[1] Binnig, G.; Röhrer, H. *Helv. Phys. Acta.* **1982**, *55*, 726

[2] Gimzewski. J. K.; Humbert, A.; Bednorz, J. G.; Rehl, B. *Phys. Rev. Lett.* **1985**, *55*, 951

[3] Wilson, I. H. in *Surface Science Techniques*, **1994**, *Elsevier Science Ltd.*

[4] Attard, G.; Barnes, C. in *Surfaces*, **1998**, *Oxford University Press Inc. New York*

[5] Zheng, N. J.; Knipping, U.; Tong, I. S. T. *J. Vac. Sci. Technol*, **1998**, *A6*, 457

[6] Einstein, A. *Ann. Phys.* **1905**, *17*, 132

[7] Auger, P. J. Phys. *Radium*, **1925**, *6*, 205

[8] Linsmeier, C. *Vacuum*, **1994**, *45*, 673

[9] Koompman, T. *Physica*, **1993**, *1*, 104

[10] Fuggle, J. C.; Fabian, D. J.; Watson, L. M. *J. Elec. Spec. Rel. Phenom*, **1976**, *9*, 99

[11] Gelius, U; Basilier, E.; Svensson, S.; Bergmark, T.; Siegbahn, K. *J. Elec. Spec. Rel. Phenom.* **1974**, *2*, 2005

[12] Proctor, A.; Sherwood, P. M. A. *Anal. Chem.*, **1980**, *52*, 2315

[13] Shirley, D.A. *Phys. Rev. B*, **1972**, *5*, 4709

[14] Carley A. F.; Roberts, M. W. *Proc. R. Soc. Lond. A*, **1978**, *363* 403

[15] Madey, T. E.; Yates, J. T.; Erickson, N. E. *Chem. Phys. Lett.*, **1973**, *19*, 487

[16] Scofield, J. H. *J. Elec. Spec. Rel. Phenom.*, **1976**, *8*, 126

# *Chapter 2*

## *Interaction of aniline with Cu(110) surfaces*

### 2.1 Introduction

The interaction of aniline ($PhNH_2$) vapour with clean and oxidised Cu(110) surfaces, and an aniline/dioxygen coadsorption has been investigated using scanning tunnelling microscopy and x-ray photoelectron spectroscopy. The investigation focuses on the extent of adsorption at room temperature and the structures formed. Emphasis is placed on the reaction with oxidised Cu(110).

### 2.2 The interaction of aniline with metal surfaces

The only previous investigation of the interaction of aniline with copper surfaces is a TPD/HREELS study on Cu(110)[1]. TPD results showed aniline desorbing from a weakly-bound multilayer state at 195K, and a chemisorbed state at 300K. It was concluded that the products detected above 300K were from a dissociative process, and not from adsorbed molecular aniline, as desorption temperatures for benzene and ammonia are 270K and 255K, respectively.

HREELS results from the same paper indicated that the aromatic ring of the aniline molecule is orientated approximately parallel to the surface. The presence of certain modes at a very low intensity indicated a slight tilt of the ring, however. HREELS also showed the presence of two NH stretching modes in the multilayer state at 100K, but only one in the chemisorbed state at 300K. It was concluded that the product of the reaction of aniline with Cu(110) is $C_6H_5NH$, and that it bonds to the surface via the nitrogen atom. There is also a weak interaction between the aromatic ring and the surface.

The reaction of aniline with silver surfaces has been investigated on both Ag(111)[2] and Ag(110)[3]. TPD results showed that aniline adsorbs molecularly on Ag(111) without decomposition below 250K. LEED showed no evidence of an ordered adsorbate. HREELS indicates the aniline molecules again lie mostly parallel to the surface, at an angle of approximately 13°. The saturation coverage was determined to be approximately $1.5 \times 10^{14}$ molecules $cm^{-2}$.

On Ag(110), aniline was found to desorb from a multilayer state at 195K, a chemisorbed monolayer at 325K, as well as another state at 250K. TPD also showed a small desorption peak at 450K when background oxygen was present in the system, indicating aniline will react with surface oxygen. Desorption from a monolayer state at 325K indicates aniline is more strongly bound to Ag (110) than Ag(111).

A saturation coverage of $2.3 \times 10^{14}$ molecules $cm^{-2}$ was determined by XPS, following the reaction of aniline with Ag(110), approximately twice the maximum coverage found for benzene and phenol. The authors concluded that aniline forms two layers on Ag(110), and that desorption of the second layer is responsible for the peak at 250K in the TPD spectrum. The angle between the surface and the aromatic ring was determined to be $39 \pm 5°$ in the single layer state at 325 K, although this tilt angle is an upper limit. The majority of molecules isolated on terraces are likely to have a smaller angle.

An investigation of aniline at Ni(100) surfaces[4] found that the aromatic ring was orientated parallel to the surface, and also suggested the formation of polyaniline. TPD results of the reaction of aniline with Ni(111) surfaces indicate the formation of

a chemisorbed monolayer at 350K, which is stable on the surface up to 700K. This is much more strongly bonding than benzene at the same surface, and the paper concluded that polyaniline was also being formed at the Ni(111) surface. RAIRS shows no in plane ring vibrations at 350K, suggesting that the molecule lies parallel to the surface here as well. It was also determined that aniline interacts with the surface through both the amine group and the aromatic ring. INDO calculations suggest that the N atom prefers on top adsorption sites.

A study of aniline at Pd(110) surfaces[5], using ARUPS (angle resolved UV photoemission spectroscopy), using synchrotron radiation, TDS and LEED, give similar results to other surfaces mentioned. It was found that a $C_6H_5NH$ product was formed, and that a near-parallel surface geometry was likely. It is the only previous study to determine a structure for an adsorbate at a metal surface. LEED results showed that a densely packed c(4x2) structure was formed. Although formation of a polymer, as seen on Ni surfaces is ruled out, a configuration is proposed which might be seen as a precursor to polyaniline.

A study using STM has determined that aniline will form regions of moderately ordered p(2 x 2) and c (4 x 2) structures on Si(100)(2 x 1) surfaces.[6]

Extensive research has been conducted into the use of aniline and various derivatives to help inhibit copper corrosion in acidic solution[7-12]. A theoretical study[7] investigated the relationship between surface defects, corrosion and corrosion inhibition by aniline. The calculations showed that the corrosion inhibition by aniline is associated mainly with the interaction of the molecule with defect sites which, due to their high reactivity to external agents, are prime sites for corrosion.

## 2.3 Experimental

The combined XPS/STM instrument used in this investigation and the sample cleaning process are as discussed in chapter 1.

The aniline (99.5%, Aldrich) was kept in a glass tube attached to the gas line and allowed into the main chamber by a leak valve. It was purified by several freeze-pump-thaw cycles using a dry ice/acetone mixture, and the purity checked by mass spectrometry. The oxygen (99.998%) was obtained from Argo Ltd, the cylinder attached to the gas line and used as received.

## 2.4 The interaction of aniline with clean Cu(110) surfaces

An atomically clean Cu(110) surface was treated to exposures of aniline vapour at room temperature, up to 120L and a maximum pressure of $1 \times 10^{-6}$ mbar. The XP spectra shown in figure 2.1 reveal that a limited reaction had occurred, giving rise to a C(1s) peak at 283.7 eV. After a total exposure of 120L aniline, the carbon concentration reached a maximum of $5.2 \times 10^{14}$ $cm^{-2}$, although this final large exposure did not cause much of an increase in surface carbon concentration from the previous 10L exposure.

STM images of a clean Cu(110) surface exposed to 120L aniline vapour showed no evidence of an adsorbed species, and no reconstruction of the surface was observed (figure 2.2).

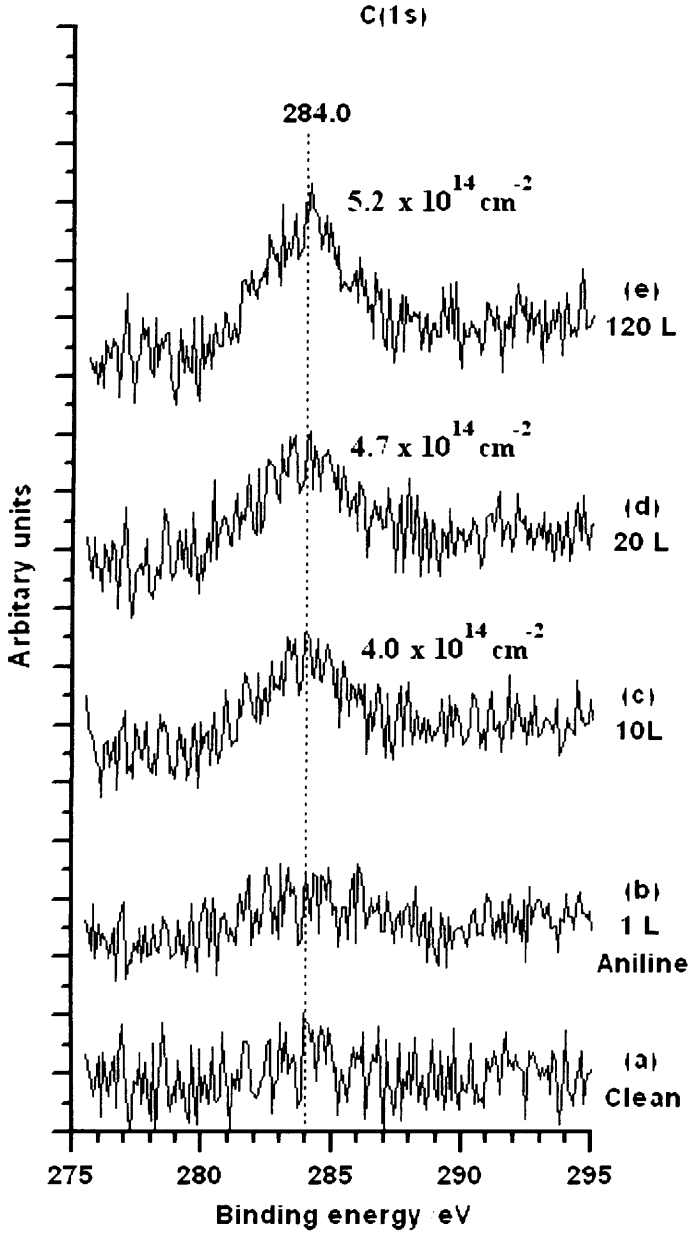


Figure 2.1: C(1s) XP spectra of the adsorption of aniline vapour at clean Cu(110) surfaces at 293K. (a) Clean, (b) Clean surface after exposure to 1L aniline, (c) 10L total exposure, (d) 20L total exposure, (e) 120L total exposure.

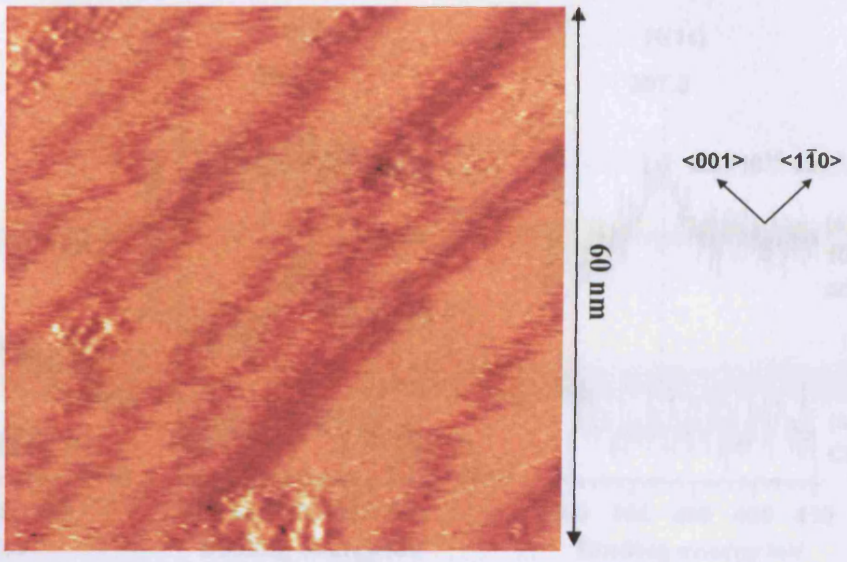


Figure 2.2: Cu(110) surface at 293 K following exposure to 120L aniline vapour. [$V_s$ = 1.22 V, $I_T$ = 2.98 nA]

## 2.5 The interaction of aniline with pre-oxidised Cu(110) surfaces

### 2.5.1 Low surface oxygen concentration

An atomically clean Cu(110) surface was exposed to 2L $O_2$ at room temperature, resulting in a partially oxidised surface with an initial oxygen surface concentration of $1.3 \times 10^{14}$ $cm^{-2}$ (figure 2.3), equivalent to approximately ¼ monolayer.

Exposure of this surface to 20L aniline vapour resulted in a facile reaction in which the surface oxygen concentration was reduced to zero. The reaction gave rise to a peak at 283.7 eV in the C(1s) region of the XP spectrum, and at 397.5 eV in the N(1s) region. The final surface concentrations were $1.6 \times 10^{15}$ $cm^{-2}$ carbon, and $2.6 \times 10^{14}$ nitrogen, giving a C:N ratio of approximately 6:1, as was expected for the aniline molecule. The ratio of final nitrogen concentration to initial oxygen concentration was 2:1, suggesting an overall reaction stoichiometry of 2 aniline: 1 oxygen.

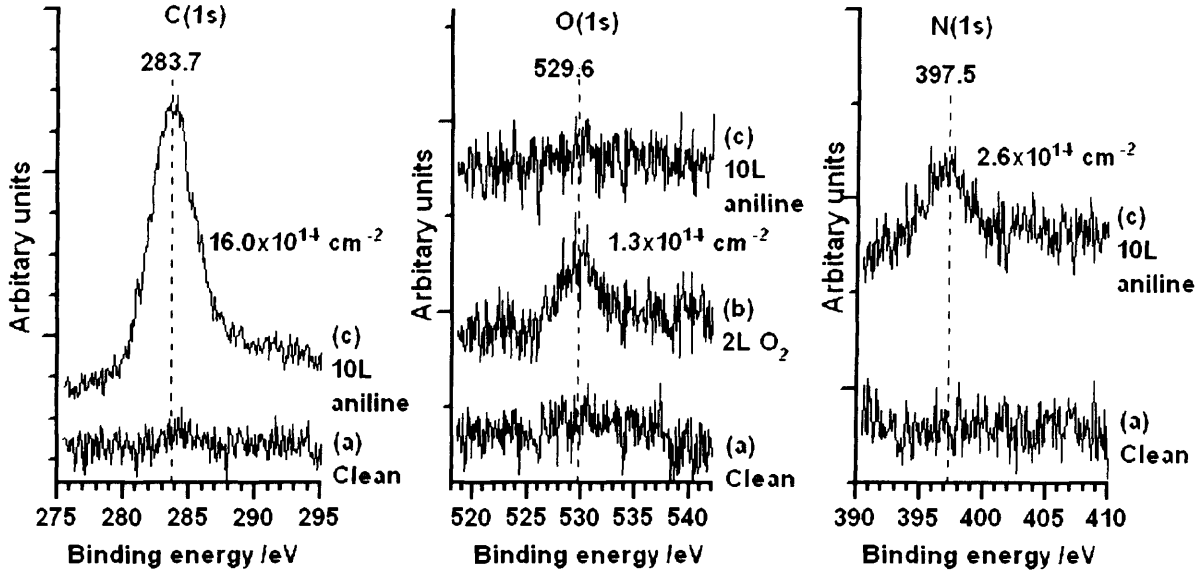


Figure 2.3: C(1s), O(1s) and N(1s) XP spectra showing aniline chemisorption at a partially oxidised Cu(110) surface at 293 K. (a) clean, (b) after a 2L dioxygen exposure, (c) after a 10L aniline vapour exposure.

### 2.5.2 High surface oxygen concentration

A partially oxidised Cu(110) surface with an oxygen concentration of $2.9 \times 10^{14}$ $cm^{-2}$, obtained by a dose of 3L dioxygen, was treated to several aniline exposures (figure 2.4). After an exposure of 4L, the reaction stoichiometry was 2 aniline: 1 oxygen. Upon further dosing, up to a total of 120L, the stoichiometry changed from 2:1 to 1:1.

Therefore, for concentrations up to approximately $2.9 \times 10^{14}$ $cm^{-2}$, the reaction stoichiometry remains 2 aniline: 1 oxygen. For concentrations greater than $2.9 \times 10^{14}$ $cm^{-2}$ but less than a monolayer ($5.5 \times 10^{14}$ $cm^{-2}$), the reaction remains facile and gives rise to identical XP peaks, however a change in stoichiometry is observed as the reaction progresses.

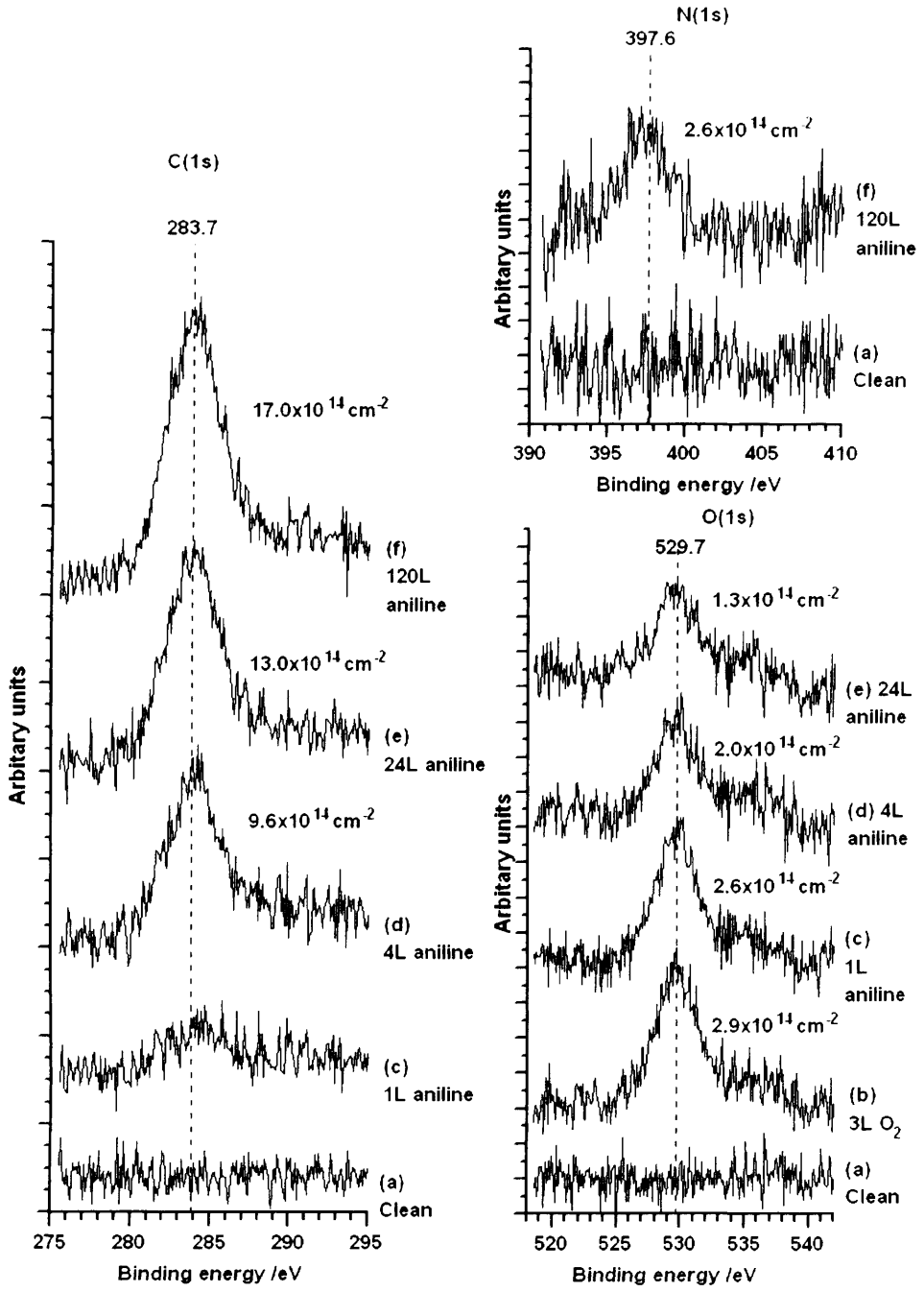


Figure 2.4: C(1s), O(1s) and N(1s) XP spectra of the reaction of aniline vapour with a partially oxidised Cu(110) surface at 293 K. (a) clean, (b) after 3L dioxygen, (c) after 1L aniline, (d) 4L aniline, (e) 24L aniline, (f) 120L aniline.

STM images of a Cu(110) surface with a initial oxygen concentration of 2.4 x $10^{14}$ $cm^{-2}$, exposed to 20L aniline, an exposure not great enough to cause a full reaction, are shown in figure 2.5. They show islands of the well-documented p(2x1)O(a) lattice, surrounded by adsorbed aniline molecules. At this point, there is no long-range order to the aniline adsorbate, although some short-range order can be observed.

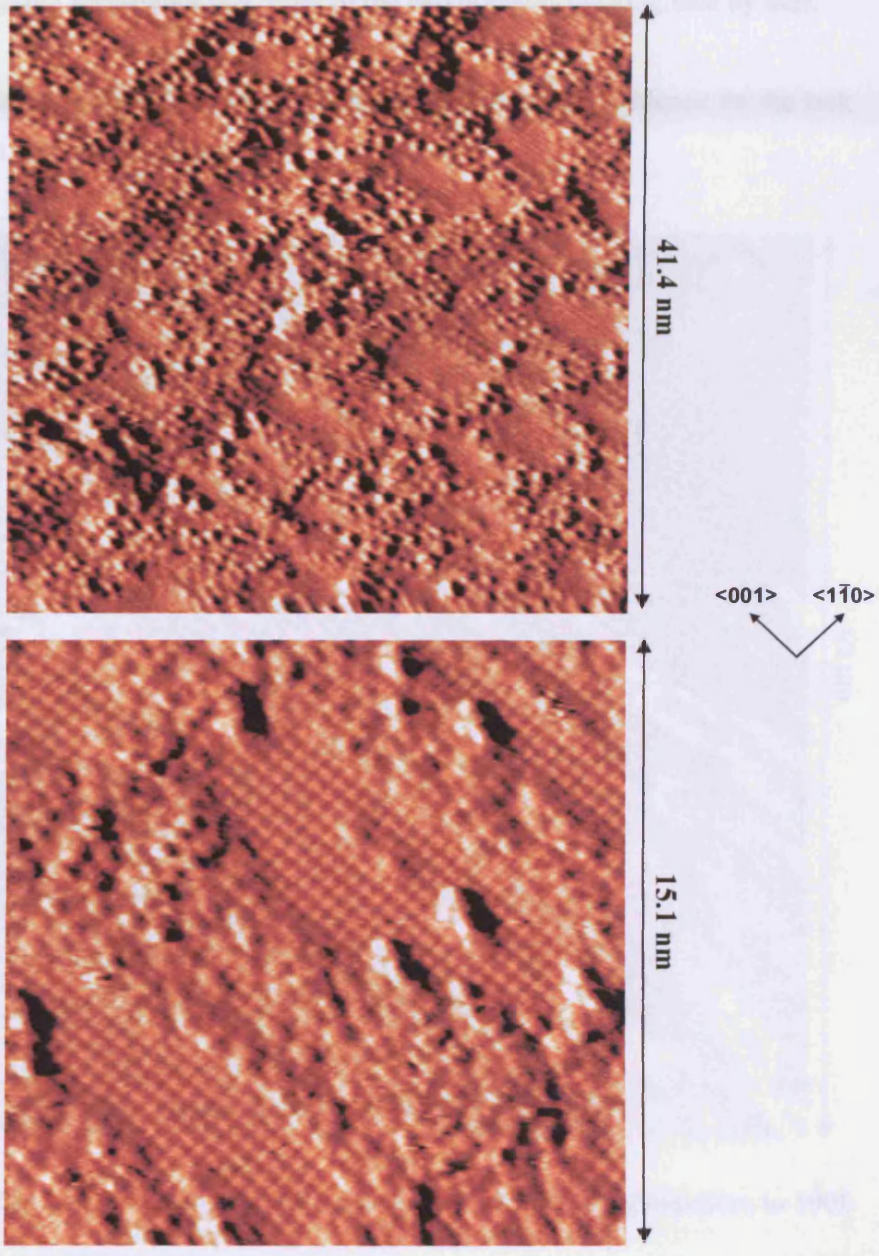


Figure 2.5: Partially oxidised Cu(110) at 293K following exposure to 20L aniline. [$V_s$ = 1.07 V, $I_T$ = 2.32 nA]

STM images obtained following the completion of this reaction, in a separate experiment with a slightly lower initial oxygen concentration, show a surface with a far more ordered adsorbate. Low resolution images show a characteristic zig-zag like structure covering the entirety of the surface (figure 2.6). Higher resolution images show that this distinctive appearance is actually a result of the aniline molecules forming separate domains of different structures on the surface (figure 2.7). The zig-zag appearance is a result of the two domains existing side by side.

There is no trace of any p(2x1) oxygen islands, confirming the evidence for the lack of an oxygen peak in the XP spectra.

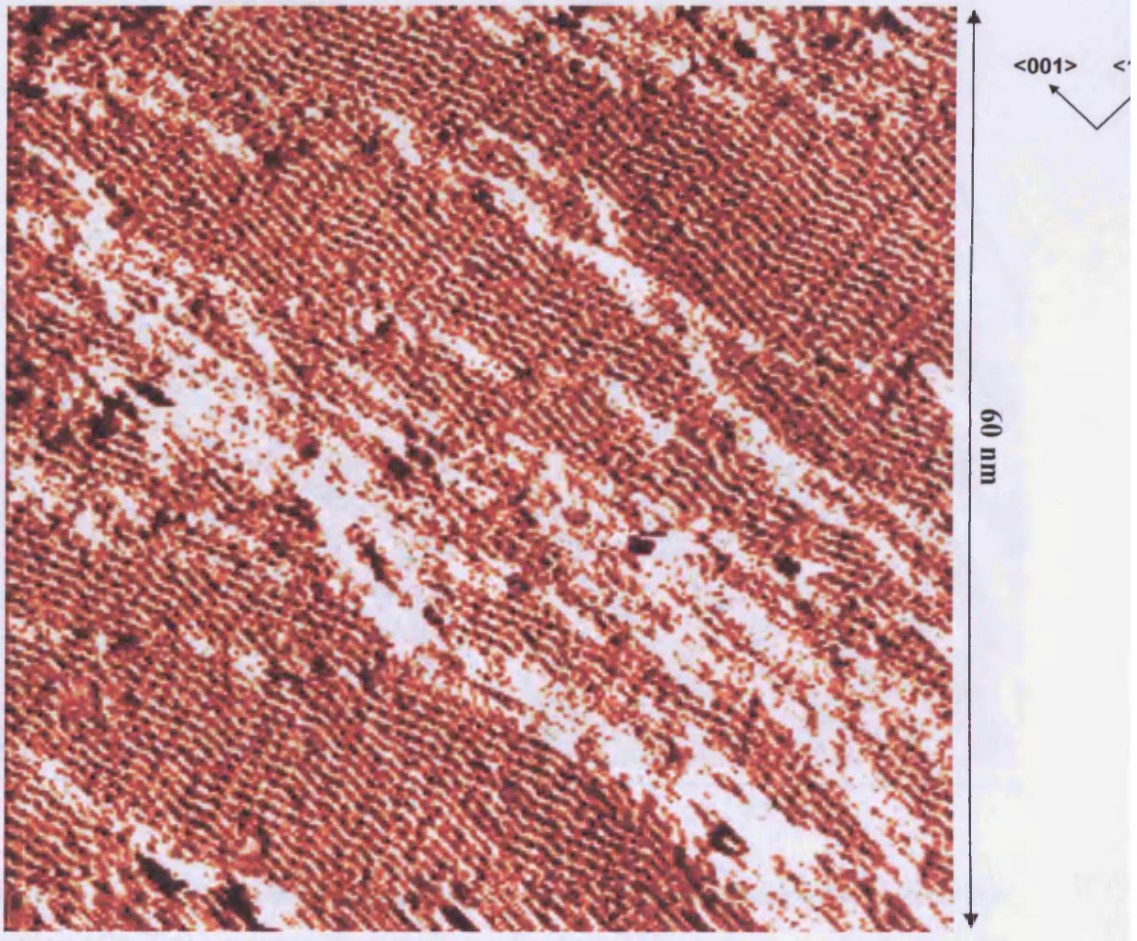


Figure 2.6: Partially-oxidised Cu(110) surface at 293 K following exposure to 100L aniline vapour. [$V_s$ = 1.22 V, $I_T$ = 3.05 nA]

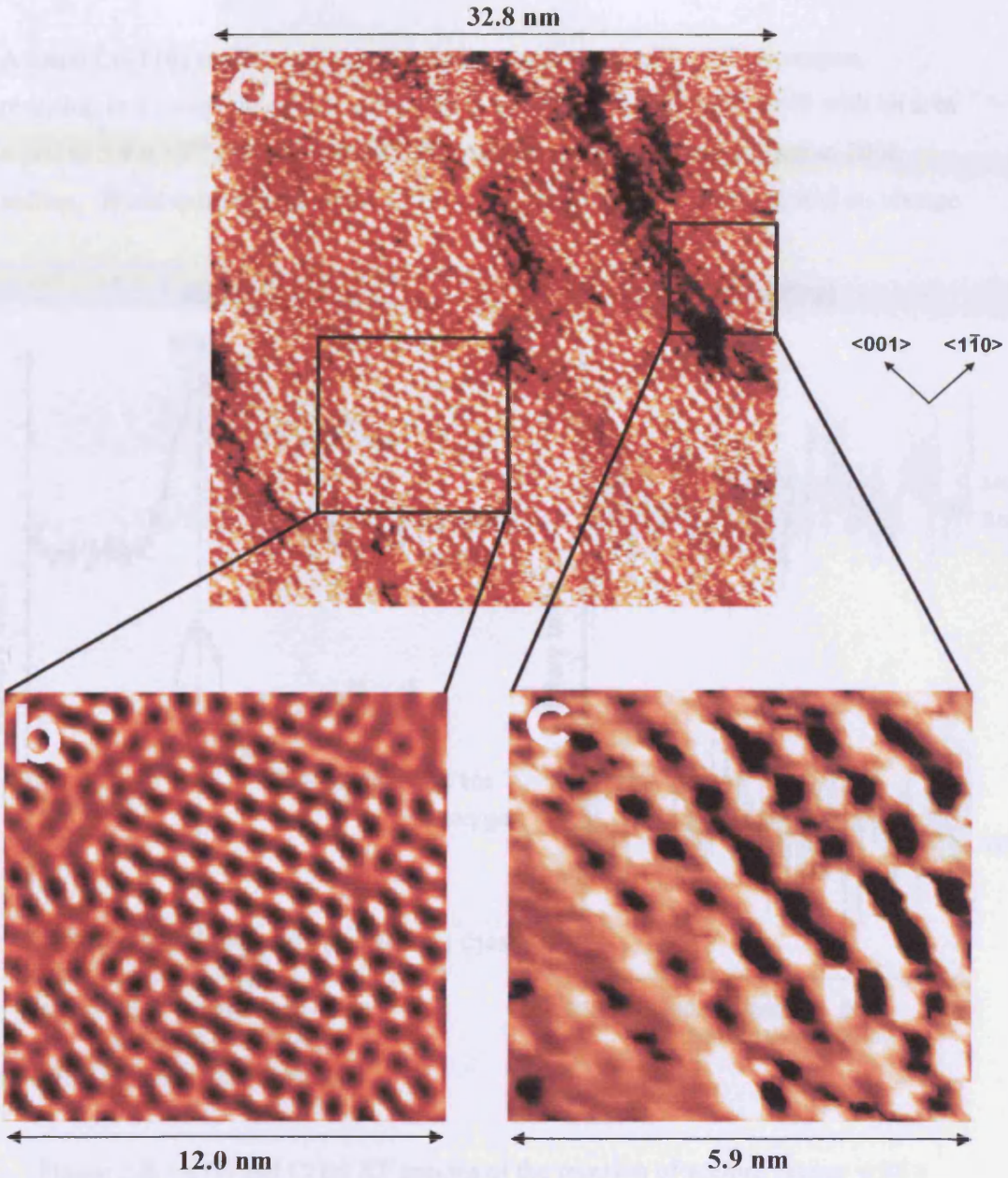


Figure 2.7: A series of STM images illustrating the different domains formed by the reaction of aniline vapour with partially oxidised Cu(110) surfaces at 293 K. Fourier transform filtering has been used on image (b) in order to show the high amount of order present more clearly. [$V_s$ = 1.01 V, $I_T$ = 2.42 nA]

### 2.5.3 Complete (2x1) oxygen monolayer

A clean Cu(110) surface at room temperature was exposed to 10L dioxygen, resulting in a complete oxygen monolayer, as evident by the O(1s) peak with an area equal to 5.4 x $10^{14}$ $cm^{-2}$ (figure 2.8). The oxidised surface was exposed to 200L aniline. There was no peak in the C(1s) of the resulting XP spectrum, and no change

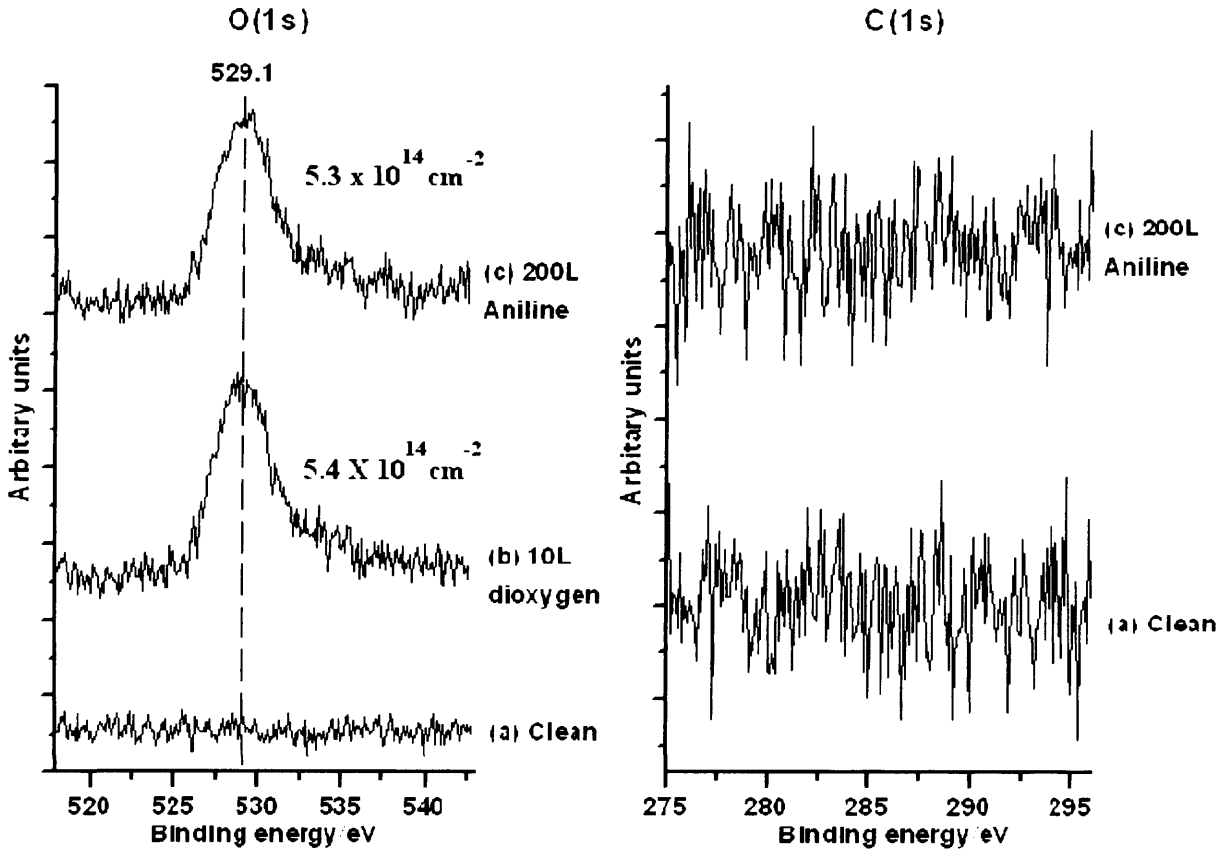


to the O(1s) peak was observed.

Figure 2.8: O(1s) and C(1s) XP spectra of the reaction of aniline vapour with a completely oxidised Cu(110) surface at 293K. (a) clean, (b) after 10L dioxygen, (c) after 200L aniline.

STM images showed the surface saturated by a p(2x1) oxygen adlayer before and after the aniline exposure(figure 2.9).

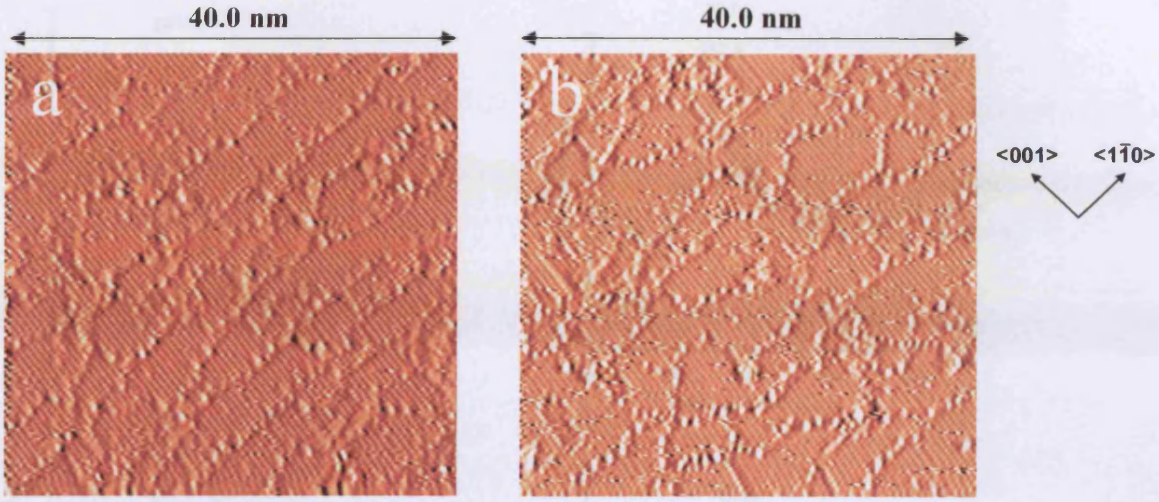


Figure 2.9: Cu(110) surface at 293K (a) following exposure to 10L dioxygen, (b) after exposure of the resulting surface to 200L aniline vapour.
[$V_s$ = 1.22 V, $I_T$ = 3.02 nA]

## 2.6 Aniline/dioxygen coadsorption at Cu(110) surfaces

A clean Cu(110) surface was exposed to 200L of a 300:1 aniline/dioxygen mixture at room temperature and studied by XPS (figure 2.10). A C(1s) peak at 284 eV and a N(1s) peak at 397.8 eV were present in the XP spectrum. No peak was found in the O(1s) region. The surface concentrations of carbon and nitrogen were determined to be $2.0 \times 10^{15}$ cm$^{-2}$ and $3.3 \times 10^{14}$ cm$^{-2}$ respectively. The C:N ratio was 6:1.

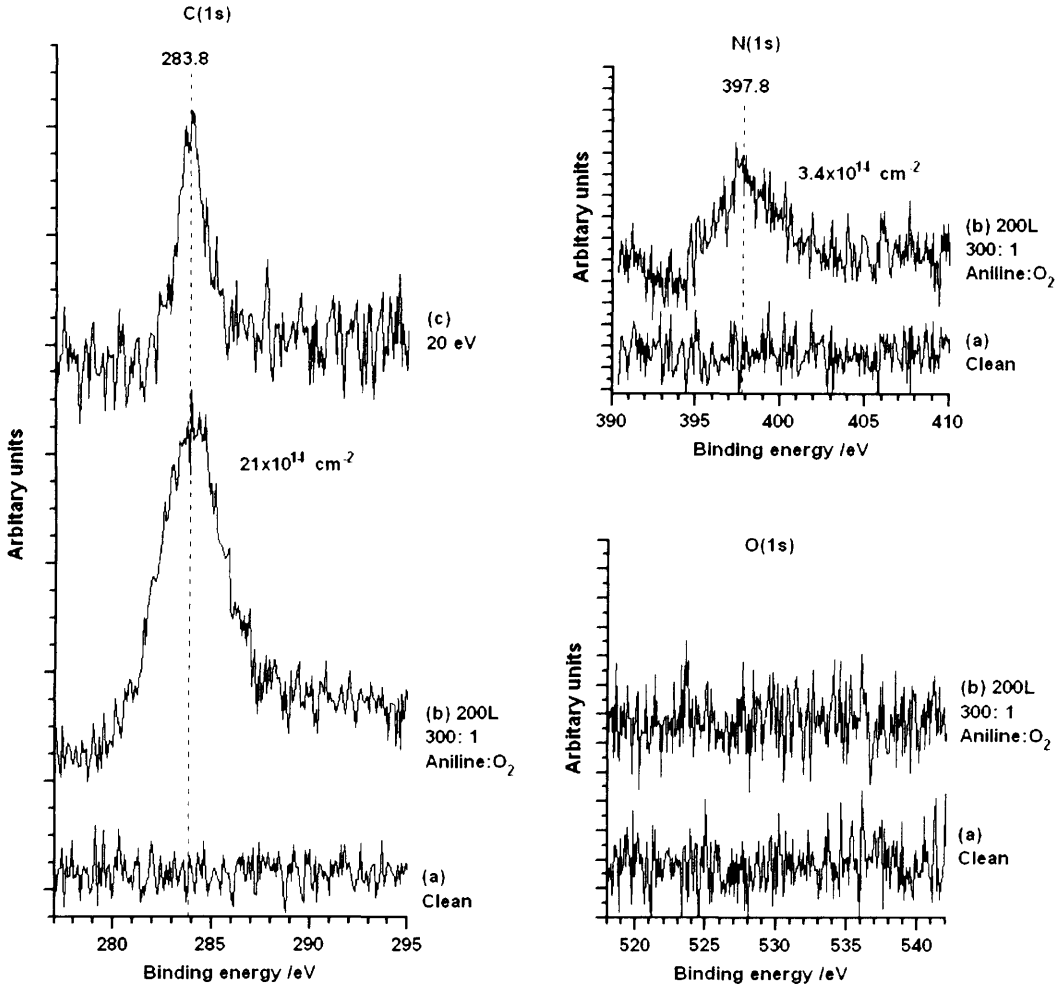


Figure 2.10: C(1s), O(1s) and N(1s) XP spectra of a 300:1 Aniline:dioxygen coadsorption at a Cu(110) surface at 293 K. (a) clean, (b) after exposure to 200L aniline/dioxygen mixture, (c) 20eV pass energy C(1s) XP spectrum.

STM images of the same surface (figure 2.11) show a similar, characteristic zig-zag appearance to that observed following the reaction with a pre-oxidised copper surface. In this instance, however, greater reconstruction of the surface has occurred, resulting in smaller, less defined terraces, apparently separated by steps of 1.2Å, characteristic of single-atom dimensions. The structure of the adsorbate appears even more ordered, and is again split into domains of differing structure. There is no evidence of an adsorbed oxygen species.

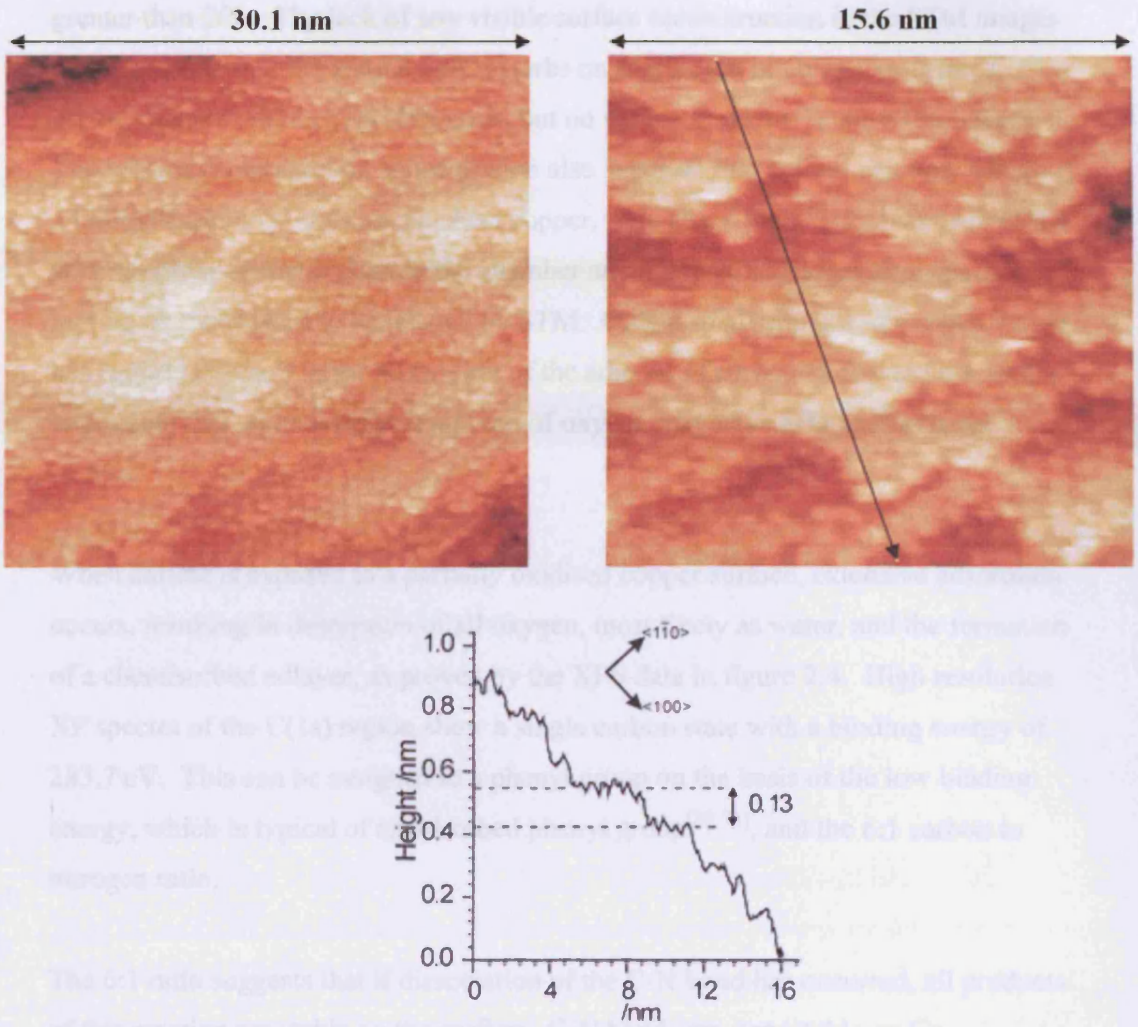


Figure 2.11: Cu(110) surface after exposure to a 300:1 aniline vapour/dioxygen mixture at 293 K. [$V_s$ = 0.59 V, $I_T$ = 2.89 nA]

## 2.7 Discussion

The XPS results show that aniline will react with clean Cu(110) surfaces at room temperature to a limited extent. This is in contrast to ammonia[13-19] and other amines, which show no adsorption unless they are dosed in the presence of oxygen. The final surface carbon concentration following a total exposure of 120L is 5.2 x $10^{14}$ $cm^{-2}$, equivalent to 0.9 x $10^{14}$ molecules $cm^{-2}$, however this is not a great deal larger than the concentration obtained after a total dose of 20L, suggesting the maximum carbon surface concentration can be attained after an exposure slightly

greater than 20L. The lack of any visible surface reconstruction in the STM images might indicate that the aniline only adsorbs on step-edges of clean Cu surfaces, giving rise to a small C(1s) XPS peak, but no visible structure in the STM images. The low maximum carbon concentration also suggests that aniline can only adsorb at a limited number of sites on the clean copper. It is also a possibility that there was a very small $O_2$ contamination in the chamber and the resulting adsorbate was too mobile on the surface to be imaged by STM. Only a small amount of oxygen would be required to result in the adsorption of the amount of carbon observed here, and it is possible that an undetectable amount of oxygen may have affected previous studies.

When aniline is exposed to a partially oxidised copper surface, extensive adsorption occurs, resulting in desorption of all oxygen, most likely as water, and the formation of a chemisorbed adlayer, as proven by the XPS data in figure 2.4. High resolution XP spectra of the C(1s) region show a single carbon state with a binding energy of 283.7 eV. This can be assigned to a phenyl group on the basis of the low binding energy, which is typical of an adsorbed phenyl group[20, 21], and the 6:1 carbon to nitrogen ratio.

The 6:1 ratio suggests that if dissociation of the C-N bond has occurred, all products of this reaction are stable on the surface. C-N bonds are very stable on Cu surfaces[22], so the breaking of this bond is unlikely. The N(1s) binding energy of 397.8 eV, points towards the formation of a phenyl-imide species, $C_6H_5N$(a), since amide species on copper surfaces typically give rise to peaks with a binding energy of 399 eV[23], and nitrides 396.5 eV[24].In contrast to this, the 2:1 aniline/oxygen reaction stoichiometry for ca. ¼ monolayer of oxygen suggests instead the formation of a phenyl-amide, $C_6H_5NH$(a). However, since the stoichiometry becomes 1:1 at higher initial oxygen surface concentrations, whilst the XP binding energy indicates that the product remains the same, the adsorbate is tentatively assigned to a phenyl-imide (equation 1). This assignment is backed up by the reaction of ammonia with preadsorbed oxygen[13-19], which follows a similar change in stoichiometry from 2:1 to 1:1 with O(a) concentration, and in that case, the formation of an imide has been proven via vibrational spectroscopy[17].

$$2PhNH_2 + O(a) \rightarrow H_2O(g) + 2PhN(a) \quad (1)$$

A proposed mechanism for the reaction of aniline with oxidised Cu(110) surfaces follows.

$$PhNH_2(g) + O(a) \rightarrow PhNH(a) + OH(a) \quad (2)$$
$$PhNH_2(g) + OH(a) \rightarrow PhNH(a) + H_2O(g) \quad (3)$$
$$2OH(a) \rightarrow O(a) + H_2O(g) \quad (4)$$

$$PhNH(a) \rightarrow PhN(a) + H(a) \quad (5)$$
$$2H(a) \rightarrow H_2(g) \quad (6)$$

$$PhNH(g) + OH(a) \rightarrow PhN(a) + H_2O(g) \quad (7)$$

At low oxygen coverages, step (7) is slow relative to steps (3) and (5), resulting in the 2:1 stoichiometry. At 293K, the amide formed by steps (2) and (3) must be unstable compared to the imide. The phenyl-amide therefore dissociates through step (5), resulting in adsorbed hydrogen which may either remain on the surface, or desorb via step (6). At higher oxygen concentrations, step (7) becomes the dominant reaction following step (2), changing the overall stoichiometry from 2:1 to 1:1. This is likely a result of either steric hindrance between two aniline molecules as the free space available gets less at higher oxygen concentrations, or the need for two sites adjacent to a chemisorbed oxygen atom, which would get scarcer as the oxygen concentration increased.

Co-adsorption experiments involving the exposure of a clean Cu(110) surface to an aniline/dioxygen mixture in a 300:1 ratio resulted in XPS peaks at 283.8 eV in the C(1s) region and 397.8 eV in the N(1s) region, with a concentration ratio of 6:1. These results are identical to those obtained for the pre-oxidised surface and therefore indicate the formation of the same phenyl-imide species. The reaction is extremely efficient, resulting in desorption of all active oxygen species, and a final aniline concentration that is greater than that obtained from reaction with a pre-

oxidised surface. This carbon concentration of $2.1x10^{15}$ $cm^{-2}$ is considered in more detail in the discussion of STM results.

STM images obtained midway through the reaction of aniline with a partially oxidised Cu(110) surface show that the aniline molecules initially adsorb onto the areas of clean copper between the p(2x1)O(a) islands. This reaction with aniline has not resulted in any change in the adsorbed oxygen structure whatsoever. This is in contrast to the reaction of pyridine with Cu(110)-O(a) surfaces[25], in which expansion of the oxygen rows into a (3x1) structure occurs. At this point in the reaction, there is no sign of long-range order to the phenyl-imide species. However, some short-range order can be observed, particularly at the edges of the oxygen islands.

The structure of oxygen adsorbed on Cu(110) surfaces is well understood. Thus, STM images that show oxygen islands together with chemisorbed phenyl-imide can be used to determine the adsorption site of the imide species. The oxygen lattice formed by the reaction of dioxygen with Cu(110) surfaces consist of added copper-oxygen chains orientated in the <100> direction (figure 2.12). The added copper atoms are situated in the hollow sites of the Cu(110) substrate and it is these atoms that are actually responsible for the maxima in the oxygen lattice as imaged by STM[26].

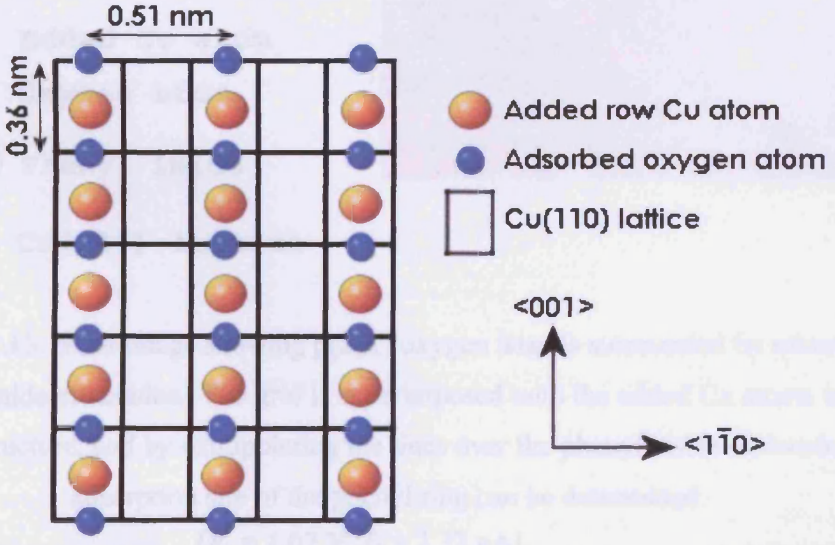


Figure 2.12: Structure formed by the dissociative chemisorption of dioxygen at Cu(110) surfaces.

Figure 2.13 shows a lattice superimposed onto an oxygen island and is extrapolated over areas of adsorbed aniline. The oxygen lattice maxima are directly in line with the aniline maxima in both the <100> and the <110> directions. Previous STM studies of similar, phenyl ring containing molecules, have shown that the maxima in the STM images are caused by the rings themselves. This, coupled with the large diameter of approximately 0.7nm of the circular features (figure 2.14) suggests it is also the phenyl rings being imaged here. It can therefore be deduced that the phenyl rings of the adsorbed imide molecules are situated in the hollow sites of the Cu(110) substrate. This conclusion has also been reached in the study of other phenyl compounds [27] and benzene[28] adsorbed at Cu(110) surfaces.

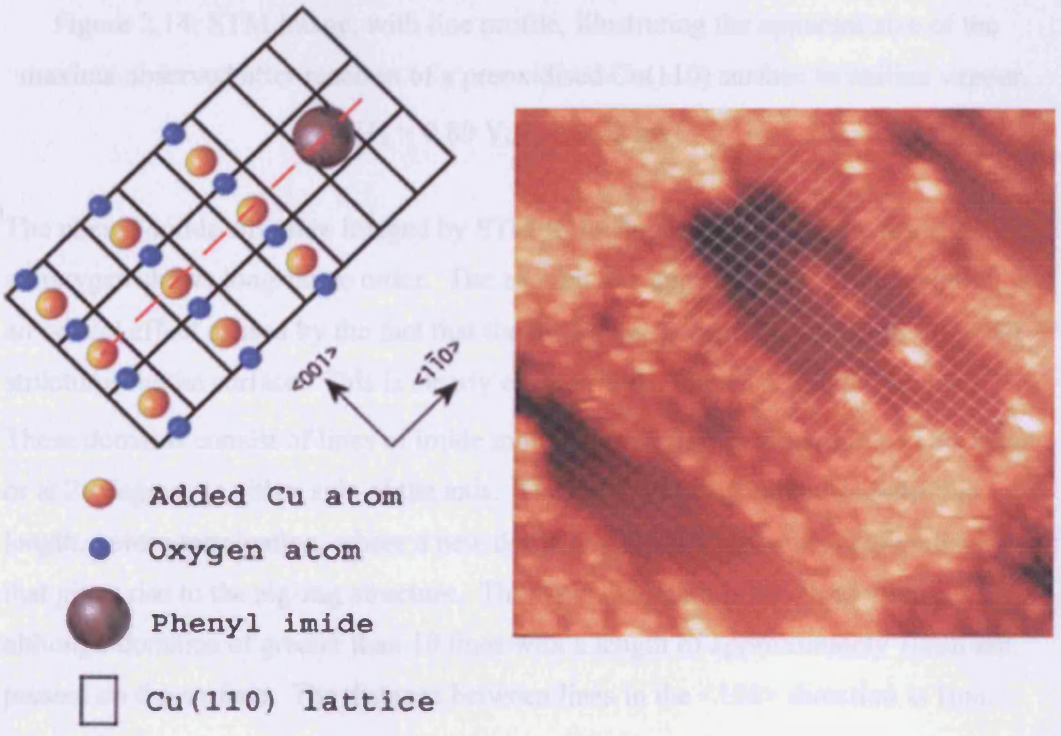


Figure 2.13: STM image showing p(2x1) oxygen islands surrounded by adsorbed phenyl imide molecules. The grid is superimposed onto the added Cu atoms in the oxygen structure, and by extrapolating the lines over the phenyl imide molecules, the adsorption site of the phenyl ring can be determined.
[$V_s$ = 1.07 V, $I_T$ = 2.32 nA]

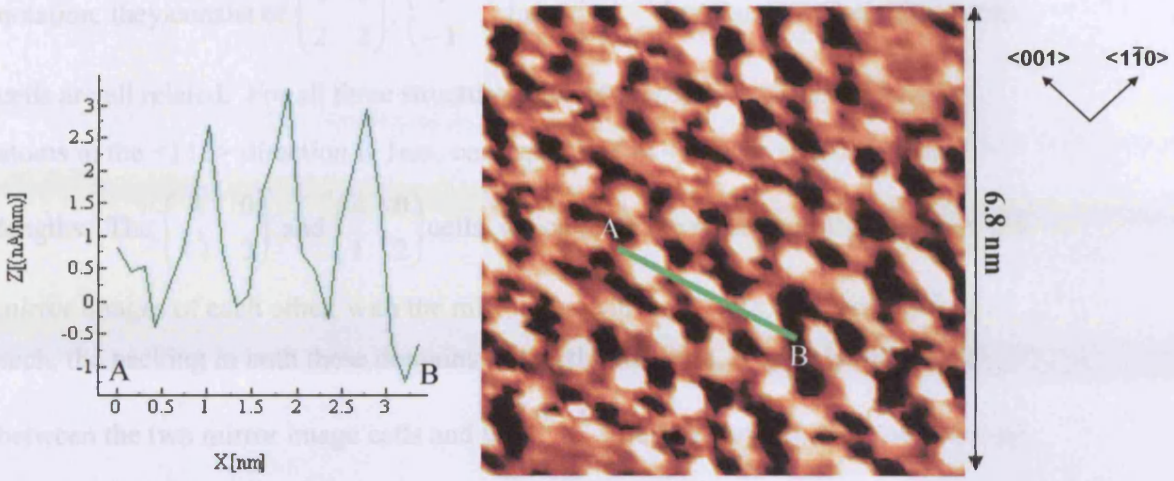


Figure 2.14: STM image, with line profile, illustrating the apparent size of the maxima observed after reaction of a preoxidised Cu(110) surface to aniline vapour. [$V_s$ = 0.80 V, $I_T$ = 3.02 nA]

The phenyl-imide structure imaged by STM following the reaction and desorption of all oxygen shows long-range order. The zig-zag like appearance at low resolution is an optical effect caused by the fact that the imide has formed 3 domains of different structures on the surface. This is clearly evident in the higher resolution images. These domains consist of lines of imide molecules running in either the <1$\bar{1}$0> axis, or at 20 degrees to either side of the axis. The lines typically extend to 3-4nm in length, before terminating, where a new domain is formed. It is this change in angle that gives rise to the zig-zag structure. The typical domain is 5-6 lines wide, although domains of greater than 10 lines with a length of approximately 10nm are present on the surface. The distance between lines in the <100> direction is 1nm.

The three different domains observed are detailed in figure 2.15. Using matrix notation, they consist of $\begin{pmatrix} 4 & 0 \\ 2 & 2 \end{pmatrix}$, $\begin{pmatrix} 4 & 0 \\ -1 & 2 \end{pmatrix}$ and $\begin{pmatrix} 4 & 0 \\ 1 & 2 \end{pmatrix}$ unit cells. These three units cells are all related. For all three structures, the intermolecular distance between atoms in the $<1\bar{1}0>$ direction is 1nm, corresponding to 4 copper substrate lattice lengths. The $\begin{pmatrix} 4 & 0 \\ -1 & 2 \end{pmatrix}$ and $\begin{pmatrix} 4 & 0 \\ 1 & 2 \end{pmatrix}$ cells, which form the most common domains, are mirror images of each other, with the mirror plane in the <100> direction, and as such, the packing in both these domains is exactly the same. The only difference between the two mirror image cells and the $\begin{pmatrix} 4 & 0 \\ 1 & 2 \end{pmatrix}$ cell, is that while the next row up in the <100> direction is shifted by one substrate atom on the $<1\bar{1}0>$ axis for the mirror image cells, the $\begin{pmatrix} 4 & 0 \\ 2 & 2 \end{pmatrix}$ structure is shifted the equivalent of two substrate lattice lengths. The areas of all three cells are identical.

It is notable that the p(4x2) structure is absent, as it has been observed on other surfaces. The fact that successive rows in the $<1\bar{1}0>$ direction are always translated at least one substrate atom, may indicate that there is steric hindrance between the phenyl-imides on the <100> axis, which stops the formation of rows of imides in the <100> axis and the formation of a p(4x2) structure.

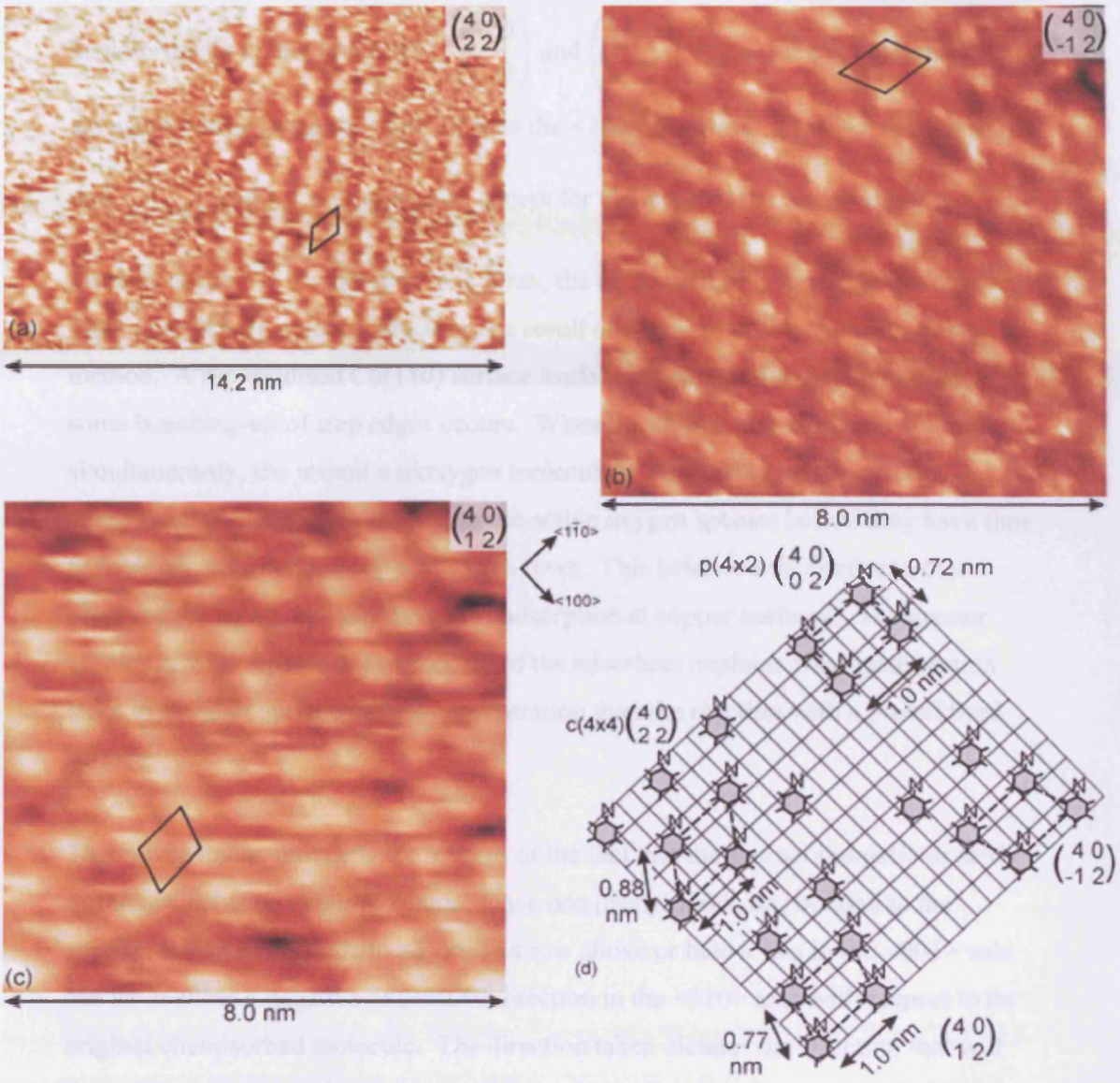


Figure 2.15: Three separate domains found at partially oxidised Cu(110) surfaces following reaction with aniline at 293K.

[(a) $V_s$ = 0.80 V, $I_T$ = 3.02 nA, (b)/(c) $V_s$ = 1.22 V, $I_T$ = 3.07 nA]

The phenyl-imide structures formed via the coadsorption of dioxygen and aniline can be described with the unit cells $\begin{pmatrix} 3 & 0 \\ -1 & 2 \end{pmatrix}$ and $\begin{pmatrix} 3 & 0 \\ 1 & 2 \end{pmatrix}$ (figure 2.16). These meshes are again mirror images of each other in the <100> direction. They are similar to the $\begin{pmatrix} 4 & 0 \\ -1 & 2 \end{pmatrix}$ and $\begin{pmatrix} 4 & 0 \\ 1 & 2 \end{pmatrix}$ unit cells, except for the fact that the intermolecular distance in the $<1\bar{1}0>$ direction is 0.76nm, the equivalent of 3 substrate spacings. This more densely packed structure is a result of the more efficient coadsorption method. A pre-oxidised Cu(110) surface leads to reconstruction of the surface and some bunching-up of step edges occurs. When the aniline and dioxygen are dosed simultaneously, the instant a dioxygen molecule is dissociated on the surface, gaseous aniline molecules react with the active oxygen species before they have time to form islands of added copper/oxygen rows. This behaviour is similar to that observed for an ammonia/dioxygen coadsorption at copper surfaces. The greater efficiency with regards to the packing of the adsorbate explains why coadsorption leads to a higher surface carbon concentration than the reaction with a preoxidised surface.

The mirror-image unit cells are a result of the fact that there is no energetic or steric difference between either structure. Once one phenyl imide has bonded to the surface, the next molecule to adsorb in a row above or below this in the <001> axis can sit in either a negative or positive direction in the <110> axis with respect to the original chemisorbed molecule. The direction taken dictates the structure that will then propagate across the surface until it meets another domain composed of its mirror-image unit cell, or a surface feature which could cause termination of that particular domain.

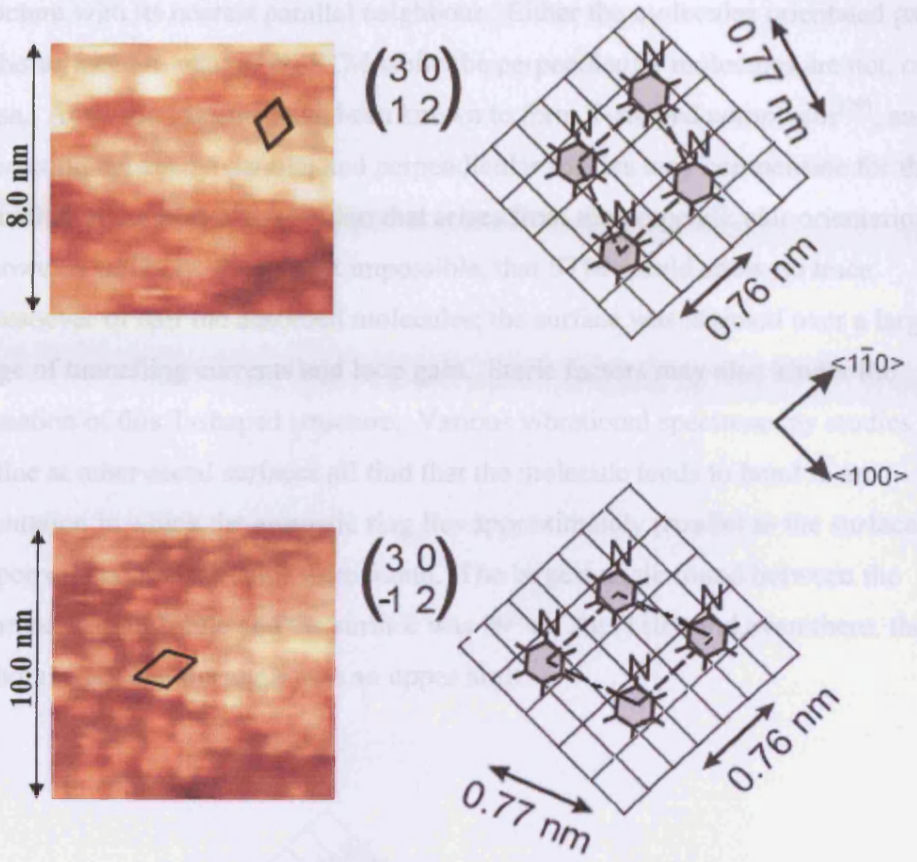


Figure 2.16: Two structures formed by the coadsorption of aniline and dioxygen at Cu(110) surfaces.

From the areas of the unit cells, it is possible to deduce the theoretical maximum surface concentration for the phenyl-imide overlayer. For the reaction with a pre-oxidised surface, the maximum phenyl-imide concentration is deduced to be $1.4 \times 10^{14}$ $cm^{-2}$, and for the coadsorption, $1.8 \times 10^{14}$ $cm^{-2}$. However, the actual concentrations as determined by XPS are $2.7 \times 10^{14}$ $cm^{-2}$ and $3.5 \times 10^{14}$ $cm^{-2}$, respectively. In both cases, the actual phenyl-imide concentration is double that predicted by STM. This indicates that the STM is only imaging half the phenyl imide molecules present on the surface, and that the unit cells must all contain 2, rather than 1, molecules.

Two models are proposed in order to account for this discrepancy. The first model involves the imide molecules adsorbing with the phenyl ring in two different orientations (figure 2.17). Half the imide molecules lie essentially parallel to the

surface, while the other half bond in a perpendicular orientation, forming a T-shaped structure with its nearest parallel neighbour. Either the molecules orientated parallel to the surface are imaged by STM while the perpendicular molecules are not, or vice-versa. Aromatic systems have been known to form T-shaped complexes[29], and the interaction between a parallel and perpendicular species may compensate for the reduction in the heat of adsorption that arises from the perpendicular orientation. It is however unlikely, though not impossible, that STM would show no trace whatsoever of half the adsorbed molecules; the surface was scanned over a large range of tunnelling currents and loop gain. Steric factors may also hinder the formation of this T-shaped structure. Various vibrational spectroscopy studies of aniline at other metal surfaces all find that the molecule tends to bond in an orientation in which the aromatic ring lies approximately parallel to the surface, and no perpendicular molecules were found. The largest angle found between the chemisorbed molecule and the surface was 39° on Ag (110), and even there, the authors stress that the angle was an upper limit.

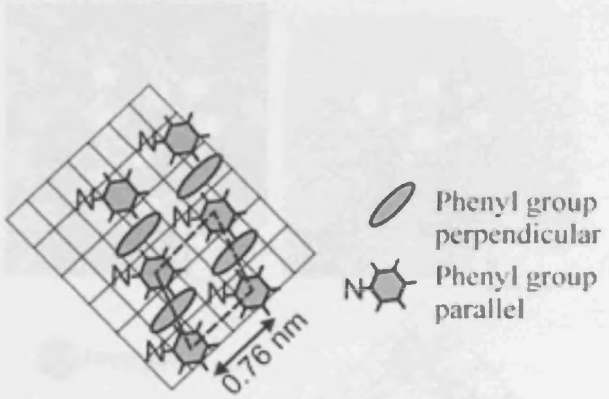


Figure 2.17: Model proposed to account for the discrepancy between the maximum phenyl imide concentration predicted by STM results, and the actual concentration determined by XPS. A t-shaped complex is formed where half the phenyl imide molecules are bonded parallel to the surface, and the other half perpendicular. Only molecules in one of the orientations are imaged by STM.

The second proposed model involves the pi-stacking of parallel pairs of phenyl imide molecules, figure 2.18 (a). If one imide molecule was stacked almost directly on top of another, in an STM image it would show up as only a single circular feature, and hence account for the 'missing' imide molecules. If this is the case, it would not be possible to determine the exact structure of these parallel pairs, but in figure 2.18 (b)-(d), we expand on the model to give a possible orientation.

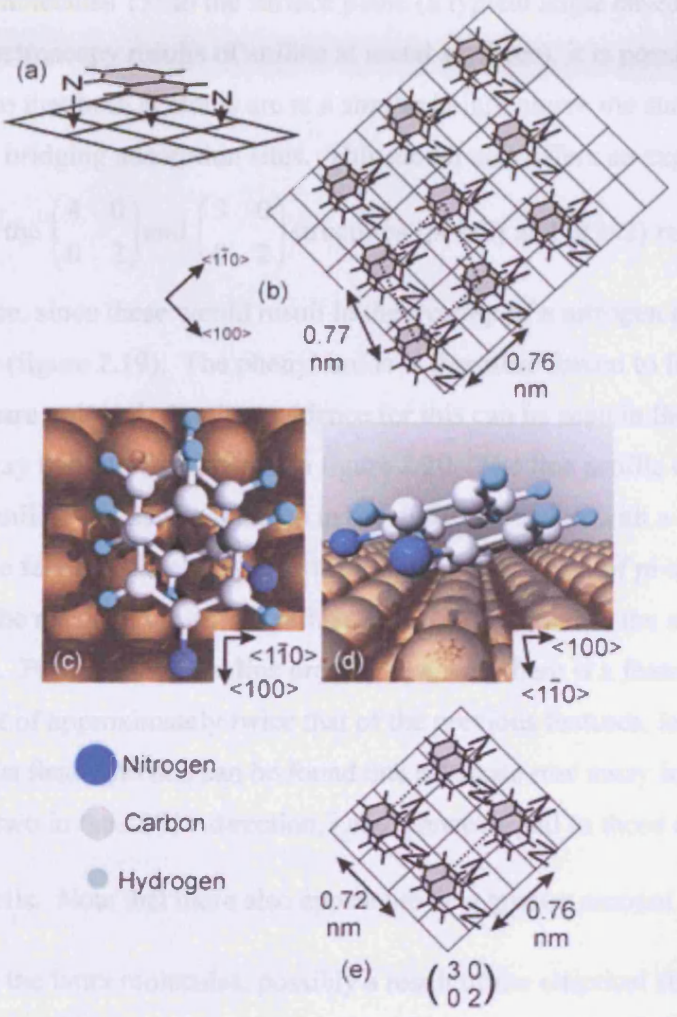


Figure 2.18: (a) Pi-stacking model to account for discrepancy between STM and XPS results, (b) - (d) Expansion of the model, (e) diagram illustrating how the proposed model might explain the lack of primitive square unit cells; both N and H atoms would need to be situated at short bridge sites.

In a pi-stacked system, the phenyl rings do not sit directly on top of each other; they are slightly offset, forming an elliptical shape. The HREELS study of the chemisorption of aniline at clean Cu(110) surfaces[1], as well as other vibrational studies on other metal surfaces[2],[3],[4], concluded that the phenyl ring lies almost, but not quite, parallel to the surface. By taking these facts into account, a possible orientation is shown in figure 2.18 (b), as well as the 3D renderings in figure 2.18 (c) and (d), using a simple ball and stick model. By tilting the pi-stacked parallel pair of phenyl-imide molecules 15° to the surface plane (a typical angle based on the vibrational spectroscopy results of aniline at metal surfaces), it is possible to rotate the two rings so that both N atoms are at a similar height above the surface, and also situated above bridging adsorption sites. This model also offers an explanation for the absence of the $\begin{pmatrix} 4 & 0 \\ 0 & 2 \end{pmatrix}$ and $\begin{pmatrix} 3 & 0 \\ 0 & 2 \end{pmatrix}$ structures (p(4x2) and p(3x2) respectively) from the surface, since these would result in the overlap of a nitrogen and a hydrogen at a bridge site (figure 2.19). The phenyl imide is therefore forced to form a structure with a non-square unit cell. Further evidence for this can be seen in the STM image obtained midway through the reaction in figure 2.20. The line profile clearly shows two adsorbed aniline molecules lined up in the <001> direction with a spacing of 1.1 nm between the features, labelled (i). It is possible that the lack of pi-stacking at this early stage in the reaction allows the aniline molecules to bond to the surface at these particular sites. Further along the line profile, however, there is a feature with an apparent height of approximately twice that of the previous features, labelled (ii). The next nearest feature to this can be found one substrate row away in the <110> direction, and two in the <001> direction, i.e. distances equal to those found in the $\begin{pmatrix} 4 & 0 \\ 1 & 2 \end{pmatrix}$ unit cells. Note that there also appears to be a greater amount of electron density around the latter molecules, possibly a result of the elliptical shape formed by a pair of pi-stacked phenyl rings. It is possible, therefore, that this STM image shows a pair of non pi-stacked phenyl-imide molecules in the formation of a p(4x2) structure, as well as two pairs of pi-stacked phenyl-imide molecules in a $\begin{pmatrix} 4 & 0 \\ 1 & 2 \end{pmatrix}$ structure.

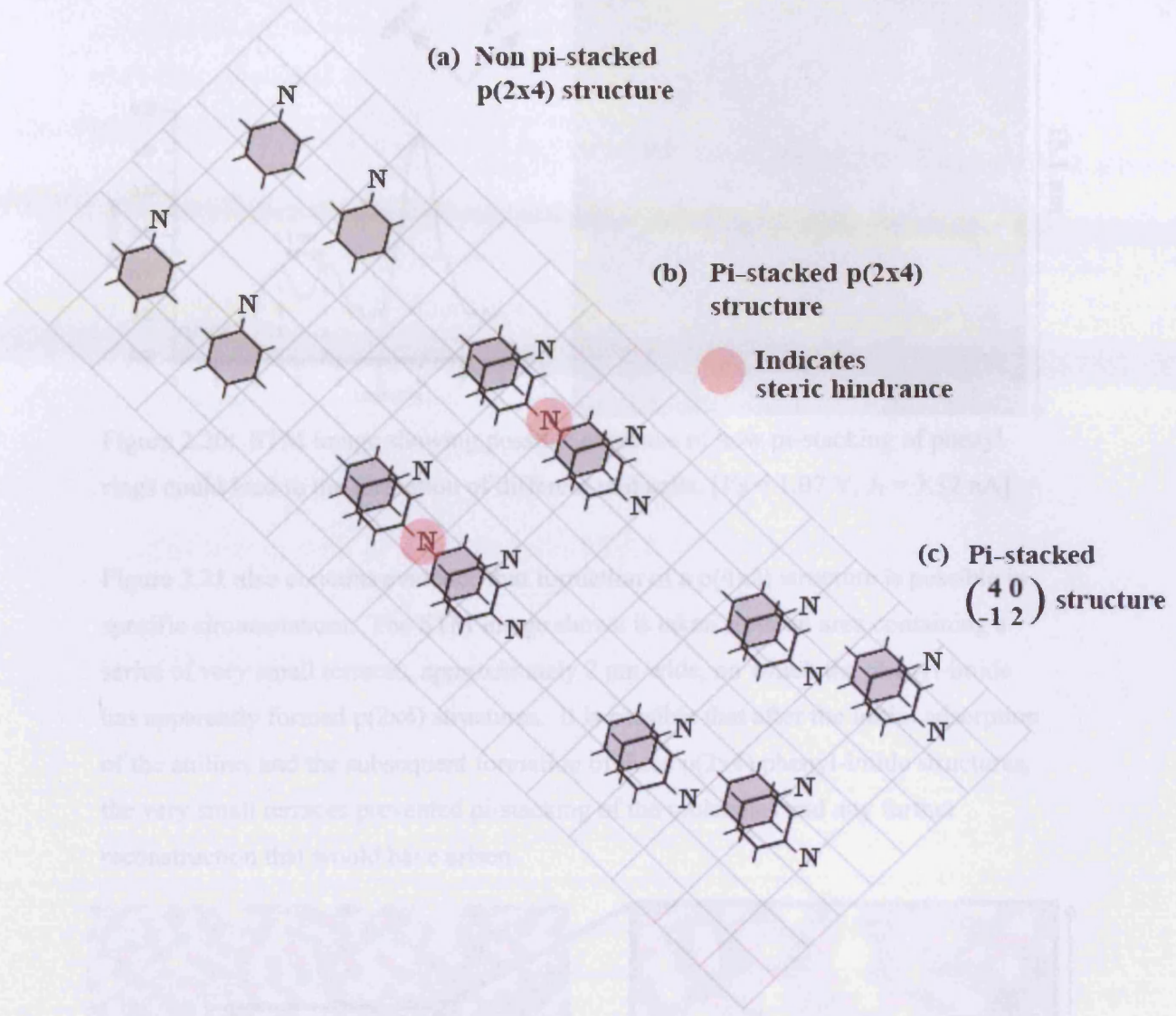


Figure 2.19: Diagram illustrating how the proposed orientation of a pi-stacked pair of phenyl-imide molecules would lead to the formation of a parallelogram shaped unit cell due to Steric hindrance between a nitrogen and hydrogen atom.

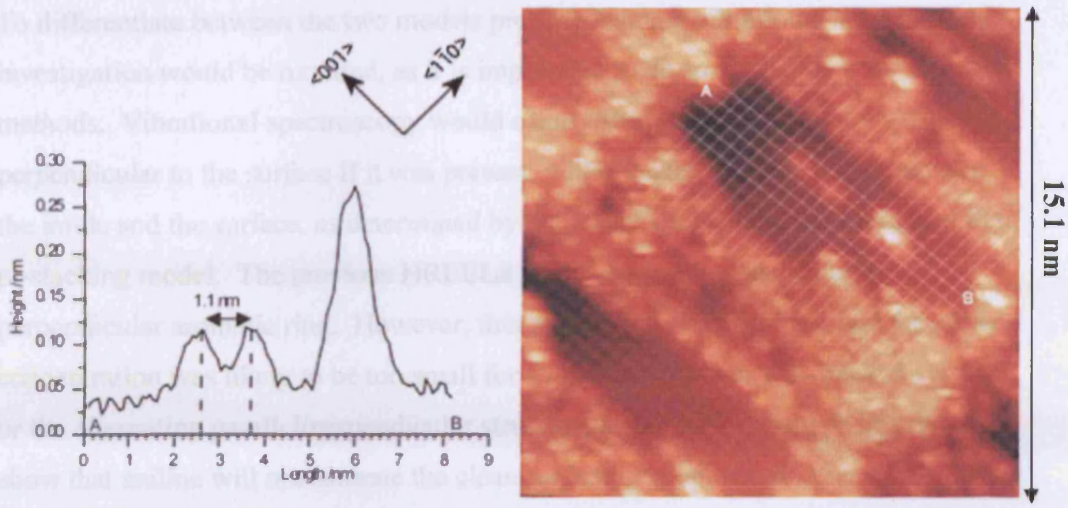


Figure 2.20: STM image showing possible evidence of how pi-stacking of phenyl rings could lead to the formation of different unit cells. [$V$s = 1.07 V, $I_T$ = 3.32 nA]

Figure 2.21 also contains evidence that formation of a p(4x2) structure is possible in specific circumstances. The STM image shown is taken from an area containing a series of very small terraces, approximately 2 nm wide, on which the phenyl-imide has apparently formed p(2x4) structures. It is possible that after the initial adsorption of the aniline, and the subsequent formation of these p(2x4) phenyl-imide structures, the very small terraces prevented pi-stacking of the molecules and any further reconstruction that would have arisen.

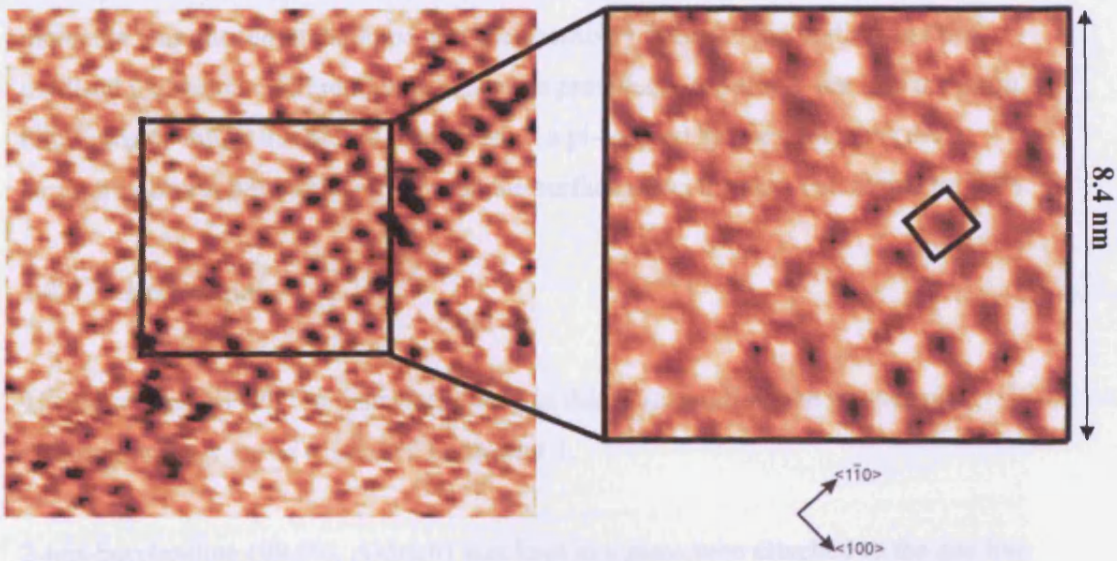


Figure 2.21: p(2x4) phenyl-imide structure found on Cu(110) after exposure of a partially oxidised Cu(110) surface to aniline vapour at 293K.
[ $V_s$ = 0.79 V, $I_T$ = 3.10 nA]

To differentiate between the two models proposed here, a vibrational spectroscopy investigation would be required, as it is impossible to do so via STM or XPS methods. Vibrational spectroscopy would clearly show the presence of a species perpendicular to the surface if it was present, whilst a change in the angle between the imide and the surface, as determined by the HREELS study[11], could support the pi-stacking model. The previous HREELS study shows no evidence of a perpendicular aromatic ring. However, this was on the clean surface, and the surface concentration was likely to be too small for formation of either a pi-stacked system, or the alternating parallel/perpendicular structure, as the XPS results in this thesis show that aniline will not saturate the clean surface at room temperature.

## 2.8 The interaction of 2-tertbutylaniline with Cu(110) surfaces

### 2.8.1 Introduction

The results of the experiments involving the interaction of aniline with oxidised Cu(110) surfaces suggest that pi-stacking of the phenyl rings may be occurring in the chemisorbed monolayer. In order to examine this theory further, the interaction of 2-tertbutylaniline, $(CH_3)_3CPhNH_2$, with the same surfaces has been investigated. This molecule was chosen in the hope that the chemistry between the aniline and the oxidised Cu surface will remain the same as previously observed, but that the extra butyl moiety might inhibit the formation of a pi-stacked species, and that the structure observed by STM will match the surface concentration calculated by XPS.

### 2.8.2 Experimental

The combined XPS/STM instrument used in this investigation and the sample cleaning process are as discussed in chapter 1.

2-tert-butylaniline (99.0%, Aldrich) was kept in a glass tube attached to the gas line and allowed into the main chamber by a leak valve. It was purified by several freeze-pump-thaw cycles using a dry ice/acetone mixture, and the purity checked by

mass spectrometry. Oxygen (99.998%, Argo Ltd) was attached to the gas line and used as received.

### 2.8.3 Clean surface

An atomically clean Cu(110) surface at 293K was exposed to a series of 2-tert-butylaniline vapour doses. XP spectra (figure 2.22) show a peak forming in the C(1s) region at 283.7 eV, which reaches maximum intensity after a total exposure of 15L, and an area equal to a carbon surface concentration of $2.1 \times 10^{15}$ $cm^{-2}$, equal to a t-butylaniline concentration of $2.1 \times 10^{14}$ $cm^{-2}$ . The N(1s) region after the same exposure shows a peak at 397.5 eV, with an area corresponding to a concentration of $2.4 \times 10^{14}$ $cm^{-2}$.

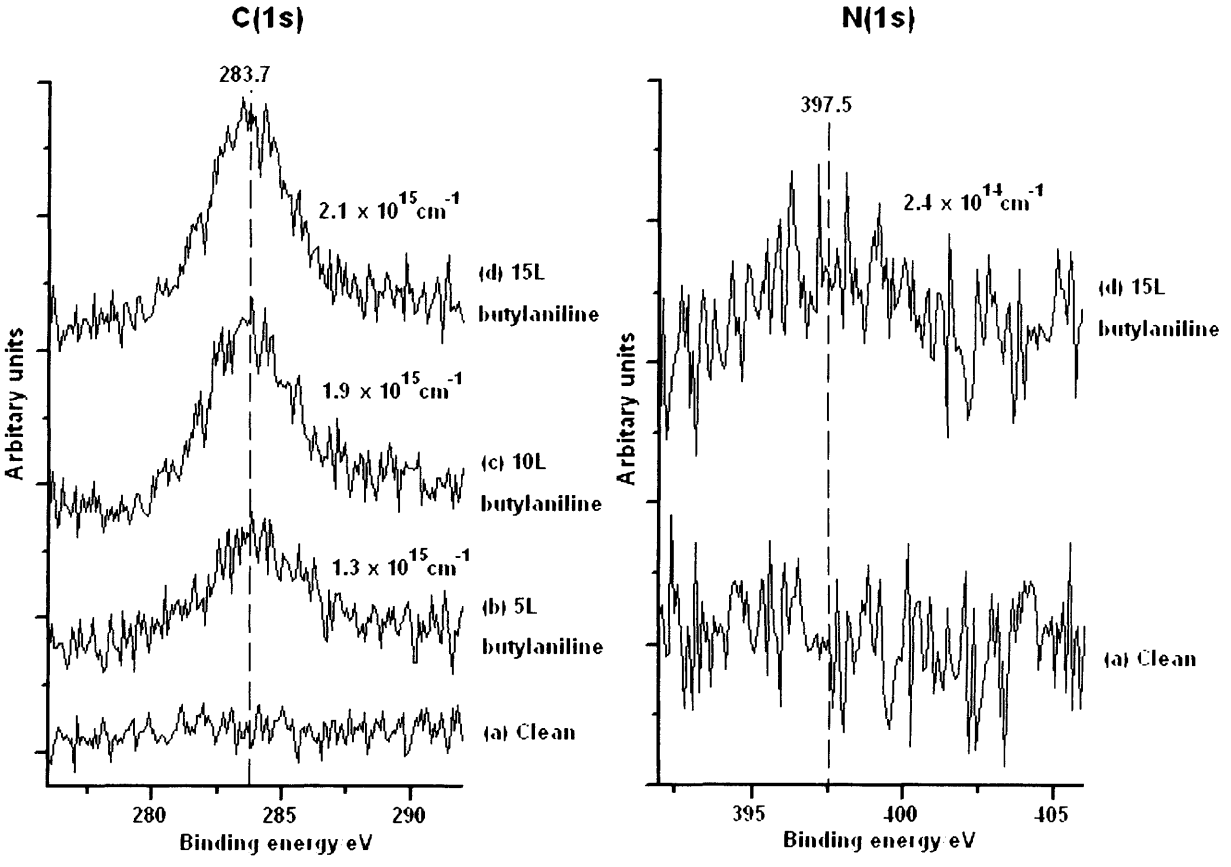


Figure 2.22: C(1s) and N(1s) XP spectra of the reaction of 2-tertbutylaniline with a clean Cu(110) surface at 293 K. (a) clean, (b) after 5L butylaniline, (c) after 10L butylaniline, (d) after 15L butylaniline.

The surface was imaged by STM (figure 2.23). The images show an adlayer comprised of circular features that mostly lacks any order. Despite the lack of long-range order, the adsorbate does seem to form semi-ordered chains orientated in approximately the <110> direction. The spacing between features in these rows is typically 0.76 nm. A uniform spacing between features or rows in other directions does not appear to exist.

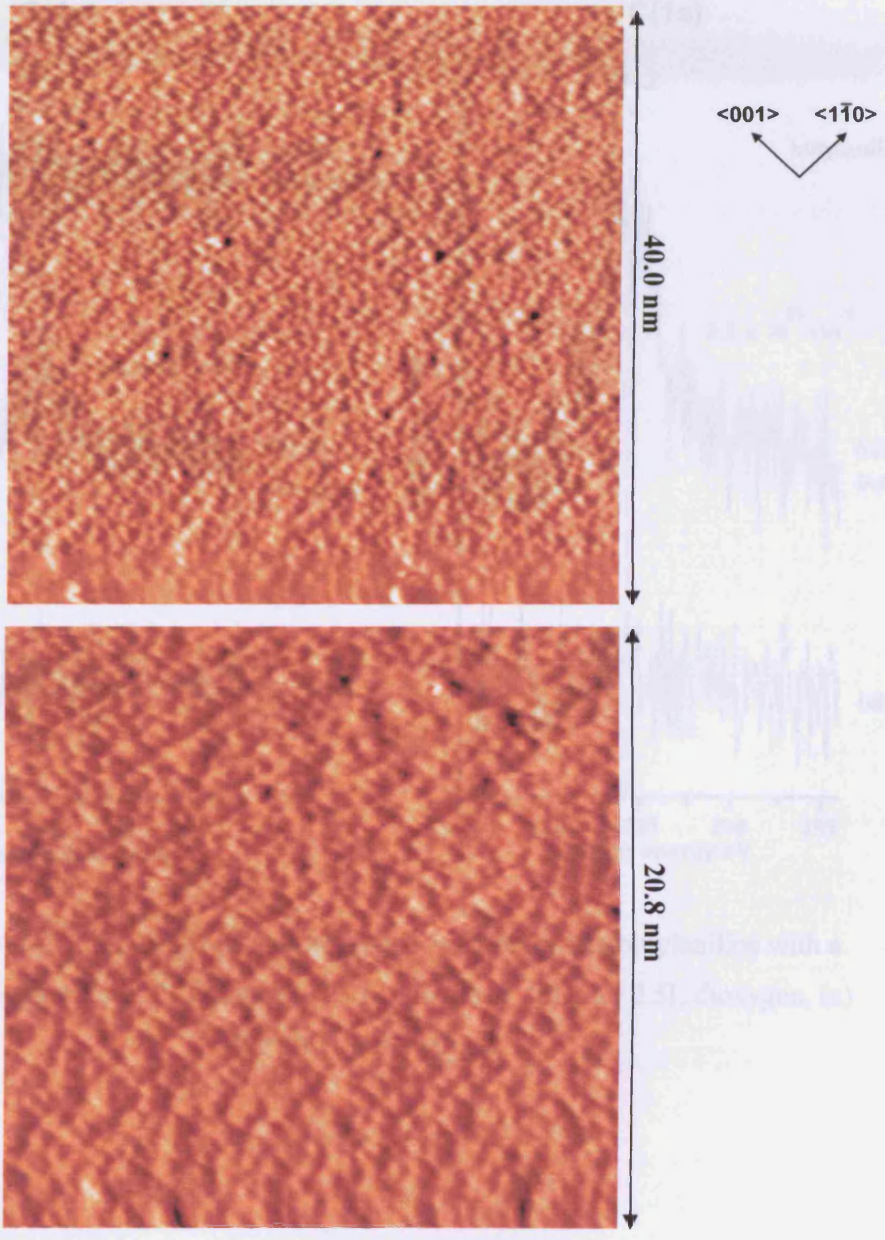


Figure 2.23: STM images of the adsorbate formed by the reaction of 2-tertbutylaniline with a clean Cu(110) surface at 293K. [$V_S$ = 1.22 V, $I_T$ = 2.52 nA]

### 2.8.4 Pre-oxidised surface

A clean Cu(110) surface at 293K was exposed to 2.5L dioxygen, resulting in a peak in the O(1s) XP spectrum equal to a surface oxygen concentration of $2.9 \times 10^{14}$ $cm^{-2}$ (figure 2.24). The partially oxidised surface was treated to a single exposure of approximately 180L 2-tertbutylaniline.

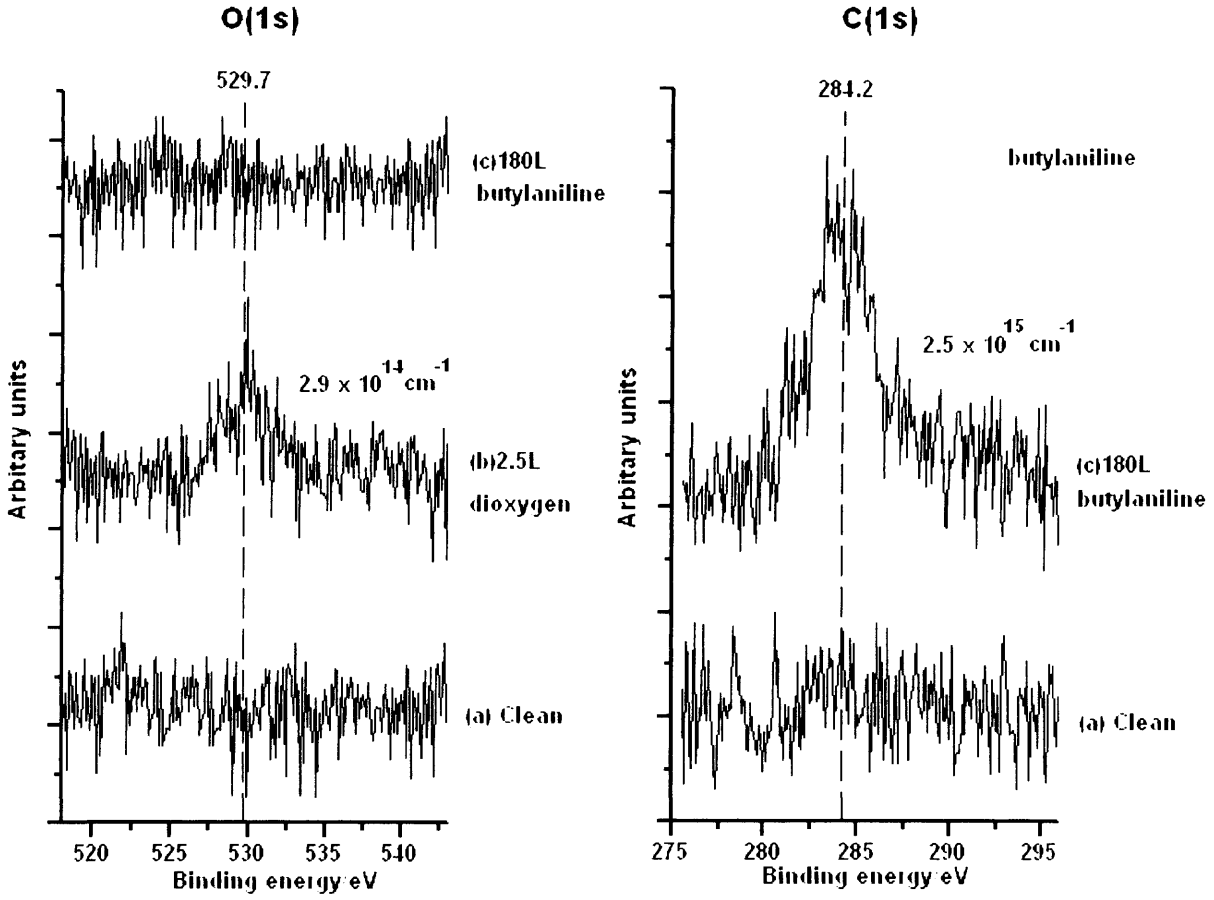


Figure 2.4: O(1s) and C(1s) XP spectra of the reaction of tert-butylaniline with a partially oxidised Cu(110) surface at 293 K. (a) clean, (b) after 2.5L dioxygen, (c) after 180L butylaniline

The resulting XP spectra show a peak in the C(1s) region at 284.2 eV with an area corresponding to a surface concentration of 2.5 x $10^{15}$ $cm^{-2}$ equal to a t-butylaniline concentration of 2.5 x $10^{14}$ $cm^{-2}$. The O(1s) peak has disappeared. The low quality of these spectra are due to problems the XPS system was experiencing at the time. The low intensities of XP peaks that were a result of these problems meant that any nitrogen on the surface did not give rise to a discernable peak, and hence the N(1s) XP spectrum is not included here.

A series of STM images of the surface are shown in figure 2.25. As was seen on the clean surface, it is covered by an adlayer of circular features. Although lower-resolution images (a) do not exhibit a great deal of long-range order, high-resolution images (b-c) show that there is a relatively high degree of short-range order to this adlayer, and as evident in image (d), small areas contain very ordered features. These features in image (d) have a spacing of 0.51 nm in the <110> direction, and 0.7 nm in the <001> direction. Although not every area of the surface is as ordered as this small section, these same spacings can be found between features across the entire surface.

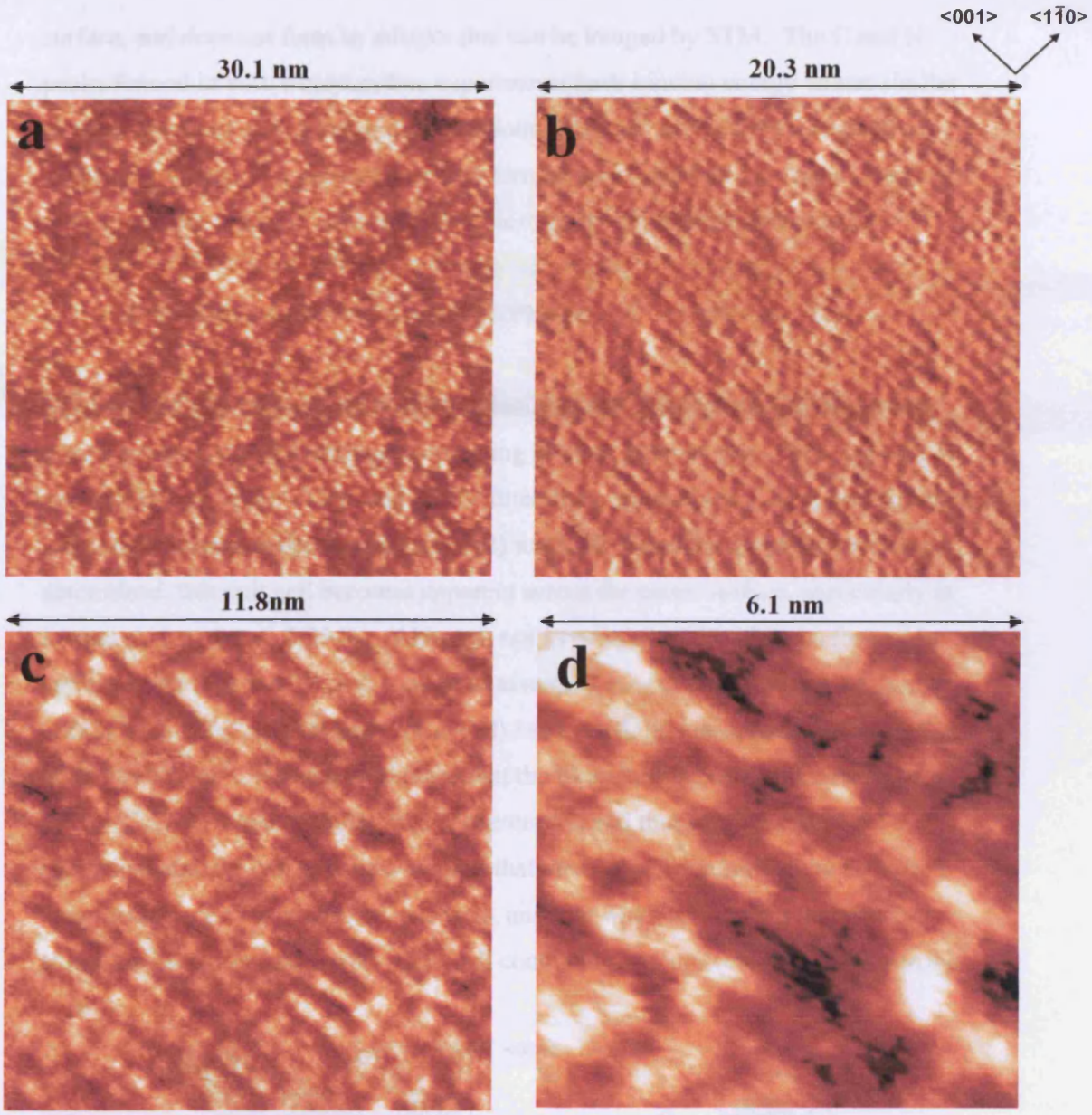


Figure 2.25: A series of STM images of the adsorbate formed after reaction of a partially oxidised Cu(110) surface with 180L 2-terbutylaniline vapour at 293 K. [(a)$V_s$ = 1.02 V, $I_T$ = 2.98 nA, (b)/(c) $V_s$ = 1.02 V, $I_T$ = 3.05 nA, (d) $V_s$ = 1.02 V, $I_T$ = 3.22 nA ]

### 2.8.5 Discussion

XP spectra show that 2-tetbutylaniline will react with both clean and partially oxidised Cu(110) surfaces at room temperature, saturating the surface. This is in contrast to the interaction of aniline with Cu(110), which does not saturate the clean

surface, and does not form an adlayer that can be imaged by STM. The C and N peaks formed in both t-butylaniline experiments have binding energy values similar to those observed during the aniline reactions, 283.7 eV and 397.5 eV respectively, suggesting that similar products are also formed here (equation 1). Again, reaction with a partially oxidised surface leads to desorption of all chemisorbed oxygen.

$$2RPhNH_2 + O(a) \rightarrow H_2O(g) + 2RPhN(a) \qquad (1)$$

STM images show that reaction of t-butylaniline with a partially oxidised surface results in an adsorbate with areas containing ordered features with a spacing of 0.51 nm and 0.72nm in the <110> and <001> directions, respectively. As shown in figure 2.26, this structure is built around a p(2x2) unit cell. Once the structure has been determined, this unit cell becomes apparent across the entire surface, particularly in images such as figure 2.25 (b). Although not as ordered as the adlayers formed by aniline, order here is high, and enough to assume the entire adlayer is based on the p(2x2) cell. A p(2x2) unit cell on Cu(110) has a maximum molecular concentration of $2.7 \times 10^{14}$ $cm^{-2}$. XP spectra showed that the t-butylaniline concentration is $2.5 \times 10^{14}$ $cm^{-2}$. The actual t-butylaniline concentration and that predicted by STM are in agreement, and we can therefore surmise that the unit cell determined by STM here only includes one t-butylaniline molecule, and that whatever process that causes aniline to form a structure with a unit cell containing two molecules is not occurring here.

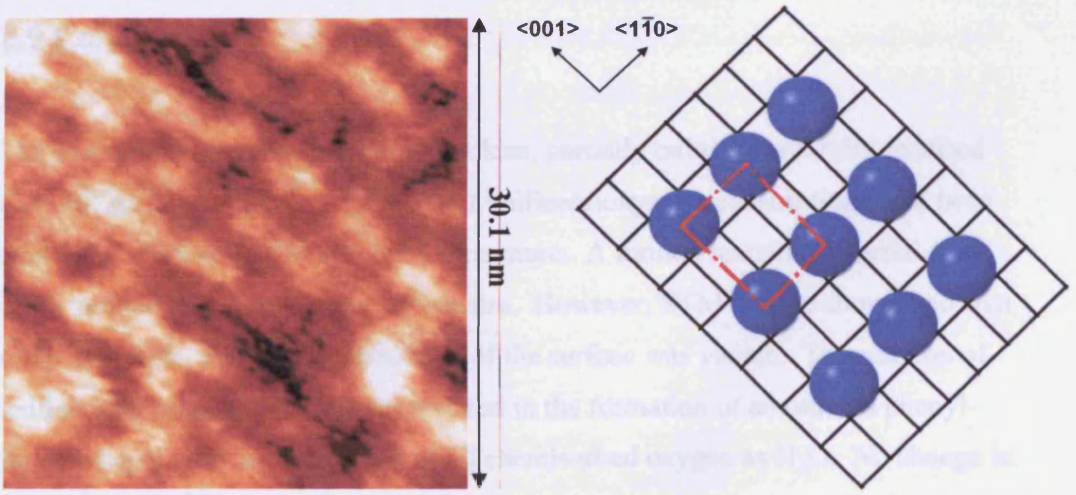


Figure 2.26: Structural diagram of the adsorbate formed by the reaction of 2-butylaniline with a partially oxidised Cu(110) surface at 293K.
[$V_s$ = 1.02 V, $I_T$ = 3.22 nA]

In the previous discussion, it was proposed that pi-stacking in the monolayer may be responsible for aniline forming parallelogram-shaped unit cells instead of primitive, square cells upon reaction with oxidised Cu(110). In the case of t-butylaniline, pi-stacking has been shown to not occur, and a primitive square unit cell is formed. It is however a more densely packed structure than may have been anticipated, especially with regards to the extra butyl moiety of the molecule. For aniline, a p(2x4) cell was theorised, however t-butylaniline has been found to instead form a smaller p(2x2) cell. The efficiency of this packing in the monolayer further emphasises the fact that the unit cell formed by phenyl-imide after the reaction of aniline with oxidised Cu(110) must contain two molecules.

The adlayer formed by the reaction of t-butylaniline with clean Cu(110) surfaces is not ordered enough to determine a unit cell, but the molecule does tend towards forming <110> orientated rows with a spacing of 0.76 nm, the equivalent of three substrate rows, between features. These ordered chains extend for lengths ranging from approximately 3 nm to 15 nm. XP spectra show a t-butylaniline surface concentration of $2.3 \times 10^{14}$ cm$^2$, approximately the same concentration observed at oxidised Cu(110), indicating, that overall, this adlayer is as densely packed as the p(2x2) structure. This essentially rules out the formation of a pi-stacked monolayer or a t-shaped complex for the reaction of 2-tertbutylaniline with clean Cu(110).

## 2.9 Conclusion

The interaction of aniline vapour with clean, partially oxidised and fully oxidised Cu(110) surfaces, together with a 300:1 aniline/dioxygen coadsorption, have been studied by XPS and STM at room temperature. A limited reaction occurred at the clean surface, as evident in the XP spectra. However, STM images showed no sign of an adsorbate, and no reconstruction of the surface was visible. The reaction of aniline with preoxidised Cu(110) resulted in the formation of an ordered phenyl-imide adlayer, and the desorption of all chemisorbed oxygen as $H_2O$. No change in the oxygen structure was observed during the reaction. At low initial surface oxygen concentrations, the reaction was determined to have a 2:1 aniline/oxygen ratio,

however as the initial oxygen concentration increased, the reaction changed to a 1:1 stoichiometry. No reaction was observed for a full oxygen monolayer. The chemisorbed phenyl-imide was found to form a mixture of three ordered domains on the surface, which can be described by $\begin{pmatrix} 4 & 0 \\ 2 & 2 \end{pmatrix}$, $\begin{pmatrix} 4 & 0 \\ -1 & 2 \end{pmatrix}$ and $\begin{pmatrix} 4 & 0 \\ 1 & 2 \end{pmatrix}$ unit meshes. A coadsorption of aniline vapour and dioxygen in a 300:1 ratio also led to a highly ordered phenyl-imide product comprised of two domains, the structures of which can be described by the mirror-image unit meshes $\begin{pmatrix} 3 & 0 \\ -1 & 2 \end{pmatrix}$ and $\begin{pmatrix} 3 & 0 \\ 1 & 2 \end{pmatrix}$, with the more densely packed structures leading to a higher surface concentration than that achieved by reaction with a preoxidised surface.

The phenyl-imide surface concentration, as determined by XPS, was found to be twice the maximum concentration predicted by the unit cells as determined by STM images. Each unit cell must therefore contain two phenyl-imide molecules as opposed to one. Two models are proposed in order to account for this discrepancy. The first involves alternating parallel and perpendicular phenyl rings with respect to the surface, where STM only images the molecules in one of the orientations. The second model involves parallel pi-stacking of the phenyl rings, where each circular feature imaged is actually two molecules on top of each other.

2-tertbutylaniline forms a moderately ordered p(2x2) adlayer when exposed to a partially oxidised Cu(110) surface. The maximum surface coverage predicted by STM is in agreement with the actual surface concentration determined by XPS, proving that the unit cell of the phenyl-imide adlayer formed by reaction of aniline with oxidised Cu(110) includes two molecules.

## 2.9 References

[1] Plank, R. V.; Dinardo, N. J.; Vohs, J. M. *Surf. Sci.* **1995**, *340*, L971.

[2] Rockey, T. J.; Yang, M.; Dai, H. *Surf. Sci.* **2005**, *589*, 42.

[3] Solomon, J. L.; Madix, R. J. *Surf. Sci.* **1991**, *255*, 12. [4] Myers, A. K.; Benziger, J. B. *Langmuir*, **1989**, *5*, 1270.

[5] Ramsey, G.; Rosina, D.; Graen, H. H. *Surf. Sci.* **1990**, *232*, 266.

[6] Rummel, R.; Ziegler, C. *Surf. Sci.* **1998**, *418*, 303.

[7] Padilla-Campos, L; Zagal, J. H.; Rangel, C. M.; Costamagna, J. *J. Molecular Structure: Theochem*, **2005**, *757*, 1

[8] Khaled, K. F.; Hackerman, N. *Electrochimica Acta*, **2004**, *49*, 485

[9] Lazarova, E.; Petkova, G.; Raicheff, R.; Neykov, G. *J. Appl. Electrochem.* **2002**, *32*, 1355.

[10] Du, T. B.; Chen, J. J.; Cao, D. Z. *J. Mater. Sci.* **2001**, *36*, 3903.

[11] Luo, H.; Guan, Y. C.; Han, K. N. *Corrosion* **1998**, *54*, 721

[12] Khaled, K. F.; Hackerman, N. *Mater. Chem. Phys.* **2003**, *82*, 949.

[13] Davies, P. R.; Keel, J. M. *Surf. Sci.* **2000**, *469*, 204.

[14] Carley, A. F.; Davies, P. R.; Roberts, M. W. *Catal. Lett.* **2002**, *80*, 25.

[15] Carley, A. F.; Davies, P. R.; Jones, R. V.; Harikumar, K. R.; Kulkarni, G. U.; Roberts, M. W. *Top. Catal.* **2000**, *11*, 299.

[16] Carley, A. F.; Davies, P. R.; Roberts, M. W.; Vincent, D. *Top. Catal.* **1994**, *1*, 35.

[17] Afsin, B.; Davies, P. R.; Pashusky, A.; Roberts, M. W.; Vincent, D. *Surf. Sci.* **1993**, *284*, 109.

[18] Afsin, B.; Davies, P. R.; Pashuski, A.; Roberts, M. W. *Surf. Sci.* **1991**, *259*, L724.

[19] Carley, A. F.; Davies, P. R.; Harikumar, K. R.; Jones, R. V.; Kulkarni, G. U.; Roberts, M. W. *Top. Catal.* **2001**, *14*, 101.

[20] Cabibil, H.; Ihm, H.; White, J. M. *Surf. Sci.* **2000**, *447*, 91.

[21] Carley, A. F.; Coughlin, M.; Davies, P. R.; Morgan, D. J.; Roberts, M. W. *Surf. Sci. Letts.* **2004**,

[22] Davies, P.R.; Keel, J.M. *Phys.Chem.Chem.Phys.* **1999**, *1*, 1383

[23] Afsin, B.; Davies, P. R.; Pashusky, A.; Roberts, M. W.; Vincent, D. *Surf. Sci.* **1993**, *284*, 109.

[24] Afsin, B.; Davies, P. R.; Pashuski, A.; Roberts, M. W. *Surf. Sci.* **1991**, *259*, L724

[25] Carley, A.F.; Davies, P.R.; Edwards, D.; Jones, R.V; Parsons, M. *Topics in Catalysis*, **2005**, *36*, 21

[26] Buisset, J.; Rust, H. P.; Schweizer, E. K.; Cramer, L.; Bradshaw, A. M. *Surf. Sci.* **1996**, *349*, L147.

[27] Carley, A. F.; Coughlin, M.; Davies, P. R.; Morgan, D. J.; Roberts, M. W. *Surf. Sci.* **2004**, *555*, L138.

[28] Rogers, B. L.; Shapter, J. G.; Ford, M. *Surf. Sci.* **2004**, *548*, 29.

[29] Hunter, C. A.; Lawson, K. R.; Perkins, J.; Urch, C. J. *J. Chem. Soc.-Perkin Trans. 2* **2001**, 651.

# *Chapter 3*

## *Interaction of dimethylamine with Cu(110) surfaces*

### 3.1 Introduction

The interaction of dimethylamine, $(CH_3)_2NH$, with clean, partially oxidised and fully oxidised Cu(110) surfaces has been investigated by XPS and STM at room temperature. The investigation focuses on the mechanism of reaction between dimethylamine and chemisorbed oxygen, the structures formed and the fate of both species.

### 3.2 The interaction of dimethylamine with metal and silicon surfaces

The most widely studied metal with respect to the surface science of dimethylamine is copper. The first investigation was conducted by Prabhakaran et al. on clean and oxidised Cu(110)[1]. HREELS results showed that dimethylamine adsorbed molecularly at 80K on the clean surface. Warming to 120K was believed to result in dehydrogenation to $(CH_3)_2N$, however doubts have arisen regarding this suggestion, as the lack of the N-H stretching mode, which was used as evidence for

dehydrogenation, may be explained as a result of the weak nature of this mode and the fact that the bond lies parallel to the surface[2]. Dimethylamine was also found to adsorb molecularly at 80K on the oxidised surface. Heating the sample to 110K in this case resulted in vibrational modes characteristic of OH and $H_2O$, indicating reaction with the adsorbed oxygen.

However, another study of the interaction of dimethylamine with Cu(110) seems to contradict these conclusions. Kelber et al. conducted a HREELS/TPD study on both clean and oxidised Cu(110), as well as oxidised polycrystalline copper[3]. On clean Cu(110), dimethylamine was found to desorb from a multilayer state at 135K, and remain adsorbed molecularly in a monolayer or sub-monolayer state up to 300K. The large discrepancies with the previous study involve the reaction with the oxidised surface. A similar spectrum to that reported by Prabhakaran was observed at 80K, but at temperatures greater than 120K, large differences are observed, the most significant being that no evidence for the formation of hydroxy species or water was found. Above room temperature, up to 320K, the spectrum was identical to that of dimethylamine chemisorbed at clean Cu(110), indicating that no N-H or C-N bond scission had occurred. This study also concluded that the main desorption peak temperature at oxidised Cu(110) was lower than that at the clean surface, suggesting that the presence of the chemisorbed oxygen actually weakens the interaction of dimethylamine with the surface. Differences in the surface oxygen coverage are proposed by the authors for the discrepancies between their results and those of Prabhakaran et al.

Raval and co-workers have conducted a RAIRS investigation of the interaction of dimethylamine with clean Cu(110) and Ni(111) surfaces[4]. Dimethylamine was seen to desorb from a multilayer state at 120K on Cu(110). Between 160K and 220K, desorption from a H-bonded second layer was observed, and a molecularly adsorbed species was seen to persist up to 300K, possibly with some H-bonding interaction. The RAIRS spectrum was compatible with the HREELS spectrum observed by Kelber at al. but details were resolved which were used to make conclusions regarding the symmetry of the adsorbed molecule. The molecule was deduced to be

adsorbed with the gas-phase $C_s$ symmetry preserved. The same was also found to be true at the Ni(111) surface. Decomposition was observed above 229K at Ni(111), and whilst the products could not be unambiguously identified, similarities to methylaminocarbyne were observed.

The interaction of dimethylamine with Cu(211) surfaces has also been studied using XPS[5]. Physisorption occurred at 80K and no change in binding energy was observed as the sample was heated. Dimethylamine desorbed molecularly with warming, with complete desorption occurring between 200K and 290K.

A RAIRS/TPD study at Pt(111) surfaces[6] revealed that dimethylamine adsorbs molecularly through the N lone pair up to 300K. At 350K, the molecule undergoes a partial dehydrogenation, forming methylaminocarbyne. At 400K, a further dehydrogenation reaction occurs, resulting in the formation of methyl isocyanide, cyanide, and species with the formula $CNCH_2$.

The interaction of dimethylamine with silicon has been studied at both (100)[7] and (111)[8] surfaces. At Si(100), an Auger/LEED and TPRS study found that the molecule adsorbs dissociatively at room temperature. It was found to chemisorb with an initial saturation coverage of 0.5ML, but adsorption was found to continue past this point, resulting in different reaction products. At low doses, partial dehydrogenation led to the formation of $H_2$, and a partial dehydrogenation reaction resulted in the production of HCN. At higher doses, an imine dehydrogenation product was observed, with N-methylmethanimine ($CH_3NCH_2$) being the most likely product.

Dimethylamine was also found to dissociate on Si(111) surfaces, forming H atoms and $(CH_3)_2N$. C(1s) and N(1s) XP spectra showed peaks at 286.4 eV and 399.1 eV respectively. An STM investigation observed the formation of two separate adsorbate structures.

## 3.3 Experimental

The combined XPS/STM instrument used in this investigation and the sample cleaning process are as discussed in chapter 1.

Dimethylamine (99.0%) and oxygen (99.998%) were obtained from Argo Ltd and used as received. Mass spectrometry was used to check purity of gases.

## 3.4 XPS studies of the interaction of dimethylamine with Cu(110) surfaces

### 3.4.1 Clean surface

An atomically clean Cu(110) surface was exposed to 200L dimethylamine vapour at 293K. C(1s) and N(1s) XP spectra show no evidence of an adsorbed species (figure 3.1).

### 3.4.2 Partially oxidised surface

A clean Cu(110) surface at room temperature was exposed to 4L dioxygen at a pressure of $2x10^{-8}$ mbar resulting in a peak in the oxygen region of the XP spectrum with an area corresponding to an oxygen surface concentration of $3x10^{14}$ $cm^{-2}$.

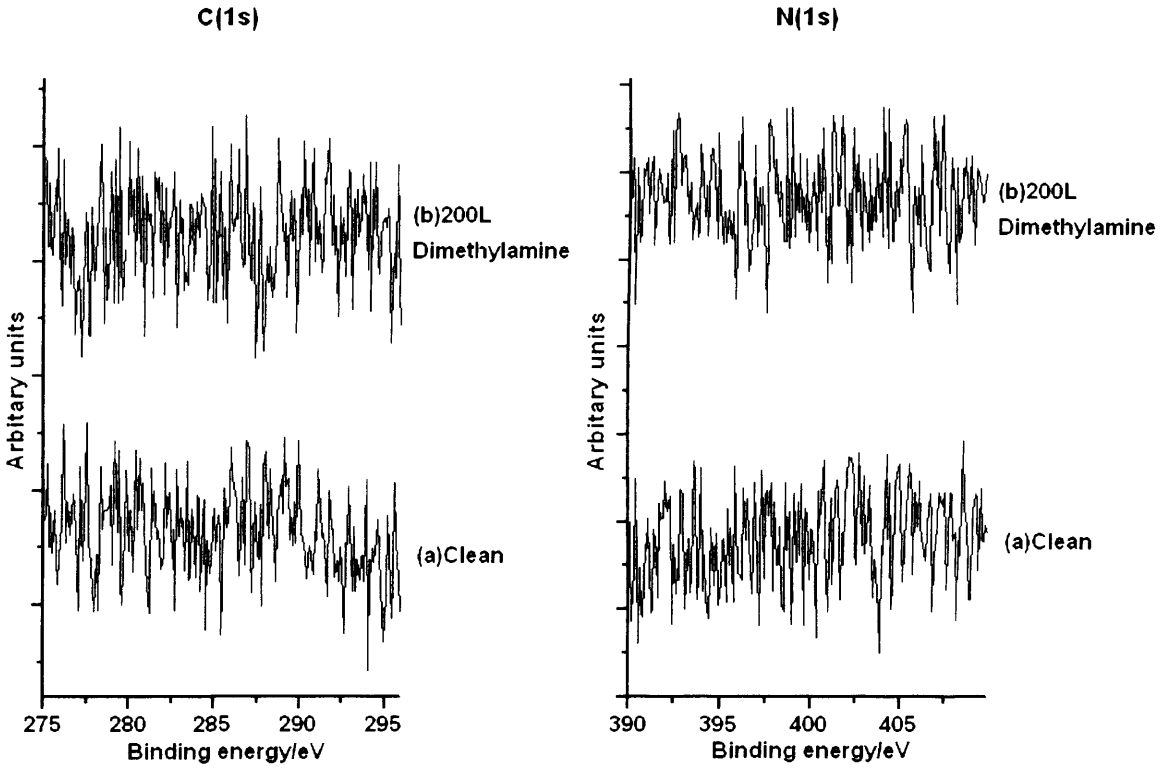


Figure 3.1: C(1s) and N(1s) XP spectra of the reaction of dimethylamine vapour with a clean Cu(110) surface at 293K. (a) clean, (b) after 200L dimethylamine.

The partially oxidised surface was exposed to two dimethylamine exposures of 5L, and a third exposure of 20L and studied by XPS after each dose (figure 3.2). The oxygen concentration was seen to get progressively smaller as the exposure to dimethylamine increased. Following the final exposure, the surface oxygen concentration was reduced to $0.6 \times 10^{14}$ $cm^{-2}$. After the initial dimethylamine exposure, the C(1s) XP region showed a small peak with a binding energy of 285.6 eV. This peak increased slightly during subsequent dimethylamine exposures, eventually giving rise to a final carbon concentration of $1.6 \times 10^{14}$ $cm^{-2}$, which would correspond to a dimethylamine concentration of $8 \times 10^{13}$ $cm^{-2}$. No evidence of an adsorbed nitrogen species was found in the XP spectrum.

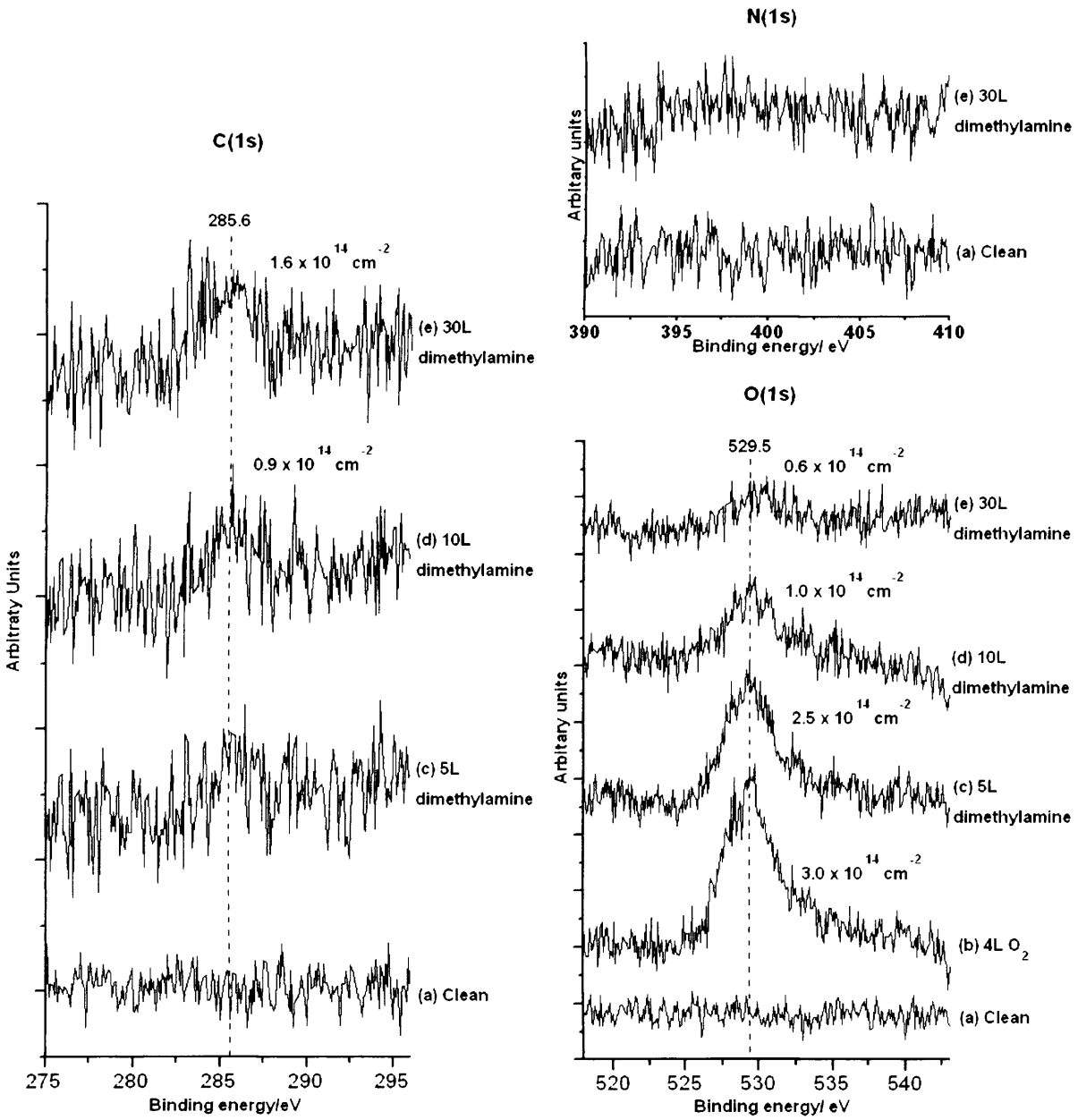


Figure 3.2: C(1s), O(1s) and N(1s) XP spectra showing the reaction of dimethylamine with a partially oxidised Cu(110) surface at 293 K. (a) clean, (b) after 4L dioxygen, (c) after a 5L dimethylamine exposure, (d)10L dimethylamine, (e) 30L dimethylamine.

### 3.4.3 Completely oxidised surface

A fully oxidised Cu(110) surface, obtained by exposure to 15L dioxygen, was exposed to two 5L doses and a final 50L dose of dimethylamine vapour and studied by XPS (Figure 3.3). After 5L, a small peak was observed in the C(1s) XP spectra, with an area equivalent to 1.7 x $10^{14}$ $cm^{-2}$. The surface oxygen concentration decreased by 1 x $10^{13}$ $cm^{-2}$. After 60L dimethylamine, the carbon concentration had increased to 2.4 x $10^{14}$ $cm^{-2}$ whilst the oxygen concentration was now 3.9 x $10^{14}$ $cm^{-2}$.

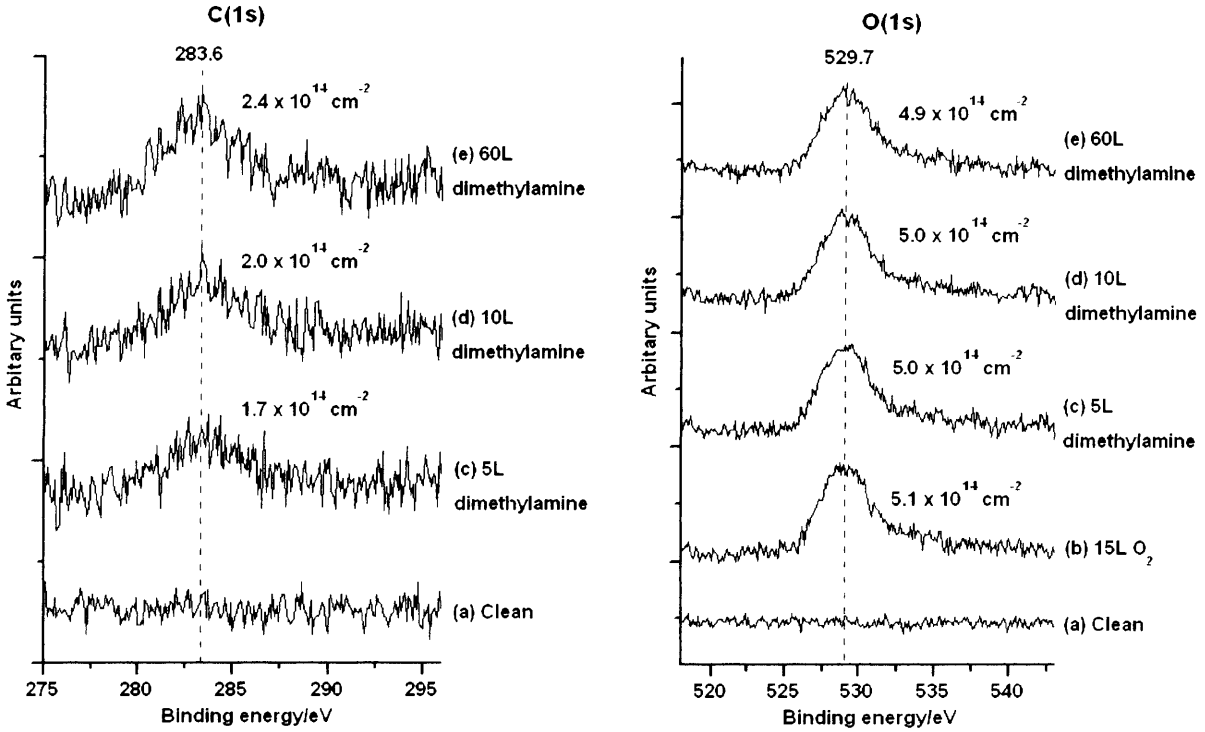


Figure 3.3: C(1s) and O(1s) XP spectra showing the reaction of dimethylamine with a fully oxidised Cu(110) surface at 293 K. (a) clean, (b) after a 15L dioxygen exposure, (c) after a 5L dimethylamine exposure, (d) 10L dimethylamine, (e) 60L dimethylamine.

## 3.5 STM studies of the interaction of dimethylamine with Cu(110) surfaces

### 3.5.1 Clean Surface

A clean Cu(110) surface at 293Kwas exposed to 200L dimethylamine vapour whilst being imaged by STM. No reconstruction of the surface occurred, and no evidence of an adsorbate was found (figure 3.4).

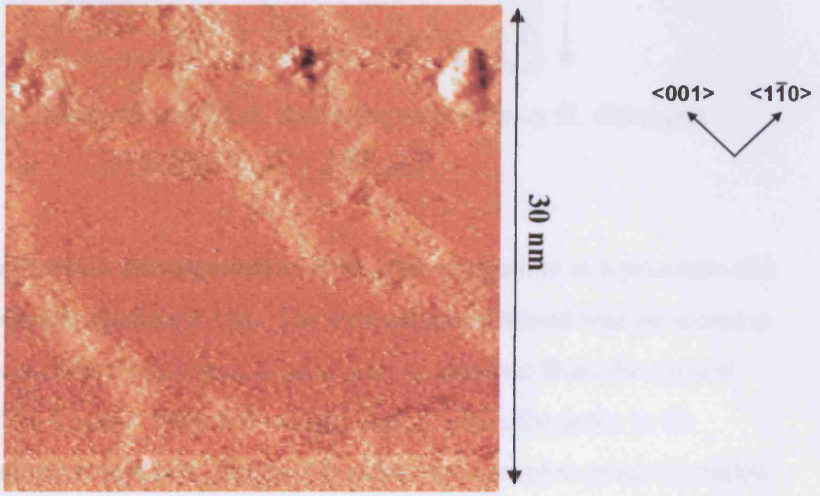


Figure 3.4: Cu(110) surface after exposure to 200L dimethylamine vapour at 293K. [$V_s$ = 0.52 V, $I_T$ = 2.99 nA]

### 3.5.2 Pre oxidised surface – short dimethylamine exposure

An atomically clean Cu(110) surface was exposed to 5L dioxygen at a pressure of 1 x $10^{-8}$ mbar and a temperature of 293K, and imaged by STM. Figure 3.5 shows the resulting surface, on which approximately half a monolayer of oxygen is adsorbed. The image shows the characteristic Cu-O chains, with an inter-row spacing of 0.5nm in the <110> direction.

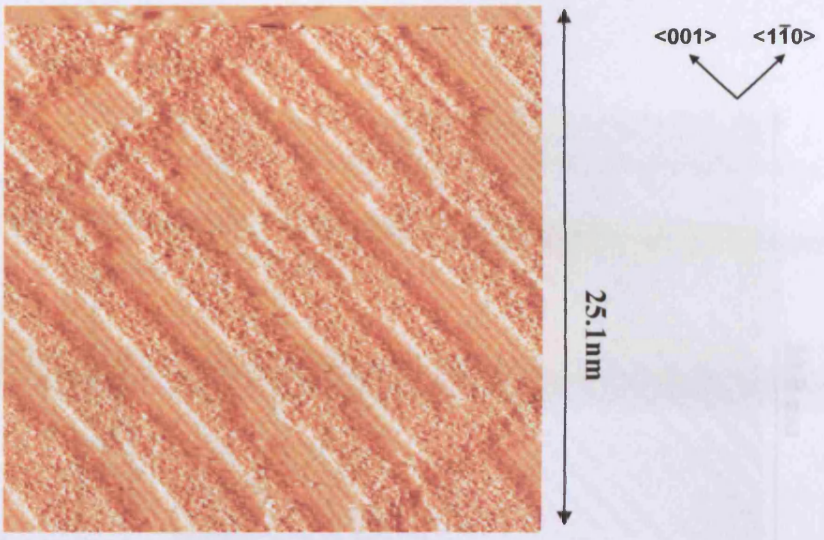


Figure 3.5: Cu(110) surface at 293K following exposure to 5L dioxygen
[$V_s$ = 0.54 V, $I_T$ = 2.84 nA]

The partially oxidised surface was exposed to 108L dimethylamine at a pressure of 3 x $10^{-7}$ mbar, whilst being imaged by STM. The first effect observed was an increase in the spacing between oxygen rows which were seen to increase from the typical 0.51nm to 0.76nm. The distance between oxygen atoms inside the rows in the <011> direction remained at 0.36nm. Figure 3.6 shows the complete transformation of all p(2x1) O(a) islands into an expanded structure. After approximately 40 minutes, the STM image became noisy and was lost. The sample was heated to 450 K for 60 minutes, at which point, the STM image quality improved to reveal the presence of p(2x1) O(a) islands on the surface (Figure 3.7). The surface oxygen concentration at this point is approximately half the concentration before the dimethylamine exposure.

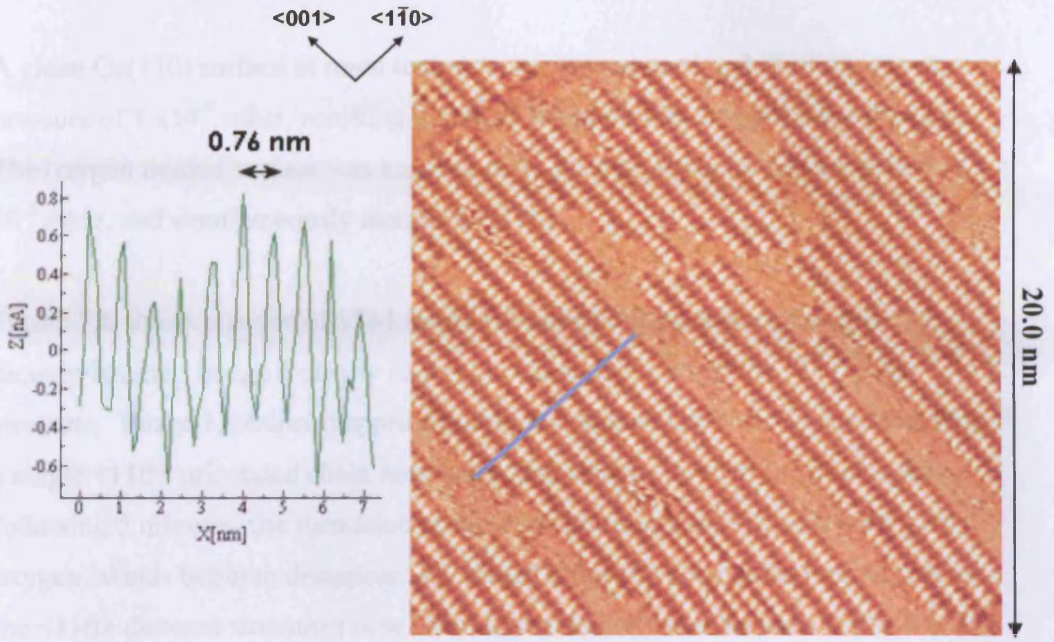


Figure 3.6: Expanded (3x1) oxygen islands adsorbed at a Cu(110) surface at 293K following the reaction of dimethylamine vapour with unexpanded p(2x1)O(a) islands. [$V_S$ = 0.04 V, $I_T$ = 3.11 nA]

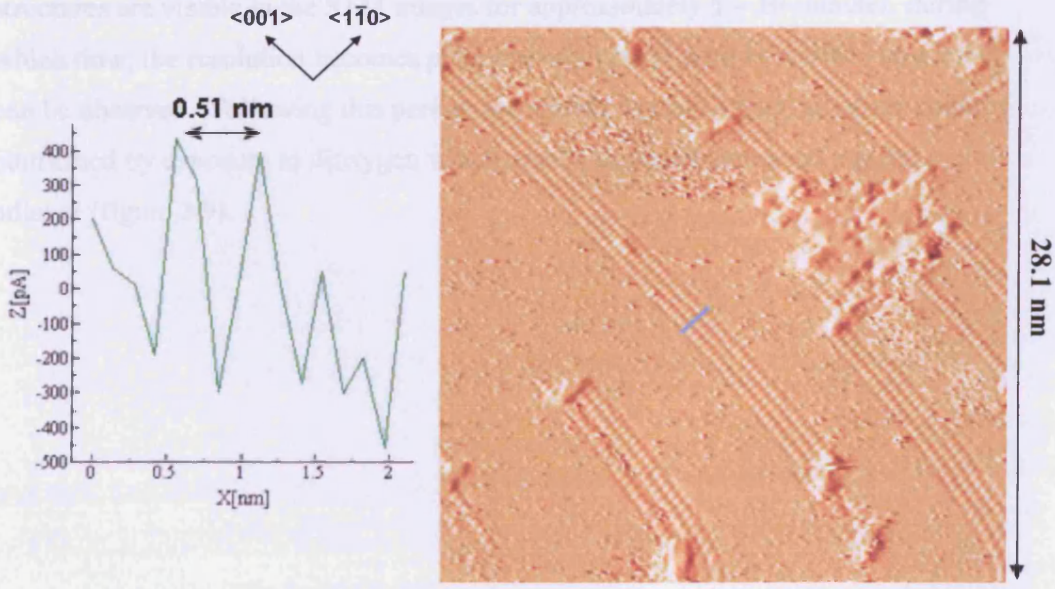


Figure 3.7: p(2x1) O(a) islands remaining at the Cu(110) surface following heating and cooling to 293K. [$V_S$ = 0.04, $I_T$ = 2.94 nA]

### 3.5.3 Pre oxidised surface – long dimethylamine exposure

A clean Cu(110) surface at room temperature was exposed to 3.6L dioxygen at a pressure of 1 x$10^{-8}$ mbar, resulting in a high initial surface oxygen concentration. The oxygen treated surface was exposed to 11.4L dimethylamine at a pressure of 1 x $10^{-8}$ mbar, and simultaneously imaged by STM.

Figure 3.8 shows a series of STM images obtained during this exposure to dimethylamine. Image *a* clearly shows the expanded rows of the (3x1)O(a) structure. Image *b*, obtained approximately one minute later, shows the formation of a single <110> orientated chain next to an O(a) island. Over the course of the following 5 minutes, the formation of these structures continues, whilst the (3x1) oxygen islands begin to disappear. By image *f*, few oxygen chains remain, whereas the <110> directed structures now cover approximately half the area being studied. These structures are approximately 0.7nm wide with a spacing of 1.0nm between each peak. No discernable structure is evident in the rows themselves.

Following complete replacement of the (3x1) oxygen islands, the <110> orientated structures are visible in the STM images for approximately 5 – 10 minutes, during which time, the resolution becomes progressively poorer until no surface structures can be observed. Following this period, the surface appears clean, an observation confirmed by exposure to dioxygen which results in the formation of a p(2x1) adlayer (figure 3.9).

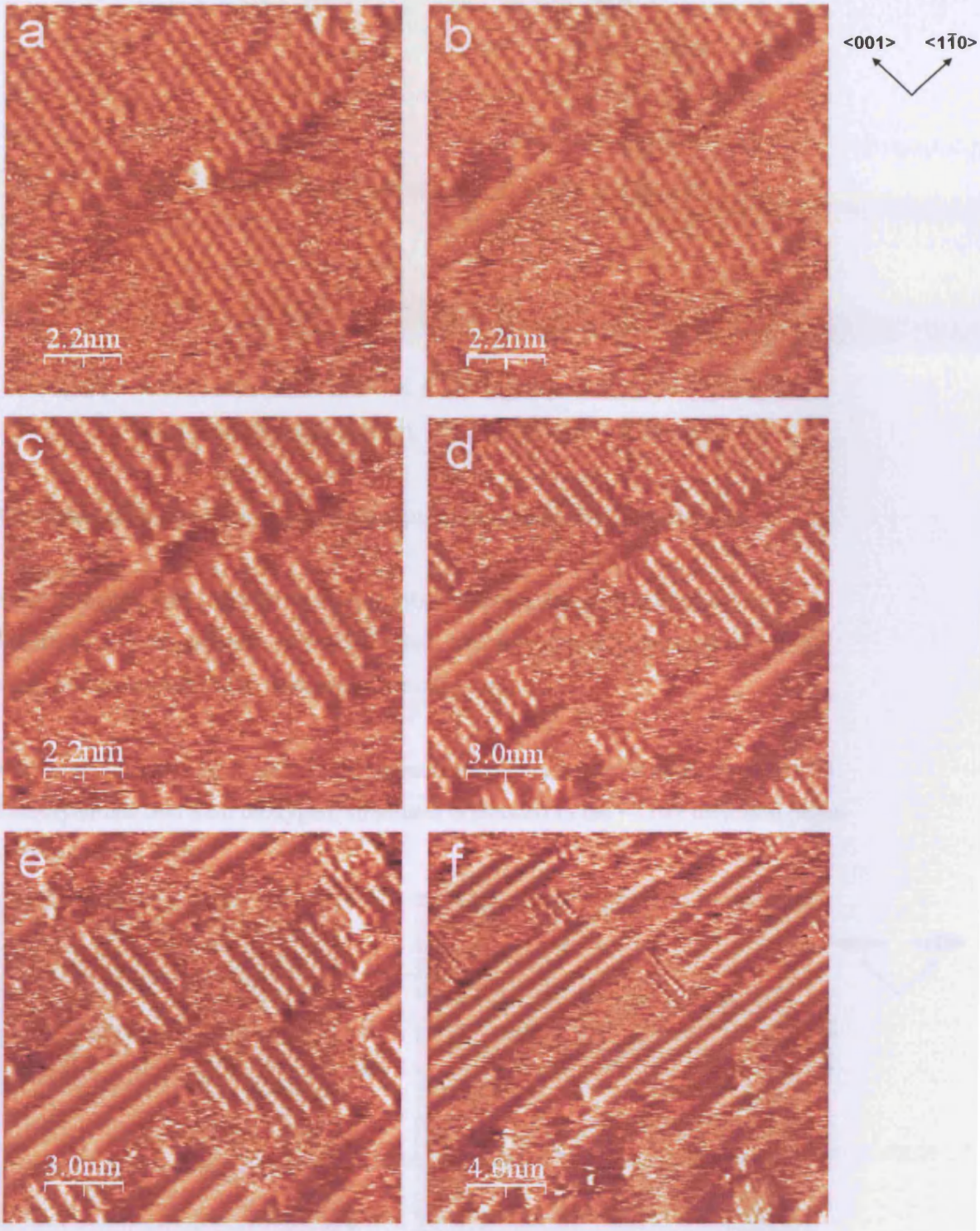


Figure 3.8: Series of successive STM images following exposure of a partially oxidised Cu(110) surface to dimethylamine vapour at 293K.

[$V_s$ = 0.80 V, $I_T$ = 2.28 nA]

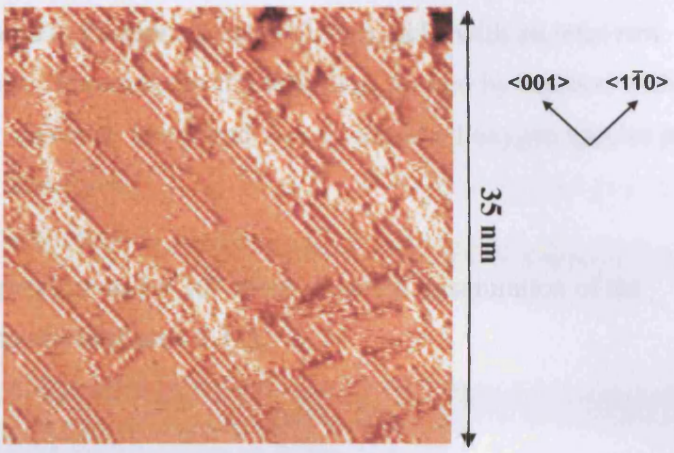


Figure 3.9: Cu(110) surface at 293 K following exposure to dioxygen upon desorption of amide product. [$V_S$ = 0.76 V, $I_T$ = 2.45 nA]

### 3.5.4 Dimethylamine/dioxygen coadsorption at a clean Cu(110) surface

An atomically clean Cu(110) surface at 293K was simultaneously exposed to dimethylamine at a pressure of 1 x $10^{-8}$ mbar, and dioxygen at a pressure of 1 x $10^{-9}$ mbar, and imaged by STM throughout the exposure.

After approximately 60 minutes, corresponding to an exposure of approximately 36L dimethylamine and 3.6L dioxygen, structures orientated in the <110> direction began to form (Figure 3.10).

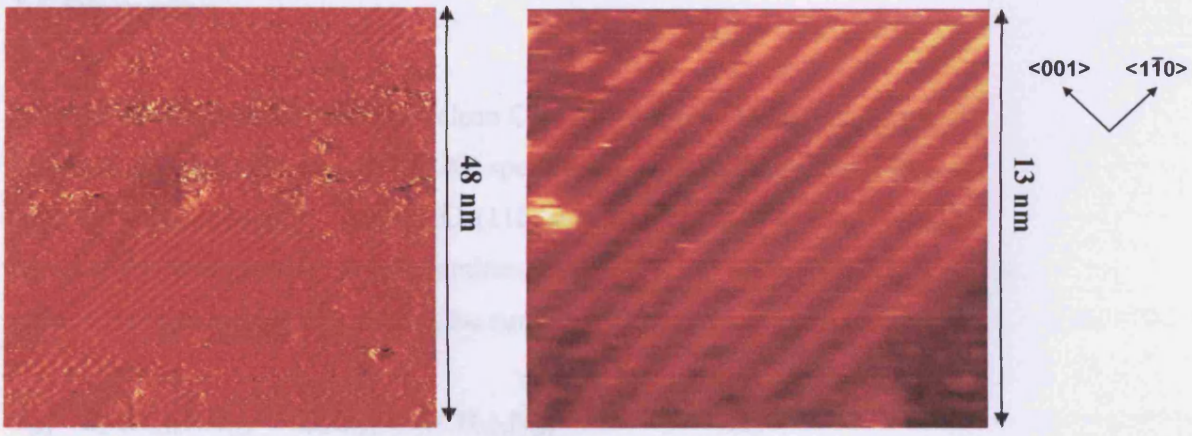


Figure 3.10: Cu(110) surface at 293K following simultaneous exposure to 36L dimethylamine and 3.6L dioxygen. [$V_S$ = 0.90 V, $I_T$ = 2.84 nA]

These structures were found to be approximately 0.7nm wide, with an inter-row spacing of 1.1nm, the same dimensions as the structures formed by reaction with a pre-oxidised surface. No evidence was found for any adsorbed oxygen species prior to the formation of these structures.

Increasing the dioxygen pressure to 5 x $10^{-8}$ mbar, resulted in saturation of the surface by p(2x1) O(a) structures (figure 3.11).

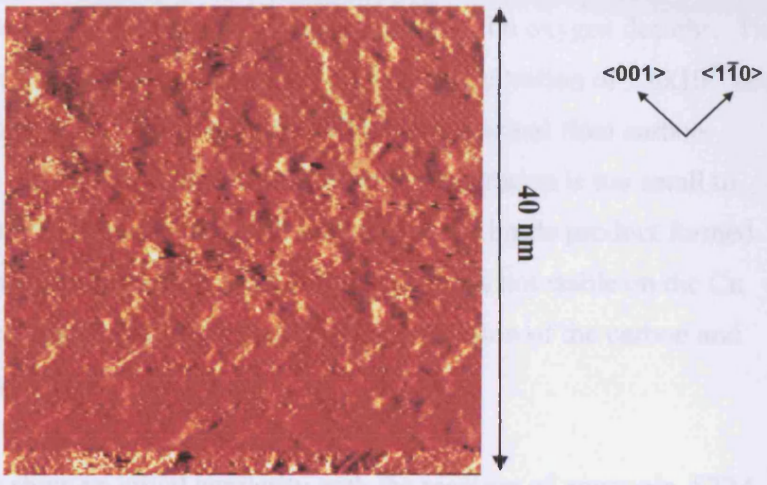


Figure 3.11: Cu(110) surface at 293K saturated with p(2x1)-O(a) as a result of an increase in the dioxygen:dimethylamine ratio [$V_S$ = 1.01 V, $I_T$ = 2.97 nA]

## 3.6 Discussion

Dimethylamine does not react with clean Cu(110) surfaces. However, as was the case with aniline and ammonia[9,10], XP spectra show that the adsorption of dimethylamine at partially oxidised Cu(110) surfaces results in the desorption of oxygen. By analogy with the other amines, the oxygen has presumably desorbed as water, leaving an amide adsorbed at the surface (equation 1).

$$O_{(a)} + 2(CH_3)_2NH_{(g)} \rightarrow H_2O_{(g)} + 2(CH_3)_2N_{(a)} \qquad (1)$$

The C(1s) binding energy of 285.6 eV supports the assignment of an amide, as a similar binding energy was observed for a dimethylamide product on Cu(211)[5]. A C(1s) binding energy of 286.6 eV has been recorded for molecular dimethylamine adsorbed at copper surfaces[11]. Unfortunately, the N(1s) signal was not strong enough to form a discernable peak in the spectrum. It is believed that decomposition under the X-rays may have been responsible for the poor XP spectra.

In contrast to the reaction with aniline, the XPS results show that there is no large increase in the surface carbon and nitrogen concentration as the oxygen desorbs. The 2:1 stoichiometry of equation 1 suggests a final carbon concentration of $9.6 \times 10^{14}$ $cm^{-2}$ and a nitrogen concentration of $4.8 \times 10^{14}$ $cm^{-2}$, whereas the actual final carbon concentration is only $1.6 \times 10^{14}$ $cm^{-2}$, and the nitrogen concentration is too small to give rise to a discernable XP peak. It is clear that, unlike the imide product formed by the reaction with aniline, the amide product formed here is not stable on the Cu surface and undergoes a further reaction that leads to desorption of the carbon and nitrogen containing species.

While the XP spectra show an initial similarity with the reaction of ammonia, STM images show that the adsorption of dimethylamine at partially oxidised Cu(110) surfaces results in a reaction that is at first similar to that observed upon adsorption of pyridine at the same surfaces[12]. Upon exposure to dimethylamine vapour, the spacing between rows of the O(a) islands increases rapidly from 0.51nm to 0.76nm This transformation corresponds to a change from a p(2x1) structure into a (3x1) phase. This change in the oxygen island structure was also observed during the reaction of pyridine vapour with partially oxidised Cu(110) surfaces. Figure 3.12 compares these two structures. Both the oxygen atoms and the added row copper atoms are shifted apart in the <110> direction so that there are now two substrate row between them, as opposed to one. The distance between oxygen atoms in the <011> direction remains the same at 0.36nm.

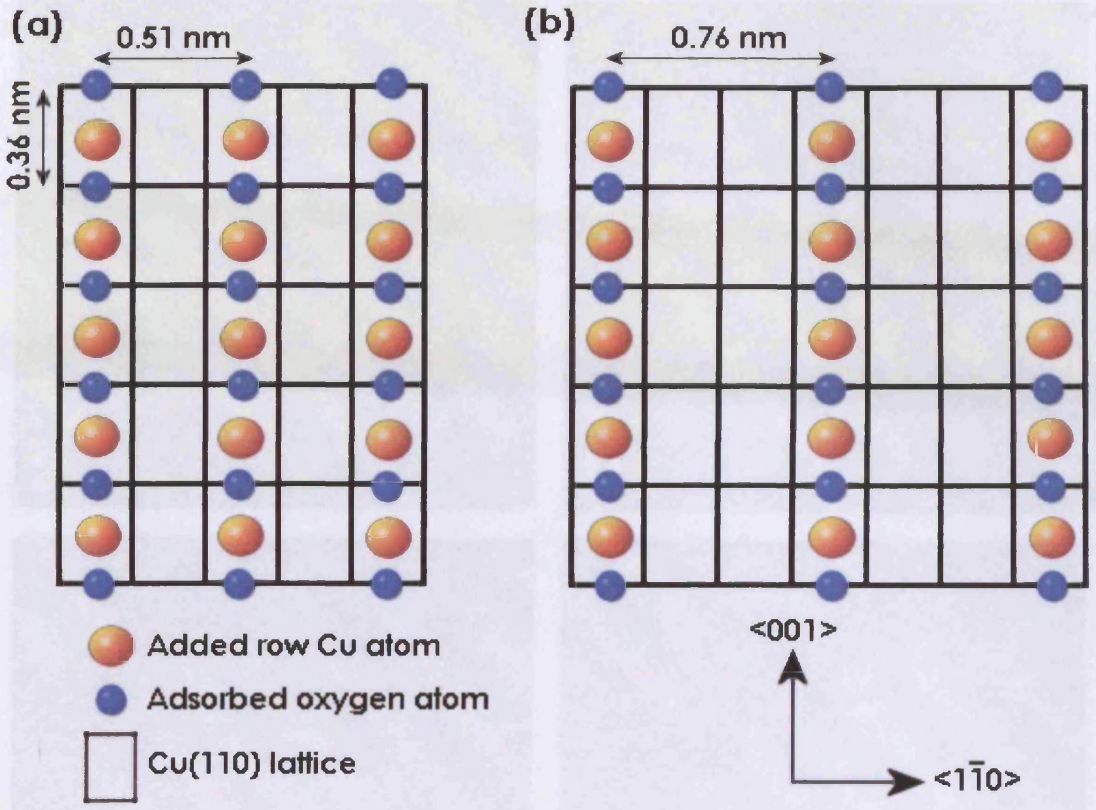


Figure 3.12: Structural diagrams of (a) normal chemisorbed oxygen on Cu(110), (b) expanded Cu(110)-O(a) structure formed by reaction with dimethylamine, as well as other compounds.

It has been concluded that pyridine adsorbs on top of the Cu-O chains, and the evidence suggests that the same is true for dimethylamine. Figure 3.13 shows a series of high resolution STM images of the (3x1) phase, with three rows of interest marked (i), (ii), and (iii). Throughout the series, row (ii) seemingly oscillates freely between rows (i) and (iii). It appears as though the row is split into two sections, with one section being close to row (i) and the other close to row (iii), but this is likely a result of the slow upwards scanning of the STM, and the movement of the row is too fast to be captured. This movement would be difficult if an adsorbate was present between the rows, indicating a lack of an adsorbed species between the rows, and therefore suggesting adsorption occurs on top of the Cu-O chains.

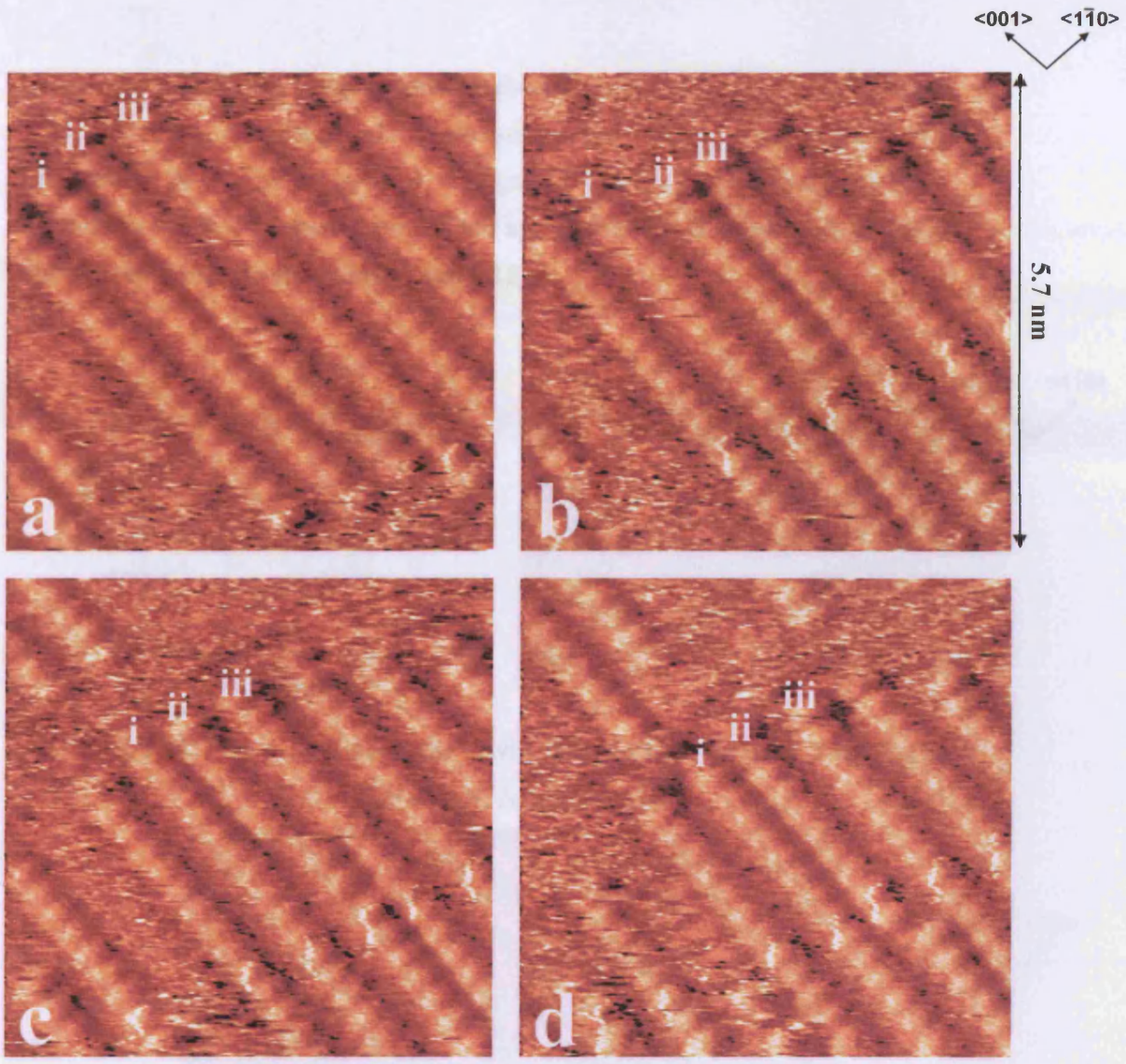


Figure 3.13: Series of STM images showing the movement of an O(a) row in the (3x1)-O(a) structure formed by the reaction of dimethylamine with partially oxidised Cu(110) surfaces at 293K. [$V_S$ = 0.18 V, $I_T$ = 2.69 nA]

Figure 3.8 shows that as the (3x1) oxygen islands desorb, new structures form along the <110> direction, which eventually replace all (3x1) islands. These structures are only stable for a period of up to 10 minutes, after which they too desorb leaving a completely clean surface. The structures are poorly resolved along the chains, with no visible maxima/minima, and are approximately 0.7nm wide, with an inter-row spacing of 1nm, peak to peak, and a gap of 0.36nm between each row. in the <110>

direction (figure 3.14). They are shown adsorbed across two substrate rows in the <001> direction, covering two four-fold hollow sites, however the exact adsorption sites cannot be determined by STM. The gap of 0.36 nm between structures is equivalent to one Cu substrate row. Their apparent height is comparable to that of the expanded oxygen structures (figure 3.15).

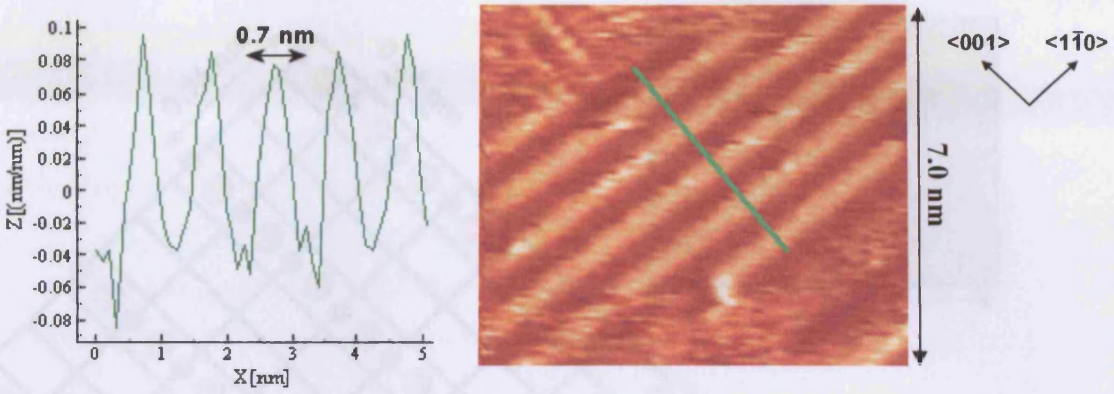


Figure 3.14: Line profile across the newly formed <100> orientated structures.
[$V_s$ = 0.80 V, $I_T$ = 2.28 nA]

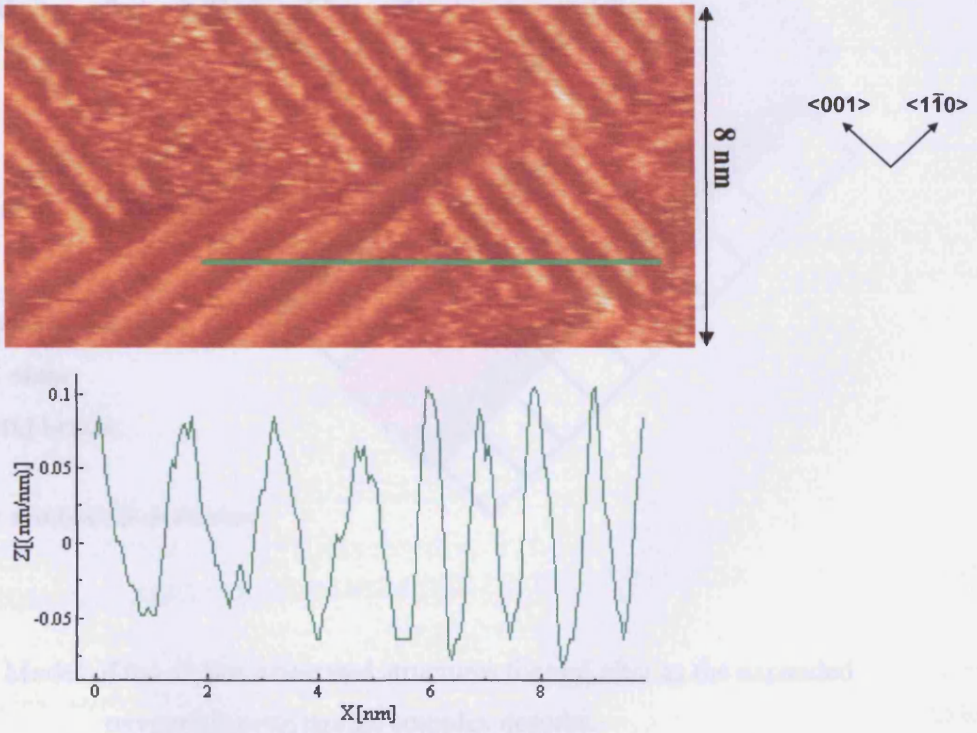


Figure 3.15: Line profile illustrating the apparent height difference between the adsorbed oxygen islands and the new <100> orientated structures.
[$V_s$ = 0.80 V, $I_T$ = 2.28 nA]

A model of these structures, together with the expanded O(a) islands, is shown in figure 3.16. Similar surface features have been observed following the reaction of ammonia with Cu-O, although in that case, the product was determined to be an imide species[13].

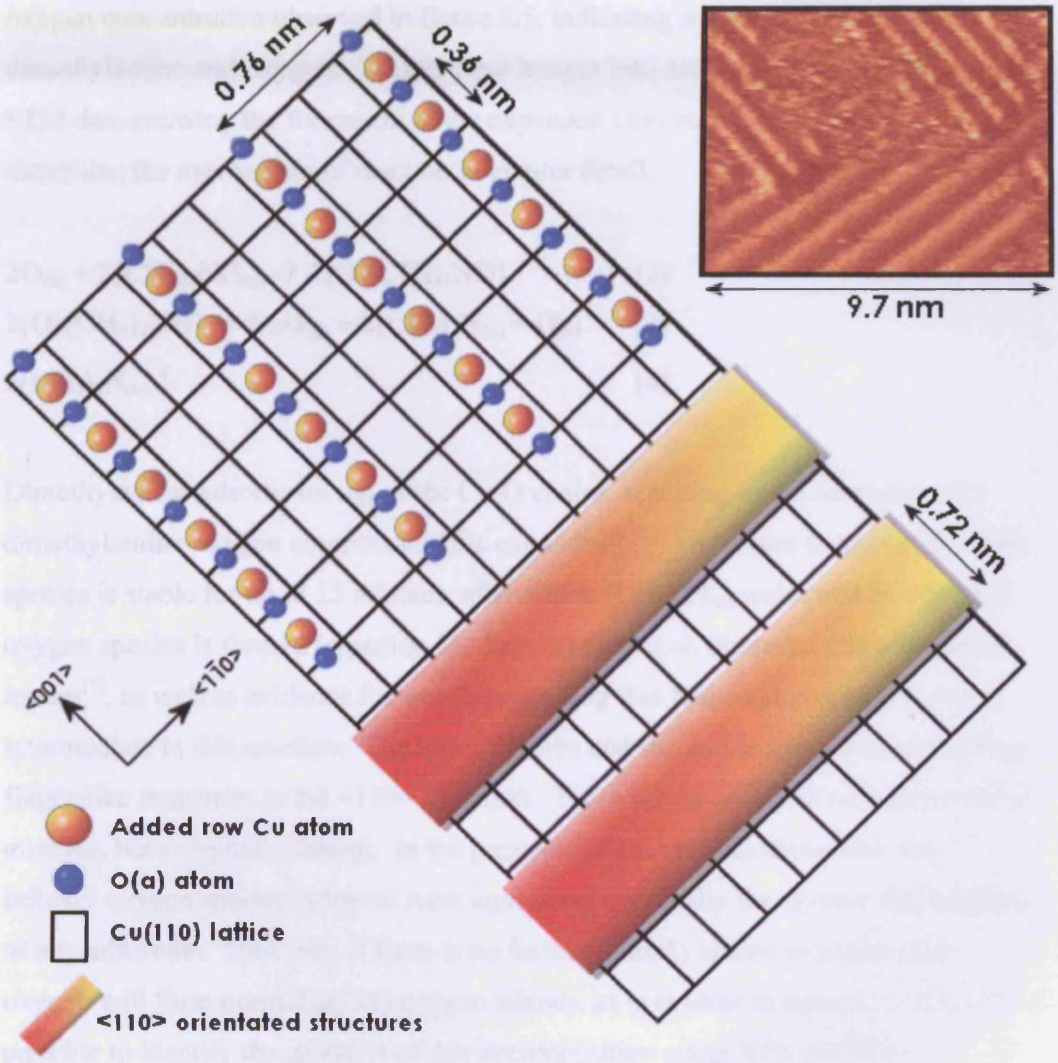


Figure 3.16: Model of the <110> orientated structures formed after as the expanded oxygen-dimethylamine complex desorbs.

The experiments discussed so far have all been conducted in the presence of excess dimethylamine vapour. Figure 3.6 shows the rapid formation of the (3x1) O(a) structure upon exposure to dimethylamine. The dimethylamine dose was then stopped, after which the STM image was lost. Upon heating and cooling, the image was regained to reveal the normal (2x1) oxygen islands (figure 3.7) The surface oxygen concentration is estimated from the STM images to be half that of the initial oxygen concentration observed in figure 3.5, indicating a 2:1 reaction between dimethylamine and oxygen. Taking these images into account, together with the STM data showing the formation of the expanded O(a) structures, it is possible to determine the mechanism of reaction in greater detail.

$$2O_{(a)} + 2(CH_3)_2NH_{(g)} \rightarrow 2[O\text{-}(CH_3)_2NH] \quad (2)$$

$$2[O\text{-}(CH_3)_2NH] \rightarrow H_2O_{(g)} + 2(CH_3)_2N_{(a)} + O_{(a)} \quad (3)$$

$$2(CH_3)_2N_{(a)} \uparrow \quad (4)$$

Dimethylamine adsorbs on top of the Cu-O chains, resulting in the formation of a dimethylamine-oxygen complex and the expanded (3x1) structure (equation 2). This species is stable for up to 15 minutes, after which $(CH_3)_2N_{(a)}$, water and an adsorbed oxygen species is formed (equation 3). Prabhakaran et al. observed OH vibrational modes[1], as well as evidence for water, suggesting that hydroxyl groups may be an intermediate in this reaction. The water desorbs and the amide species form the long finger-like structures in the <110> direction. These are again stable on a timescale of minutes, but eventually desorb. In the presence of excess dimethylamine, the leftover oxygen species is free to react again, and eventually the surface will be clean of any adsorbate. However, if there is no further dimethylamine available, the oxygen will form normal p(2x1) oxygen islands, as is evident in figure3.7. It is not possible to identify the products of this decomposition using XPS and STM techniques, but two possible reactions are shown in equations (5) and (6).

$$(CH_3)_2N_{(a)} \rightarrow HCN_{(g)} + CH_{4(g)} + H_{2(g)} \quad (5)$$

$$(CH_3)_2N_{(a)} \rightarrow CH_3NCH_{2(g)} + H_{(a)} \quad (6)$$

Equation (5) involves the breaking of a C-N bond, which is very stable at Cu surfaces, and is therefore considered unlikely. The product of the reaction in equation (6), $CH_3NCH_{2(g)}$ (N-methylmethanimine), has previously been observed following adsorption of dimethylamine in high doses at Si(100) surfaces[7]. Lower doses of dimethylamine at the same surface lead to the formation of HCN and $H_2$.

A coadsorption of dioxygen and dimethylamine vapour in a 10:1 ratio lead to the formation of <110> orientated structures forming on the surface before any adsorbed oxygen islands were observed. Their dimensions, 0.7nm wide, with a spacing of 1.1nm (figure 3.17), are the same as the <110> structures formed by reaction with a pre-oxidised surface, and we therefore conclude they are comprised of the same species. This suggests that the formation of the (3x1) structure is not a pre-requisite for the reaction of dimethylamine with oxidised Cu(110); the structures will form so long as there is an active oxygen species available. The following is a probable mechanism for the coadsorption of dimethylamine and dioxygen. As soon as an oxygen species becomes active at the surface, it can react with dimethylamine (equation 7), forming the <110> amide chains, which then decompose and desorb, possibly via the reactions detailed in equations (5) or (6).

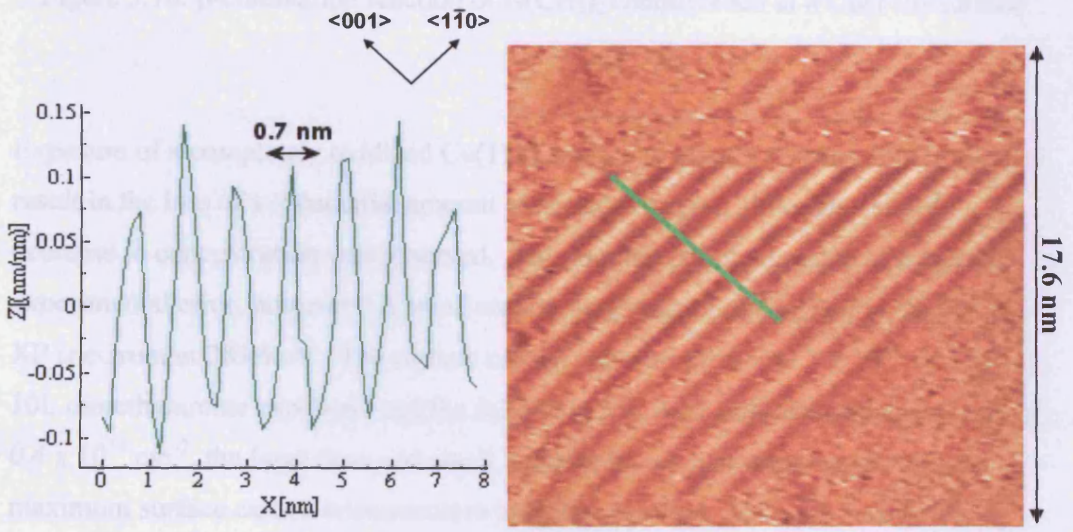


Figure 3.17: Line profile across the features formed by a coadsorption of dimethylamine vapour and dioxygen at Cu(110) surfaces.

[$V_s$ = 0.90 V, $I_T$ = 2.84 nA]

$$O_{(a)} + 2(CH_3)_2NH_{(g)} \rightarrow H_2O_{(g)} + 2(CH_3)_2N_{(a)} \qquad (7)$$

A coadsorption of dioxygen and ammonia resulted in very similar structures[114], although as previously mentioned, the product was assigned to an imide rather than an amide. However, those imide structures were found to be stable on the Cu surface for long periods of time at 293K. This difference in stability between the two products may be due to the fact that the imide formed by the ammonia/dioxygen coadsorption has two bonds between the N and the Cu surface, and no β hydrogens, whereas the $(CH_3)_2N$ product contains β hydrogens and only a single bond to the surface. It is possible therefore for $(CH_3)_2N$ to undergo a β-elimination reaction (figure 3.18), leading to the N-methylmethanimine product in equation (6).

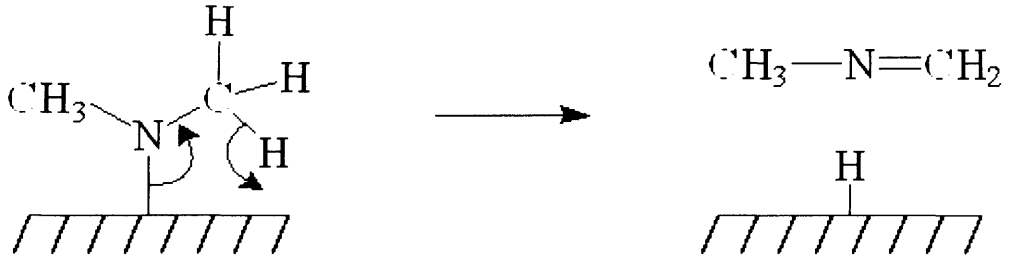


Figure 3.18: β-elimination reaction of $N(CH_3)_2$ chemisorbed at a Cu(110) surface

Exposure of a completely oxidized Cu(110) surface to dimethylamine vapour did not result in the loss of a substantial amount of surface oxygen, although a small decrease in concentration was observed. This amount is not a great deal larger than experimental error, however. A small carbon peak was also observed in the C(1s) XP spectrum at 283.6 eV. The surface carbon concentration was 2 x $10^{14}$ $cm^{-2}$ after 10L dimethylamine exposure, and the following 50L dose only caused an increase of 0.4 x $10^{14}$ $cm^{-2}$, the large dose and small increase in concentration suggesting the maximum surface carbon concentration had been reached. No peak was visible in the N(1s) XP spectrum, although such a small concentration would not be expected to give rise to a discernable peak. Clearly, dimethylamine cannot react with fully

oxidized Cu(110) in the same manner as it can with partially oxidized Cu(110). The limited adsorption observed here probably occurs at step edges or at surface defects in the (2x1) adlayer. Unlike the reaction with partially oxidized Cu(110), it appears that the small amount of adsorbed product formed here is stable on the surface. It is possible that the saturated surface leaves no room for the formation of the amide species, and so the dimethylamine-oxygen complex may be stable, assuming the dimethylamine has indeed found sites on the oxygen covered surface where it is still possible for such a structure to form.

These results may help explain the different conclusions reached by the previous vibrational spectroscopy studies[1,3]. It appears, as previously suggested by Kelber et al. that the discrepancies are indeed a result of different initial surface oxygen coverages. A partially oxidized surface leads to the formation of water, as observed by Prabhakaran et al. Furthermore, their observation of $(CH_3)_2N$ is also supported by the results presented here, suggesting that the disappearance of the N-H stretching mode is indeed caused by the breaking of that bond, and is not a result of the bond being parallel to the surface. A fully oxidized surface leads to the results similar to those published by Kelber, i.e. no OH or $H_2O$ vibrational modes would be observed, as the complete oxygen monolayer is unreactive to dimethylamine.

The only discrepancy between the results presented here and previous studies is that dimethylamine was not observed to adsorb at 293K at clean Cu(110) surfaces, whereas all TPD and vibrational spectroscopy results show adsorption up to 300K. This may be due to the relatively long time period required for a complete XPS scan, compared to the small amount of time required to obtain results using other techniques such as TPD or RAIRS. Another possible explanation lies in the fact that the experiments documented here all involved dosing at room temperature, whereas in the previous studies, dimethylamine was dosed at low temperature, and the sample heated. The Raval study[4] suggests that some H-bonding may be occurring in the monolayer state up to 300K. It is possible that this H-bonded structure cannot form when the dimethylamine is dosed at room temperature, and so the extra thermal stability afforded by the H-bonding, allowing adsorption up to 300K, is not present.

Oxygen contamination in the previous studies may also offer an explanation for the different desorption temperatures, but it is unlikely that such high contamination would go unnoticed.

## 3.7 CONCLUSIONS

The adsorption of dimethylamine at clean, partially and completely oxidised Cu(110) surfaces has been studied by STM and XPS. The results presented here show no evidence of dimethylamine adsorption on clean Cu(110) at room temperature.

Dimethylamine readily adsorbs at partially oxidised Cu(110), causing the structure of the chemisorbed oxygen islands to expand, resulting in a change from p(2x1) to p(3x1) domains. The dimethylamine-oxygen complex formed decomposes into water, which desorbs, an adsorbed oxygen species, and an amide product, $(CH_3)_2N$, which forms structures orientated in the <110> direction. The amide is stable for a period of approximately 10 minutes at 293K, after which it desorbs. The most likely desorption mechanism is a β-hydride elimination, resulting in the formation of $CH_3NCH_2$.

If dimethylamine vapour is still present in the chamber, the adsorbed oxygen species formed from the initial dimethylamine-oxygen decomposition is free to react with dimethylamine vapour again, a process which eventually leads to the desorption of all surface oxygen. If no dimethylamine vapour is present, normal p(2x1)O(a) islands are formed.

Reaction with a fully oxidised surface does not result in significant oxygen desorption. Minor dimethylamine adsorption occurs, believed to happen only at step edges and other surface defects, and the product of this interaction is stable on the surface at room temperature. The lack of free space on the oxidised surface may impede the formation of the amide, and hence account for the stability of the adsorbed product under such conditions.

## 3.8 References


[1] Prabhakaran, K.; Sen, P.; Rao, C.N.R. *Surf. Sci.* **1986**, *169*, L301

[2] Kang, D.; Trenary, M. Surf. Sci. **2002**, *519*, 40

[3] Kelber, J.A.; Rogers, Jr, J.W.; Banse, B.A.; Koel, B.E. App. Surf. Sci. **1990**, 193

[4] Chalker, S.; Haq, S.; Birtill, J.J.; Nunney, T.S.; Raval, R. Surf. Sci. **2006**, *Article in press*

[5] Davies, P.R.; Keel, J.M. Surf. Sci. 2000, 469

[6] Kang, D.; Trenary, M. *Surf. Sci.* **2002**,*519*, 40

[7] Mulcahy, C. P. A.; Carman, A. J.; Casey, S. M. *Surf. Sci.* **2000**, *459*,1

[8] Cao, X.; Hamers, R. J. *Surf. Sci.* **2003**, *523*, 241

[9] Carley, A. F.; Davies, P. R.; Roberts M. W.; Vincent, D. *Top. Catal.* **1994**, *1*, 35

[10] Afsin, B.; Davies, P. R.; Pashusky, A.; Roberts, M. W.; Vincent, D. *Surf. Sci.* **1993**, *284*, 109.

[11] Davies, P.R.; Keel, J.M. Catal. Lett. **1999**, *58*, 99

[12] Carley, A.F.; Davies, P.R,; Edwards, D.; Jones, R.V; Parsons, M. *Topics in Catalysis*, **2005**, *36*, 21

[13] Davies, P. R.; Keel, J. M.; *PCCP*, **1999**, *1*, L383

[14] Afsin, B.; Davies, P. R.; Pashuski, A.; Roberts, M. W. *Surf. Sci.* **1991**, *259*, L2742

# *Chapter 4*

## *Interaction of ethylamines with Cu(110) surfaces*

### 4.1 Introduction

The interaction of ethylamine, $CH_3CH_2NH_2$, and diaminoethylamine, $NH_2CH_2CH_2NH_2$ with clean, partially oxidised and fully oxidised Cu(110) surfaces have been studied at room temperature by XPS and STM. The study focuses on the reactions of these compounds with chemisorbed oxygen islands and the structures formed. The reactions of 2,2,2-trifluoroethylamine with the same surfaces have also been studied in order to determine the effect of the gas phase basicities of these compounds on their reactions with oxidised Cu(110)

### 4.2 The interaction of ethylamine and diaminoethane with metal surfaces

A TPRS, XPS and EELS investigation into the interaction of ethylamine with clean and oxidised Ag(110) surfaces has been conducted by Madix and co workers[1]. On the clean surface, ethylamine was found to adsorb molecularly at 110K. Desorption from a multilayer state occurred at 160K, and from monolayer states from 150K to 400K. It was determined by XPS that ethylamine bonds through the lone pair of the N atom in the monolayer.

It was found that ethylamine stabilises oxygen adsorbed on the Ag(110) surface, possibly as a result of H-bonding, resulting in molecular oxygen desorption at 235K, 50K above the normal desorption temperature. At 110K, formation of ethylamide, $CH_3CH_2NH$, and hydroxyl groups occurs at the oxidised surface. At 280K, chemisorbed ethylimide($CH_3CH_2N$) is formed, resulting in the desorption of water. Ethylimide undergoes further reactions at 370K to form, acetonitrile, hydrogen and regenerated ethylamine. Deuterium labelling experiments show how preadsorbed oxygen activates the N-H bond, whereas clean Ag(110) does not activate this bond.

TPD and HREELS experiments involving ethylamine at clean Ni(111) surfaces[2] show it adsorbs molecularly at 150K, again through the N lone pair. It then undergoes a dehydrogenation reaction to form $CH_3CN$, which desorbs at 350K.

The reaction of ethylamine at clean W(100) surfaces have been studied, as well as W(100)-O and W(100)-C[3]. On the clean surface, large exposures resulted only in trace amounts of $CH_4$ and $NH_3$. The oxidised surface was found to be inert with respect to C-H, C-N and N-H bond scission, resulting in molecular ethylamine desorption up to 550K. The W(110)-C surface was found to be more reactive, resulting in ethylene and acetonitrile, with the latter being the major product.

The interaction of diaminoethane with Pt(111) surfaces has been studied using RAIRS and TPD[4]. Molecular adsorption occurs between 80K and 300K. At 360K, RAIRS shows that the molecule rearranges to form a species that is identified as diaminoethane ($H_2NCH_2CH_2NH_2$). Above this temperature decomposition to aminomethyidyne, $CNH_2$ takes place.

## 4.3 Experimental

The combined XPS/STM instrument used in this investigation and the sample cleaning process are as discussed in chapter 1.

Ethylamine (99.0%, Aldrich) and diaminoethane (99.5%, Aldritch) were kept in glass tubes attached to the gas line and allowed into the main chamber by a leak valve. They were purified by several freeze-pump-thaw cycles using a dry ice/acetone mixture, and the purity checked by mass spectrometry. Oxygen (99.998%, Argo was attached to the gas line and used as received.

## 4.4 The interaction of ethylamine with Cu(110) surfaces

### 4.4.1 Clean surface

A clean Cu(110) surface at 293K was exposed to 500L ethylamine vapour at a pressure of 1 x $10^{-7}$ mbar and studied by XPS (figure 4.1). No peaks were found in either the C(1s) or N(1s) XP regions.

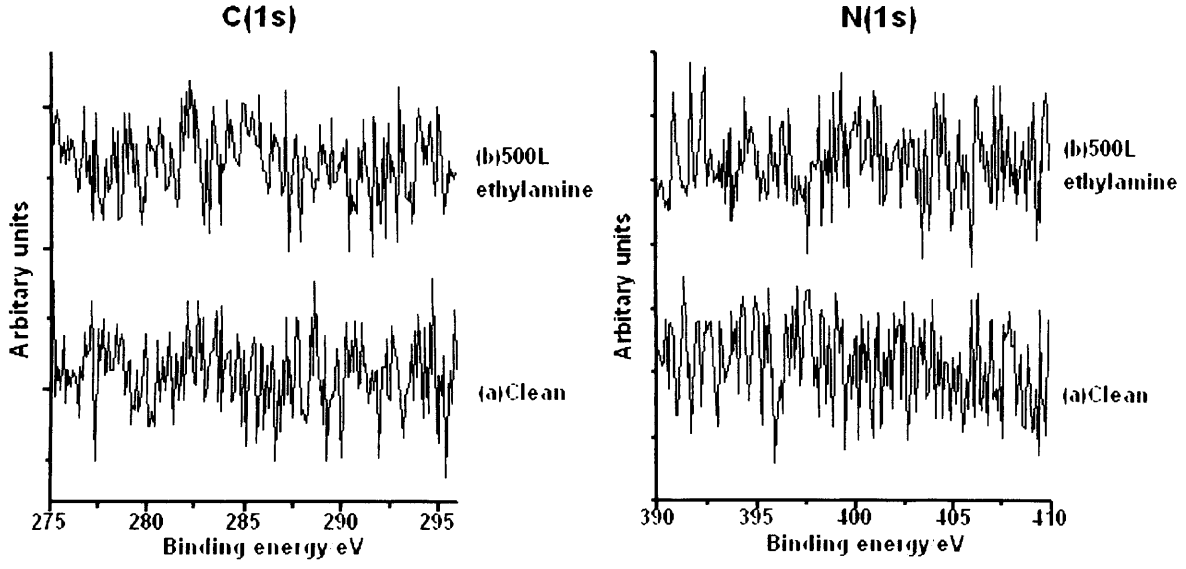


Figure 4.1: C(1s) and N(1s) XP spectra of the reaction of ethylamine vapour with a clean Cu(110) surface at 293K.

STM images of the surface showed no evidence of an adsorbed species (figure 4.2).

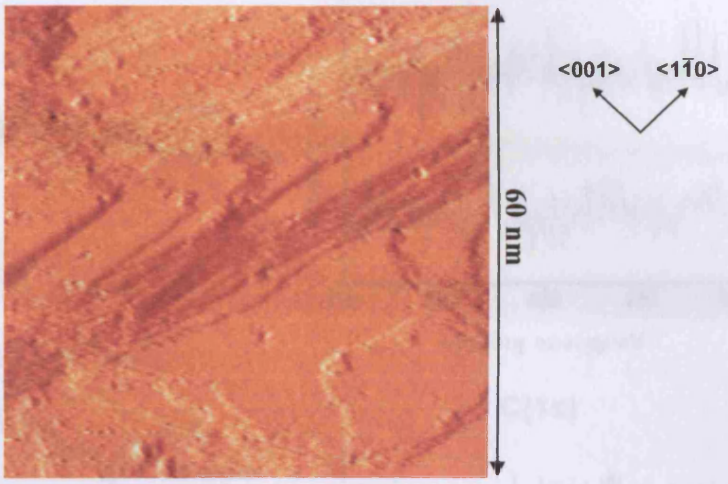


Figure 4.2: Cu(110) surface following exposure to 500L ethylamine at 293K

[$V_s$ = 1.22 V, $I_T$ = 2.65 nA]

### 4.4.2 Partially oxidised surface

An atomically clean Cu(110) surface was exposed to 2L dioxygen, resulting in a peak in the oxygen region of the XP spectrum at 529.7 eV(figure 4.3) with a calculated surface concentration of 3.2 x $10^{14}$ $cm^{-2}$; the equivalent of approximately 3/4 monolayer.

The partially oxidised Cu surface was exposed to 108L ethylamine vapour at a pressure of 1 x $10^{-7}$ mbar , which resulted in the loss of the oxygen peak from the XP spectrum. There was no evidence in the XPS for an adsorbed carbon or nitrogen species after reaction.

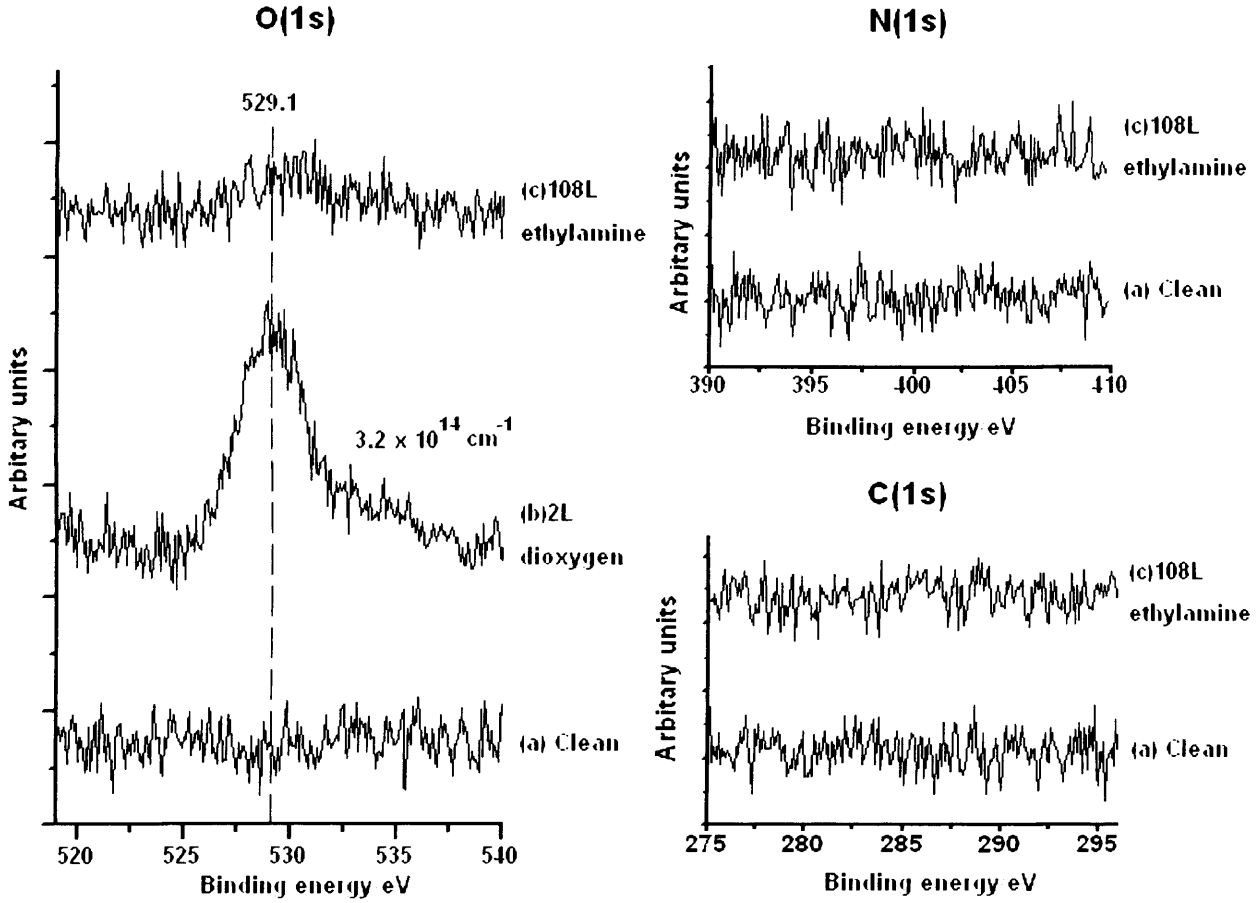


Figure 4.3: O(1s) and C(1s) XP spectra of the reaction of ethylamine vapour with a partially oxidised Cu(110) surface at 293K. (a) clean, (b) after 2L dioxygen, (c) after 108L ethylamine.

An atomically clean Cu(110) surface was exposed to 5L dioxygen at a pressure of 5 x $10^{-8}$ mbar, resulting in the partially oxidised surface shown in the STM image of figure 4.4.

This surface was exposed to ethylamine vapour at a pressure of 1 x $10^{-8}$ mbar and imaged continuously by STM.

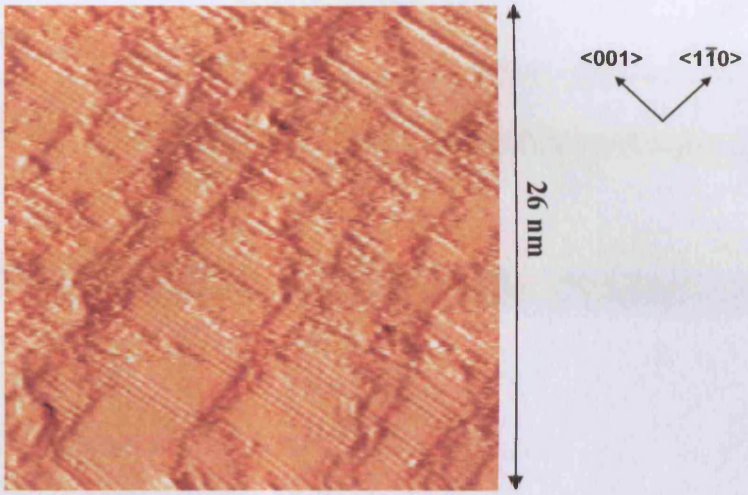


Figure 4.4: Cu(110) surface following exposure to 5L dioxygen
[$V_s$ = 0.22 V, $I_T$ = 3.11 nA]

After approximately 5 minutes of ethylamine exposure, the spacing between Cu-O chains in the (2x1) O(a) islands began to increase from 0.51nm to 0.76nm, forming (3x1) structures similar to those observed previously after reaction of oxidised Cu(110) with pyridine and dimethylamine (figure 4.5 A). While the transformation of unexpanded O(a) islands continued, the islands that had already undergone expansion began to disappear from the image, (Figure 4.5 B – C). By figure 4.5 D, approximately 20 minutes after the start of the ethylamine exposure, the surface appeared devoid of any adsorbed species. In order to confirm the cleanliness of the surface, it was exposed to dioxygen, which resulted in saturation by p(2x1) O(a) structures (figure 4.6).

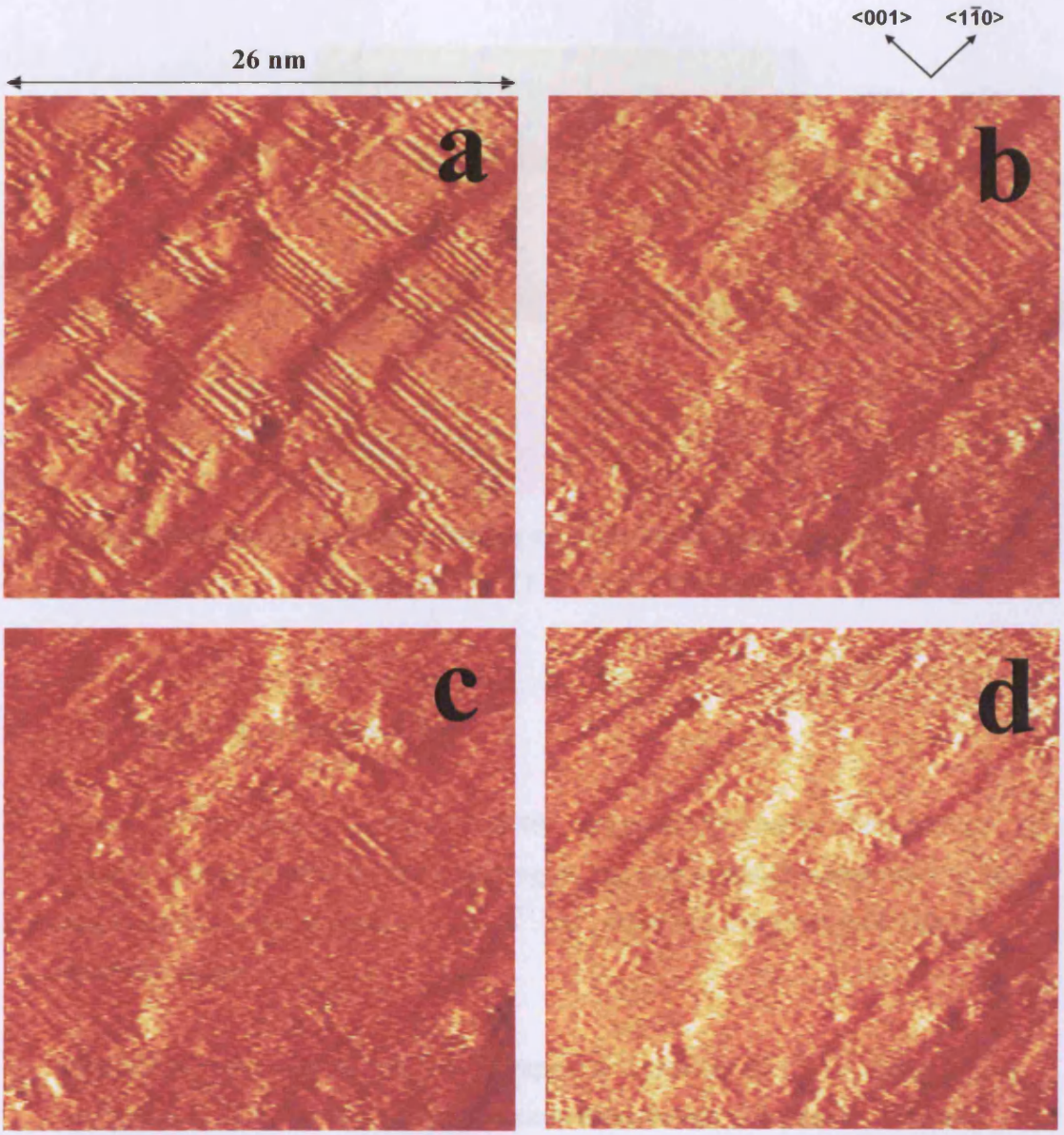


Figure 4.5: A series of STM images detailing the reaction ethylamine vapour with a partially oxidised Cu(110) surface. [$V_S$ = 0.18 V, $I_T$ = 3.10 nA]

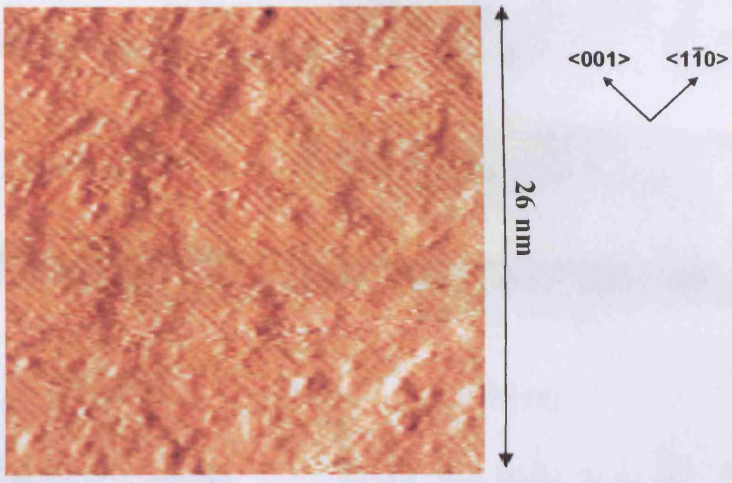


Figure 4.6: Cu(110) surface following exposure to dioxygen after reaction with ethylamine. [$V_S$ = 1.22 V, $I_T$ = 2.67 nA]

### 4.4.3 Completely oxidised surface

A clean Cu(110) surface was exposed to 40L dioxygen. XP spectra of the surface (figure 4.7) shows a peak in the oxygen region, the area of which corresponds to an oxygen surface concentration of 5.4 x $10^{14}$ $cm^{-1}$, equal to a complete monolayer of adsorbed oxygen.

An initial exposure of 200L ethylamine vapour at a pressure of 1 x $10^{-7}$ mbar led to a small decrease in the surface oxygen concentration, but no C(1s) peak. A further dose of 500L at a pressure of 1 x $10^{-6}$ mbar resulted in the loss of almost all the surface oxygen. No peak was found in the C(1s) XP spectrum.

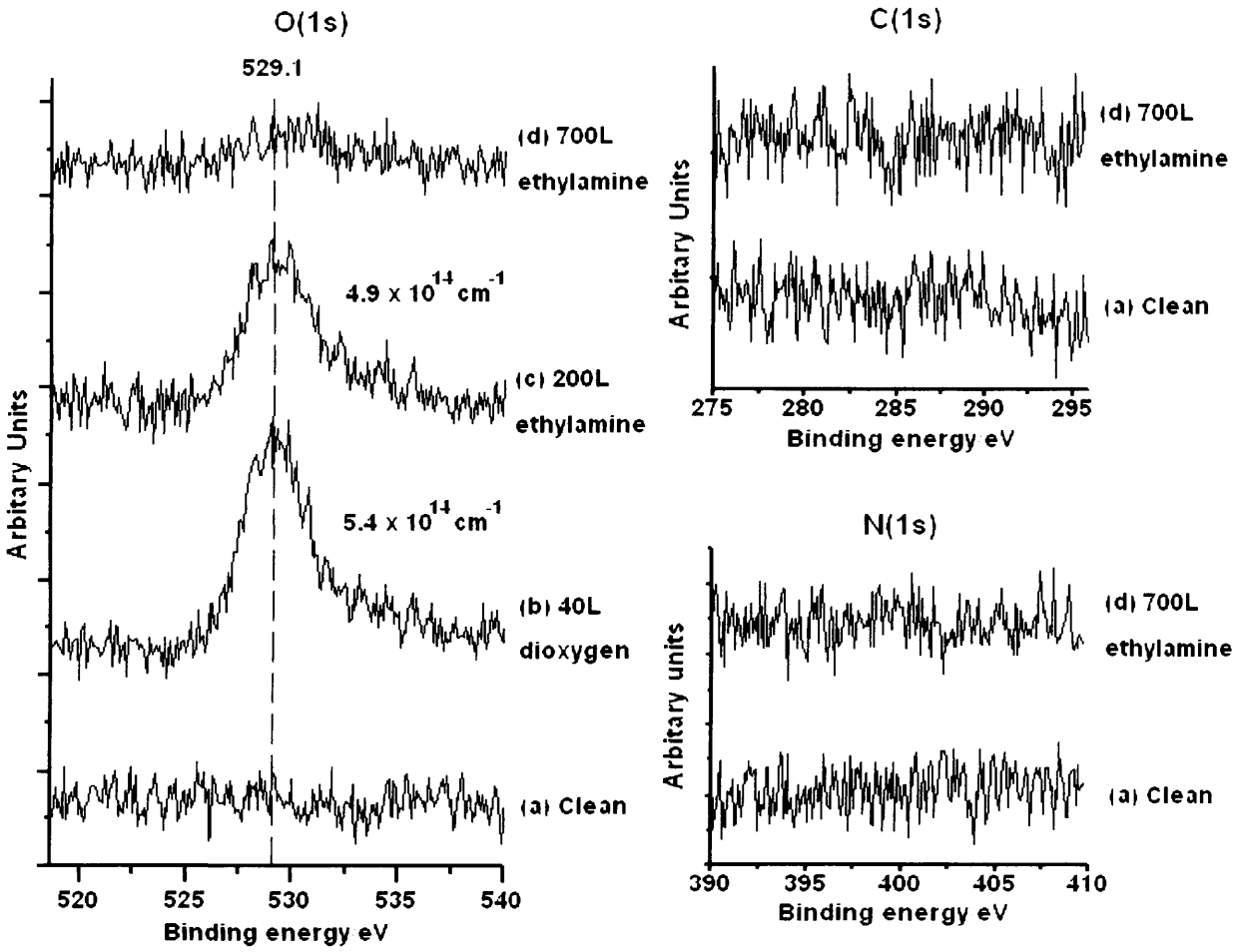


Figure 4.7: O(1s) and C(1s) XP spectra of the reaction of ethylamine vapour with a completely oxidised Cu(110) surface at 293K. (a) clean, (b) after 40L dioxygen, (c) after 200L ethylamine, (d) after a total exposure of 700L ethylamine

A clean Cu(100) surface was exposed to 90L dioxygen, resulting in a surface completely covered in the p(2x1)O(a) structure (figure 4.8 A).

The surface was exposed to ethylamine vapour at a pressure of $5 \times 10^{-7}$ mbar whilst being imaged by STM. As the dosing progressed, image quality degraded, as can be seen in figure 4.8 B. This type of behaviour generally indicates that some kind of process is occurring at the surface. After 15 minutes of exposure to ethylamine vapour, the image quality improved, and STM images now showed an apparently

clean surface (figure 4.8 C). Cleanliness of the surface was proven by a further dose of dioxygen, which resulted in the formation of new (2x1) O(a) islands (figure 4.8 D).

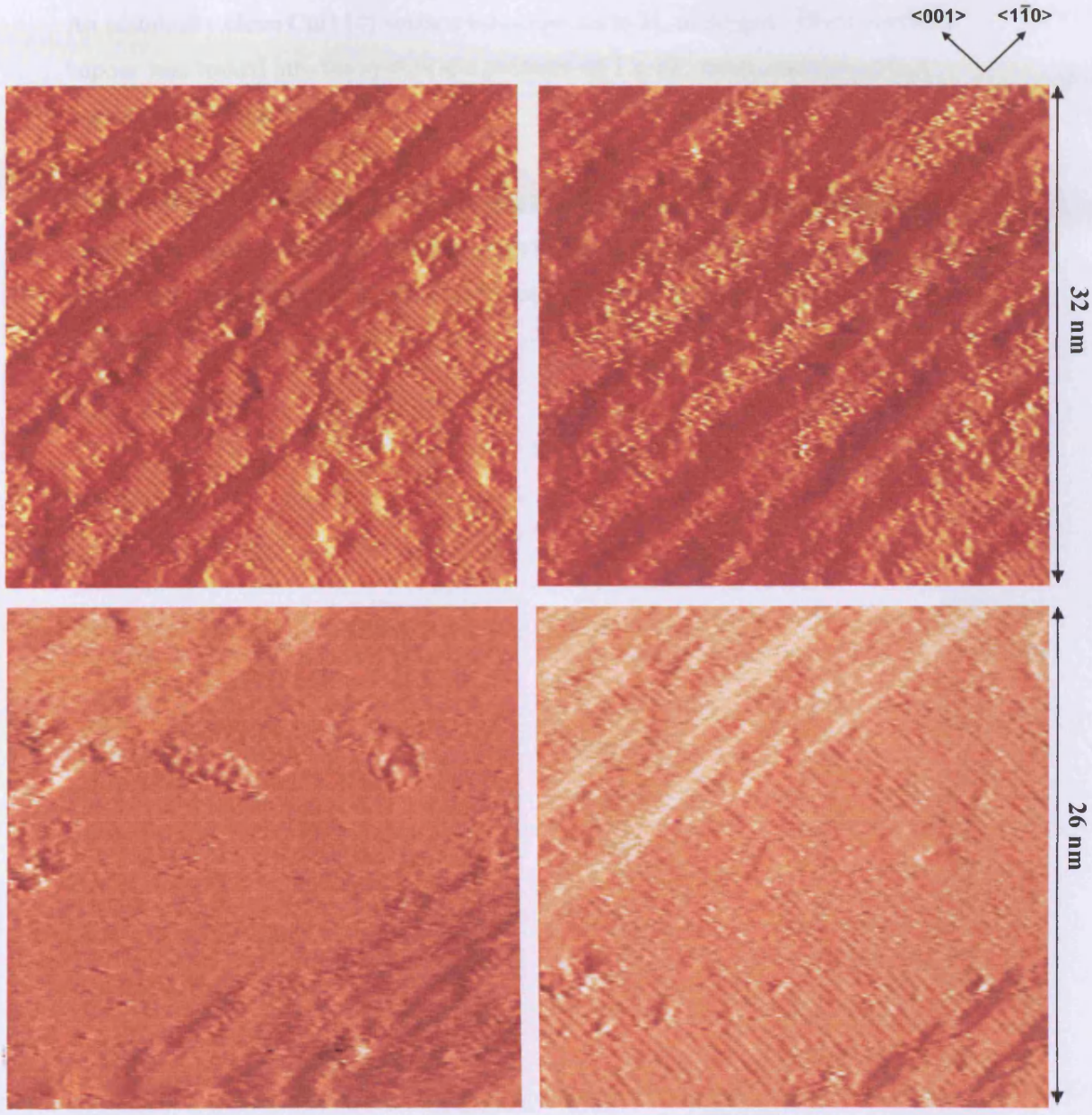


Figure 4.8: A series of STM images detailing the reaction of a fully oxidised Cu(110) surface with ethylamine vapour at 293 K. (a) completely oxidised Cu(110) surface, (b) – (c) during ethylamine dose, (d) after another oxygen dose.

[(a)/(b) $V_s$ = 0.62 V, $I_T$ = 2.70 nA, (c) $V_s$ = 0.62 V, $I_T$ = 3.12 nA, (d) $V_s$ = 0.56 V, $I_T$ = 3.17 nA]

## 4.5 The interaction of diaminoethane ($NH_2CH_2CH_2NH_2$) with partially oxidised Cu(110) surfaces

An atomically clean Cu(110) surface was exposed to 3L dioxygen. Diaminoethane vapour was leaked into the system at a pressure of 1 x $10^{-7}$ mbar, and the surface continuously imaged by STM.

Figure 4.9 shows, in detail, the progressive expansion of the oxygen islands and eventual desorption of all adsorbed species that occurred during the exposure. Each image took approximately 50 seconds to record, and no images were discarded from this series.

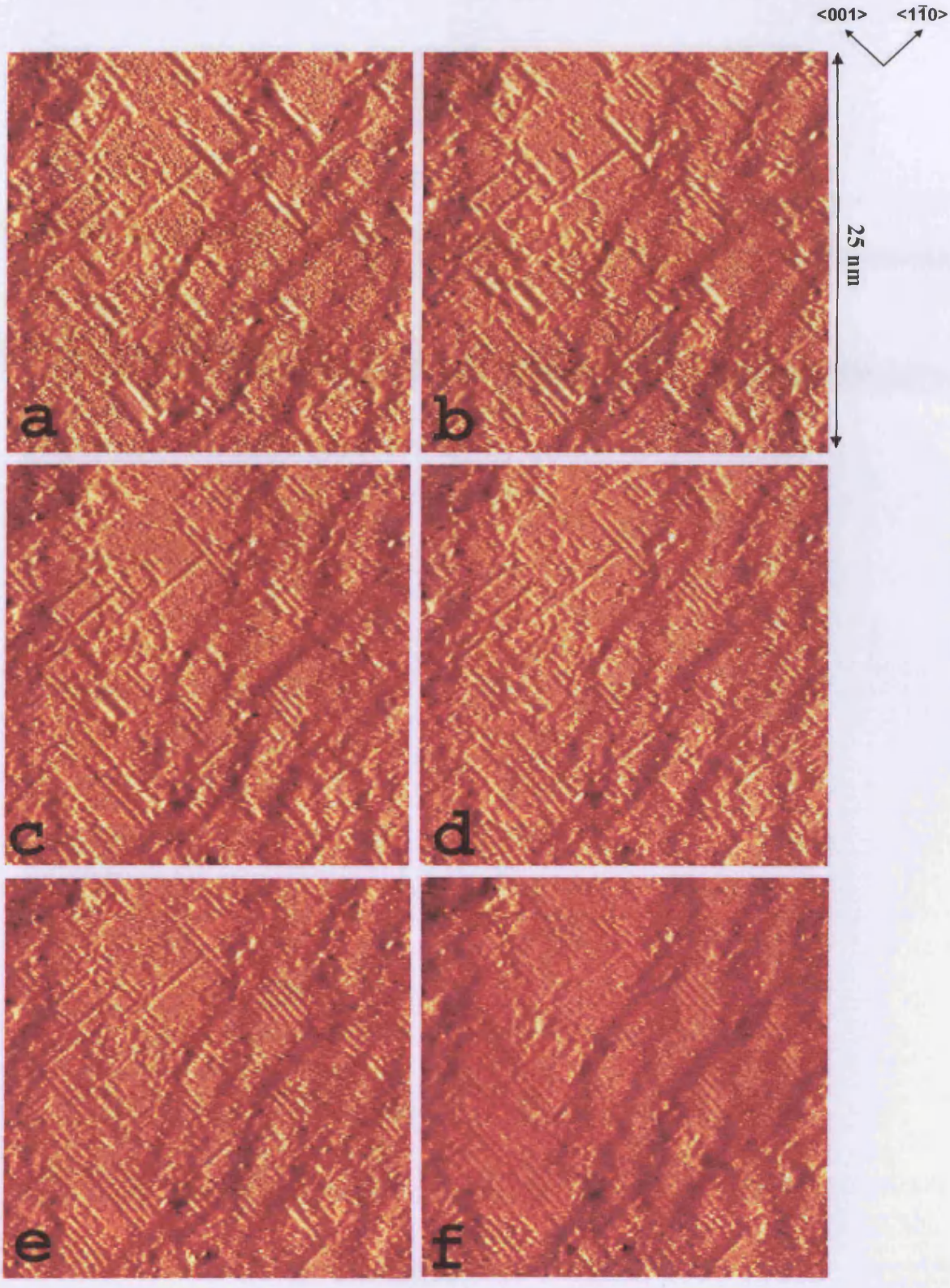
<001>
<1$\bar{1}$0>
25 nm
a
b
c
d
e
f

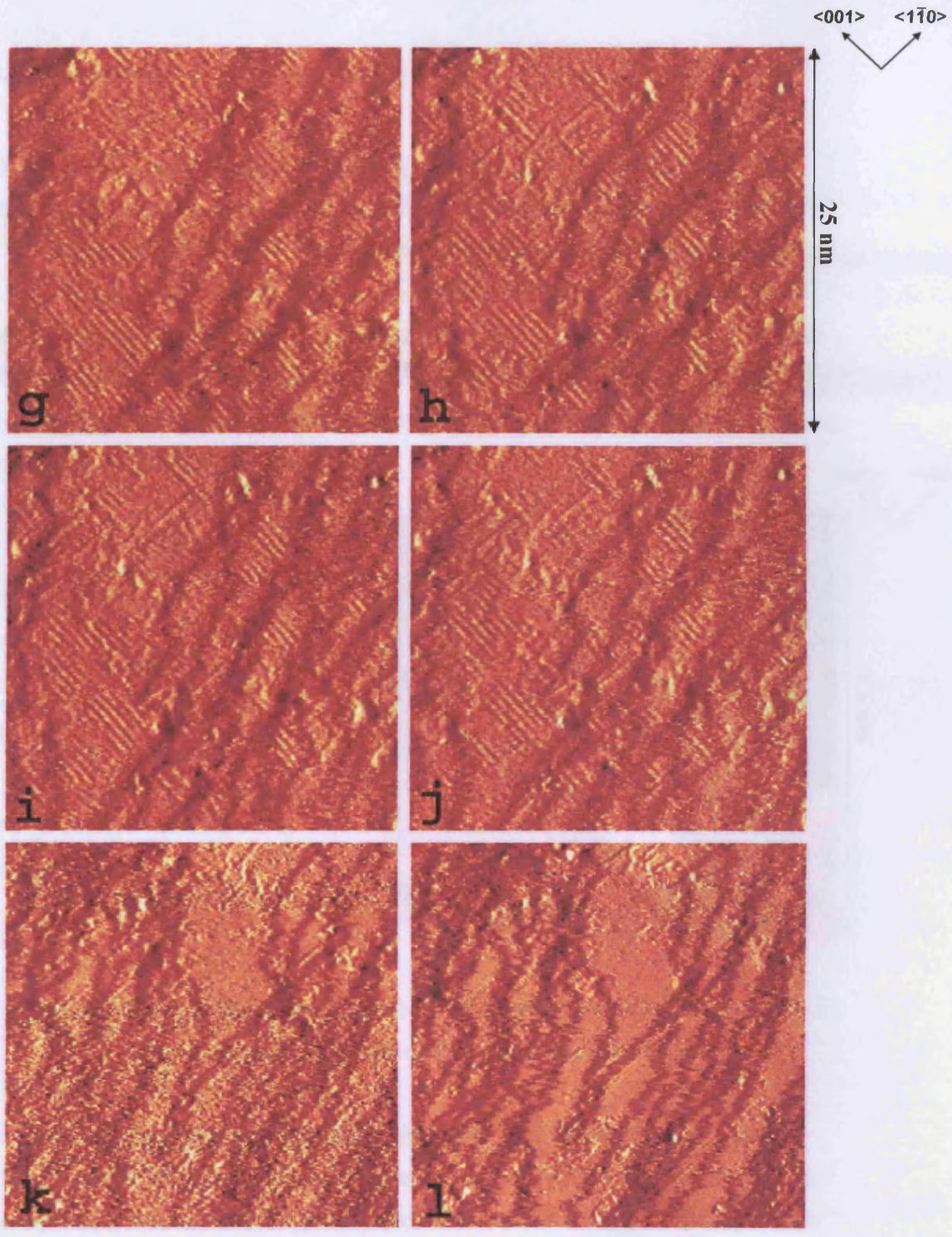


Figure 4.9: Series of STM images detailing the reaction of a partially oxidised Cu(110) surface at 293K with diaminoethylamine vapour at a pressure of 1 x $10^{-7}$ mbar. [$V_S$ = 1.22 V, $I_T$ = 3.10 nA]

## 4.6 Discussion

Upon exposure of a partially oxidised Cu(110) surface to ethylamine vapour, the characteristic Cu-O rows chains of the p(2x1) O(a) islands are seen to expand in the <110> direction, the inter row spacing increasing from 0.51nm to approximately 0.76nm (figure 4.10). The distance between atoms within the chains in the <100> direction remains at 0.36nm. This expanded structure is the familiar (3x1) structure observed during the reaction of pyridine[5] and dimethylamine[5] with oxidised Cu(110) surfaces. Formation of this structure is clearly a common occurrence during the reaction of amines with Cu-O.

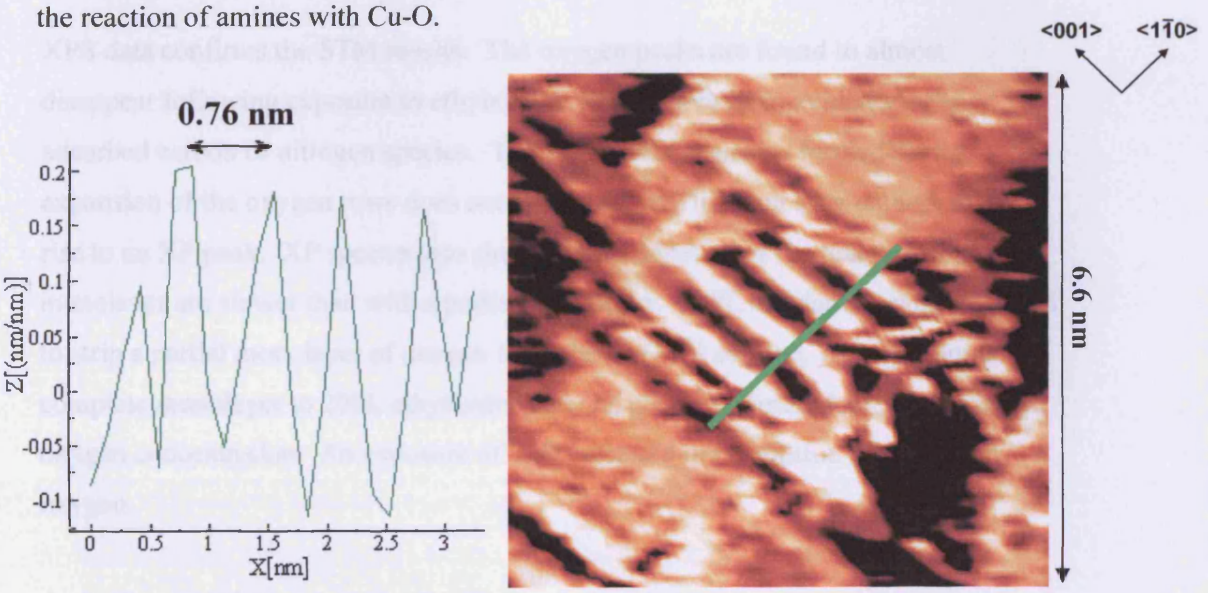


Figure 4.10: Line profile across expanded O(a) structure formed by the reaction of ethylamine with pre-oxidised Cu(110) surface at 293 K.

In contrast to the reaction with pyridine, the reaction of ethylamine with oxidised Cu(110) continues past the formation of an expanded O(a) structure resulting in its desorption, effectively stripping the surface of all adsorbed oxygen, leaving a clean surface in its wake. No new structures were seen to form as the expanded O(a) structures desorbed, as was observed with dimethylamine.

Ethylamine will react with both partial, and complete oxygen monolayers, the latter being an interesting result, since the mechanism for reaction with a partially oxidised surface involves expansion of the oxygen rows to a (3x1) structure. Expansion of the rows for a complete oxygen monolayer is obviously impossible, yet ethylamine will still strip the copper of all surface oxygen. This differs from the pattern observed with the reactions of dimethylamine at oxidised Cu(110), where the initial oxygen concentration directly affected which reactions would occur. Exposure of a completely oxidised surface to dimethylamine resulted only in limited adsorption, and no reaction with the oxygen monolayer was observed.

XPS data confirms the STM results. The oxygen peaks are found to almost disappear following exposure to ethylamine, whilst there is no evidence of an adsorbed carbon or nitrogen species. The intermediate species formed during expansion of the oxygen rows does not have a surface lifetime long enough to give rise to an XP peak. XP spectra also show that the kinetics of the reaction with a full monolayer are slower than with a partial monolayer. 108L ethylamine was sufficient to strip a partial monolayer of oxygen from the Cu(110) surface, yet exposure of a complete monolayer to 200L ethylamine only resulted in a small decrease in surface oxygen concentration. An exposure of 700L resulted in desorption of almost all oxygen.

As in the case of the reactions of aniline and dimethylamine with oxidised Cu surfaces, the oxygen-containing leaving group is almost certainly $H_2O$. It has been shown that at 110K, ethylamine will react with oxygen adsorbed at Ag(110) surfaces[1], forming a hydroxy group, which, at higher temperatures, will either react with another hydroxy group or an amine/amide species, forming water, which desorbs. This is also a possible mechanism for the reaction at Cu(110) surfaces, and is detailed in the following equations.

$$CH_3CH_2NH_2 + O_{(a)} \rightarrow CH_3CH_2NH_{(a)} + OH_{(a)} \qquad (1)$$

Upon formation of the hydroxyl group (equation 1), the reaction can take different paths. Two hydroxyl groups can combine to form water and a lone oxygen species, which proceeds to react with an adsorbed amide group, resulting in a new hydroxyl species (equations 2 – 3). The cycle then reverts back to equation 1.

$$2\ OH_{(a)} \rightarrow H_2O_{(g)} + O_{(a)} \quad (2)$$

$$O_{(a)} + CH_3CH_2NH_{(a)} \rightarrow OH_{(a)} + CH_3CH_2N_{(a)} \quad (3)$$

The second possible path involves the adsorbed hydroxy groups reacting directly with the adsorbed amine or amide species (equations 4 – 5). Both reaction pathways result in the formation of water, which desorbs, and eventually $CH_3CH_2N$, which is either not stable on the surface, or undergoes another reaction into a species which desorbs.

$$OH_{(a)} + CH_3CH_2NH_{2(a)} \rightarrow H_2O_{(g)} + CH_3CH_2NH_{(a)} \quad (4)$$

$$OH_{(a)} + CH_3CH_2NH_{(a)} \rightarrow H_2O_{(g)} + CH_3CH_2N_{(a)} \quad (5)$$

It is also possible that the amide species does not react any further with adsorbed oxygen or hydroxyl groups. Instead, it may undergo a β-hydride elimination reaction, forming $CH_3CHNH$ (figure 4.11). The hydrogen formed would then be free to react with adsorbed hydroxyl groups and desorb as water. This third pathway is detailed in equations 6 and 7.

$$CH_3CH_2NH_{(a)} \rightarrow CH_3CHNH_{(g)} + H_{(a)} \quad (6)$$

$$H_{(a)} + OH_{(a)} \rightarrow H_2O_{(g)} \quad (7)$$

It is not possible to determine which reactions are occurring at the surface using STM and XPS techniques. Reactions similar to those shown in equations 2-5, which lead to the formation of $CH_3CH_2N$, have been previously observed at Ag surfaces. However the β-hydride elimination mechanism is analogous to the reaction proposed for the desorption of $(CH_3)_2N_{(a)}$ from the surface after reaction of dimethylamine with partially oxidized Cu(110). Also, the imides formed by the reaction of other

amines studied by the group (ammonia and aniline) with oxidized Cu(110) have both been stable on the surface at room temperature. If an imide is formed here, it goes against this trend, as it is clearly not stable at 293K.


Figure 4.11: β-elimination reaction of $CH_3CH_2NH$ chemisorbed at a Cu(110) surface.

STM images of the reaction of diaminoethane with an oxidised Cu(110) surface show exactly the same pattern of O(a) row expansion to a (3x1) structure (figure 4.12), followed by desorption. The extra amino moiety, therefore, does not appear to affect the reaction. It is not possible to determine if it has an effect on the kinetics as there are too many variables, but there is no obvious difference. The (3x1) O(a) structure formed by both species has approximately the same lifetime of between 3 and 8 minutes.

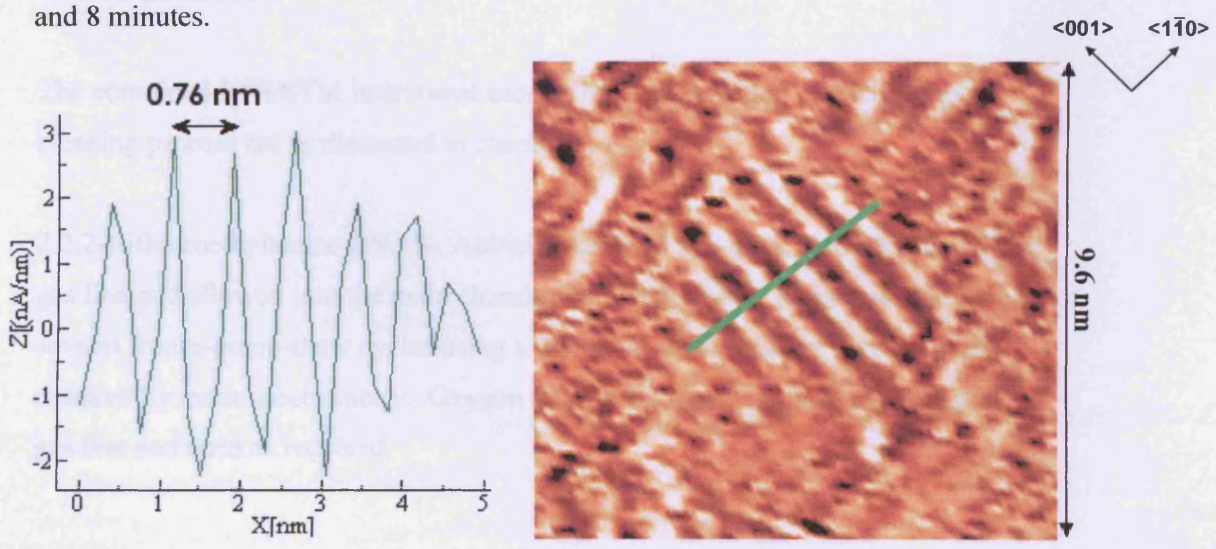


Figure 4.12: Line profile across expanded O(a) structure formed by the reaction of diaminoethane vapour with a pre-oxidised Cu(110) surface at 293K.

## 4.7 The interaction of 2,2,2-trifluoroethylamine with Cu(110) surfaces

### 4.7.1 Introduction

The differences observed in the reactions of amines; aniline, dimethylamine, pyridine and ethylamine could be due to two main factors, steric and the gas phase basicity of those compounds.

Our interest lies in 2,2,2-trifluoroethylamine due to the fact that it is structurally similar to ethylamine, yet has a much lower gas-phase basicity; 812.9 KJ $mol^{-1}$, as opposed to 870.0 kJ $mol^{-1}$. This is the lowest basicity of all amine compounds studied by the group at Cu surfaces thus far, and so the reaction of trifluoroethylamine at Cu(110) may help determine what role, if any, the gas phase basicity of these compounds plays in their interaction with oxidised Cu surfaces, with no change in steric properties.

### 4.7.2 Experimental

The combined XPS/STM instrument used in this investigation and the sample cleaning process are as discussed in chapter 1.

2,2,2-trifluoroethylamine (99.5%, Aldrich) was kept in a glass tube attached to the gas line and allowed into the main chamber by a leak valve. It was purified by several freeze-pump-thaw cycles using a dry ice/acetone mixture, and the purity checked by mass spectrometry. Oxygen (99.998%, Argo Ltd) was attached to the gas line and used as received.

### 4.7.3 Clean surface

A clean Cu(110) surface was exposed to 300L 2,2,2-trifluoroethylamine vapour at 293K. The STM images showed no sign of an adsorbed species (figure 4.13)

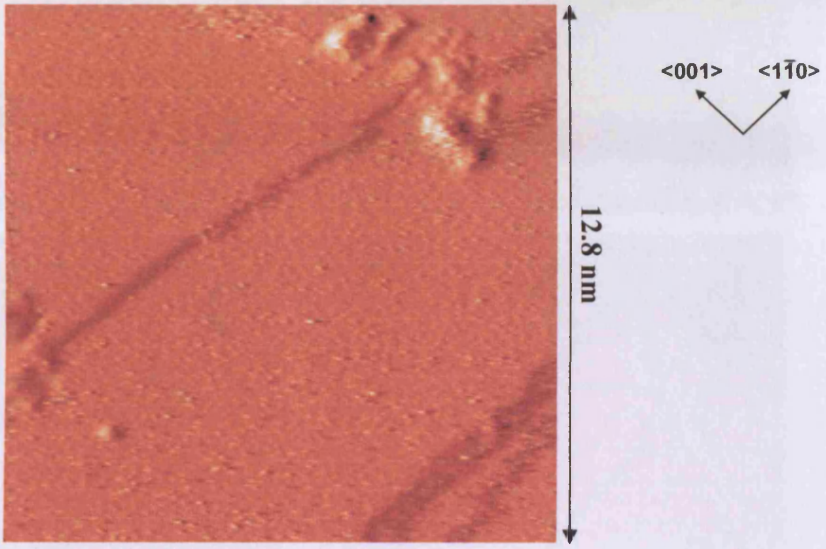


Figure 4.13: Cu(110) surface following exposure to 300L trifluoroethylamine vapour at 293K. [$V_S$ = 0.68 V, $I_T$ = 2.65 nA]

### 4.7.4 Low O(a) coverage

An atomically clean Cu(110) surface was exposed to 1L dioxygen and imaged by STM. The resulting image, figure 4.14 A, shows a partially oxidised surface with a low concentration of p(2x1)O(a) islands.

The oxidised surface was exposed to 2,2,2-trifluoroethylamine vapour at a pressure of 5 x $10^{-8}$ mbar whilst being imaged by STM (figure 4.14 B-F). As the exposure progresses, the O(a) islands are seen to disappear. By image F, the surface appears clean. There is a time period of approximately 50 seconds between each image in this series, and no images were omitted.

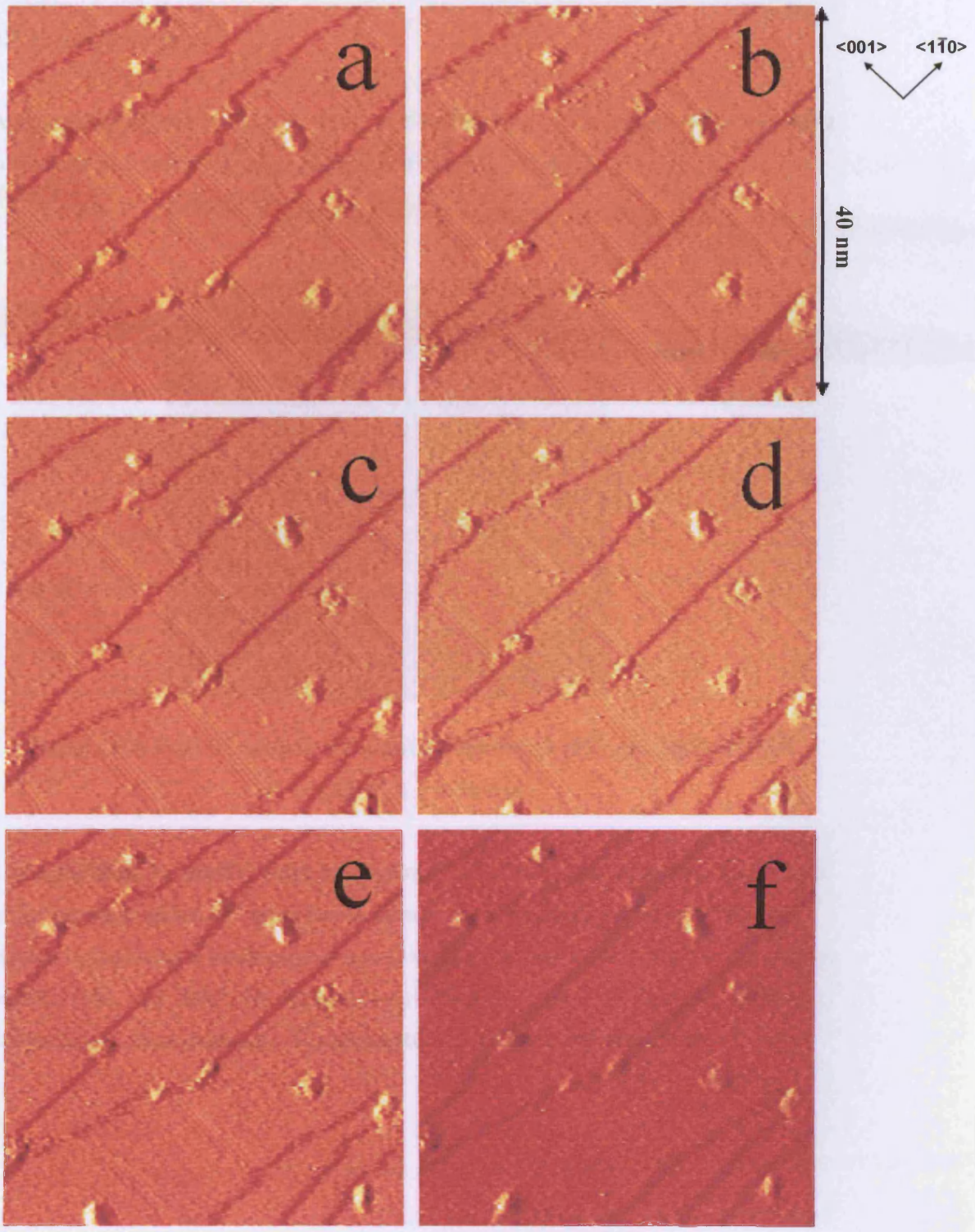


Figure 4.14: A series of STM images detailing the reaction of a partially oxidised Cu(110) surface at 293K with 2,2,2 trifluoroethylamine vapour.

[$V_s$ = 0.64 V, $I_T$ = 2.10 nA]

### 4.7.5 O(a) monolayer

A clean Cu(110) surface was exposed to 40L dioxygen. STM images of the resulting surface show a complete p(2x1)O(a) monolayer (figure 4.15).

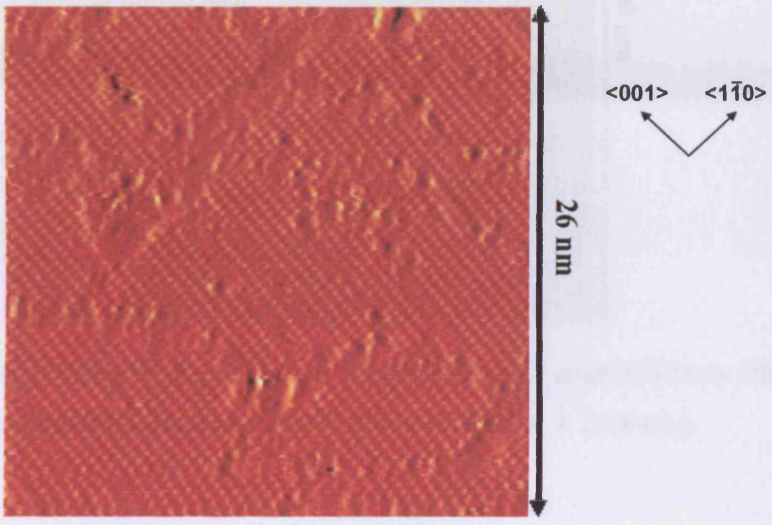


Figure 4.15: Cu(110) surface at following exposure to 40L dioxygen at 293K.
[$V_s$ = 0.53 V, $I_T$ = 2.40 nA]

The completely oxidised surface was exposed 2,2,2-trifluoroethylamine vapour at an initial pressure of 2 x $10^{-8}$ mbar for 25 minutes whilst being imaged by STM. No change in the oxygen structure, nor any desorption was observed. Further exposures of 60L, 120L and 1800L did not lead to a reaction. Figure 4.16 shows the surface following the final exposure. The complete p(2x1)O(a) monolayer remains.

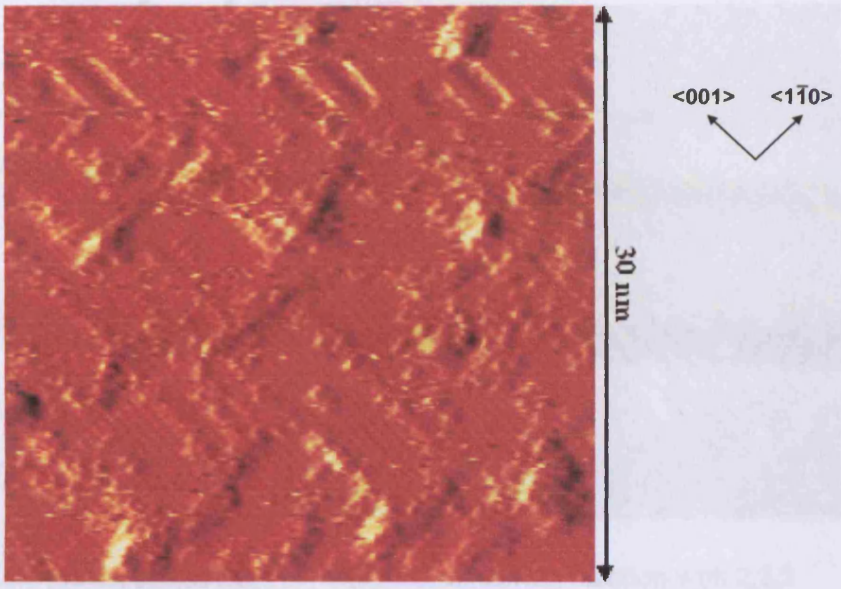


Figure 4.16: Oxidised Cu(110) surface following exposure to approximately 2000L 2,2,2 trifluoroethylamine at 293K. [$V_S$ = 0.78 V, $I_T$ = 2.98 nA]

### 4.7.6 Discussion

The reaction of 2,2,2 trifluoroethylamine with oxidised Cu(110) has both similarities and discrepancies with the reaction of ethylamine with the same surfaces. Both molecules readily react with O(a) islands, effectively 'stripping' the surface of all surface oxygen. However, while STM images show that ethylamine forms an intermediate species wherein the p(2x1)O(a) islands expand, STM images show no evidence of an expanded oxygen structure(figure 4.17), nor any other intermediate species, following the exposure of p(2x1)O(a) islands to trifluoroethylamine vapour. Instead, the oxygen islands appear to simply desorb.

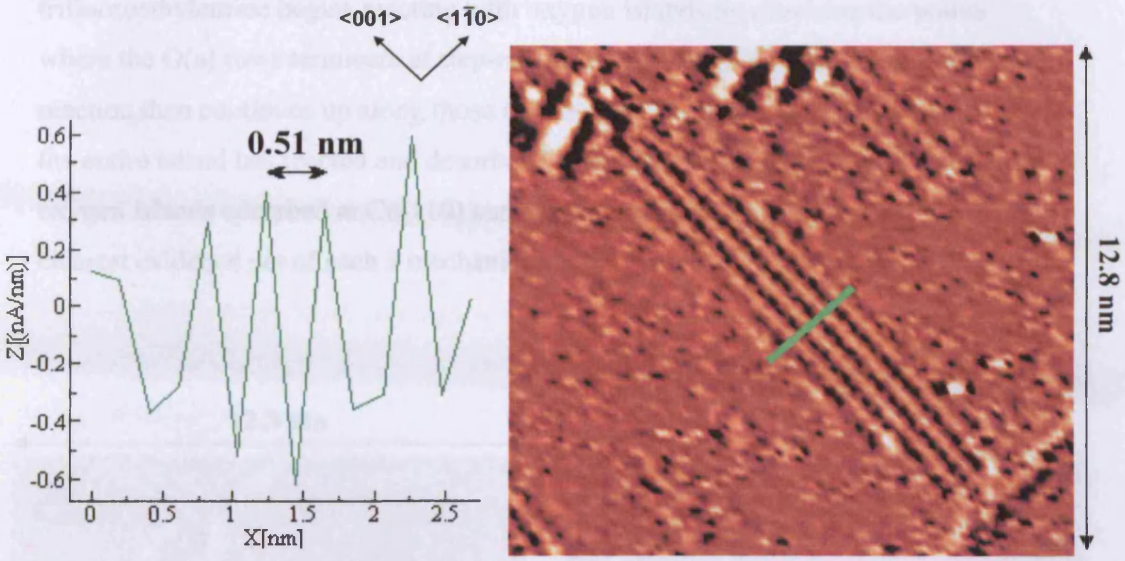


Figure 4.17: Line profile across Cu(110)-O(a) islands during reaction with 2,2,2 trifluoroethylamine at 293 K. [$V_S$ = 0.64 V, $I_T$ = 2.10 nA]

Figure 4.18 contains a series of zoomed-in STM images that detail this desorption process. Image (a) shows two p(2x1) O(a) islands; one five adsorbate rows wide, extending across the entire width of the terrace, the other a smaller island consisting of only two oxygen/added copper rows, but still extending from step to step across the terrace. At this point, the surface was being exposed to 2,2,2 trifluoroethylamine vapour at a pressure of 5 x $10^{-8}$ mbar. Image (b) shows the surface approximately 50 seconds later. The larger island has not undergone any changes; however the smaller island no longer extends from step to step. Oxygen atoms have desorbed from one end of both chains, shortening the island by 3.3 nm. 50 seconds later, image (c) shows that the chains have lost a further 3.5 nm in length, while the larger island remains unchanged. Image (d) was taken a further 100 seconds into the exposure. The smaller island has now almost completely desorbed, and the larger island is now also reacting with the trifluoroethylamine. The two outermost rows on the left of the image are desorbing, causing a shortening of the rows from the bottom step up, whilst the single outermost row on the right side of the oxygen island is desorbing from the top terrace downwards. By the next image, stored 50 seconds later, both islands have completely desorbed (image (f)). These images clearly show that the

trifluoroethylamine begins reacting with oxygen islands by attacking the points where the O(a) rows terminate at step-edges (and possibly other defects). The reaction then continues up along those chains that are on the edges of the island until the entire island has reacted and desorbed. Ammonia is believed to react with oxygen islands adsorbed at Cu(110) surfaces in a similar manner[6-12], but this is the clearest evidence yet of such a mechanism.

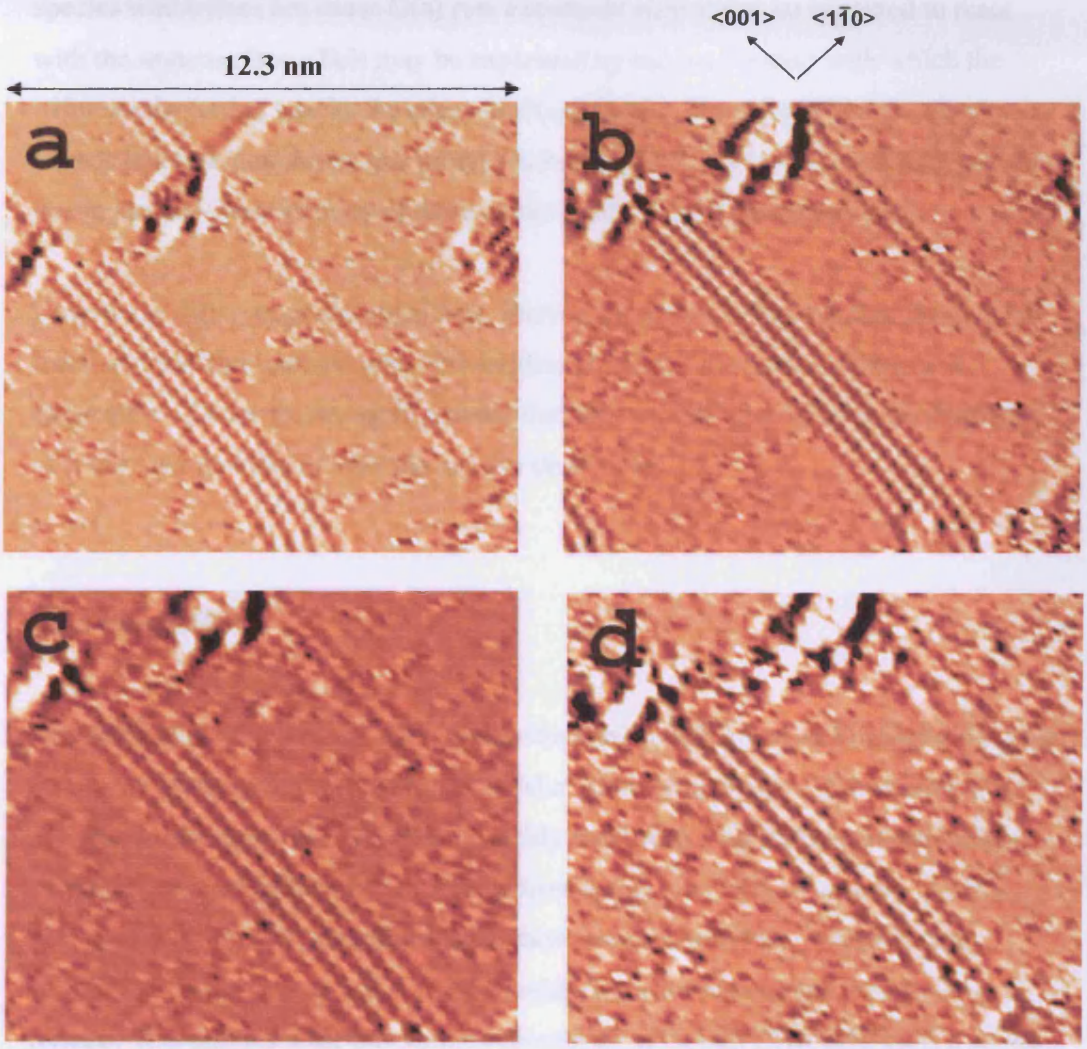


Figure 4.18: Zoomed-in view of the progressive desorption of two Cu(110)-O(a) islands during reaction with 2,2,2 trifluoroethylamine vapour at 293K.

[$V_s$ = 0.64 V, $I_T$ = 2.10 nA]

The other main difference between ethylamine and trifluoroethylamine lies in their reaction with fully oxidised Cu surfaces. Both STM and XPS show that ethylamine will react with a full oxygen monolayer, resulting in a clean Cu surface. STM images obtained during the exposure of a fully oxidised Cu surface to trifluoroethylamine indicate that no reaction occurred, even following a very large dose. In many respects, this is a curious result. If a species that causes expansion of the oxygen rows can undergo reaction with a full oxygen monolayer, then a similar species which does not cause O(a) row expansion might also be expected to react with the same surface. This may be explained by the mechanism with which the trifluoroethylamine attacks the edges of O(a) islands. Since there are no edges to the islands in a full monolayer, this process is hampered. Another possible explanation lies in the gas-phase basicity of these compounds. This is discussed later.

Despite the differences discussed here, there is no reason to believe that the general reactions of trifluoroethylamine with oxidised Cu(110) deviates with those of ethylamine. Certainly, we again assume that the main driving force is the formation of water, and that that is what the oxygen desorbs as.

## 4.8 Conclusions

The reactions of ethylamine and diaminoethylamine with clean and oxidised Cu(110) have been investigated with XPS and STM at room temperature. Ethylamine does not react with clean Cu(110) but will readily react with a partially oxidised surface causing expansion of the oxygen islands from p(2x1) to (3x1) structures. After a period of no more than several minutes, these structures desorb, resulting in an atomically clean surface. Upon reaction with chemisorbed oxygen, $CH_3CH_2N_{(a)}$ is formed. It is unclear what this species desorbs as, although $CH_3CHNH_{(g)}$ is a strong possibility. Ethylamine reacts with fully oxidised Cu(110), stripping the surface of all oxygen. No reconstruction of the oxygen lattice occurs in this case.

The extra amino moiety possesed by diaminoethane does not appear to have any effect on its interaction with oxidised Cu(110) as the reaction progressed in the exact same way as was observed with ethylamine.

The interaction of 2,2,2-trifluoroethylamine with clean, partially oxidised and fully oxidised Cu(110) has also been investigated by STM at room temperature. Both clean and fully oxidised Cu(110) surfaces are inert to trifluoroethylamine, however the molecule reacts with a partially oxidised surface, causing desorption of all surface oxygen without any reconstruction of the oxygen islands and resulting in a clean surface.

## 4.9 References

[1] Madix, R.J.; Thornburg, D. M. *Surf. Sci.* **1990**, *226*, 61

[2] Gardin, D. E.; Somarjai, G. A. *J. Phys. Chem*, **1992**, *96*, 9424

[3] Pearlstine, K. A.; Friend, C. M. *J. Am. Chem. Soc.* **1986**, *108*, 5837.

[4] Kang, D. H.; Trenary, M. *Surf. Sci.* **2000**, *470*, L13.

[5] Carley, A.F.; Davies, P.R.; Edwards, D.; Jones, R.V; Parsons, M. *Topics in Catalysis*, **2005**, *36*, 21

[6] Davies, P. R.; Keel, J. M. *Surf. Sci.* **2000**, *469*, 204

[7] Carley, A. F.; Davies, P. R.; Roberts, M. W. *Catal. Lett.* **2002**, *80*, 25.

[8] Carley, A. F.; Davies, P. R.; Jones, R. V.; Harikumar, K. R.; Kulkarni, G. U.; Roberts, M. W. *Top. Catal.* **2000**, *11*, 299.

[9] Carley, A. F.; Davies, P. R.; Roberts, M. W.; Vincent, D. *Top. Catal.* **1994**, *1*, 35.

[10] Afsin, B.; Davies, P. R.; Pashusky, A.; Roberts, M. W.; Vincent, D. *Surf. Sci.* **1993**, *284*, 109.

[11] Afsin, B.; Davies, P. R.; Pashuski, A.; Roberts, M. W. *Surf. Sci.* **1991**, *259*, L724.

[12] Carley, A. F.; Davies, P. R.; Harikumar, K. R.; Jones, R. V.; Kulkarni, G. U.; Roberts, M. W. *Top. Catal.* **2001**, *14*, 101.

# Chapter 5

## Trends in the reactions of amines with oxidised Cu(110) surfaces

Table 1 gives the gas-phase basicity of the amines studied in this thesis, together with that of other amine compounds previously studied by the group.

| **Compound** | **Gas-phase basicity/ kJ mol$^{-1}$** |
|---|---|
| Diaminoethane | 912.5 |
| Pyridine | 898.1 |
| Dimethylamine | 896.5 |
| Ethylamine | 878.0 |
| Aniline | 850.6 |
| Ammonia | 819.0 |
| Trifluroethylamine | 812.9 |

Table 5.1: the gas-phase basicity of amine compounds discussed in this thesis.

The gas phase basicity is defined as the negative of the Gibbs energy change associated with the reaction $B + H^+ \rightarrow BH^+$ in the gas phase.

When these basicity values are compared to the results of the reactions of these amines with pre-oxidised Cu(110) surfaces, certain trends become apparent. The first, and clearest of these trends concerns the transformation of normal p(2x1)O(a) islands into expanded (3x1) structures. The three compounds with the lowest basicity (trifluroethylamine, ammonia and aniline) do not cause expansion of the adsorbed oxygen lattice, whereas compounds with a basicity of 878.0 $KJmol^{-1}$ and greater (ethylamine, dimethylamine, pyridine and diaminoethane) all do. A possible explanation for this is that the higher basicity allows for stronger bonds to be formed and hence give out enough energy to allow the species to force the oxygen rows apart.

It also appears that, of the compounds which cause expansion of the oxygen rows, the higher the basicity of the compound, the more stable the product formed following reaction with chemisorbed oxygen. Exposure to ethylamine results in expanded oxygen islands that are stable for several minutes, but no other species is witnessed. Dimethylamine, with its higher gas phase basicity also causes expansion of the oxygen rows, but another structure is observed following desorption of the oxygen which is again stable on the surface for several minutes. Pyridine, which has a basicity higher than both ethylamine and dimethylamine, forms an expanded oxygen structure, which is completely stable at room temperature.

There is however a discrepancy in this trend, as the compound with the highest gas phase basicity, diaminoethane, forms an expanded O(a) structure that is only stable for minutes. A probable explanation for this is that only one of the amino moieties reacts with the surface, and that despite the higher basicity, in this case it essentially behaves exactly the same as ethylamine, which is indeed what the results show.

The three amines with the lowest basicities will not react with a complete oxygen monolayer, although the trend here for compounds with a higher basicity is not as clear. The only compound in the top half of the table to not react at all with a full O(a) monolayer is pyridine, which is also the only amine with a high basicity to form a stable chemisorbed product on Cu(110) at 293K. Both ethylamine and

diaminoethane will readily react with a Cu(110) surface saturated in oxygen, resulting in a clean surface, whereas a limited reaction occurs when such a surface is exposed to dimethylamine vapour. It is probable that dimethylamine can only adsorb at step-edges in this case, in a similar manner to that seen when ammonia reacts with a full oxygen monolayer at Cu(110) at 375K.

Thus, the gas-phase basicity values may explain the differences in the reaction of ethylamine and trifluoroethylamine with oxidised Cu(110) surfaces. Although both molecules share certain structural characteristics, there is a marked difference in their basicity. Ethylamine has a gas-phase basicity of 878.0 $KJmol^{-1}$, 65.1 $KJmol^{-1}$ higher than that of trifluoroethylamine, which has the lowest basicity of all the amines studied thus far. Following the trends highlighted here, ethylamine, with its high basicity, causes expansion of the chemisorbed oxygen lattice, and can react with a complete oxygen monolayer. Trifluoroethylamine however, with its low basicity, does not cause O(a) row expansion, and cannot react with a full O(a) monolayer.

Another clear trend can be seen when the abilities of these compounds to undergo a β-elimination reaction are considered. As previously mentioned, a β-elimination mechanism may be responsible for the desorption of the chemisorbed products formed by the reactions of dimethylamine and ethylamine with partially oxidised Cu(110). In fact, every amine studied thus far that contains β hydrogen atoms that could undergo such an elimination (dimethylamine, ethylamine, diaminoethane and 2,2,2 trifluoroethylamine) do not form a stable chemisorbed bond to the surface at room temperature. The other three amines either do not contain β hydrogen atoms (ammonia), or the carbon atoms they are bonded to are part of a Π system (aniline and pyridine), and as such cannot undergo a β-elimination reaction, as a C-H bond in a hybridised system has a higher strength than an aliphatic carbon. The chemisorbed products formed by these compounds at oxidised Cu(110) surfaces are stable for days at room temperature. These results suggest that the β-elimination mechanism proposed for the reaction of ethylamine with oxidised Cu(110) is the pathway being followed, and that an imide is not formed.

# *Chapter 6*

## *The interaction of 4,4-diaminobenzophenone with Cu(110) surfaces*

### 6.1 Introduction

The interaction of 4,4-diaminobenzophenone (figure 6.1) with clean Cu(110) surfaces has been investigated by STM and XPS at room temperature. Diaminobenzophenone is a solid at room temperature, unlike the other molecules studied in this thesis. It was chosen in order to compare the amine functionality of larger organic molecules with the simpler amines.

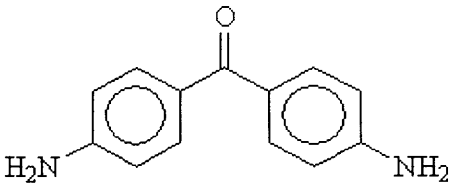


Figure 6.1: Diaminobenzophenone

## 6.2 Experimental

The combined XPS/STM instrument used in this investigation and the sample cleaning process are as discussed in chapter 1.

4,4-diaminobenzophenone (98%, Aldrich) was placed in a Knudsen cell, which was heated to 453K, then opened to the system for varying amounts of time depending on the required exposure.

## 6.3 XPS studies of the interaction of 4,4-diaminobenzophenone with Cu(110) surfaces

An atomically clean Cu(110) surface at 293 K was exposed to 4,4 diaminobenzophenone from a Knudsen cell set to a temperature of 453K for 2 minutes and studied by XPS (figure 6.2). Extensive adsorption occurred, resulting in a peak in the C(1s) spectrum at 283.5 eV with an area equivalent to a surface concentration of $2.8 \times 10^{15}$ $cm^{-2}$, corresponding to $2.2 \times 10^{14}$ benzophenone molecules $cm^{-2}$. Peaks were also present in the N(1s) spectra at 398.1 eV, with an area equal to $4.3 \times 10^{14}$ $cm^{-2}$, and the O(1s) spectra at 530.4 eV, the area of which was equal to $2.6 \times 10^{14}$ $cm^{-2}$. The C:N ratio, therefore, is approximately 13:2, whilst the N:O ratio is approximately 2:1. These are in agreement with the expected stoichiometry.

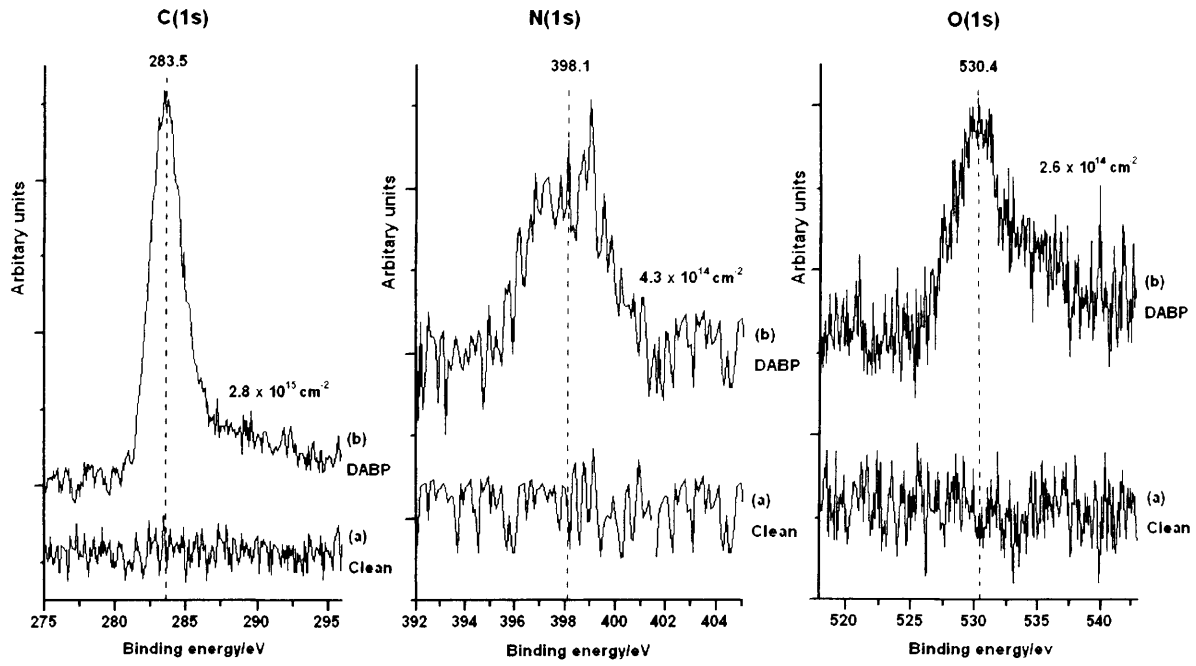


Figure 6.2: C(1s), N(1s) and O(1s) XP spectra of the chemisorption of 4,4 diaminobenzophenone at a Cu(110) surface at 293 K. (a) clean, (b) after exposure to diaminobenzophenone dosed from a Knudsen cell at 453 K.

## 6.4 STM studies of various coverages of diaminobenzophenone adsorbed at Cu(110) surfaces

Atomically clean Cu(110) surfaces at 293K were exposed to varying amounts of diaminobenzophenone via a Knudsen cell. XPS was used to determine the surface carbon concentration following each exposure. Three concentrations were then studied by STM in order to investigate the effects of surface concentration on the structure of the adsorbate. The C(1s) spectra of the chosen concentrations are shown in figure 6.3.

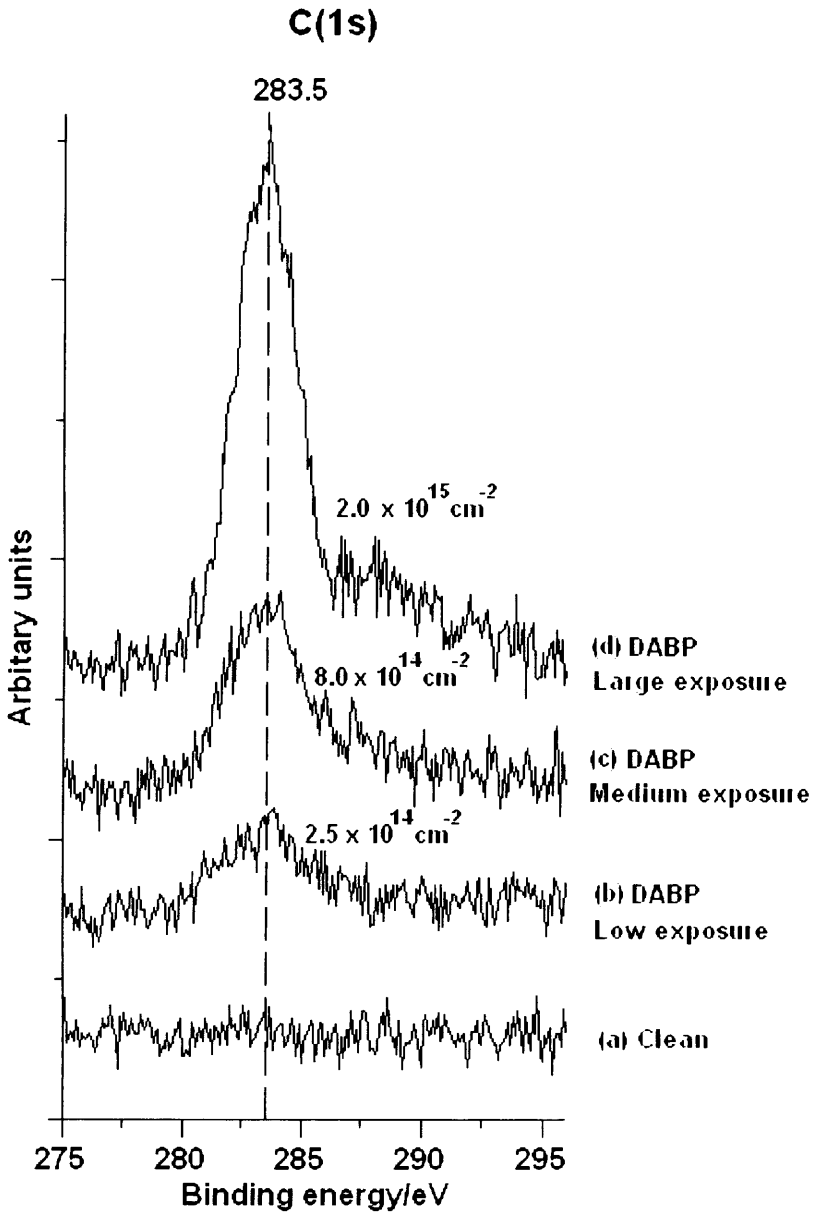


Figure 6.3: C(1s) XP spectra of various coverages of diaminobenzophenone adsorbed at Cu(110) surfaces

### 6.4.1 Low coverage, $\sigma_C = 2.5 \times 10^{14}$ cm$^{-2}$

The lowest surface carbon concentration imaged by STM was 2.5 x $10^{14}$ cm$^{-2}$, figure 6.3 (b). This is the equivalent of 2 x $10^{13}$ diaminobenzophenone molecules cm$^{-2}$.

STM did not image any adsorbate on the majority of the surface, as was expected for a small surface carbon concentration. However, several areas were found containing ordered adsorbed structures. An example of these areas is show in figure 6.4. In the following discussion, this feature will be labelled structure '(a)'. The structure covers the entire width of a 6.5 nm wide terrace for a length of approximately 25 nm. Resolution is poor within the structure, but it is comprised of features running in the <001> direction, approximately 1.3 nm wide, with an apparent gap of 0.5 nm between each feature.

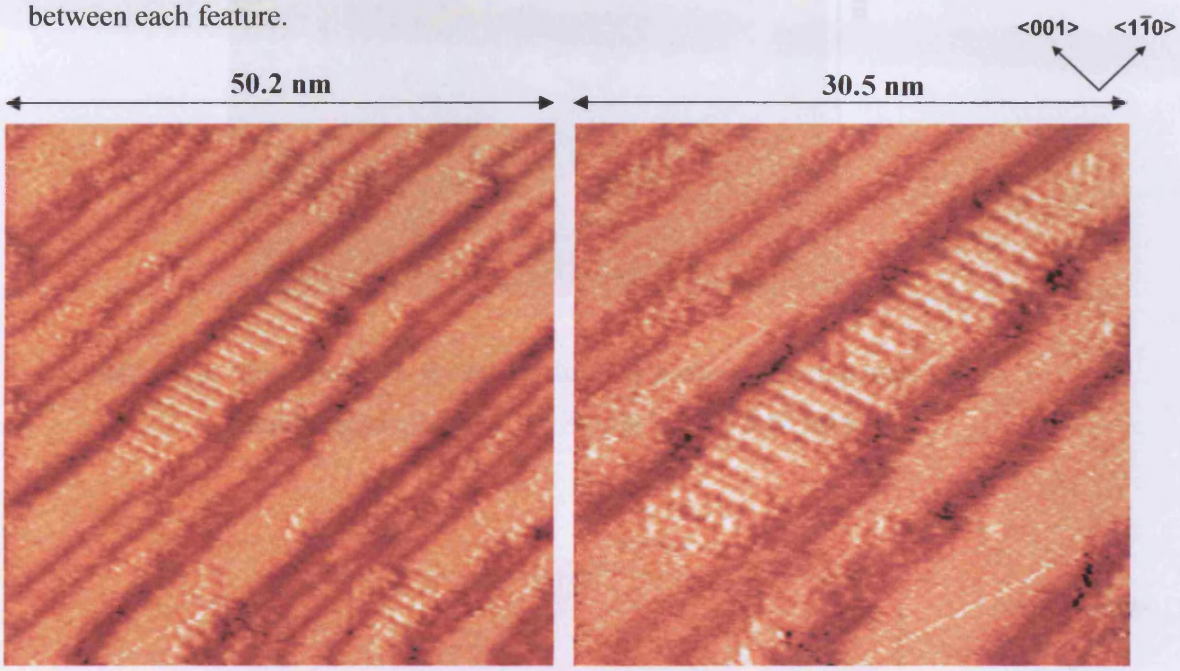


Figure 6.4: Structure '(a)'. Found on Cu(110) with a surface carbon concentration of $2.5 \times 10^{14}$ cm$^{-2}$, following exposure to 4,4 diaminobenzophenone. [$V_s$ = 0.56 V, $I_T$ = 2.89 nA]

The second area of ordered structure, structure '(b)' can be seen in the STM image of figure 6.5. It shows an entire terrace, approximately 7nm wide, covered in a species with a high amount of order. It is clearly different to structure (a). The structure itself is relatively complicated. It contains pairs of features aligned approximately 20° anti-clockwise from the <001> direction. Rows of these pairs run in a direction 35° clockwise from the <001> direction.

Figure 6.6 shows both structures (a) and (b) in the same STM image.

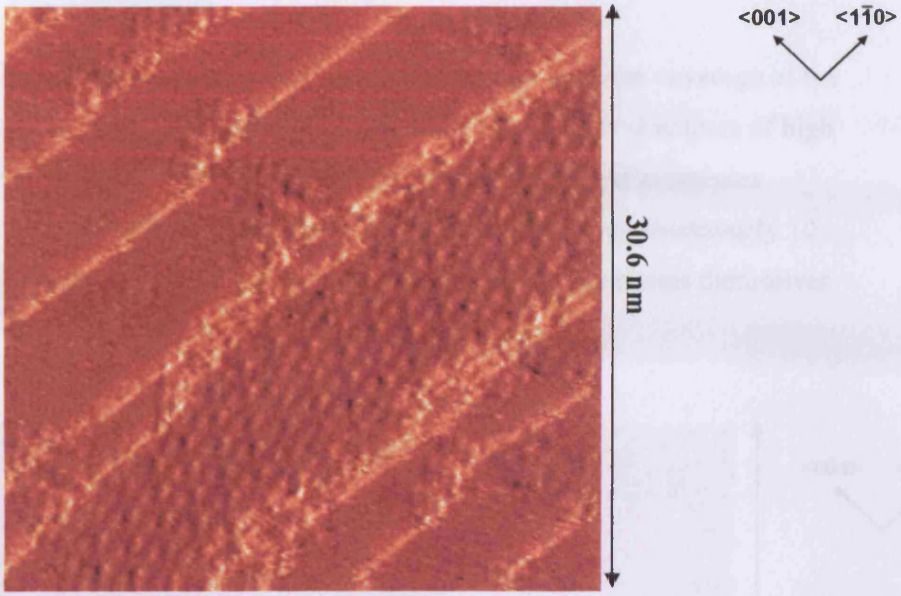


Figure 6.5: 'Structure (b)'. Found on Cu(110) surface after exposure to 4,4 diaminobenzophenone. [$V_S$ = 1.00 V, $I_T$ = 2.65 nA]

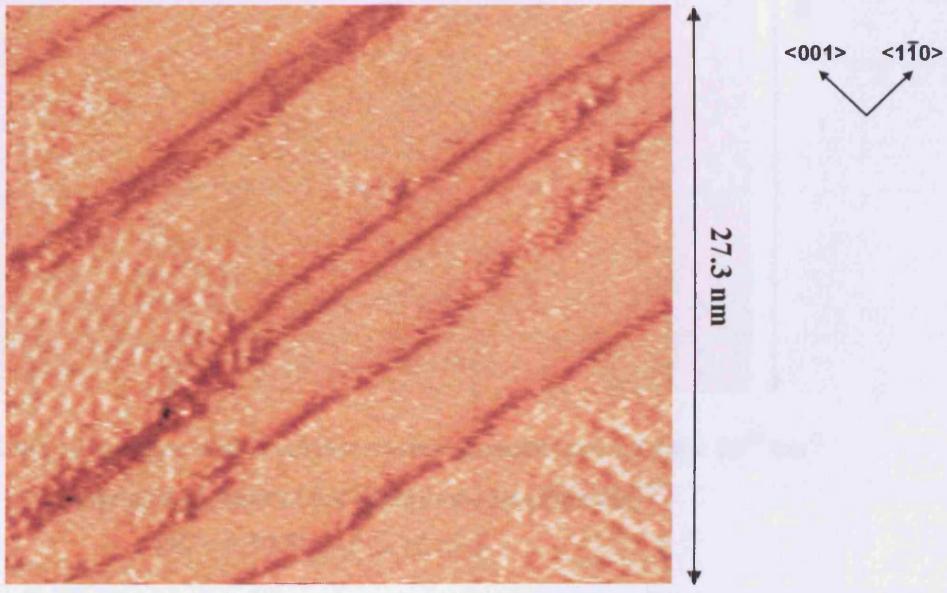


Figure 6.6: STM image containing both structure (a) and (b) found on a Cu(110) surface following exposure to 4,4 diaminobenzophenone.
[$V_s$ = 1.00 V, $I_T$ = 3.10 nA]

### 6.4.2 Medium Coverage, $\sigma_C = 8.0 \times 10^{14}$ cm$^{-2}$

Figure 6.7 shows an STM image of a Cu(110) surface with a medium coverage of 6 x $10^{13}$ diaminobenzophenone molecules cm$^{-2}$. There are two distinct structures of high order on a 40nm wide terrace, as well as approximately 20 chains of molecules running in the <100> direction. These chains range from 2 nm to approximately 10 nm in length, with a spacing of 0.5 nm between the maxima in the chains themselves (figure 6.8).

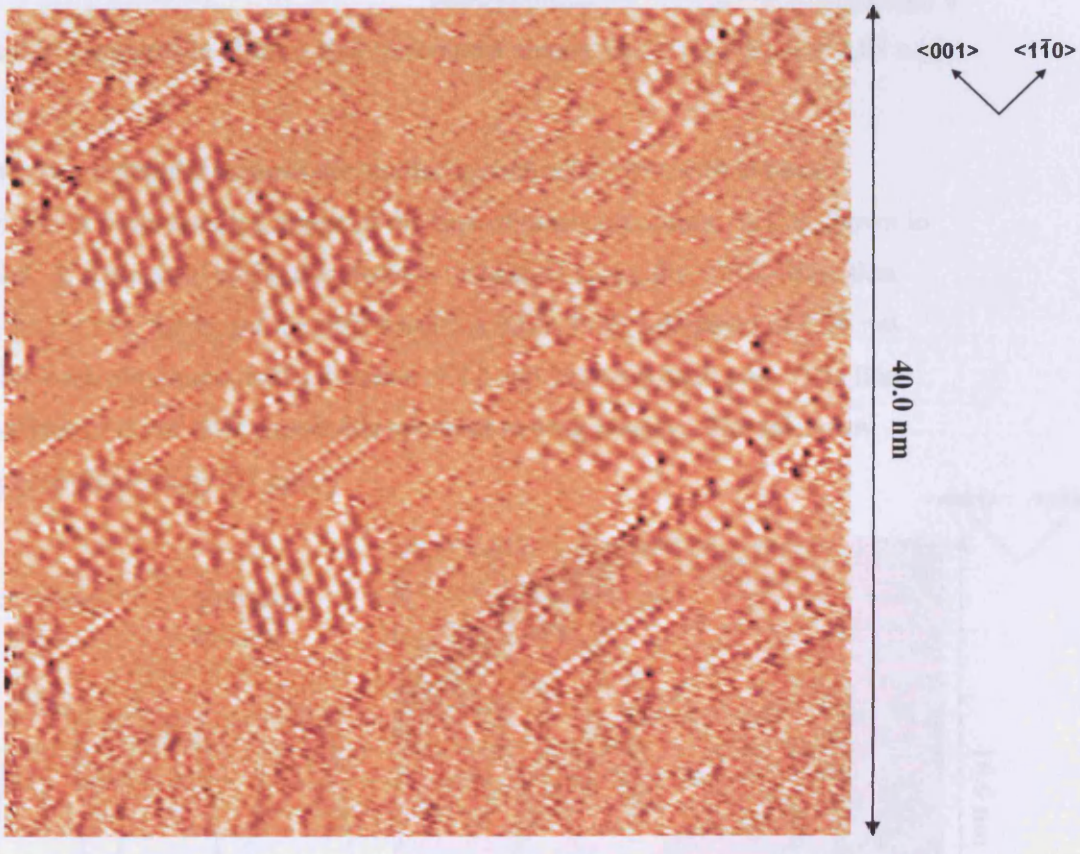


Figure 6.7: Cu(110) surface with a surface carbon concentration of 8 x $10^{14}$ cm$^{-2}$ following exposure to 4,4 diaminobenzophenone.
[$V_s$ = 0.50 V, $I_T$ = 3.12 nA]

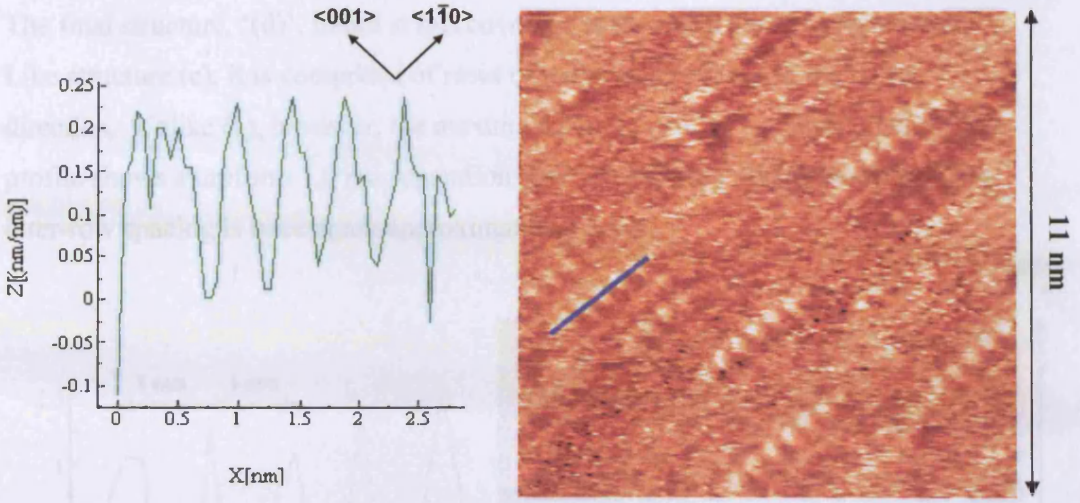


Figure 6.8: Line profile of the <100> orientated chains. [$V_S$ = 0.67 V, $I_T$ = 2.89 nA]

The other two ordered structures are similar to each other, but with certain differences. A more detailed image of the first of these structures, '(c)' is shown in figure 6.9. It consists of rows of molecules orientated along the <110> direction. Within these rows, the bright maxima appear in pairs, with a distance of 0.76 nm separating each maximum, and a distance of 1.1 nm between each pair. The line profile of one of these rows shows this apparent pairing clearly. The inter-row spacing is approximately 1.1 nm.

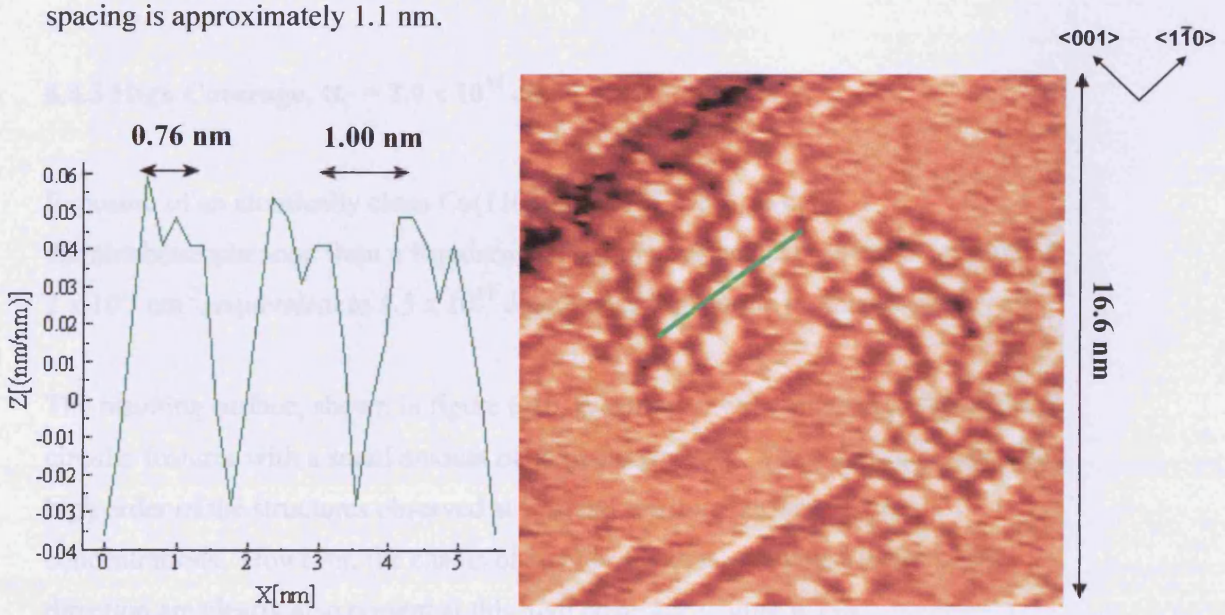


Figure 6.9: Detailed view of structure (c). [$V_s$ = 0.50 V, $I_T$ = 3.12 nA]

The final structure, '(d)', found at this coverage is shown in detail in figure 6.10. Like structure (c), it is comprised of rows of molecules running in the <110> direction. Unlike (c), however, the maxima do not appear to be paired, and the line profile shows a uniform 1.0 nm separation between maxima within the rows. The inter-row spacing is once again approximately 1.1 nm.

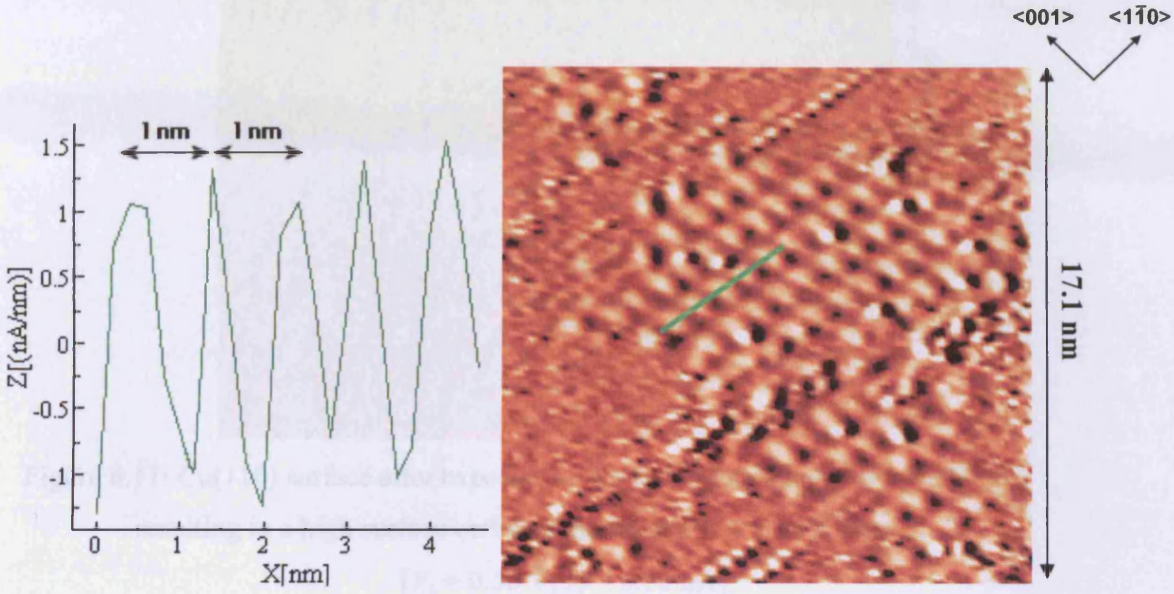


Figure 6.10: Detailed view of structure (d).[$V_s$ = 0.50 V, $I_T$ = 3.12 nA]

### 6.4.3 High Coverage, $\sigma_C = 2.0 \times 10^{15}$ cm$^{-2}$

Exposure of an atomically clean Cu(110) surface at 293 K to 4,4 diaminobenzophenone from a Knudsen cell led to a surface carbon concentration of $2 \times 10^{15}$ cm$^{-2}$, equivalent to $1.5 \times 10^{14}$ diaminobenzophenone molecules cm$^{-2}$.

The resulting surface, shown in figure 6.10, is saturated with relatively well-defined circular features with a small amount of short-range order. They do not possess the high order of the structures observed at low and medium surface carbon concentrations. However, the chains of smaller features orientated in the <110> direction are clearly also present at this high coverage (figure 6.12).

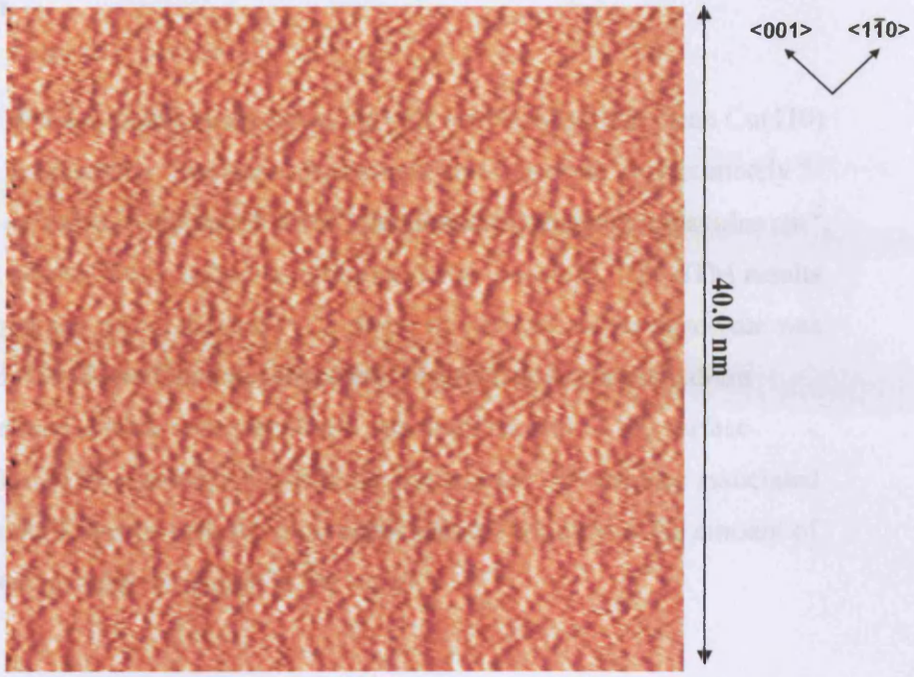


Figure 6.11: Cu(110) surface after exposure to 4,4 diaminobenzophenone at 293 K, resulting in a high surface carbon concentration of 1 x $10^{15}$ $cm^{-2}$.
[$V_s$ = 0.50 V, $I_T$ = 3.10 nA]

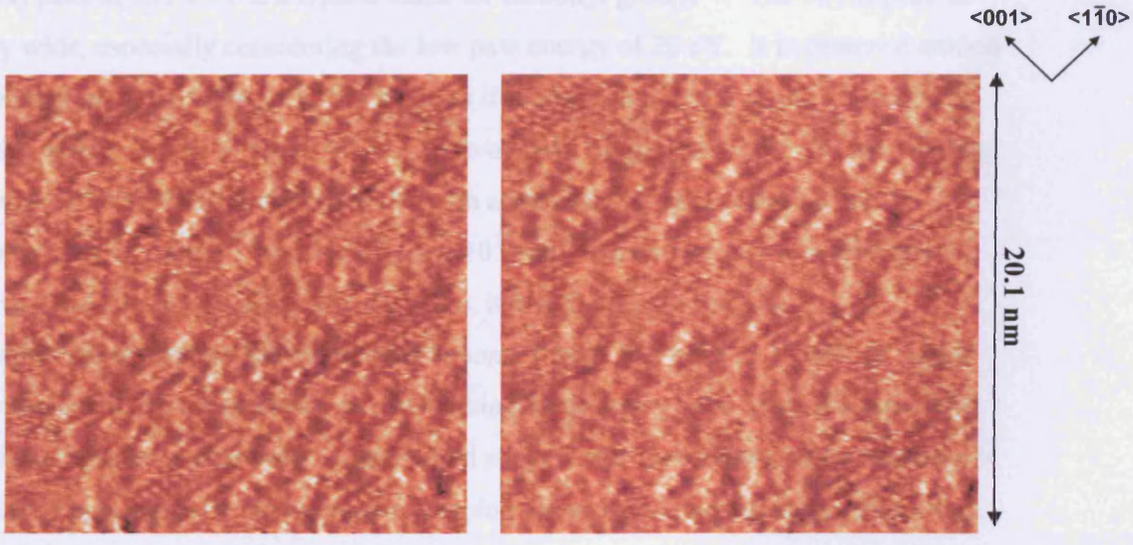


Figure 6.12: Chains of features orientated in the <110> direction at a Cu(110) surface with high 4,4 diaminobenzophenone coverage.
[$V_s$ = 2.00 V, $I_T$ = 3.10 nA]

## 6.5 Discussion

XP spectra show that 4,4 diaminobenzophenone will readily adsorb at clean Cu(110) surfaces at room temperature. Surface carbon concentrations up to approximately 5 x $10^{15}$ $cm^{-2}$ were recorded, equal to 3.8 x $10^{14}$ diaminobenzophenone molecules $cm^{-2}$, although it is not known if this is the maximum coverage possible. The STM results suggest such a coverage is past the point of a single monolayer, as the adsorbate was found to be much less ordered than the structures observed at low and medium diaminobenzophenone surface concentrations. Accurate control of the surface coverage was found to be extremely difficult due the number of variables associated with dosing from the Knudsen cell; the most significant of which was the amount of diaminobenzophenone solid remaining in the k-cell.

The C(1s) peak at 283.5 eV of figure 6.2 is typical of the values found for phenyl rings[1,2], and is similar to the binding energies observed for the reaction of aniline with oxidised Cu(110), as well as that of phenyl iodide at the same surface. The O(1s) peak at 531.1 eV is a typical value for carbonyl groups[3]. The N(1s) peak is very wide, especially considering the low pass energy of 20 eV. It is centered around a binding energy of 398.6 eV, but looks as if it may contain two peaks. A curve fit of the peak is shown in figure 6.13. The two peaks suggested by the fit have binding energies of 398.87 eV and 396.94 eV, with areas equal to concentrations of approximately 2.5 x $10^{14}$ $cm^{-2}$ and 1.72 x $10^{14}$ $cm^{-2}$ respectively. If two different nitrogen species are present on the surface, it would suggest that the diaminobenzophenone has dissociated in some form. The peak at 398.87 eV could be assigned to an amine group, as similar binding energies have been observed for various physisorbed amines[4]. This would suggest that the interaction between the N and the Cu is not the main interaction keeping the molecule adsorbed on the surface. This is in contrast to aniline, which was found to form an imide and bond to the Cu surface through the N atom. At this point, it is harder to assign the second peak. The C:N:O ratio was found to be constant at 13:2:1 for every experiment, indicating that the products of any dissociation upon adsorption are stable on the surface. Since the XP spectrum was taken at a high coverage, it is also possible that the second peak is

due to a physisorbed second layer. STM images support this, as order in the monolayer is seen to break down at higher coverages, however, sub-monolayer coverages did not give rise to a N(1s) peak intense enough to confirm this.

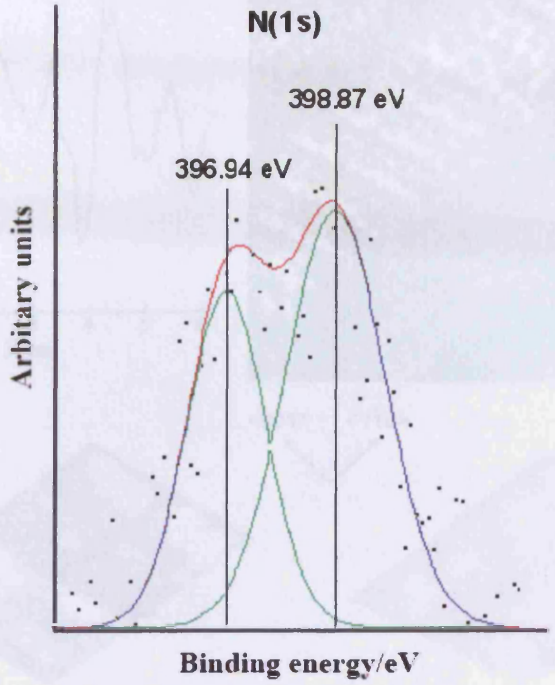


Figure 6.13: Curve fit of the N(1s) XP spectrum obtained after exposure of a Cu(110) surface to 4,4 diaminobenzophenone, illustrating how the two peaks shown in green could possibly give rise to the wide N peak centered at 398.1 eV.

STM images of 4,4 diaminobenzophenone adsorbed at Cu(110) surfaces in low and medium surface concentrations apparently show the presence of four distinct, ordered structures; two per concentration. Figure 6.14 shows a high contrast black and white STM image of structure (a). Due to the high contrast, the structure of the columns is clearer, and they appear to consist of pairs of bright maxima orientated in the <110> direction. The spacing between each maximum is 0.76 nm, with a separation of 1.0 nm between each pair along the <110> axis. These values are exactly the same as the dimensions between maxima in the <110> orientated rows of structure (c). The inter-row spacing for both structures is also the same, at 1.1 nm.

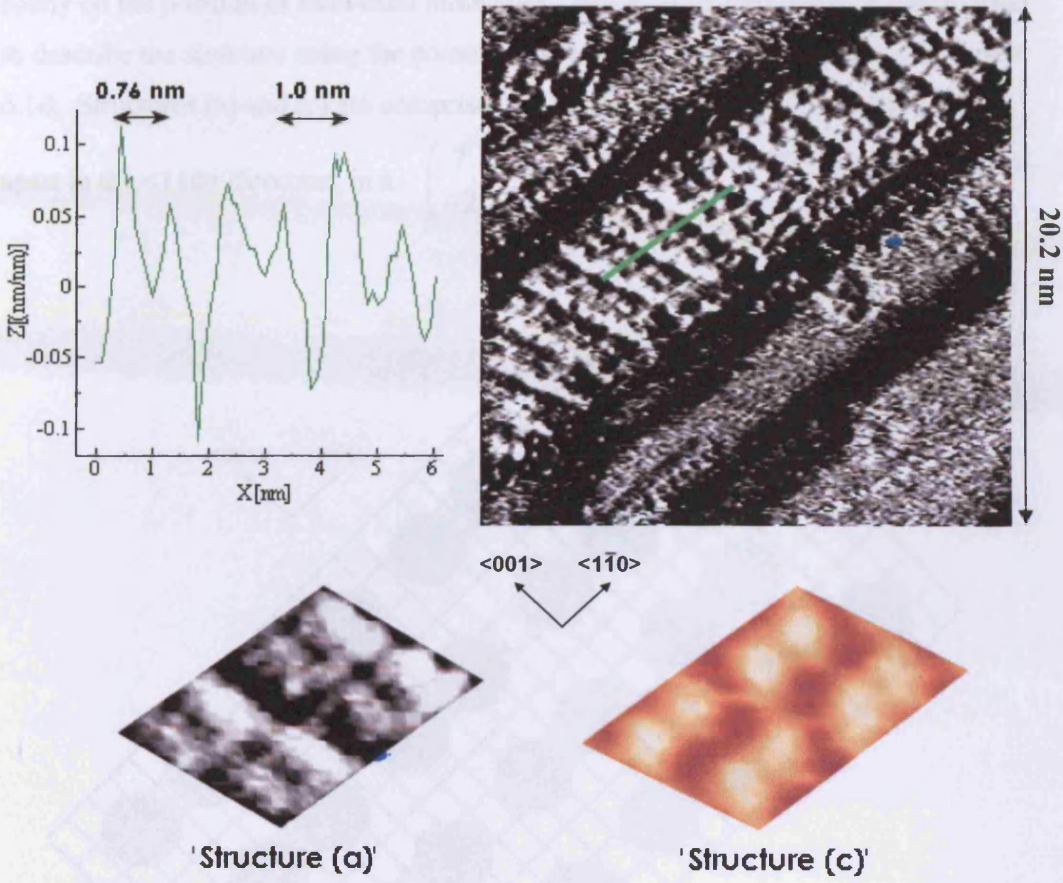


Figure 6.14: High contrast greyscale image of structure (a) with line profile across green line. Also shown are two sections of structures (a) and (c) highlighting similarities between the two.

We therefore conclude that structures (a) and (c) are the same. Initial dissimilarities were probably due to different scanning conditions and also the fact that structure (a) extended completely across a small terrace, whereas structure (c) only covered part of a much larger terrace. This had the effect of emphasizing the column-like features of structure (a).

Figure 6.15 shows a model of this structure on a Cu(110) lattice. The spacing of 1.0 nm between pairs and 0.76 within the pairs in the <110> direction are equivalent to four and three substrate rows, respectively. Due to the two different spacing in these rows, it is impossible to describe this structure using simple matrix notation based

solely on the position of individual molecules. However, matrix notation can be used to describe the structure using the points in the center of the pairs, as shown in figure 6.16. Structures (a) and (c) are comprised of pairs of molecules, 3 substrate rows apart in the <110> direction, in a $\begin{pmatrix} 7 & 0 \\ -2 & 3 \end{pmatrix}$ unit cell.

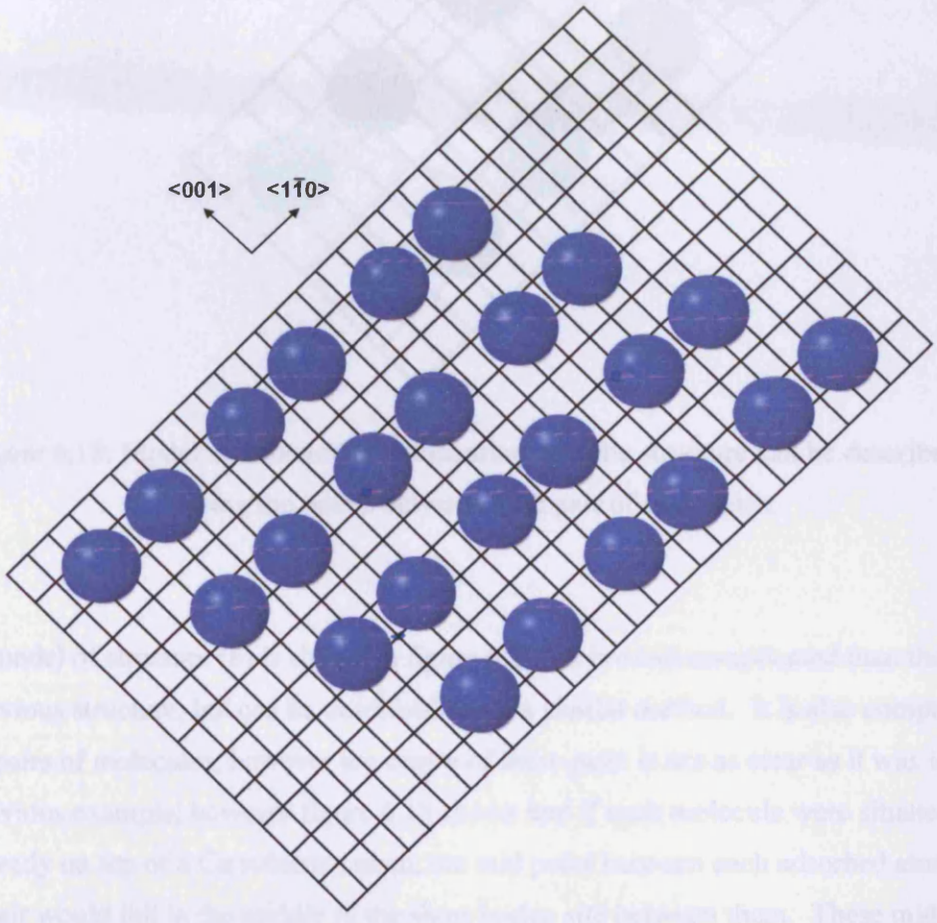


Figure 6.15: Model of structure (a)/(c)

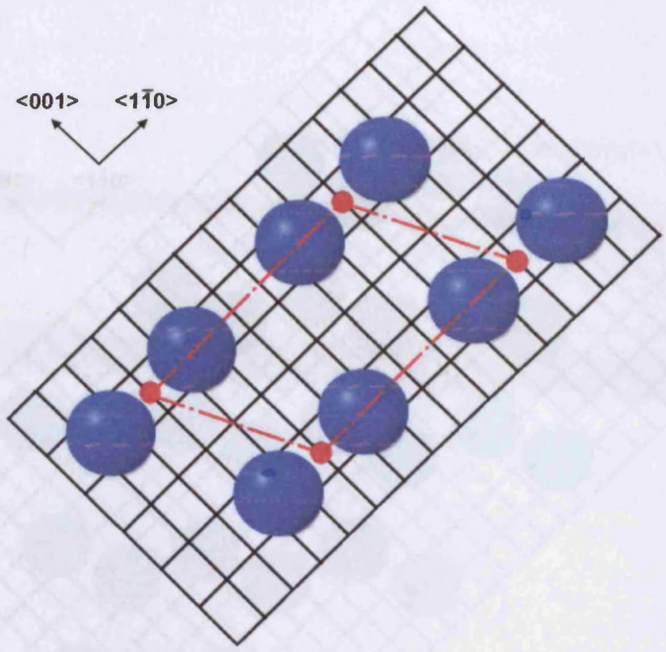


Figure 6.18: Model of structure (b) illustrating how the structure can be described by using the points between each pair of molecules.

A model of structure (b) is shown in figure 6.17. It is more complicated than the previous structure, but can be described using a similar method. It is also comprised of pairs of molecules, however the centre of these pairs is not as clear as it was in the previous example; however figure 6.18 shows that if each molecule were situated directly on top of a Cu substrate atom, the mid point between each adsorbed atom in a pair would fall in the middle of the short bridge site between them. These mid-point sites can then be described by the matrix $\begin{pmatrix} 7 & 0 \\ -4 & 3 \end{pmatrix}$.

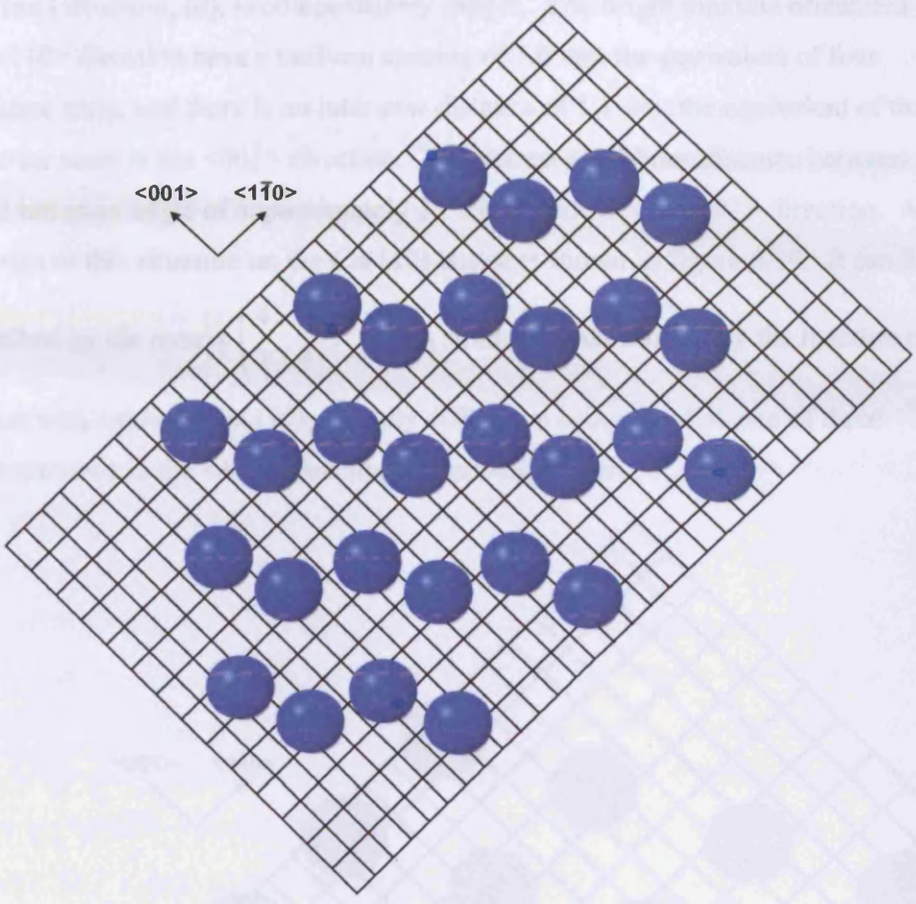


Figure 6.17: Model of structure (b).

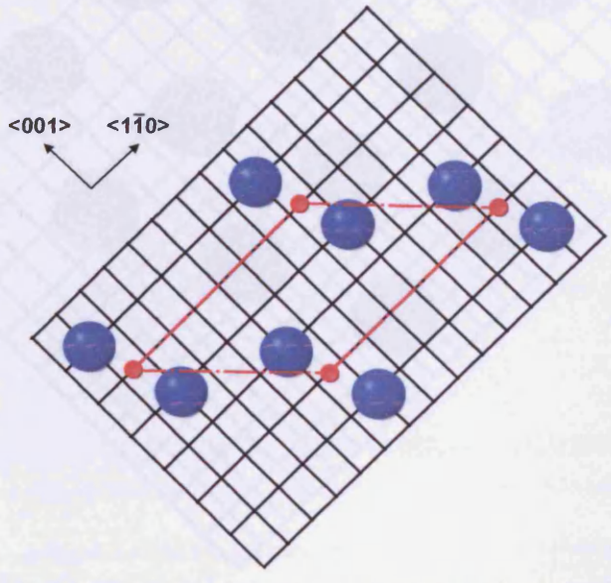


Figure 6.18: Model of structure (b) illustrating how the structure can be described by using the points between each pair of molecules.

The final structure, (d), is comparatively simple. The bright maxima orientated in the <110> direction have a uniform spacing of 1.0 nm, the equivalent of four substrate rows, and there is an inter-row distance of 1.1 nm, the equivalent of three substrate rows in the <001> direction. The nearest neighbour distance between rows is 1.2 nm at an angle of approximately 25° either side of the <001> direction. A diagram of this structure on the Cu(110) lattice is shown in figure 6.19. It can be described by the matrix $\begin{pmatrix} 4 & 0 \\ 2 & 3 \end{pmatrix}$. This is similar to that formed by the reaction of aniline with oxidised Cu(110), the only difference being the distance of three substrate rows in the <110> direction as opposed to two.

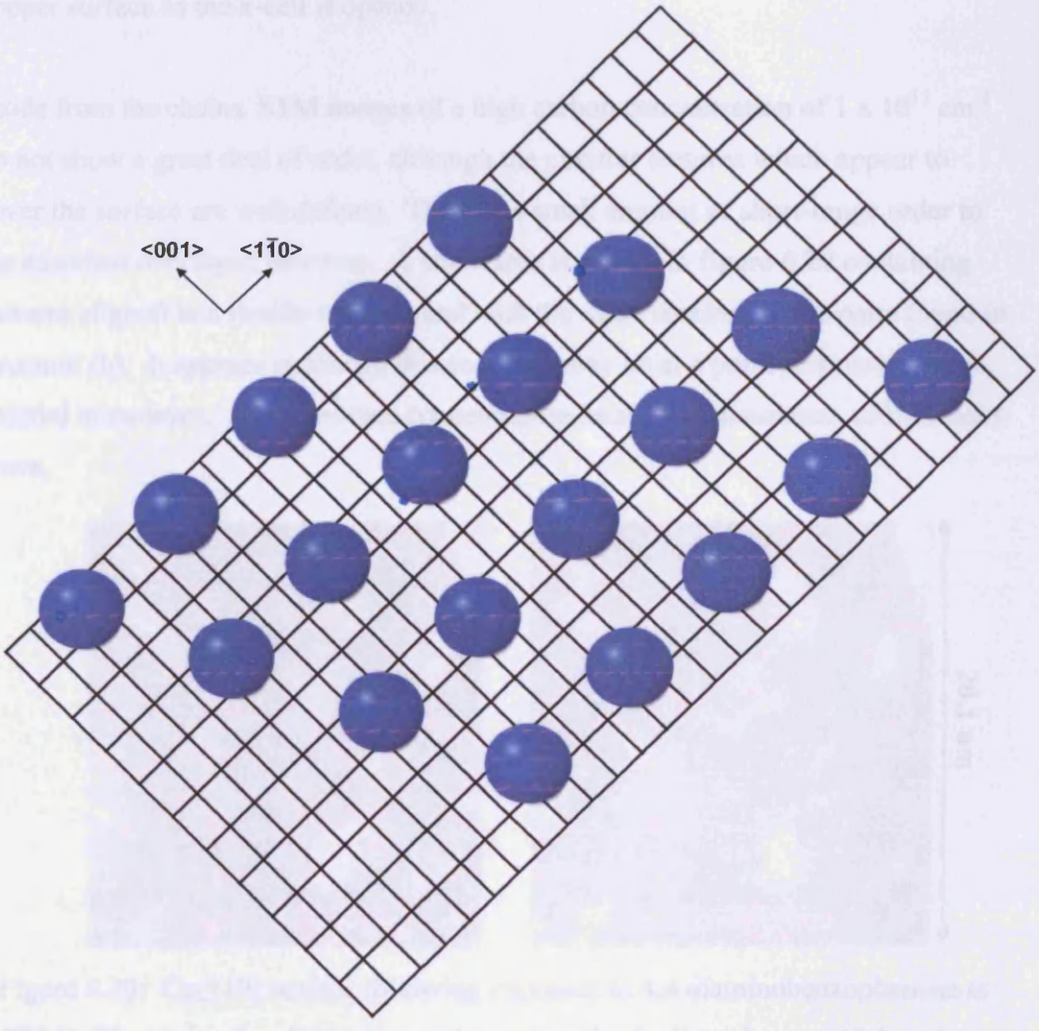


Figure 6.19: Model of structure (d).

The other features observed at medium, as well as high, coverage, were the chains running in the <110> direction. These chains were not observed at low coverage, although the reason for this may simply be that they were present in a low concentration. They were only observed as single chains; no island-like structures formed from groups of these chains were found. The spacing between features in a chain is 0.5 nm. The chains are probably composed of chemisorbed nitride atoms, although their origin is unclear. It is unlikely that the copper surface has caused C-N bond scission, and the structures do not appear to exist in a very large concentration. It is possible that some dissociation of diaminobenzophenone occurs on the walls of the k-cell at high temperatures. The dissociated nitrogen atoms then adsorb at the copper surface as the k-cell is opened.

Aside from the chains, STM images of a high carbon concentration of 1 x $10^{15}$ $cm^{-2}$ do not show a great deal of order, although the circular features which appear to cover the surface are well defined. There is a small amount of short-range order to the adsorbed overlayer, however. A small area is shown in figure 6.20 containing features aligned in a similar manner, and with the same spacing, to the pairs found in structure (b). It appears as though this coverage may be at a point just past a single, ordered monolayer. As the surface concentration exceeds a monolayer, order breaks down.

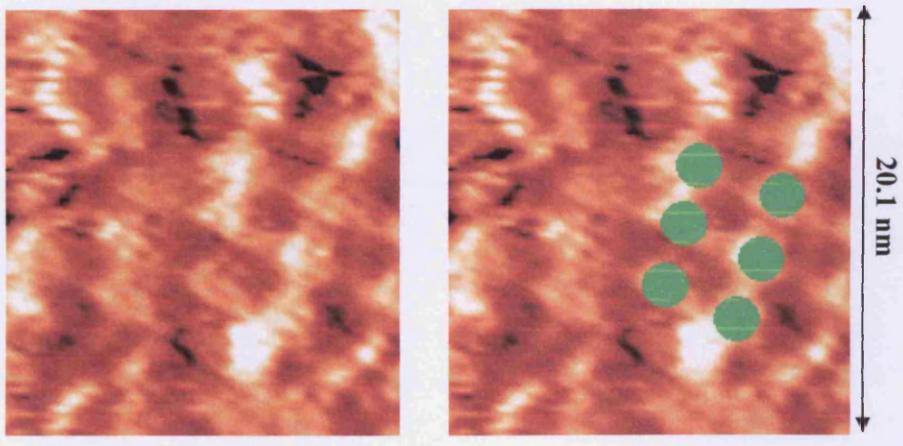


Figure 6.20: Cu(110) surface following exposure to 4,4 diaminobenzophenone at 293 K, illustrating the short-range order to the adsorbed overlayer at high carbon coverages. [$V_S$ = 0.52 V, $I_T$ = 3.10 nA]

## 6.6 Conclusions

The adsorption of 4,4-diaminobenzophenone at clean Cu(110) surfaces has been investigated by STM and XPS. At sub-monolayer coverages, the compound forms three different highly ordered structures. The first can be described using by a $\begin{pmatrix} 4 & 0 \\ 2 & 3 \end{pmatrix}$ unit mesh. The others are based around a pair of molecules, forming $\begin{pmatrix} 7 & 0 \\ -4 & 3 \end{pmatrix}$ and $\begin{pmatrix} 7 & 0 \\ -2 & 3 \end{pmatrix}$ lattices. XPS suggests that formation of a second, physisorbed layer occurs. This is backed-up by the fact that order is seen to break down at higher coverages.

## 6.7 References

[1] Cabibil, H.; Ihm, H.; White, J. M. *Surf. Sci.* **2000**, *447*, 91.

[2] Carley, A. F.; Coughlin, M.; Davies, P. R.; Morgan, D. J.; Roberts, M. W. *Surf. Sci. Letts.* **2004**

[3] Takahagi T.; Shimada I.; Fukuhara M.; Morita K.; Ishitani A. *J. Polym. Sci. Part A, 1986*, **24**, 3101

[4] Barber M.; Connor J.A.; Guest M.F.; Hillier I.H.; Schwarz M.; Stacey M. *J. Chem. Soc. Faraday Trans. II,* **1973**, *69*, 551

# *Appendix A*
## *Publications*

*STM and XPS studies of the oxidation of aniline at Cu(110) surfaces*
- Davies, P. R.; Edwards, D.; Richards, D. *J. Phys. Chem. B.* **2004,** *108*, 18630

*Molecularly resolved studies of the reactions of pyradine and dimethylamine with oxygen at a Cu(110) surface*
- Carley, A. F.; Davies, P. R.; Edwards, D. E.; Jones, R. V.; Parsons, M. *Topics in Catalysis,* **2005**, *36*, 21

*Aromatic interactions in the close packing of phenyl-imides at Cu(110) surfaces*
- Davies, P. R.; Edwards, D.; Richards, D. *Surf. Sci.* **2004**, *573*, 284

18630 *J. Phys. Chem. B* **2004,** *108,* 18630−18639

# STM and XPS Studies of the Oxidation of Aniline at Cu(110) Surfaces

**Philip R. Davies,* Dyfan Edwards, and Darran Richards**

*School of Chemistry, Cardiff University, P.O. Box 912, Cardiff CF10 3TB, U.K.*

*Received: May 27, 2004; In Final Form: September 8, 2004*

Aniline chemisorption at clean and partially oxidized Cu(110) surfaces at 293 K is compared with the reaction of a 300:1 aniline/dioxygen mixture at the same surface using STM and XPS. Limited dissociation occurs at the clean surface but in the presence of chemisorbed oxygen efficient oxy-dehydrogenation takes place with water desorption and the formation of chemisorbed phenyl imide ($C_6H_5N(a)$) with a reaction stoichiometry that changes with coverage. The adsorption site of the phenyl group is identified by STM to be the 2-fold hollow and it is proposed that the nitrogen is situated over the short bridge site. Chemisorptive replacement of oxygen gives a maximum phenyl imide concentration of $2.8 \times 10^{14}$ molecules $cm^{-2}$ at which coverage the surface is dominated by a mixture of three ordered domains with structures described by $\begin{pmatrix} 4 & 0 \\ 2 & 2 \end{pmatrix}$, $\begin{pmatrix} 4 & 0 \\ -1 & 2 \end{pmatrix}$, and $\begin{pmatrix} 4 & 0 \\ 1 & 2 \end{pmatrix}$ unit meshes. Adsorption of aniline and dioxygen mixtures however results in phenyl imide concentrations up to $3.4 \times 10^{14}$ $cm^{-2}$ molecules $cm^{-2}$ and a highly ordered biphasic structure characterized by $\begin{pmatrix} 3 & 0 \\ -1 & 2 \end{pmatrix}$ and $\begin{pmatrix} 3 & 0 \\ 1 & 2 \end{pmatrix}$ domains. A discrepancy between the concentrations measured by XPS and those calculated from the STM structures is discussed in terms of $\pi$-stacking of the phenyl rings in the adsorbed monolayer. Finally the chemistry of aniline is compared with that of ammonia and the importance of the NH bond strength and the basicity of the amine discussed.

## Introduction

Amines have applications in many interface related areas including corrosion inhibition,[1−5] adhesion,[6−10] and heterogeneous catalysis.[11,12] In the latter case, amines are commonly used not only as reactants but also as catalyst modifiers.[12−14] Pfaltz, for example, has shown[15] that a basic nitrogen group is a necessary component of chiral modifiers for the hydrogenation of α-functionalized ketones.[16−20] The interaction of the amine functionality with the surface is therefore a subject of some importance in surface science. Our own interest in amine surface chemistry stems from studies of ammonia oxidation[21−30] and of the interaction of pyridine with surface oxygen, where intermolecular complexes between pyridine and both molecular oxygen transients[31] and chemisorbed atomic oxygen[32,33] have been demonstrated. In this paper, we consider the reaction of aniline with oxygen at Cu(110) surfaces. Aniline has a lower basicity ($pK_b = 9.37$) than either ammonia ($pK_b = 4.75$) or pyridine ($pK_b = 8.75$), and the reaction with oxygen may also be sterically hindered by the phenyl ring.

Previous studies of aniline surface chemistry have concentrated on adsorption at clean metal[34−44] or clean silicon surfaces[45,46] using temperature-programmed desorption (TPD) and vibrational spectroscopy (HREELS). It has been reported[47] that the molecule dissociates at clean Cu(110) surfaces to give an amide (PhNH(a)) in which the phenyl ring lies approximately parallel to the surface but there have been no structural studies of the reaction.

## Experimental Section

Experiments were conducted using a combined variable temperature STM/XPS instrument (Omicron Vacuum Physik) equipped with a dual Al Kα and Mg Kα photon source. Except where stated otherwise, XP spectra were recorded with a pass energy of 100 eV resulting in typical peak half-widths of ca. 2.0 eV. Spectra were obtained by the combination of 10−20 individual scans over a 25 eV wide region, with a total acquisition time of between 10 min (O(1s) and Cu (2p) spectra) to 20 min (C(1s) and N(1s) spectra). The spectra were calibrated to the clean Cu($2p_{3/2}$) peak at 932.7 eV. XPS data was acquired using commercial software (Spectra, Ron Unwin) and analyzed using software developed in-house. Surface concentrations were calculated from XP peak areas using the method discussed previously.[48,49] We estimate the error in surface concentrations of oxygen to be $\pm 1.5 \times 10^{13}$ $cm^{-2}$ and to be slightly greater in the case of carbon and nitrogen, which have weaker signals.

The dimensions of the sample were 7 mm by 7 mm with a thickness of approximately 0.5 mm, it was cut to within 0.5° of the (110) plane and polished mechanically down to 0.25 μm. Cleaning involved cycles of $Ar^+$ sputtering (0.75 keV, 20 μA $cm^{-2}$ for 20 min) and annealing for 60 min at 900 K. This resulted in flat terraces approximately 10−20 nm wide in the STM images. Sample cleanliness was checked by XPS. Gases were dosed via a leak valve at pressures of between $10^{-9}$ and $5 \times 10^{-7}$ mbar. The aniline (Aldrich, 99.5%) was subjected to several freeze pump thaw cycles using a dry ice/acetone slush and its purity was monitored with in-situ mass spectrometry. Oxygen (Argo Ltd, 99.998%) was used as received.

## Results

**3.1. XPS Investigations.** *3.1.1. Aniline Adsorption at Clean and Preoxidized Cu(110) Surfaces.* In contrast to ammonia[28] and other amines[50] which do not react with clean copper surfaces, Figure 1a shows that exposure of a clean Cu(110)

* Corresponding author. E-mail: daviespr@cf.ac.uk.

10.1021/jp047697l CCC: $27.50 
Published on Web 11/06/2004

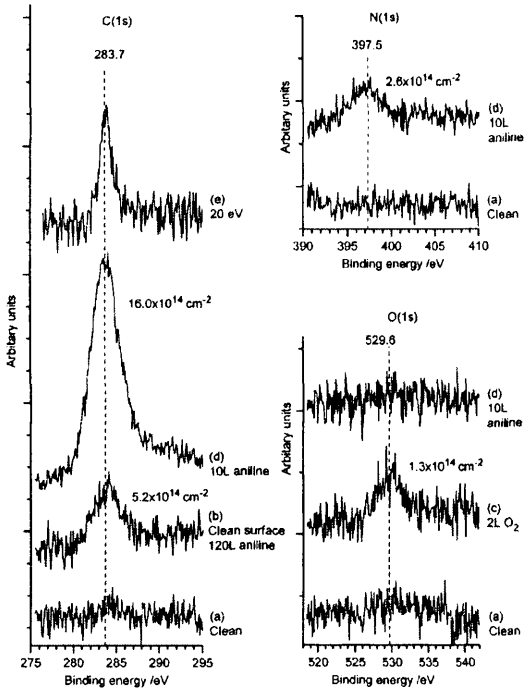


**Figure 1.** XP C(1s). N(1s), and O(1s) spectra comparing aniline adsorption at clean and partially oxidized Cu(110) surfaces at 293 K: (a) clean surface; (b) clean Cu(110) surface after exposure to 120 langmuir of aniline at 293 K: (c) clean surface after exposure to 2 langmuir of $O_2$(g): (d) surface in part c after exposure to 10 langmuir of aniline. (e) C(1s) spectrum of the surface in part d recorded at 20 eV pass energy to establish the presence of a single carbon state.

surface to aniline at 293 K leads to some adsorption with a single peak appearing in the XP C(1s) region at a binding energy of 283.7 eV, which reaches maximum intensity after ca. 120 L (1 langmuir = $10^{-6}$ Torr s)

The surface concentration of carbon, calculated from the XP peak area, is 5.2 × $10^{14}$ $cm^{-2}$. The corresponding N(1s) spectrum shows some intensity increase but the peak is too weak to calculate a reliable concentration.

More extensive adsorption results when aniline is dosed in the presence of preadsorbed oxygen. Figure 1c shows an XP O(1s) spectrum of a Cu(110) surface with an initial oxygen concentration of 1.3 × $10^{14}$ $cm^{-2}$. When this surface is exposed to 10 langmuir of aniline at 293 K, Figure 1d, a facile reaction occurs resulting in the desorption of all the oxygen, presumably as water,[28] and its replacement by a species containing carbon and nitrogen with binding energies of 283.7 and 397.5 eV respectively. The carbon:nitrogen ratio calculated from the XP peak areas is 6:1, and the nitrogen concentration (2.6 × $10^{14}$ $cm^{-2}$) is twice that of the initial oxygen concentration. Exposures up to 120 langmuir gave rise to no further adsorption. High resolution spectra of the C(1s) region, Figure 1e, show only a single carbon state at the surface and this can be assigned on the basis of the carbon/nitrogen ratio and the characteristically low binding energy to a phenyl group.[51,52] The N(1s) peak binding energy of 397.5 eV is characteristic of imide chemisorbed at copper surfaces, amides and nitrides typically giving rise to peak binding energies at 399 and 396.5 eV respectively.[28,29] These assignments are discussed in more detail below.

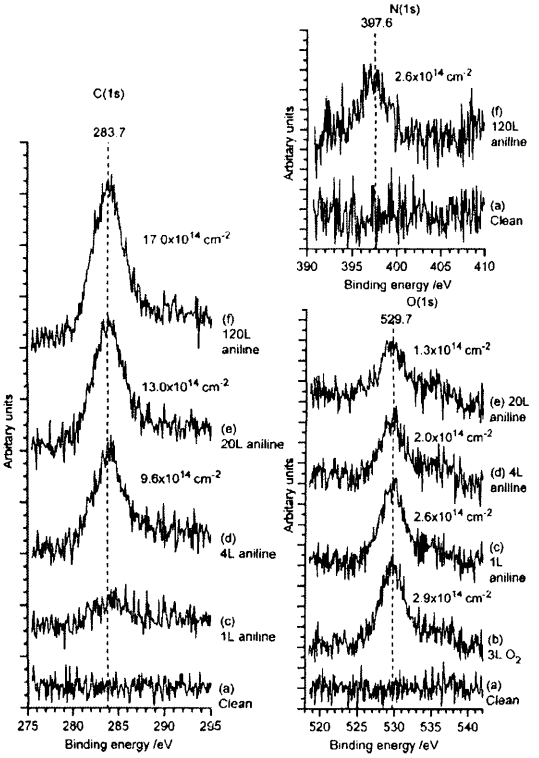


**Figure 2.** XP C(1s), N(1s), and O(1s) spectra of the chemisorption of aniline at 293 K at a Cu(110) surface with a higher initial oxygen concentration than that shown in Figure 1. Note the change in the ratio of phenyl groups added to oxygen removed from 2:1 after 4 langmuir of aniline to 1:1 after 120 langmuir: (a) clean surface; (b) surface after exposure to 3 langmuir of $O_2$(g): (c) surface after exposure to 1 langmuir of aniline; (c) surface after exposure to 4 langmuir of aniline; (d) surface after exposure to 8 langmuir of aniline: (e) surface after exposure to 20 langmuir of aniline; (f) surface after exposure to 120 langmuir of aniline.

For oxygen concentrations greater than ca. 2.5 × $10^{14}$ $cm^{-2}$ but less than a monolayer (5.5 × $10^{14}$ $cm^{-2}$), reaction with aniline remains facile at room temperature with identical XP binding energies indicating that the reaction product is the same as that observed at lower oxygen concentrations. However, there is a marked change in stoichiometry as the reaction progresses. Figure 2 shows that for an oxygen concentration of 2.9 × $10^{14}$ $cm^{-2}$, exposure to aniline results, after 4 langmuir, in a 2:1 aniline:oxygen reaction stoichiometry (parts b and d), but this changes to 1:1 with a further exposure of 20 langmuir (parts d and e). For initial oxygen concentrations close to a monolayer, reaction is limited in extent at room temperature and the reaction stoichiometry is 1:1. A monolayer of preadsorbed oxygen completely inhibits aniline reaction for exposures up to 200 langmuir at room temperature.

*3.1.2. Coadsorption of Aniline and Dioxygen at Clean Cu(110) Surfaces.* Figure 3 shows XP spectra obtained after the clean copper surface was exposed to 200 langmuir of a 300:1 aniline:oxygen mixture at 293 K. The total oxygen exposure is 0.7 langmuir but the XP data shows no oxygen at the surface. Instead, peaks in the C(1s) and N(1s) regions at binding energies of 283.8 and 397.8 eV indicate the presence of the same species observed after aniline reaction with *preadsorbed* oxygen. The

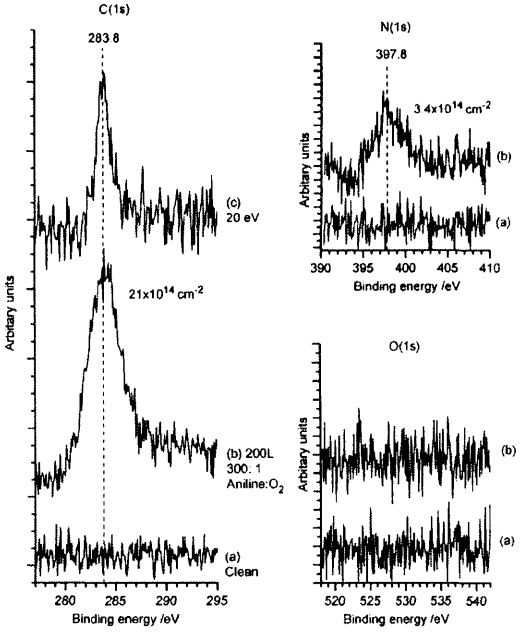


**Figure 3.** XP C(1s), N(1s), and O(1s) spectra of the adsorption of aniline and dioxygen at a Cu(110) surface in a 300:1 mixture at 293 K: (a) clean surface; (b) surface after exposure to 200 langmuir of mixture; (c) high resolution 20 eV pass energy spectrum of the surface in part b.

coadsorption of reactants results not only in an efficient reaction that converts all of the oxygen adsorbing at the surface but also in a higher concentration of the phenyl imide product than was obtained through sequential adsorption of the reactants, the final carbon concentration being $2.1 \times 10^{15}$ cm$^{-2}$.

**3.2. STM Investigations.** *3.2.1. Aniline Adsorption at Clean and Preoxidized Cu(110) Surfaces.* No ordered adlayer structures were observed by STM for aniline reaction with the clean Cu(110) surface, and no reaction was evident in the STM images when a surface with a monolayer of oxygen present ($5.5 \times 10^{14}$ cm$^{-2}$) was exposed to aniline. At oxygen coverages below $5 \times 10^{14}$ cm$^{-2}$, however, aniline adsorption is observed at step edges and at defect sites in the lattice; a typical image is shown in Figure 4a for an initial oxygen concentration of $4.8 \times 10^{14}$ cm$^{-2}$. At lower oxygen concentrations the imide product from the aniline can be imaged simultaneously with the p(2 × 1)O(a) lattice. Figure 4b shows the characteristic p(2 × 1) oxygen islands surrounded by the phenyl imide product after a surface with an initial oxygen concentration of $2.4 \times 10^{14}$ cm$^{-2}$ was exposed to 20 langmuir of aniline at room temperature. The phenyl imide structure does not exhibit long range order, but some evidence for local structure is present, related to the unit cells described in more detail below. It is also clear from Figure 4b that aniline adsorption does not result in any expansion of the oxygen lattice in the ⟨1$\bar{1}$0⟩ direction as was observed in the case of pyridine[32] and some other amines.[50]

The majority of imide features appear 0.1 nm above the oxygen although some features 0.3 nm above are also observed. Figure 4, parts c and d. Extrapolating the oxygen (2 × 1) lattice over imide covered areas in Figure 4b establishes that, in both the ⟨100⟩ and ⟨1$\bar{1}$0⟩ directions, the imide features are in line with the maxima in the oxygen p(2 × 1) lattice.

Improved long range order in the phenyl imide adlayer was obtained when low oxygen coverages were completely removed by reaction with aniline. Images were obtained for carbon concentrations of around $1.6 \times 10^{14}$ cm$^{-2}$, corresponding to an imide concentration of $2.7 \times 10^{14}$ cm$^{-2}$, and in all cases had a characteristic "zigzag" appearance at low resolution; examples are shown in Figure 5. The zigzag appearance arises from ordered sets of lines which occur in domains generally 3−4 nm in length (though several extend to 9 nm) and 5−6 lines wide (approximately 5−6 nm although some involve more than 10 lines over approximately 10 nm.) The lines, are orientated either along the ⟨1$\bar{1}$0⟩ axis or at ±20 degrees to it. In the ⟨100⟩ direction, the spacing between the lines is 1.0 nm.

Individual molecular features are also observed in the STM images, examples are shown in Figure 6, parts a and b with a close up of the molecularly resolved features near to two step edges in Figure 6c. The adsorbed imides are approximately 0.7 nm in diameter with height corrugations between features of ~0.05 nm. No details were resolved within these features. The imides are best imaged with a positive sample bias and closely resemble those observed[53,54] following the dissociative adsorption of phenyl iodide, they are assigned to the phenyl ring of the imide.

In Figure 7, parts a−c, molecularly resolved images of each of the three characteristic domains are shown. The unit cells for all three structures have in common a 1.0 nm vector in the ⟨1$\bar{1}$0⟩ direction corresponding to four times the substrate lattice and, as we discuss in more detail below, can be described in matrix notation[55] by $\begin{pmatrix} 4 & 0 \\ 2 & 2 \end{pmatrix}$, $\begin{pmatrix} 4 & 0 \\ -1 & 2 \end{pmatrix}$, and $\begin{pmatrix} 4 & 0 \\ 1 & 2 \end{pmatrix}$ unit cells.

Figure 8a shows an STM image obtained from a surface on which an oxygen concentration of $2.4 \times 10^{14}$ cm$^{-2}$ was exposed to 200 langmuir of aniline. Although molecular scale features can still be resolved after reaction, there is no long-range order and little evidence for short-range order except for a tendency for features to align in the ⟨110⟩ direction.

*3.2.2. Coadsorption of Aniline and Dioxygen at Clean Cu(110) Surfaces.* Parts b and c of Figure 8 show STM images corresponding to the XP data in Figure 3 obtained after a clean Cu(110) surface was exposed to 200 langmuir of a 300:1 aniline/oxygen mixture at 293 K and which gave a final carbon concentration of $2.1 \times 10^{15}$ cm$^{-2}$. There are two major differences between the image in Figure 8b and that in Figure 8c and those obtained when oxygen is preadsorbed. First, the surface is characterized by considerably shorter terraces than those of the clean surface, and the profile in Figure 8d shows that nearly all the steps at the surface are of single atomic dimensions (the interplane spacing for a Cu(110) surface being 0.13 nm) whereas at the clean and partially oxidized surfaces, steps are typically bunched in twos or threes. Second, a high degree of adsorbate ordering is present after coadsorption. The phenyl imide adlayer can be described with $\begin{pmatrix} 3 & 0 \\ -1 & 2 \end{pmatrix}$ and $\begin{pmatrix} 3 & 0 \\ 1 & 2 \end{pmatrix}$ unit meshes which are clearly related, by a compression in the ⟨1$\bar{1}$0⟩ direction, to the lower coverage $\begin{pmatrix} 4 & 0 \\ -1 & 2 \end{pmatrix}$ and $\begin{pmatrix} 4 & 0 \\ 1 & 2 \end{pmatrix}$structures identified above.

## 4. Discussion

**4.1. Identification of the Chemisorbed Reaction Product.** We consider first the identity of the surface species resulting

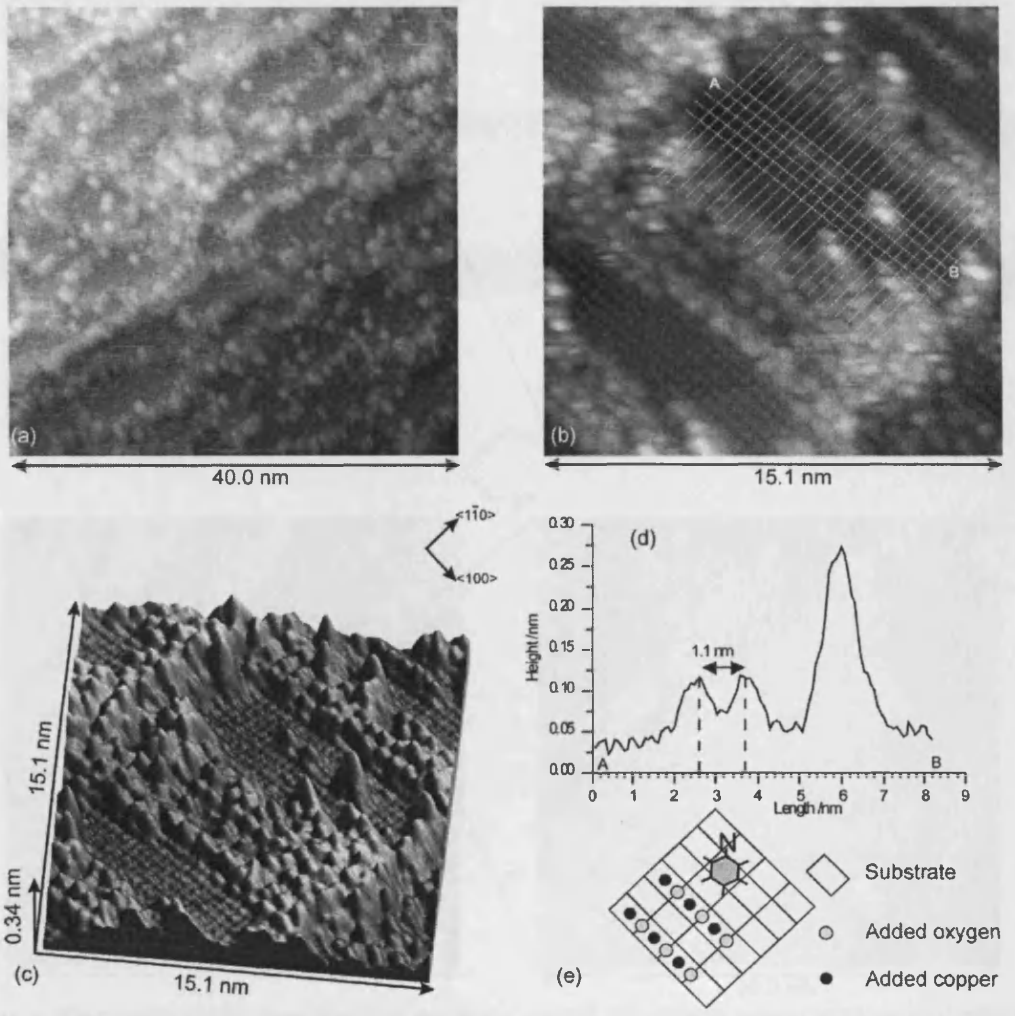


**Figure 4.** STM images recorded after the reaction of aniline with different concentrations of preadsorbed oxygen at a Cu(110) surface at 293 K: (a) initial oxygen concentration of $4.8 \times 10^{14}$ cm$^{-2}$ exposed to 20 langmuir of PhI at 293 K. $V_S = +1.22$ V, $I_T = 1.80$ nA; (b) initial oxygen concentration of $2.4 \times 10^{14}$ cm$^{-2}$ exposed to 20 langmuir of PhI at 293 K, $V_S = +1.07$ V, $I_T = 2.32$ nA. The grid superimposed on the image extrapolates the p(2 × 1)*O*(*a*) structure over the adsorbed imide. (c) 3d rendering of the topography from part b. (d) Line profile along AB in part b. (e) Model of proposed adsorption site of phenyl imide together with the p(2 × 1)O(a) lattice.

from the reaction of aniline with oxygen. The XP data indicates that the same species is formed under all the conditions studied here. The C(1s) binding energy of 293.7 eV and the 0.7 nm diameter features in the STM images agree well with previous studies[53,54] of phenyl groups at copper surfaces, and the consistent 6:1 C:N ratio with the N(1s) binding energy of 397.8 eV indicate that the C−N bond remains intact. The adsorbed species can therefore be assigned to either an amide ($C_6H_5NH$-(a)) or an imide ($C_6H_5N$(a)) with the latter being indicated by the N(1s) binding energy of 397.8 eV; amides giving N(1s) binding energies in the region of 399 eV. The presence of the phenyl imide is confirmed by the reaction stoichiometry. Although the 2:1 aniline/oxygen ratio at low oxygen concentrations suggests an amide, with water being produced through steps 1 and 2 or step 3, the 1:1 the stoichiometry at high oxygen concentrations establishes the formation of a phenyl imide through step 4.

$$PhNH_2(g) + O(a) \rightarrow PhNH(a) + OH(a) \quad (1)$$

$$PhNH_2(g) + OH(a) \rightarrow PhNH(a) + H_2O(g) \quad (2)$$

$$2OH(a) \rightarrow O(a) + H_2O(g) \quad (3)$$

$$PhNH_2(g) + O(a) \rightarrow PhN(a) + H_2O(g) \quad (4)$$

These observations can be rationalized with a model in which step 4 is slow relative to (1) and (2) or (3) at low oxygen coverages but is dominant at high surface coverages, perhaps because of steric hindrance between the two aniline reactants or the need for two adjacent adsorption sites. The phenyl imide formed from (1) and/or (2) must be unstable at the surface with

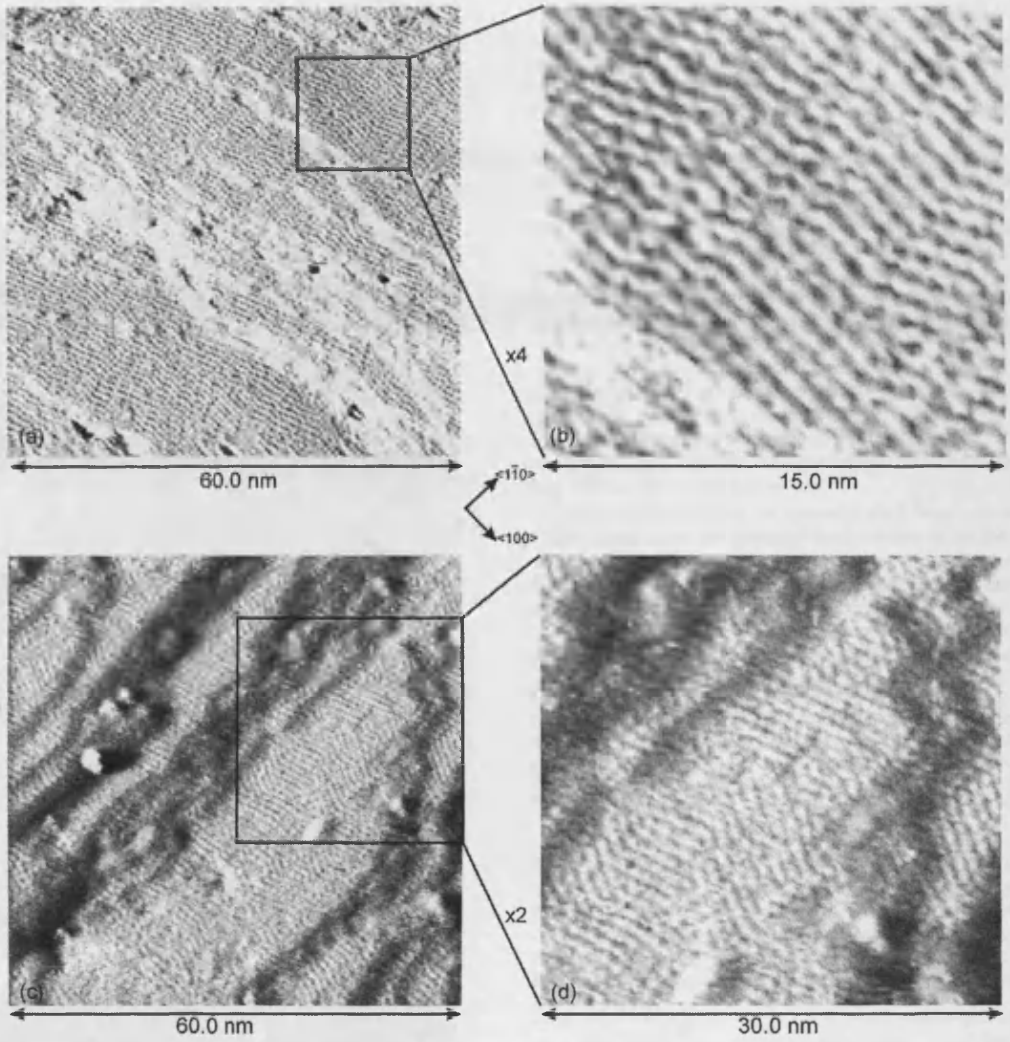


**Figure 5.** STM images showing the characteristic domain structure of a monolayer of phenyl imide generated by the reaction of aniline with preadsorbed oxygen at a Cu(110) surface at 293 K: (a and b) $V_S = 1.22$ V, $I_T = 3.05$ nA; (c and d) $V_S = 1.01$ V, $I_T = 2.42$ nA.

respect to the phenyl imide at 293 K, dissociating to give adsorbed hydrogen (step 5) which either remains at the surface or desorbs without further reaction with oxygen (step 6).

$$\mathrm{PhNH(a)} \rightarrow \mathrm{PhN(a)} + \mathrm{H(a)} \quad (5)$$

$$2\mathrm{H(a)} \rightarrow \mathrm{H_2(g)} \quad (6)$$

Similar stoichiometric changes have been observed[28] when ammonia reacts with chemisorbed oxygen suggesting a common mechanism; in that case, vibrational spectroscopy has shown that the product at room temperature is indeed the imide (NH(a)).

A detailed understanding of the reaction between ammonia and oxygen at copper surfaces has been developed in recent years. Where oxygen is preadsorbed, ammonia reacts with the ⟨100⟩ ends of the Cu−O chains[27,56] but if the oxygen transients that precede the chemisorbed islands can be intercepted (through low temperatures[57,58] or coadsorption at room temperature[28]) reaction is significantly faster and more selective. The nature and role of the oxygen transients has been discussed in detail elsewhere for a number of different systems,[23] but we emphasize here the extensive step movement that accompanies the coadsorption of aniline and dioxygen and the highly ordered adsorbate structure that results. These changes point to a very "flexible" surface during reaction. In addition, we note the high surface concentration of phenyl imide ($3.4 \times 10^{14}$ molecules $cm^{-2}$) that results from the coadsorption reaction. Assuming a square unit cell, this structure would have a *maximum* intermolecular spacing of 0.55 nm, the approximate van der Waals radius for the molecule is 0.6 nm.[59] In comparison, the equivalent imide (NH(a))[24] and phenoxy species[59] form c($2 \times 4$) and c($4 \times 2$) structures at Cu(110) surfaces respectively with

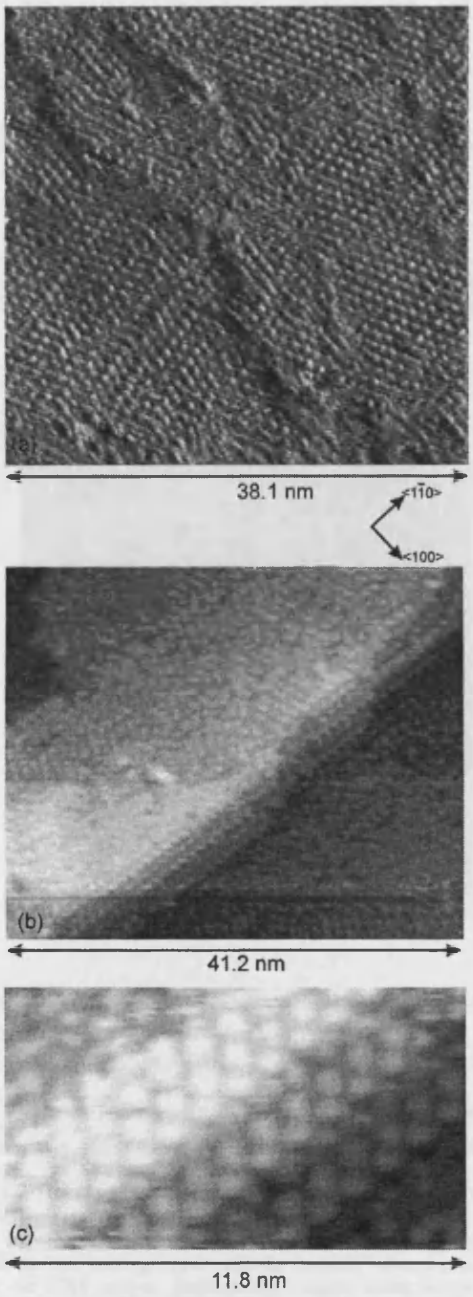


**Figure 6.** STM images showing atomically resolved domain structure of a monolayer of phenyl imide generated by the reaction of aniline with preadsorbed oxygen at a Cu(110) surface at 293 K: (a) $V_S$ = 1.22 V, $I_T$ = 3.02 nA; (b) $V_S$ = 1.26 V, $I_T$ = 3.66 nA; (c) close up of ordered imide structure at a step edge, $V_S$ = 1.27 V; $I_T$ = 3.65 nA.

maximum concentrations of $2.6 \times 10^{14}$ molecules $cm^{-2}$. We return to this point in the discussion of the structures revealed by the STM images of the coadsorbed system below.

**4.2. The Adsorption Site of the Imide.** We consider next the adsorption site of the phenyl imide. From the size of the features imaged here and their similarity to those observed after adsorption of phenyl iodide at a Cu(110) surface, we conclude that it is the phenyl group that is imaged by STM. Figure 4b establishes that, in both the ⟨100⟩ and ⟨1$\bar{1}$0⟩ directions, these features are in line with the maxima in the oxygen lattice. The oxygen lattice consists of added copper−oxygen chains orientated in the ⟨100⟩ direction and STM images the copper rather than the oxygen atoms.[60] Furthermore, the added copper atoms are known to be situated in the hollow sites of the Cu(110) substrate. The extrapolation in Figure 4b therefore indicates that the phenyl rings are also located over a hollow site in the substrate lattice. This is in agreement with the adsorption sites identified for both phenyl species[53] and benzene[61] at Cu(110) surfaces. Interestingly, the favored adsorption site of NH(a) at Cu(110) surfaces is the short bridge site,[62,63] and as Figure 4e shows, if the phenyl imide is drawn using C−C and C−N bond lengths of 0.14 nm, typical values for aromatic molecules,[64] the nitrogen can be situated in the short bridge site with the phenyl ring situated above the hollow site.

Three ordered structures are observed when "high" coverages of the phenyl imide are obtained from reaction of aniline with chemisorbed oxygen, Figure 7, parts a−c. The structure in Figure 7a can be described with a centered rectangle unit cell with the long axis 1.4 nm in length in the ⟨100⟩ direction. This agrees well with a c(4 × 4) mesh (using Wood's notation) but for the present purposes a more useful description is the primitive unit cell given in matrix notation[55] by $\begin{pmatrix} 4 & 0 \\ 2 & 2 \end{pmatrix}$. The two other structures shown in Figure 7, parts b and c, are mirror images of each other about the ⟨100⟩ axis, with rhomboid unit cells ~0.8 nm long at ±20° to the ⟨100⟩ axis; these correspond well with $\begin{pmatrix} 4 & 0 \\ -1 & 2 \end{pmatrix}$ and $\begin{pmatrix} 4 & 0 \\ 1 & 2 \end{pmatrix}$ unit meshes, respectively.

Models showing the relationship between the three structures are given in Figure 7d with the phenyl groups centered at the adsorption sites determined from Figure 4. Each has a spacing in the ⟨1$\bar{1}$0⟩ direction of 1.0 nm with the second "row" of phenyl imide two lattice spacings away in the ⟨100⟩ direction. The different structures are obtained by translating successive rows by ±1 or ±2 lattice positions in the ⟨1$\bar{1}$0⟩ direction. Interestingly, the p(4 × 2) structure, i.e. $\begin{pmatrix} 4 & 0 \\ 0 & 2 \end{pmatrix}$ in which successive rows of phenyl imide are aligned in the ⟨100⟩ direction, is not observed. Since this structure results in a smaller imide−imide nearest neighbor distance (0.72 nm) than the other three, its absence may indicate steric hindrance between adsorbed phenyl imides in the ⟨100⟩ direction. Although the exposure of the surface to aniline and dioxygen simultaneously results in a higher phenyl imide surface concentration, the minimum separation of the adsorbed molecules in the $\begin{pmatrix} 3 & 0 \\ 1 & 2 \end{pmatrix}$ structure remains greater than this value at 0.76 nm.

**4.3. Adsorbate Ordering at the Cu(110) Surface.** One of the most interesting observations from these experiments is the discrepancy between the coverages calculated from the STM images and the surface concentrations measured by XPS. If each feature in the STM images represents a phenyl imide then the three structures produced from reaction with preadsorbed oxygen have maximum surface coverages of $^1/_8$th of a monolayer, equivalent to a surface carbon concentration of $8.1 \times 10^{14}$ $cm^{-2}$. The XPS data shows an actual carbon concentration of $16 \times 10^{14}$ $cm^{-2}$. In the case of the coadsorption experiment, the

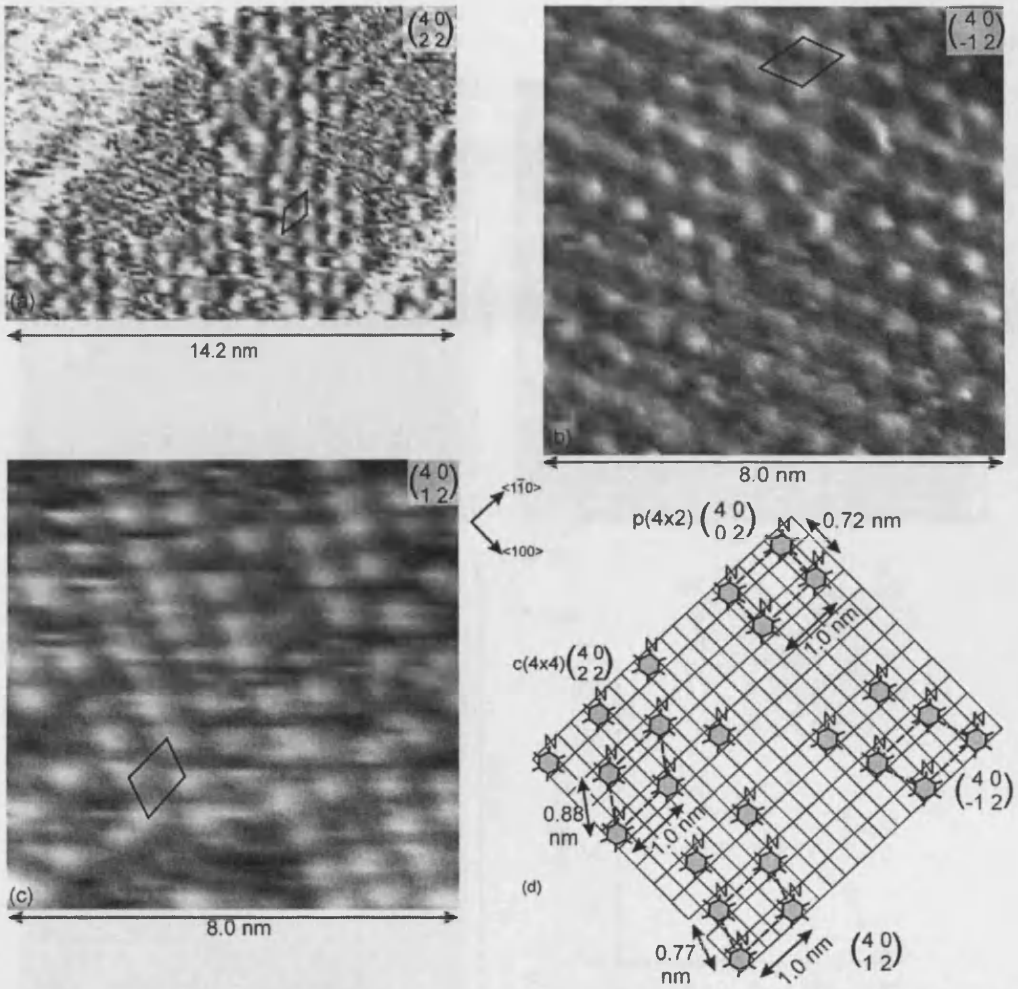


**Figure 7.** STM images of the three different domains present at a Cu(110) surface after the reaction of aniline with preadsorbed oxygen at 293 K: (a) $\begin{pmatrix} 4 & 0 \\ 2 & 2 \end{pmatrix}$, C(4 × 4) structure, $V_S = 0.80$ V, $I_T = 3.02$ nA; (b) $\begin{pmatrix} 4 & 0 \\ -1 & 2 \end{pmatrix}$, $V_S = 1.22$ V, $I_T = 3.07$ nA; (c) $\begin{pmatrix} 4 & 0 \\ 1 & 2 \end{pmatrix}$, $V_S = 1.22$ V, $I_T = 3.07$ nA. (d) Schematic showing possible structural models based on the adsorption site determined in Figure 4

$\begin{pmatrix} 3 & 0 \\ 1 & 2 \end{pmatrix}$ mesh has a maximum surface coverage of $^1/_6$th of a monolayer, equivalent to a carbon concentration of $1.1 \times 10^{14}$ cm$^{-2}$. The XPS data shows an actual carbon concentration of $2.1 \times 10^{14}$ cm$^{-2}$. We conclude that the unit cells shown by the STM contain two phenyl imide species.

Parts a and b of Figure 9 show two models which account for the high packing density and the "missing" phenyl groups in the STM images. Both models suggest strong aromatic interactions between the adsorbates. In Figure 9a, the phenyl rings are orientated in an edge-to-face T-shaped structure in which every other phenyl group is orientated perpendicular to the surface. Generally, phenyl rings bond parallel to metal surfaces, but the reduction in the heat of adsorption that results from the perpendicular orientation of half the rings could be compensated for by the formation of the T-shaped complex, which is known[65] to be a favorable structure for close packed aromatic systems. The alternative model, in Figure 9b, involves parallel phenyl pairs, a form of $\pi$-stacking, with the coordination of both nitrogens to the surface achieved by tilting the rings away from the surface plane. Parts c and d of Figure 9 show a possible model in which the lower phenyl ring is situated above a hollow site with the nitrogen atom in the short bridge site. The phenyl ring of the second molecule is parallel to the first, 0.15 nm above it and rotated by 65°, placing the nitrogen group above another short bridge site. By tilting the two phenyl rings at approximately 15° to the surface plane, around an axis which includes neither nitrogen atom, it is possible to bring the nitrogen of the upper ring to a similar height to that of the lower molecule. Surface vibrational spectroscopy has indicated that the phenyl ring is *close* to parallel to the surface,[47,66] but to date, these studies have concerned aniline reactions only with clean surfaces where the surface concentration of phenyl imide may not be high enough to force the formation of the $\pi$-stacked complex. Many other similar arrangements are possible for the

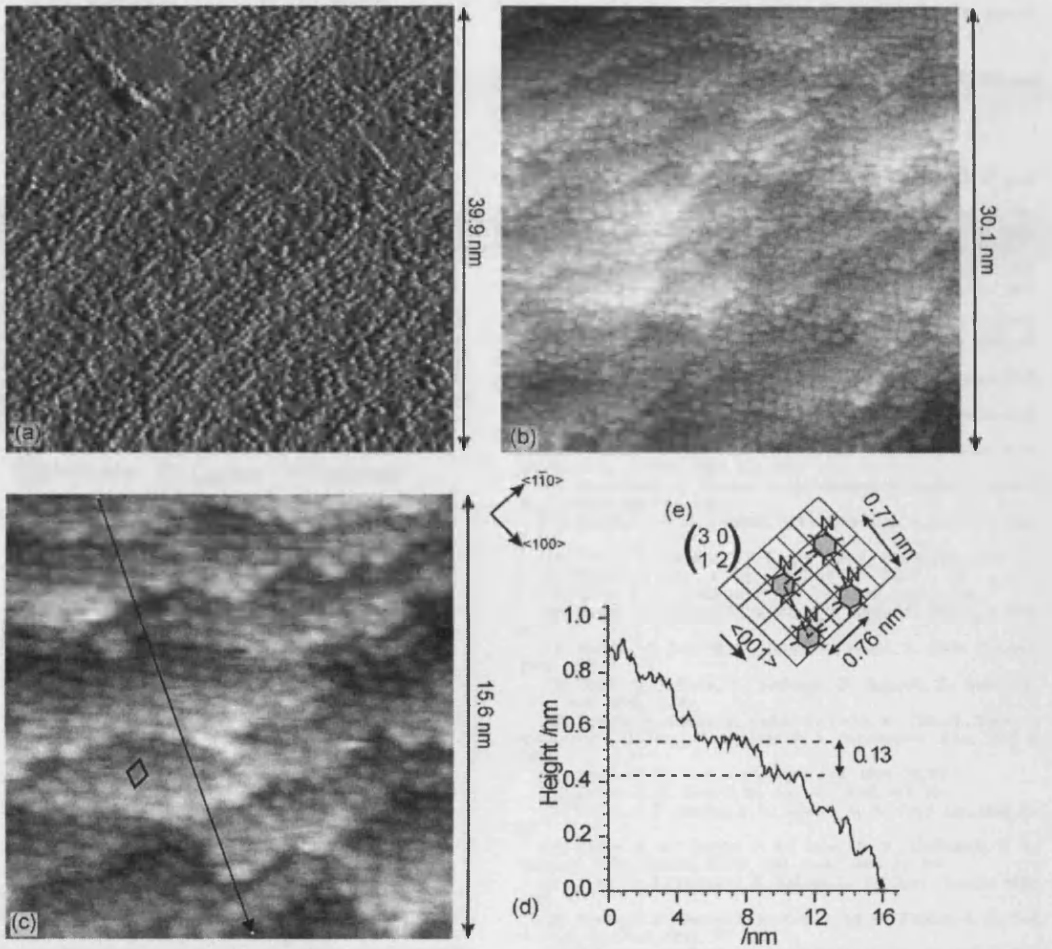


**Figure 8.** Comparison of STM images of high coverages of phenyl imide produced from (a) Cu(110) surface with an initial oxygen concentration of $2.4 \times 10^{14}$ cm$^{-2}$ exposed to 200 langmuir of aniline at 293 K, $V_S = 0.95$ V, $I_T = 1.93$ nA and (b) clean Cu(110) surface exposed to 200 langmuir of a 300:1 aniline/dioxygen mixture at 293 K, $V_S = 0.95$ V, $I_T = 2.04$ nA. (c) Close up of another area of the crystal after coadsorption, $V_S = 0.59$ V, $I_T = 2.89$ nA. (d) Line profile along line in part c showing short terraces and single atomic steps. (e) Model of the $\begin{pmatrix} 3 & 0 \\ 1 & 2 \end{pmatrix}$ structure using the adsorption site determined in Figure 4.

phenyl imide complex with the nitrogen atoms in different sites, but the model presented here has the advantage of a compact structure which would be consistent with the 0.7 nm diameter of the features observed in the STM images and also offers a explanation for the absence of the $\begin{pmatrix} 4 & 0 \\ 0 & 2 \end{pmatrix}$ and $\begin{pmatrix} 3 & 0 \\ 0 & 2 \end{pmatrix}$ structures from the surface, since these would result in the overlap of a nitrogen and a hydrogen at a bridge site, Figure 9f.

$\pi$-Stacking is associated with aromatic systems with reduced electron densities and differing polarizations, which conditions may be induced, in the present case by the interaction of the lower ring with the surface, the $\pi$-stacking interaction compensating for the reduced adsorption energy of the upper phenyl. $\pi$-Stacking of aromatic groups has been employed in the construction of 3-d supramolecular structures from large molecules such as porphyrins[67] and has been reported for smaller molecules deposited from solution[68,69] The present results, however, suggest that $\pi-\pi$ interactions play a significant role in the close packing of aromatic groups in a monolayer deposited from vacuum.

### 5. Conclusions

The reaction of aniline with surface oxygen has many characteristics in common with the equivalent reaction with ammonia, in particular, a similar dependence of the reaction stoichiometry on coverage suggesting similar reaction mechanisms, and a single imide product. The reaction with aniline is facile at room temperature, indicating that the weaker basicity of this molecule either does not affect the reaction or else is compensated for by the overall higher heat of adsorption of the phenyl ring and the weaker NH bond ($335 \pm 13$ kJ mol$^{-1}$ in aniline, $460 \pm 8$ kJ mol$^{-1}$ in ammonia[70]). There was no indication of the formation of an intermediate structure involving an expanded $(2 \times 1)$O(a) lattice as has been observed with pyridine and other amines.[32,50] By simultaneous imaging of the phenyl imide and the $p(2 \times 1)$O(a) lattice, the phenyl group

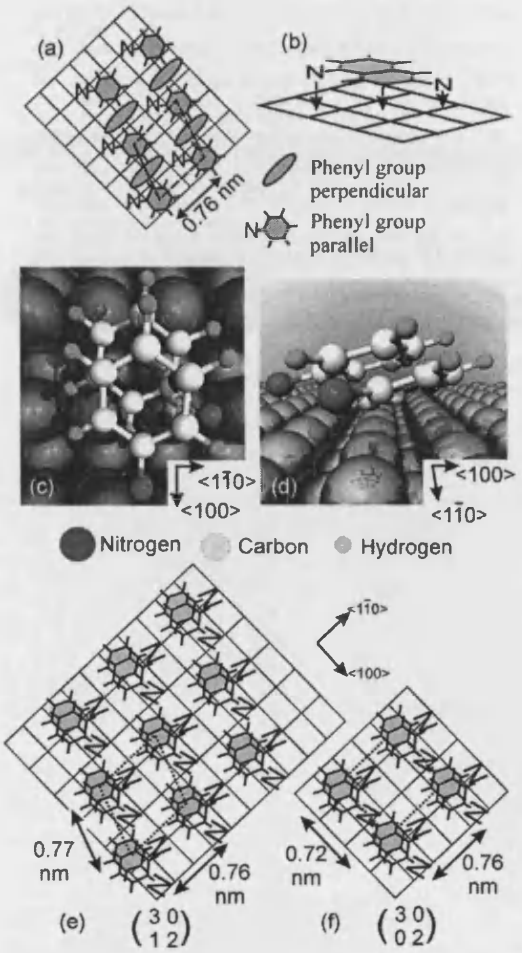


**Figure 9.** Models to account for the discrepancy between surface concentrations of phenyl imide calculated from STM and XP data: (a) edge-to-face. T-shaped packing of phenyl rings; (b) schematic of face-to-edge $\pi$-stacking model; (c) top and (d) side views of ball-and-stick drawing of the $\pi$-stacking model with phenyl rings tilted by 15° to surface plane; (e and f) models for the 2d structures of the phenyl imide dimers.

was shown to lie above the substrate hollow site, in this position the nitrogen atom of the imide can be placed over the short bridge site, the favored site for NH(a).

The maximum concentration of phenyl imide observed following exposure of *preadsorbed* oxygen to aniline was determined by XPS to be $2.6 \times 10^{14}$ cm$^{-2}$. At this concentration the phenyl imide adlayer forms domains of three closely related ordered structures described by $\begin{pmatrix} 4 & 0 \\ 2 & 2 \end{pmatrix}$, $\begin{pmatrix} 4 & 0 \\ -1 & 2 \end{pmatrix}$, and $\begin{pmatrix} 4 & 0 \\ 1 & 2 \end{pmatrix}$ unit cells. Adsorption of aniline and dioxygen mixtures however leads to closer packing of the phenyl imides with a concentration calculated from the XPS spectra of $3.4 \times 10^{14}$ cm$^{-2}$ and an ordered adlayer described by $\begin{pmatrix} 3 & 0 \\ 1 & 2 \end{pmatrix}$ and $\begin{pmatrix} 3 & 0 \\ -1 & 2 \end{pmatrix}$ unit cells.

The surface concentrations calculated from the XPS for the ordered phenyl imide structures are twice that calculated from the unit cells revealed by the STM. Furthermore, the high phenyl imide concentrations indicate a nearest neighbor distance that is less than the van der Waals radius of the molecule. To account for these observations it is proposed that attractive $\pi-\pi$ interactions between the phenyl imide adsorbates give rise to $\pi$-stacking in the monolayer.

**Acknowledgment.** This work was supported by EPSRC and The Royal Society.

### References and Notes

(1) Lazarova, E.; Petkova, G.; Raicheff, R.; Neykov, G. *J. Appl. Electrochem.* **2002**, *32*, 1355.
(2) Khaled, K. F.; Hackerman, N. *Electrochim. Acta* **2004**, *49*, 485.
(3) Du, T. B.; Chen, J. J.; Cao, D. Z. *J. Mater. Sci.* **2001**, *36*, 3903.
(4) Luo, H.; Guan, Y. C.; Han, K. N. *Corrosion* **1998**, *54*, 721.
(5) Khaled, K. F.; Hackerman, N. *Mater. Chem. Phys.* **2003**, *82*, 949.
(6) Gaillard, F.; Joly, J. P.; Peillex, E.; Romand, M. *J. Adhes.* **2000**, *72*, 317.
(7) Li, Z. F.; Ruckenstein, E. *J. Colloid Interface Sci.* **2002**, *251*, 343.
(8) Harun, M. K.; Lyon, S. B.; Marsh, J. *Prog. Org. Coat.* **2003**, *46*, 21.
(9) Johnsen, B. B.; Olafsen, K.; Stori, A. *Int. J. Adhes. Adhes.* **2003**, *23*, 157.
(10) Marsh, J.; Minel, L.; Barthes-Labrousse, M. G.; Gorse, D. *Appl. Surf. Sci.* **1998**, *133*, 270.
(11) Penzien, J. C.; Haessner, C.; Jentys, A.; Kohler, K.; Muller, T. E.; Lercher, J. A. *J. Catal.* **2004**, *221*, 302.
(12) Bronnimann, C.; Bodnar, Z.; Aeschimann, R.; Mallat, T.; Baiker, A. *J. Catal.* **1996**, *161*, 720.
(13) Huntsman, W. D.; Madison, N. L.; Schlesinger, S. I. *J. Catal.* **1963**, *2*, 498.
(14) Struijk, J.; Scholten, J. J. F. *Appl. Catal., A* **1992**, *82*, 277.
(15) Pfaltz, A.; Heinz, T. *Top. Catal.* **1997**, *4*, 229.
(16) Wells, P. B.; Wilkinson, A. G. *Top. Catal.* **1998**, *5*, 39.
(17) Bartok, M.; Felfoldi, K.; Szollosi, G.; Bartok, T. *Catal. Lett.* **1999**, *61*, 1.
(18) Bartok, M.; Felfoldi, K.; Torok, B.; Bartok, T. *Chem. Commun.* **1998**, 2605.
(19) Torok, B.; Felfoldi, K.; Szakonyi, G.; Balazsik, K.; Bartok, M. *Catal. Lett.* **1998**, *52*, 81.
(20) Tungler, A.; Mathe, T.; Tamai, T.; Fodor, K.; Toth, G.; Kajtar, J.; Kolossvary, I.; Herenyi, B.; Sheldon, R. A. *Tetrahedron: Asym.* **1995**, *6*, 2395.
(21) Davies, P. R.; Keel, J. M. *Catal. Lett.* **1999**, *58*, 99.
(22) Davies, P. R.; Keel, J. M. *Surf. Sci.* **2000**, *469*, 204.
(23) Carley, A. F.; Davies, P. R.; Roberts, M. W. *Catal. Lett.* **2002**, *80*, 25.
(24) Carley, A. F.; Davies, P. R.; Jones, R. V.; Harikumar, K. R.; Kulkarni, G. U.; Roberts, M. W. *Top. Catal.* **2000**, *11*, 299.
(25) Carley, A. F.; Davies, P. R.; Roberts, M. W. *Chem. Commun.* **1998**, 1793.
(26) Carley, A. F.; Davies, P. R.; Roberts, M. W.; Thomas, K. K.; Yan, S. *Chem. Commun.* **1998**, 35.
(27) Carley, A. F.; Davies, P. R.; Roberts, M. W.; Vincent, D. *Top. Catal.* **1994**, *1*, 35.
(28) Afsin, B.; Davies, P. R.; Pashusky, A.; Roberts, M. W.; Vincent, D. *Surf. Sci.* **1993**, *284*, 109.
(29) Afsin, B.; Davies, P. R.; Pashuski, A.; Roberts, M. W. *Surf. Sci.* **1991**, *259*, L724.
(30) Carley, A. F.; Davies, P. R.; Harikumar, K. R.; Jones, R. V.; Kulkarni, G. U.; Roberts, M. W. *Top. Catal.* **2001**, *14*, 101.
(31) Carley, A. F.; Yan, S.; Roberts, M. W. *J. Chem. Soc., Faraday Trans.* **1990**, *86*, 2701.
(32) Carley, A. F.; Davies, P. R.; Jones, R. V.; Kulkarni, G. U.; Roberts, M. W. *Chem. Commun.* **1999**, 687.
(33) Davies, P. R.; Shukla, N. *Surf. Sci.* **1995**, *322*, 8.
(34) Thornburg, D. M.; Madix, R. J. *Surf. Sci.* **1990**, *226*, 61.
(35) Sasaki, T.; Aruga, T.; Kuroda, H.; Iwasawa, Y. *Surf. Sci.* **1992**, *276*, 69.
(36) Maseri, F.; Peremans, A.; Darville, J.; Gilles, J. M. *J. Electron Spectrosc. Relat. Phenom.* **1990**, *54*, 1059.
(37) Sasaki, T.; Aruga, T.; Kuroda, H.; Iwasawa, Y. *Surf. Sci.* **1991**, *249*, L347.
(38) Gardin, D. E.; Somorjai, G. A. *J. Phys. Chem.* **1992**, *96*, 9424.
(39) Erley, W.; Hemminger, J. C. *Surf. Sci.* **1994**, *316*, L1025.
(40) Erley, W.; Xu, R.; Hemminger, J. C. *Surf. Sci.* **1997**, *389*, 272.
(41) Chen, J. J.; Winograd, N. *Surf. Sci.* **1995**, *326*, 285.
(42) Birtill, J. J.; Ridley, P.; Liddle, S.; Nunney, T. S.; Raval, R. *Ind. Eng. Chem. Res.* **2001**, *40*, 553.
(43) Barlow, S. M.; Haq, S.; Raval, R. *Langmuir* **2001**, *17*, 3292.

(44) Xu, X. P.; Friend, C. M. *J. Vac. Sci. Technol. A—Vac. Surf. Films* **1991**, *9*, 1599.
(45) Bitzer, T.; Alkunshalie, T.; Richardson, N. V. *Surf. Sci.* **1996**, *368*, 202.
(46) Rummel, R. M.; Ziegler, C. *Surf. Sci.* **1998**, *418*, 303.
(47) Ashton, M. R.; Jones, T. S.; Richardson, N. V.; Mack, R. G.; Unertl, W. N. *J. Electron Spectrosc. Relat. Phenom.* **1990**, *54*, 1133.
(48) Carley, A. F.; Roberts, M. W. *Proc. R. Soc. London, Ser. A* **1978**, *363*, 403.
(49) Carley, A. F.; Davies, P. R.; Jones, R. V.; Harikumar, K. R.; Kulkarni, G. U.; Roberts, M. W. *Surf. Sci.* **2000**, *447*, 39.
(50) Carley, A. F.; Davies, P. R.; Edwards, D.; Parsons, M.; Roberts, M. W. Manuscript in preparation.
(51) Cabibil, H.; Ihm, H.; White, J. M. *Surf. Sci.* **2000**, *447*, 91.
(52) Carley, A. F.; Coughlin, M.; Davies, P. R.; Morgan, D. J.; Roberts, M. W. *Surf. Sci. Lett.* **2004**, in press.
(53) Carley, A. F.; Coughlin, M.; Davies, P. R.; Morgan, D. J.; Roberts, M. W. *Surf. Sci.* **2004**, *555*, L138.
(54) Weiss, P. S.; Kanma, M. M.; Graham, T. M.; Stranick, S. J. **1998**, *14*, 1284.
(55) Park, R. L.; Madden, H. H., Jr. *Surf. Sci.* **1968**, *11*, 188.
(56) Guo, X. C.; Madix, R. J. *Faraday Discuss.* **1996**, 139.
(57) Carley, A. F.; Davies, P. R.; Kulkarni, G. U.; Roberts, M. W. *Catal. Lett.* **1999**, *58*, 93.
(58) Sueyoshi, T.; Sasaki, T.; Iwasawa, Y. *J. Phys. Chem.* **1996**, *100*, 1048.
(59) Guo, X. C.; Madix, R. J. *Surf. Sci.* **1995**, *341*, L1065.
(60) Buisset, J.; Rust, H. P.; Schweizer, E. K.; Cramer, L.; Bradshaw, A. M. *Surf. Sci.* **1996**, *349*, L147.
(61) Rogers, B. L.; Shapter, J. G.; Ford, M. *Surf Sci* **2004**, *548*, 29.
(62) Davies, P. R.; Keel, J. M. *Phys. Chem. Chem. Phys.* **1999**, *1*, 1383.
(63) Hirschmugl, C. J.; Schindler, K. M.; Schaff, O.; Fernandez, V.; Theobald, A.; Hofmann, P.; Bradshaw, A. M.; Davis, R.; Booth, N. A.; Woodruff, D. P.; Fritzsche, V. *Surf. Sci.* **1996**, *352*, 232.
(64) Walker, B. W.; Stair, P. C. *Surf. Sci.* **1981**, *103*, 315.
(65) Hunter, C. A.; Lawson, K. R.; Perkins, J.; Urch, C. J. *J. Chem. Soc., Perkin Trans. 2* **2001**, 651.
(66) Plank, R. V.; Dinardo, N. J.; Vohs, J. M. *Surf. Sci.* **1995**, *340*, L971.
(67) Gesquiere, A.; De Feyter, S.; De Schryver, F. C.; Schoonbeek, F.; van Esch, J.; Kellogg, R. M.; Feringa, B. L. *Nano Lett.* **2001**, *1*, 201.
(68) Pinheiro, L. S.; Temperini, M. L. A. *Surf. Sci.* **1999**, *441*, 45.
(69) Pinheiro, L. S.; Temperini, M. L. A. *Surf. Sci.* **2000**, *464*, 176.
(70) *CRC Handbook of Chemistry and Physics*, 59th ed.; Weast, R. C., Ed.; CRC Press Inc: Boca Raton, FL, 1979; pp F215.

*Topics in Catalysis Vol. 36, Nos. 1–4, August 2005 (© 2005)*
DOI: 10.1007/s11244-005-7859-1



# Molecularly resolved studies of the reaction of pyridine and dimethylamine with oxygen at a Cu(110) surface

Albert F. Carley, Philip R. Davies*, Dyfan Edwards, Rhys V. Jones, and Martin Parsons
*School of Chemistry, Cardiff University, Cardiff CF10 3AT, United Kingdom*

Pyridine and dimethylamine have been studied at clean and oxidised Cu(110) surfaces as model systems for the interaction of amines with heterogeneous catalysts using scanning tunnelling microscopy and X-ray photoelectron spectroscopy. Both molecules interact strongly with sub monolayer concentrations of chemisorbed oxygen causing a change from the well known p(2 × 1)O(a) islands to a (3 × 1) structure. XPS shows a 1:1 correspondence between the concentration of surface oxygen and that of chemisorbed pyridine but the stoichiometry of the dimethylamine/oxygen system could not be directly measured because of a slow reaction which results in the desorption of oxygen as water and the formation of a chemisorbed amide. The amide also decomposes at room temperature and desorbs leaving a clean surface. However, the 2:1 stoichiometry of the dimethylamine/oxygen reaction suggests a 1:1 dimethylamine:oxygen ratio in the (3 × 1) structure. The results of the study are interpreted in terms of an amine–oxygen complex, which may provide a general model for the interaction of amines with oxygen at metal surfaces.

**KEY WORDS:** dimethylamine; pyridine; XPS; STM; amide; surface; Cu(110), amine oxide.

## 1. Introduction

With the advent of STM, the high mobility of adsorbates and substrates under mild reaction conditions was unmistakable [1], with obvious implications for the modelling of heterogeneous catalytic mechanism. At about the same time, other experimental evidence was accruing, from more established techniques [2,3], that highlighted the role of short lived species and further emphasised the deficiencies of the "chess board" model as a basis for understanding surface reaction mechanisms. However, the dynamic nature of the surface has not made the issue of surface structure redundant; in many cases an improved knowledge of the detailed local atomic structure, which STM makes possible even in relatively disordered systems, has improved our understanding of the factors affecting surface reaction kinetics and hence, of catalytic mechanisms. The oxidation of methanol is a case in point, an understanding [4] of the role of oxygen and methoxy islands and the importance of the interface between them, having led to an explanation of the different pathways that have been observed for this reaction under different experimental conditions [5,6]. Similarly, the kinetics of ammonia oxidation at Cu(110) surfaces were explained with a Monte Carlo model [7] of the atomic structure of the partial oxygen adlayer based upon evidence provided by STM. We have been studying the role of local atomic structure in surface reaction mechanisms by STM, and in this paper we continue our studies of the interaction of amines with oxygen [8–13].

The surface chemistry of amines is important in a number of catalytic processes, including the catalytic oxidative decomposition of amines in effluent [14,15] and the commercial production of amines. In the latter case, Baiker and co-workers have reported [16–19] the synthesis of alkylamines over copper catalysts with a product distribution much closer to that required by industry than the present methanol amination process, and with the added environmental advantage of using carbon dioxide as the feedstock. Amines also play an important role in modifying the selectivity and activity of other catalytic reactions. For example, palladium [20] and ruthenium [21] based hydrogenation catalysts are enhanced by amine modification and the enantioselective hydrogenation of α-functionalised ketones and olefins over platinum [22] requires a modifier containing a basic nitrogen atom [23–26] and the presence of oxygen [27].

With very few exceptions [28–30], previous studies of amine surface chemistry have considered adsorption only at clean metal [28,31–35] or silicon surfaces [36–38] and utilised in the main temperature programmed desorption (TPD) and vibrational spectroscopy (RAIRS and HREELS). We have, on the contrary, studied reactions with other adsorbed species, particularly oxygen [11,13,39–41]. In this paper we are interested in the way in which the nitrogen of an amine group interacts with an adsorbed oxygen state. Previous work [42] has hinted that at Cu(110) surfaces the presence of ammonia in the gas phase results in a weakening of the oxygen–metal interaction and thus a greater mobility of the oxygen islands over the metal surface. This could be attributed to hydrogen bonding between the transiently adsorbed ammonia molecules and the surface oxygen, but a study of pyridine at Cu(111) surfaces [8] and a

* To whom correspondence should be addressed.
E-mail: daviespr@cf.ac.uk

1022-5528/05/0800-0021-0 © 2005 Springer Science+Business Media, Inc.

preliminary study of pyridine on Cu(110) [11] has suggested a different pathway involving the formation of a surface pyridine-oxide from the interaction between the nitrogen lone pair and the surface oxygen. This resulted, on Cu(110), in a change in the local structure of the chemisorbed oxygen. To explore this mechanism further we have recently investigated [9,10] the adsorption of aniline at Cu(110) surfaces. Aniline is a significantly weaker base than pyridine but unlike pyridine is still capable of hydrogen bonding interactions. No changes in the local structure of the oxygen were evident however, although the dehydrogenation of the aniline via Eq. 1, was so rapid, that changes may have been occurring on a timescale that could not be followed with STM.

$$2PhNH_2(g) + O(a) \rightarrow 2PhN(a) + H_2O(g) + H_2(g) \quad (1)$$

In the present study we explore the nature of the pyridine–oxygen interaction and the mechanism by which the pyridine–oxygen complex forms and compare it to the effect of dimethylamine ($(CH_3)_2NH$) adsorption, a stronger base than either ammonia or pyridine.

## 2. Experimental

Experiments were conducted on a combined variable temperature STM/XPS instrument (Omicron Vacuum Physik) equipped with a dual Alkα and Mgkα photon source. XP spectra were recorded with a pass-energy of 50 eV except where stated otherwise. This resulted in typical peak half-width of ca 1.8 eV. Spectra were obtained by the combination of 10–20 individual scans over a 25 eV wide region, with total acquisition time of 15 min (O(1s) and Cu (2p) spectra) to 30 min (C(1s) and N(1s) spectra). The spectra were calibrated against the clean Cu($2p_{3/2}$) peak at 932.7 eV. XPS data were acquired using commercial software (DAT125, Omicron). XP peak areas were used to calculate surface concentrations according to the method discussed previously [43,44]. This results in an error in surface concentration for oxygen of about $\pm 3 \times 10^{13}$ cm$^{-2}$ but slightly more in the case of carbon and nitrogen, which have weaker signals.

The dimensions of the sample were 7 mm by 7 mm with a thickness of approximately 0.5 mm, cut to within 0.5 degrees of the (110) plane and polished mechanically down to 0.25 μm. Cleaning involved cycles of $Ar^+$ sputtering (0.76 keV, 20 μA cm$^{-2}$ for 20 min) and annealing for 60 min at 900 K. Sample cleanliness was checked by XPS. Pyridine (Aldrich, 99.8%) was further purified by several freeze-pump-thaw cycles before dosing; dimethylamine (Argo Ltd, 99.0%) and oxygen (Argo Ltd, 99.998%) were used as received. Gases were dosed via a leak valve at pressures of between $10^{-9}$ and $5 \times 10^{-7}$ mbar and their purity confirmed with *in situ* mass spectrometry.

## 3. Results

### 3.1. The adsorption of pyridine at clean and partially oxidised Cu(110) surfaces

After exposures to pyridine of over 100 L no adsorption was detected by XPS at clean Cu(110) surfaces at room temperature. At 160 K, physisorption of pyridine takes place as evidenced by peaks in the C(1s) and N(1s) regions of the photoelectron spectrum at binding energies of 285.1 eV and 399.0 eV respectively. However, STM images of the surface after pyridine adsorption at this temperature do not show the presence of the pyridine, (figure 1(a)), perhaps because the relatively weak interaction between molecule and surface results in movement of the adsorbate during the STM scan; similar effects have been seen with other adsorbates [44–46]. On warming, the desorption of pyridine is complete by room temperature. At partially preoxidised surfaces the interaction of pyridine is much stronger, but at low temperatures the STM shows no apparent effect on the preadsorbed oxygen structure. Figure 1(b) shows an STM image recorded at 160 K of a Cu(110) surface at which approximately $4 \times 10^{14}$ cm$^{-2}$ of oxygen had been chemisorbed at room temperature before cooling to 160 K and exposure to 3.3 L of pyridine. The p(2 × 1) O(a) lattice is clearly visible in the image with the characteristic Cu–O chains spaced 0.51 nm in the $<1\bar{1}0>$ direction as indicated by the black arrows. In a gap between two oxygen islands, indicated by the white arrow (i) there is some evidence for "doughnut" shaped features with a diameter of approximately 0.5 nm comparable with the van der Waals radius of the pyridine molecule. These features were never observed in the absence of pyridine and we tentatively assign them to pyridine molecules trapped between the two oxygen islands and thus prevented from moving away from the STM tip during scanning. On warming, the partially oxidised surface with the pyridine present is restructured with the <100> orientated Cu–O chains moving apart in the $<1\bar{1}0>$ direction to a separation of 0.76 nm. The pyridine is much more strongly adsorbed in the presence of oxygen and remains at the surface until at least 400 K, whereupon XPS shows complete desorption of the pyridine, (presumably molecularly since there is no loss of oxygen), and the p(2 × 1) oxygen islands are reformed.

The restructuring of the p(2 × 1) oxygen islands also occurs when pyridine is adsorbed at room temperature. Figure 1(c) and (d) show a partially oxidised surface ($\sigma_O = 2.5 \times 10^{14}$ cm$^{-2}$) before and after exposure to 5 L of pyridine at ~293 K. There are three features to note; the increased separation of the Cu–O chains from 0.51 nm to ~0.76 nm indicated by the black arrows; the retention of the 0.36 nm separation between the maxima along the Cu–O chains in the <100> direction; and the position of the maxima within the "Cu–O" chains after pyridine adsorption which coincide with the maxima of the clean surface surrounding the oxygen island.

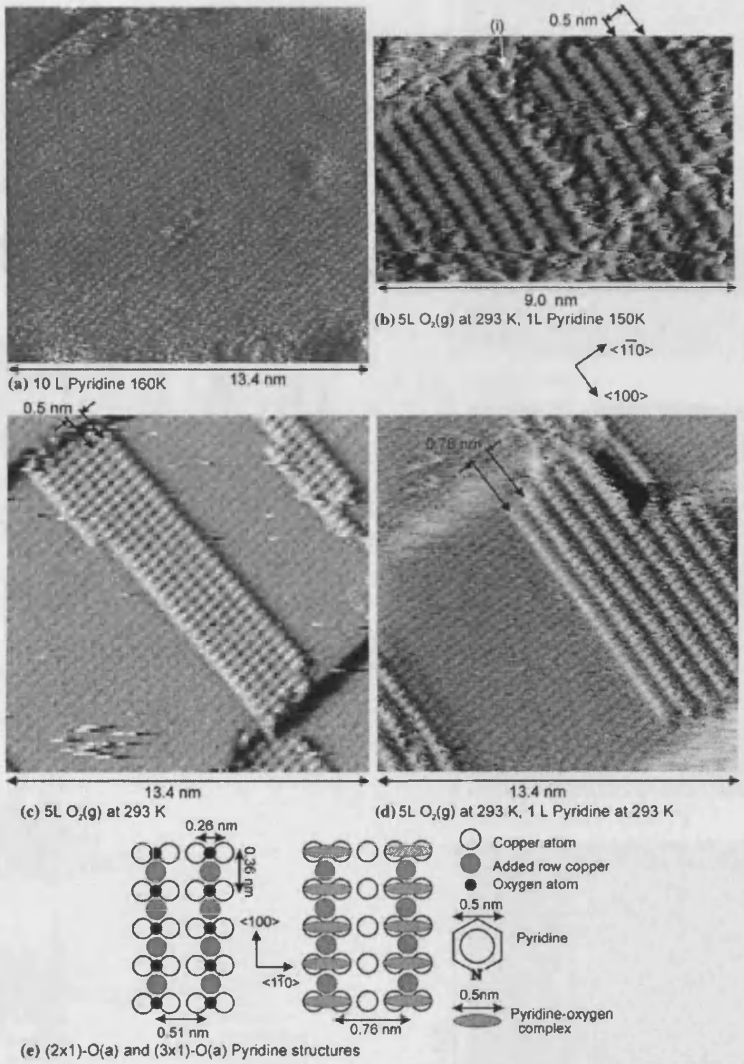


Figure 1. A comparison of STM images of the adsorption of pyridine at clean and preoxidised Cu(110) surfaces. (a) Clean Cu(110) exposed to 10 L pyridine at 160 K, $V_S = 0.95$ V, $I_T = 1.93$ nA. (b) Partially oxidised Cu(110) exposed to 1 L pyridine at 150 K, $V_S = 1.05$ V, $I_T = 2.53$ nA. (c) Partially oxidised Cu(110) at 293 K, $V_S = -1.03$ V, $I_T = 2.93$ nA. (d) Partially oxidised Cu(110) exposed to 1 L pyridine at 293 K, $V_S = -0.11$ V, $I_T = 2.79$ nA. (e) Models of the (2 × 1)O(a) and (3 × 1)O(a)/Py structures.

Figure 1(e) shows a model comparing the accepted structure of the p(2 × 1) O(a) lattice on Cu(110) with the new (3 × 1) structure, this suggests that the maxima in the pyridine-controlled structure corresponds to the oxygen sites within the chains.

The STM images in 1(d) and the model in 1(e) suggest a 1:1 correspondence between the pyridine and surface oxygen. This is confirmed by the XP spectra in figure 2 which show the effect of a 345 L saturation exposure of pyridine, at room temperature, on a Cu(110) surface with an initial oxygen concentration of $2.9 \times 10^{14}$ cm$^{-2}$. There is no evidence in the O(1s) region for the pyridine having any discernable effect on the preadsorbed oxygen but carbon and nitrogen peaks do appear in the spectra at binding energies of 285.1 eV and 399.0 eV respectively, (figure 2(b)). The final C:N:O ratio at the surface, calculated from the photoelectron spectra as described above, is 5:1:1 corresponding exactly with molecular adsorption of the pyridine in a 1:1 complex with the surface oxygen. To probe the stability of the complex the

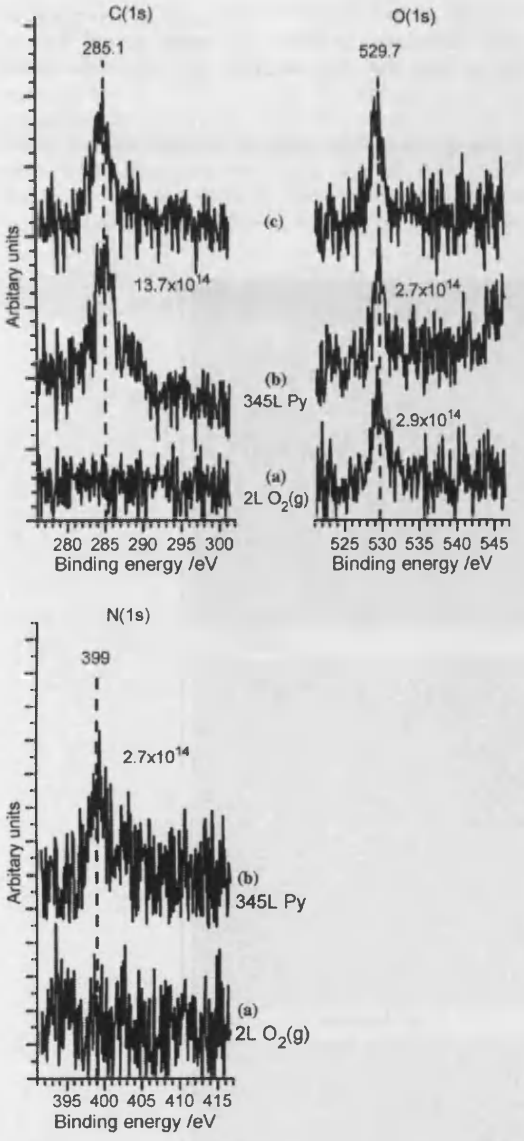


Figure 2. XP spectra of the adsorption of pyridine at a preoxidised Cu(110) surface. (a) Clean. (b) 2 L $O_2$(g). (c) 345 L pyridine at room temperature.

surface was left overnight at room temperature; the subsequent XP spectra 2(c) show no change in either binding energy or surface concentration.

More detailed information on the effect of the pyridine on the oxygen comes from figure 3 which shows an area of the Cu(110) surface with a low initial

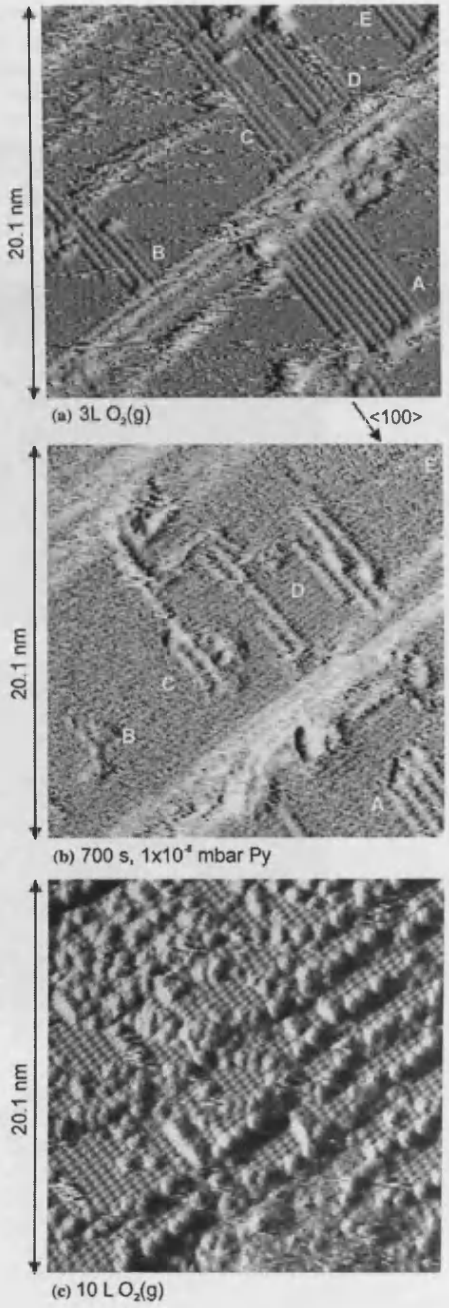


Figure 3. The effect of pyridine on low oxygen concentrations at a Cu(110) surface. (a) Surface before pyridine dose, $V_s = -2.23$ V, $I_T = 2.84$ nA. (b) During pyridine adsorption, $V_s = -1.73$ V, $I_T = 2.08$ nA. (c) After 10 L $O_2$, $V_s = 0.85$ V, $I_T = 2.08$ nA.

oxygen coverage ($\sigma_O \sim 2 \times 10^{14}$ cm$^{-2}$) before, figure 3 (a) and during figure 3(b) pyridine adsorption. The initial adsorption of pyridine was too fast to be captured by the STM images, the expansion of the oxygen chains occurring within the space of a single image, but the changes in island size and/or position are shown. Island A has been reduced from eight chains to four and moved towards the right of the image which has also allowed it to move closer to the bottom of the image and away from the upper step edge. Island B has all but vanished whereas island C retains two chains though they are now separated by 0.76 nm. Island D has split into two and the two chains in the right hand half of the islands are in the process of moving during the image shown in figure 3(b). Heating the surface to 400 K results in the desorption of the pyridine, leaving a $(2 \times 1)$ O(a) structure. On the other hand, exposure of the pyridine

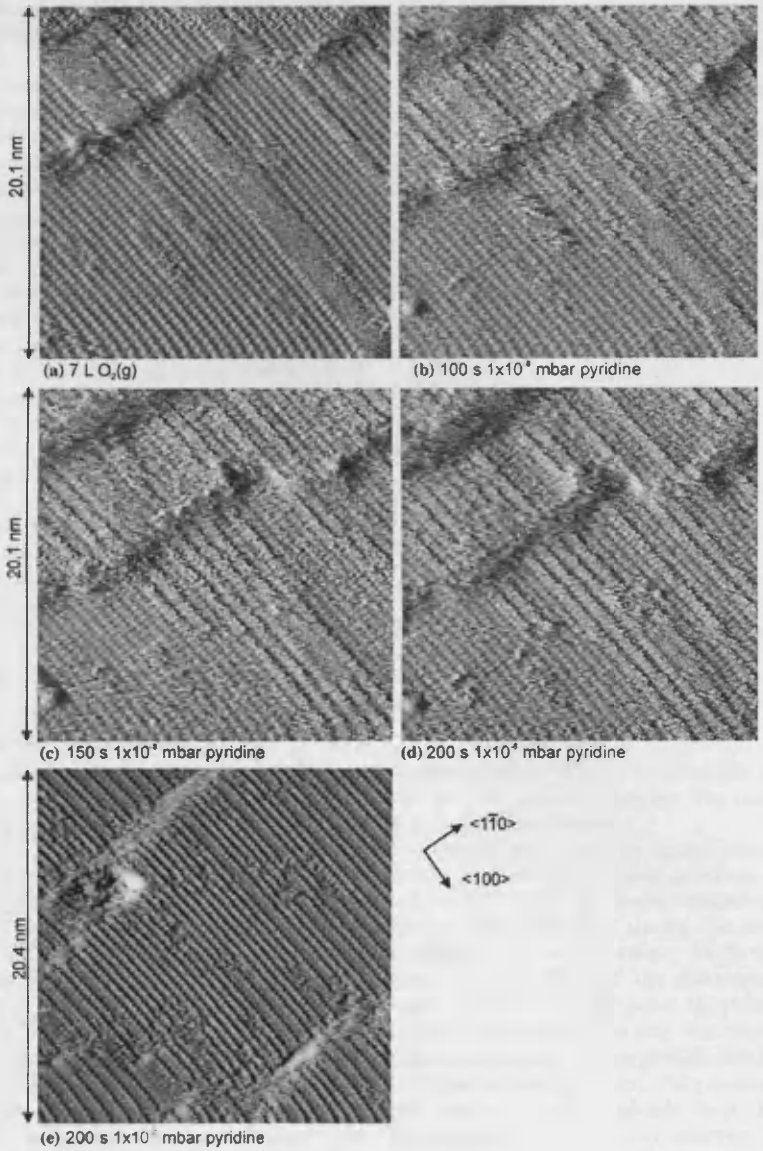


Figure 4. The effect of pyridine on high oxygen concentrations at a Cu(110) surface. (a) Adsorption of 7 L $O_2$(g), $V_s = 0.04$ V, $I_T = 3.00$ nA. (b)–(d) During pyridine exposure at $1 \times 10^{-8}$ mbar, $V_s = 0.04$ V, $I_T = 3.11$ nA. (e) After pyridine exposure, $V_s = -0.04$ V, $I_T = 2.94$ nA.

covered surface to oxygen results in the development of a p(2 × 1) lattice decorated with 0.5 nm diameter features often collected at step edges, (figure 3(c)).

### 3.2. *The adsorption of pyridine in the presence of high coverages of surface oxygen*

At higher oxygen coverages, the effects of pyridine adsorption can be followed more easily because the high surface concentration limits the mobility of the surface adsorbates. In figure 4, a surface with an initial oxygen concentration of $\sim 4.5 \times 10^{14}$ cm$^{-2}$ was monitored by STM during an exposure to pyridine of $1 \times 10^{-8}$ mbar. Before exposure to pyridine, figure 4(a), the images show a surface almost completely covered in oxygen but with a small number of areas of clean surface also present. After 100 s of pyridine exposure, figure 4(b), the chains on each side of the clean surface areas have expanded, reducing the area of the clean surface, furthermore there is an increase in "noise" on these chains with the atomic detail in the <100> direction becoming obscured on some of them. After another 50 s exposure, figure 4(c), the clean areas of copper have narrowed further and several broad, noisy chains are apparent to either side of the clean areas. After 200 s all the clean areas of the surface are covered in the broader noisy chains but areas originally covered in the close packed p(2 × 1) O(a) structure have not been affected, see for example the lower left hand corner of image figure 4(d) which still retains the atomically resolved p(2 × 1) O(a) structure. Further exposures to pyridine do not result in any other changes to the surface structure which now exhibits mixed areas of atomically resolved p(2 × 1) and (3 × 1) structures, (figure 4(e)). Pyridine does not adsorb at a Cu(110) surface precovered with a (2 × 1) monolayer of oxygen.

### 3.3. *The adsorption of dimethylamine at clean and partially oxidised Cu(110) surface*

Dimethylamine was not detected by XPS at clean Cu(110) surfaces after exposures at room temperature of up to 200 L but it does react with preadsorbed surface oxygen. A surface with an initial oxygen concentration of $3.0 \times 10^{14}$ cm$^{-2}$ was exposed to dimethylamine, (figure 5). After a total exposure of 30 L of dimethylamine, $0.6 \times 10^{14}$ cm$^{-2}$ of the oxygen is still present at the surface: by analogy with ammonia [7,47], the remaining $2.4 \times 10^{14}$ cm$^{-2}$ of oxygen has presumably desorbed as water, Eq. 2.

$$O(a) + 2(CH_3)_2NH(g) \rightarrow H_2O(g) + 2(CH_3)_2N(a) \quad (2)$$

The 2:1 stoichiometry of reaction (2) implies a final nitrogen concentration of $4.8 \times 10^{14}$ cm$^{-2}$ and a final carbon concentration of $9.6 \times 10^{14}$ cm$^{-2}$. However, in the XP spectra nitrogen is not detected at all and only a small part of the carbon remains by the end of the experiment. Clearly, the amide product undergoes a further reaction leading to desorption of both nitrogen and carbon containing species. The nature of this reaction is discussed below.

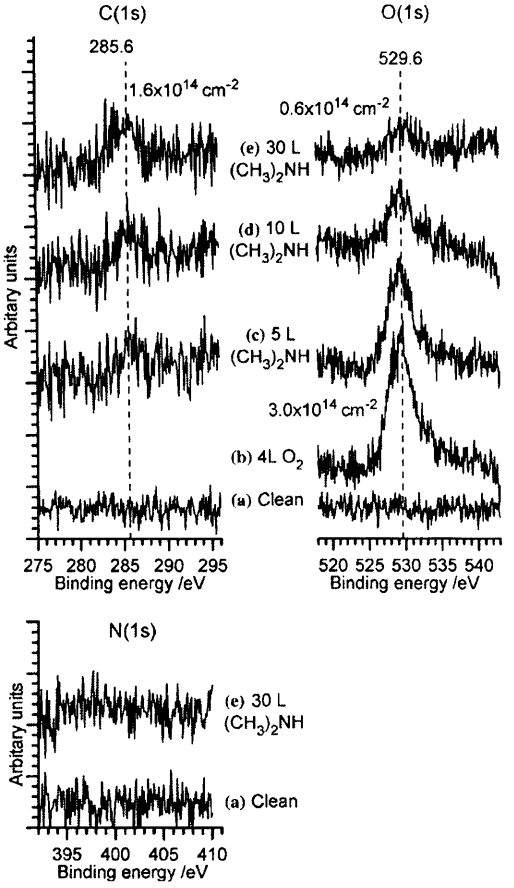


Figure 5. XP spectra of the adsorption of dimethylamine at a preoxidised Cu(110) surfaces. (a) Clean. (b) 4 L $O_2$(g). (c) 5 L dimethylamine at room temperature. (d) 10 L. (e) 30 L.

Figure 6 shows the structural effects of dimethylamine exposure on a low coverage of oxygen ($\sigma_O \sim 1.5 \times 10^{14}$ cm$^{-2}$) at room temperature, the STM images being recorded during the exposure to dimethylamine at $5 \times 10^{-8}$ mbar. As in the case of pyridine, the first effect of the dimethylamine is a very rapid expansion of the p(2 × 1) lattice, the beginning of the transformation having been captured in the top right hand corner of image 6(b) (images are recorded from the bottom upwards). Fifty seconds later, figure 6 (c), the p(2 × 1)O(a) islands have been completely transformed into a (3 × 1) structure similar to that observed above for pyridine. There are no more structural changes as the exposure is increased but, in

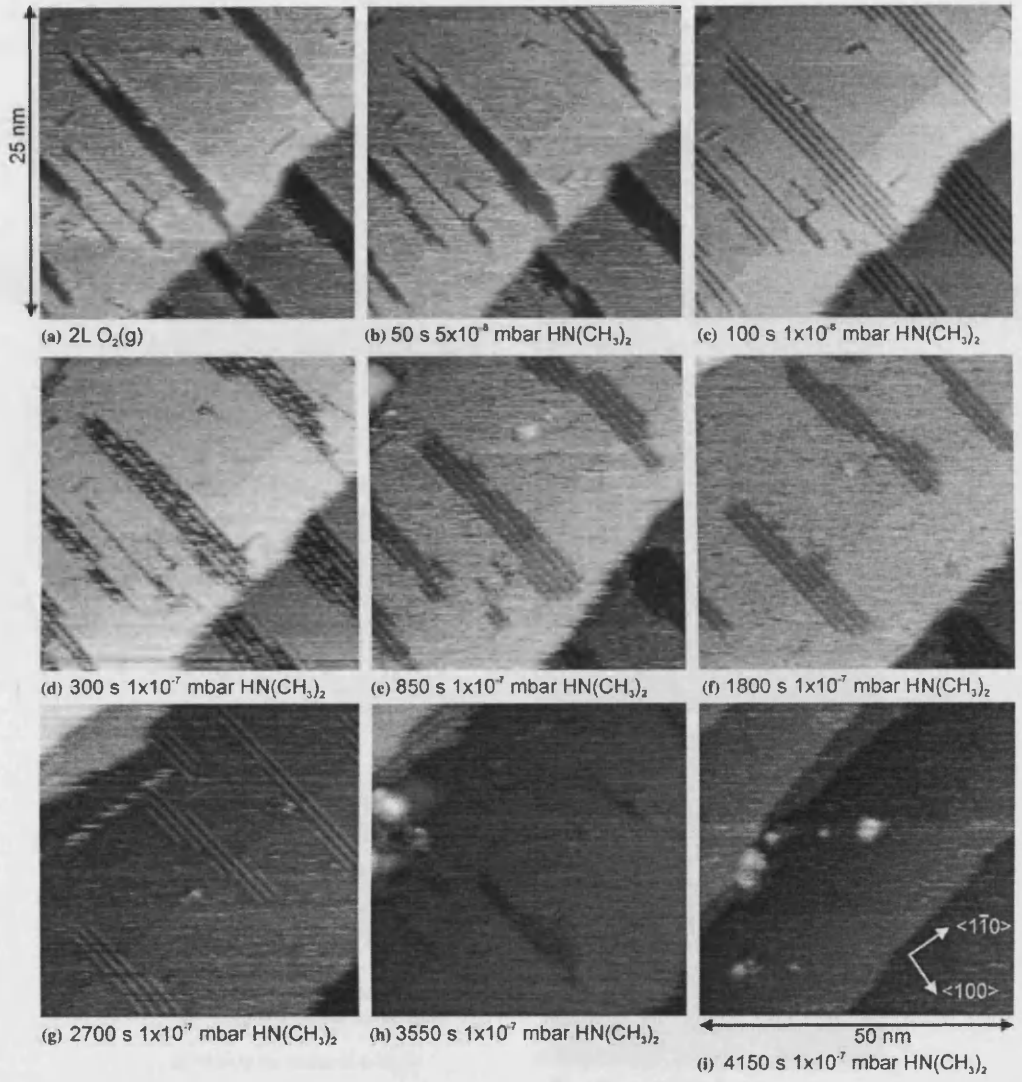


Figure 6. *In situ* STM observation of the reaction of dimethylamine with a p(2 × 1) oxygen island. $V_S = 0.41$ V, $I_T = 2.943$ nA.

contrast to pyridine, there is a slow process in which the islands steadily decrease in size, shown in images 6(d)–(h). This occurs through a shortening of the islands in the < 100 > direction, in a similar manner to the reaction of ammonia along the (2 × 1) O(a) chains [7,47]. After approximately 4000 s exposure at $1 \times 10^{-7}$ mbar no trace of the oxygen islands remains in the STM images, figure 6(i) and the XP spectra show a clean surface.

The images in figure 7 were recorded after the coadsorption of oxygen and dimethylamine in a ~1:1 mixture at a Cu(110) surface at 293 K. The advantage of the coadsorption approach is that transient oxygen states can be intercepted before the formation of less reactive oxygen islands and this can lead to high concentrations of well ordered surface species [2,10,45]. In the present case, coadsorption results in a well ordered monolayer, characterised in the main by a (3 × 1) unit cell but with a limited number of (2 × 1) features also present. Figure 7(a) shows a typical area of the surface with a close up of several chains in 7(b), a line profile along the dotted arrow in (b) is shown in (c) showing the 0.5 nm and 0.76 nm separation of the chains. Images (b), (d) and (e) were recorded sequentially and show the

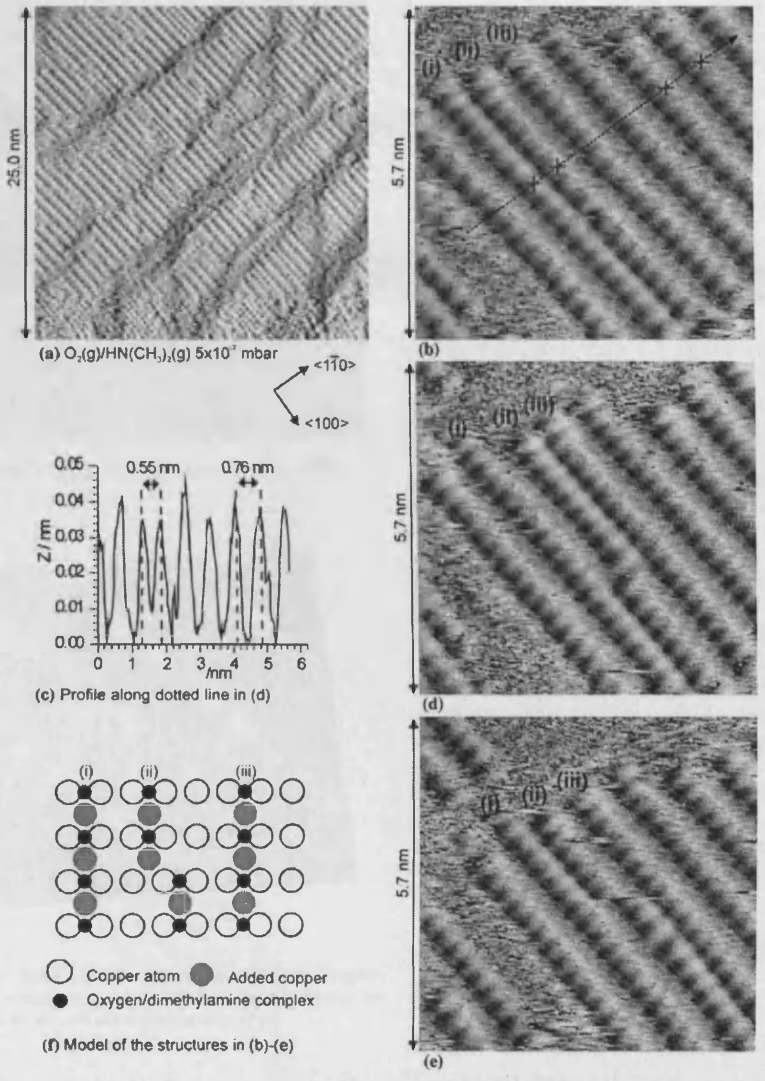


Figure 7. STM images of a Cu(110) surface after the coadsorption of oxygen and dimethylamine at $5 \times 10^{-7}$ mbar. (a) Low magnification view showing high surface coverage, $V_S = 0.72$ V, $I_T = 3.5$ nA. (b), (d) and (e) Images recorded successively of the same area of surface showing the movement of one of the oxygen/dimethylamine chains, $V_S = -0.18$ V, $I_T = 2.69$ nA. (c) line profile along the arrow in (b). (f) Schematic model of the structure in (b).

movement of a particular chain, indicated by the label (ii), during successive scans. Chain (ii) is initially 0.5 nm away from its nearest neighbour (i) but in the next scan 6(d), completed 50 s later, the chain has broken and the top half moved 0.25 nm away from (i) to within 0.5 nm of chain (iii). By the completion of the next image, 7(e), the two halves of chain (ii) have changed positions again. The model in 7(f) gives an interpretation of the structure of the chains. A closer view of chains (i)–(iii) is given in figure 8, no obvious differences between any of the chains are apparent.

### 3.4. *The adsorption of dimethylamine in the presence of high coverages of surface oxygen*

As in the case of pyridine, the evolution and subsequent decay of the $(3 \times 1)$ structure formed from the reaction of adsorbed oxygen with dimethylamine can be followed more easily at higher initial oxygen

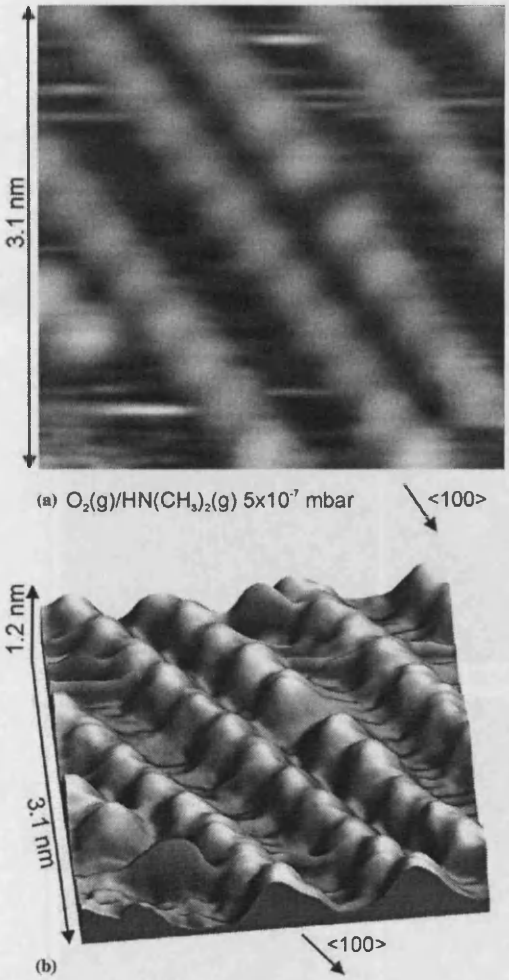


Figure 8. Close up detail of the dimethylamine/oxygen complex formed from the coadsorption of dimethylamine and oxygen (a) $V_S = -0.13$ V, $I_T = 2.69$ nA. (b) 3D representation of (a).

coverages. Figure 9 shows a sequence of images recorded during the exposure of a Cu(110) surface, with an initial oxygen concentration of $\sim 4 \times 10^{14}$ cm$^{-2}$, to dimethylamine at a pressure of $1 \times 10^{-8}$ mbar. The rapidly formed (3 × 1) structure is evident in 9(a) but subsequent scans show the development of a new structure consisting of poorly resolved rows in the $<1\bar{1}0>$ direction, which gradually replace the <100> directed chains. The new structures appear ~0.7 nm wide and are spaced 1.1 nm apart in the <100> direction; their apparent height is very similar to that of the modified oxygen chains. As the (3 × 1) structures disappear over a period of 10–15 min they are temporarily replaced by the $<1\bar{1}0>$ chains, but these too are only transiently present and over a period of 15 min the resolution of the STM images becomes progressively poorer until only the surface steps can be observed. After an hour the surface appears to be clean and this is confirmed by the adsorption of oxygen which results in the usual p(2 × 1) O(a) adlayer, figure 9(i).

### 3.5. *High coverages of preadsorbed oxygen exposed to low doses of dimethylamine*

Equation 2 shows that the removal of oxygen as water requires two dimethylamine molecules, whereas the intermediate complex suggested by the pyridine experiments involves a 1:1 amine:oxygen ratio. In the dimethylamine experiments described the decomposition of the (3 × 1) dimethylamine complex takes place in the presence of excess dimethylamine in the gas phase and the stoichiometry is therefore hidden. Figure 10 confirms the 2:1 stoichiometry of the dimethylamine oxidation. Oxygen was adsorbed at room temperature until a coverage of approximately half a monolayer was present ($\sigma_O \sim 2.7 \times 10^{14}$ cm$^{-2}$), 10(a). The partially oxidised surface was then exposed to 110 L of dimethylamine sufficient to convert all of the (2 × 1) O(a) structures to the (3 × 1) complex, 10(b). The surface was scanned continuously by STM for approximately 40 min after which the image became noisy and features could no longer be resolved. At this stage the sample was heated to ~450 K and, after equilibriating at this temperature for 60 min the surface could once again be imaged. The STM now shows a well resolved p(2 × 1) oxygen structure, 10(c) with a surface coverage of a quarter of a monolayer. The overall stoichiometry of the reaction is summarised in Eq. 3.

$$\begin{aligned} 2\mathrm{O(a)} + 2(\mathrm{CH_3})_2\mathrm{NH(g)} &\rightarrow 2[\mathrm{O} - (\mathrm{CH_3})_2\mathrm{NH}] \\ &\rightarrow \mathrm{H_2O}(\uparrow) + 2(\mathrm{CH_3})_2\mathrm{N}(\uparrow) + \mathrm{O(a)} \end{aligned} \quad (3)$$

## 4. Discussion

The present data confirms the 5:1:1 C:N:O stoichiometry of the pyridine–oxygen complex on Cu(110) and shows that it is formed on isolated oxygen chains or on the <100> edges of the p(2 × 1) oxygen islands, extending into the islands in a chain by chain mechanism. Chain expansion is inhibited at low temperatures, indicating a small activation energy for formation, and at high coverages where chain movement is not possible. The fact that pyridine is not adsorbed in the presence of a monolayer of oxygen suggests that the increased separation of the oxygen chains is not simply due to steric interactions of adjacent pyridine molecules, but is an inherent requirement of the pyridine–oxygen complex. It is also interesting to note that at the Cu(111) surface [8], the extent of pyridine adsorption was much

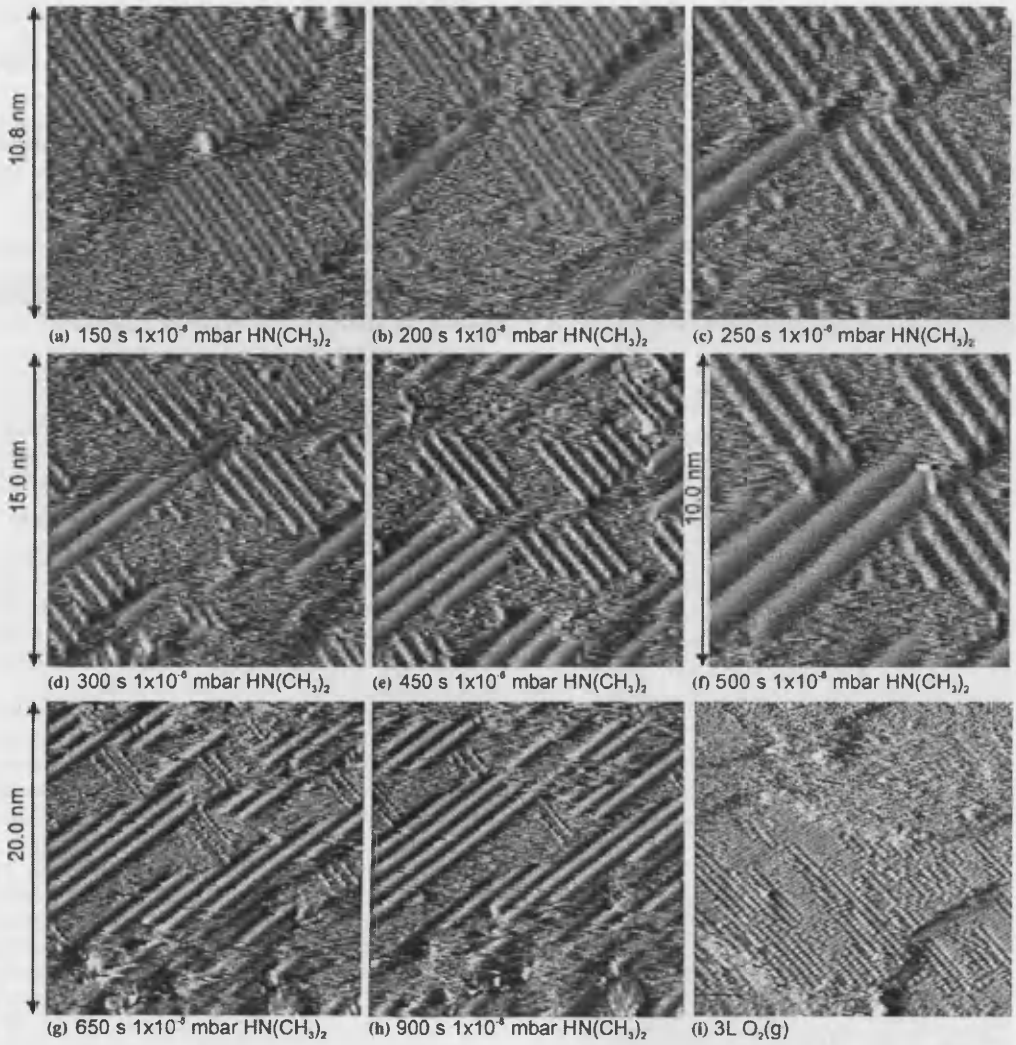


Figure 9. *In situ* STM observation of the reaction of dimethylamine with a p(2 × 1) oxygen island and the formation of "amide" rows in the $< 1\bar{1}0 >$ direction. (a)–(h) Images recorded during dimethylamine exposure, $V_S = 0.80$ V, $I_T = 2.28$ nA. (i) STM image recorded after leaving the surface for several hours and then exposing it to 3 L of oxygen, note the p(2 × 1) structure and the absence of the p(3 × 1) structure, $V_S = 0.76$ V, $I_T = 2.45$ nA.

lower than on Cu(110) with a maximum pyridine:oxygen ratio of 1:5. This may be an indication of the much reduced mobility of oxygen on Cu(111) as compared to Cu(110). There are some similarities with the oxydehydrogenation ammonia at Cu(110) of surfaces, where oxygen island edges have been shown to be the reactive sites and where oxygen island mobility seems to be enhanced by the presence of ammonia. However, *in situ* STM images [30,42] and a combined XPS/Monte Carlo model [7] of the ammonia–oxygen reaction have shown that it is the < 100 > ends of the islands that are first attacked by ammonia rather than the $< 1\bar{1}0 >$ sides. Furthermore, there was no indication in the ammonia/oxygen system for a widening of the oxygen chain separation during reaction.

Dimethylamine adsorption at the partially oxidised Cu(110) surface has a very similar effect to pyridine adsorption, with the expansion of the oxygen chain spacing in the $< 1\bar{1}0 >$ direction. The STM images show a well defined 0.36 nm spacing in the < 100 > direction, unchanged from the O(a) spacing in the p(2 × 1) structure, and identical maxima along the length of the modified chains. There is no evidence for anything adsorbed between, or next to the O–Cu chains, a point

that is reinforced by chain (ii) in figure 7 which oscillates freely between the two neighbouring chains. We conclude that, like pyridine, dimethylamine adsorbs on top of the Cu–O chains. Because of the oxydehydrogenation reaction that follows the formation of the complex, the dimethylamine/oxygen complex is relatively short lived and we do not have XP data on the dimethylamine/oxygen ratio; however, the excellent resolution and uniform nature of the maxima in the chains strongly suggest a 1:1 oxygen to dimethylamine ratio.

The oxydehydrogenation of the dimethylamine leads to water, which desorbs (Eq. 2) and an adsorbed product which shows up in the STM images as relatively wide, poorly resolved $<1\bar{1}0>$ orientated rows. Similar features have been reported in the case of imides formed from the oxidation of ammonia at Cu(110) surfaces [30,48,49] but in the present case a more reasonable assignment would be to a chemisorbed amide ($(CH_3)_2N(a)$).

$$O(a) + 2(CH_3)_2NH(g) \rightarrow H_2O(g) + 2(CH_3)_2N(a) \quad (4)$$

The 2:1 stoichiometry for this reaction and the supposition above that the dimethylamine–oxygen complex has a 1:1 ratio are consistent with the images in figure 10 which show half of the oxygen being removed after reaction with a saturation dimethylamine dose.

The amide formed from the dimethylamine/oxygen reaction is also unstable at the surface desorbing completely after 15–20 min, but we do not have any direct spectroscopic information on the products of this decomposition reaction. Nitrile formation has been suggested following the reaction of ethylamine with oxygen at Cu(110) [50] and Ag(110) [29] surfaces which, for dimethylamine, would involve breaking the C–N bond. An alternative route would be the breaking of a single C–H bond, resulting in *N*-methylenemethylamine ($CH_2=N-CH_3$) [51,52]. Both HCN and *N*-methylenemethylamine have been reported as decomposition products of dimethylamine over Si(100) [38].

## 5. Conclusions

Surface oxygen significantly increases the heat of adsorption of dimethylamine and pyridine at Cu(110) surfaces and the STM and XPS data suggest the formation of a 1:1 amine–oxygen complex which we propose is analogous to the amine oxides observed in solution and the gas phase [53]. Amine oxides may represent a general pathway for the interaction of amines with oxygen at metal surfaces but it is not clear whether such complexes compete with the oxydehydrogenation reaction (Eq. 2) or are a first step in the reaction. In the case of ammonia and aniline, there was little evidence for complex formation during reaction [10,42] but in these cases the N–H bond is relatively weak and the gas phase basicity relatively low; any complex would therefore be expected to be very short lived. We are

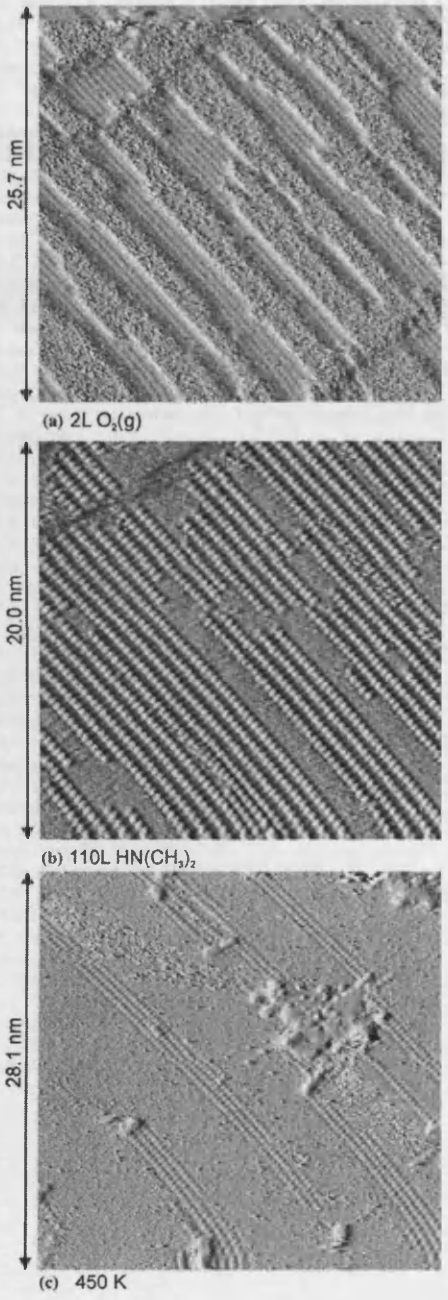


Figure 10. STM images confirming the 2:1 stoichiometry of the reaction between dimethylamine and oxygen (Eq. 2). (a) Cu(110) surface approximately half covered with the p(2 × 1)O(a) structure after exposure to 2 L $O_2$(g) at 293 K, $V_S = 0.54$ V, $I_T = 2.84$ nA. (b) STM image showing the complete conversion of the p(2 × 1) to p(3 × 1) structure after exposure to dimethylamine, $V_S = 0.04$ V, $I_T = 3.11$ nA. (c) The surface in (b) imaged at 450 K, $V_S = 0.037$ V, $I_T = 2.94$ nA.

pursuing this point in further experimental and theoretical work.

**Acknowledgements**

The authors thank Prof. M. W. Roberts for his contributions and many helpful discussions. The work was funded by EPSRC.

**References**

[1] P.S. Weiss, M.J. Abrams, M.T. Cygan, J.H. Ferris, M.M. Kamna, K.R. Krom, S.J. Stranick and M.G. Yoshikawa Youngquist, Anal. Chim. Acta 307 (1995) 355.
[2] B. Afsin, P.R. Davies, A. Pashuski and M.W. Roberts, Surf. Sci. 259 (1991) L724.
[3] A.F. Carley, P.R. Davies and M.W. Roberts, Catal. Lett. 80 (2002) 25.
[4] P.R. Davies and G.G. Mariotti, J. Phys. Chem. 100 (1996) 19975.
[5] R.J. Madix and M. Bowker, Surf. Sci. 95 (1980) 190.
[6] P.R. Davies and G.G. Mariotti, Catal. Lett. 43 (1997) 261.
[7] A.F. Carley, P.R. Davies, M.W. Roberts and D. Vincent, Top. Catal. 1 (1994) 35.
[8] P.R. Davies and N. Shukla, Surf. Sci. 322 (1995) 8.
[9] P.R. Davies, D. Edwards and D. Richards, Surf. Sci. 573 (2004) 284.
[10] P.R. Davies, D. Edwards and D. Richards, J. Phys. Chem. B 108 (2004) 18630.
[11] A.F. Carley, P.R. Davies, R.V. Jones, G.U. Kulkarni and M.W. Roberts, Chem. Commun. (1999) 687.
[12] P.R. Davies and J.M. Keel, Catal. Lett. 58 (1999) 99.
[13] A.F. Carley, P.R. Davies, K.R. Harikumar, R.V. Jones, G.U. Kulkarni and M.W. Roberts, Top. Catal. 14 (2001) 101.
[14] M. Klare, G. Waldner, R. Bauer, H. Jacobs and J.A.C. Broekaert, Chemosphere 38 (1999) 2013.
[15] M. Klare, J. Scheen, K. Vogelsang, H. Jacobs and J.A.C. Broekaert, Chemosphere 41 (2000) 353.
[16] S.V. Gredig, R. Maurer, R.A. Koeppel and A. Baiker, J. Mol. Catal. A. 127 (1997) 133.
[17] S.V. Gredig, R.A. Koeppel and A. Baiker, App. Catal. A. 162 (1997) 249.
[18] S.V. Gredig, R.A. Koeppel and A. Baiker, Catal. Today 29 (1996) 339.
[19] A. Baiker, Appl. Organomet. Chem. 14 (2000) 751.
[20] W.D. Huntsman, N.L. Madison and S.I. Schlesinger, J. Catal. 2 (1963) 498.
[21] J. Struijk and J.J.F. Scholten, Appl. Catal. A 82 (1992) 277.
[22] P.B. Wells and A.G. Wilkinson, Top. Catal. 5 (1998) 39.
[23] M. Bartok, K. Felfoldi, G. Szollosi and T. Bartok, Catal. Lett. 61 (1999) 1.
[24] M. Bartok, K. Felfoldi, B. Torok and T. Bartok, Chem. Commun. (1998) 2605.
[25] B. Torok, K. Felfoldi, G. Szakonyi, K. Balazsik and M. Bartok, Catal. Lett. 52 (1998) 81.
[26] A. Tungler, T. Mathe, T. Tarnai, K. Fodor, G. Toth, J. Kajtar I. Kolossvary, B. Herenyi and R.A. Sheldon, Tetrahedron: Asymmetry 6 (1995) 2395.
[27] S.P. Griffiths, P. Johnston and P.B. Wells, Appl. Catal. A-Gen. 191 (2000) 193.
[28] T. Sasaki, T. Aruga, H. Kuroda and Y. Iwasawa, Surf. Sci. 249 (1991) L347.
[29] D.M. Thornburg and R.J. Madix, Surf. Sci. 226 (1990) 61.
[30] X.C. Guo and R.J. Madix, Faraday Discussions (1996) 139.
[31] T.S. Nunney, J.J. Birtill and R. Raval, Surf. Sci. 428 (1999) 282.
[32] W. Erley, R. Xu and J.C. Hemminger, Surf. Sci. 389 (1997) 272.
[33] F. Maseri, A. Peremans, J. Darville and J.M. Gilles, J. Elec. Spec. Relat. Phenom. 54 (1990) 1059.
[34] D.E. Gardin and G.A. Somorjai, J. Phys. Chem. 96 (1992) 9424.
[35] J.J. Chen and N. Winograd, Surf. Sci. 326 (1995) 285.
[36] T. Bitzer, T. Alkunshalie and N.V. Richardson, Surf. Sci. 368 (1996) 202.
[37] R.M. Rummel and C. Ziegler, Surf. Sci. 418 (1998) 303.
[38] C.P.A. Mulcahy, A.J. Carman and S.M. Casey, Surf. Sci. 459 (2000) 1.
[39] P.R. Davies and N.G. Newton, Surf. Sci. 546 (2003) 149.
[40] P.R. Davies and J.M. Keel, Surf. Sci. 469 (2000) 204.
[41] A.F. Carley, P.R. Davies, M.W. Roberts, K.K. Thomas and S. Yan, Chem. Commun. (1998) 35.
[42] A.F. Carley, P.R. Davies, G.U. Kulkarni and M.W. Roberts, Catal. Lett. 58 (1999) 93.
[43] A.F. Carley and M.W. Roberts, Proc. R. Soc. London, Ser. A 363 (1978) 403.
[44] A.F. Carley, P.R. Davies, R.V. Jones, K.R. Harikumar, G.U. Kulkarni and M.W. Roberts, Surf. Sci. 447 (2000) 39.
[45] A.F. Carley, P.R. Davies, R.V. Jones, K.R. Harikumar, M.W. Roberts and C.J. Welsby, Top. Catal. 22 (2003) 161.
[46] A.F. Carley, P.R. Davies, K.R. Harikumar, R.V. Jones and M.W. Roberts, Top. Catal. 24 (2003) 51.
[47] B. Afsin, P.R. Davies, A. Pashusky, M.W. Roberts and D. Vincent, Surf. Sci. 284 (1993) 109.
[48] P.R. Davies and J.M. Keel, PCCP 1 (1999) 1383.
[49] A.F. Carley, P.R. Davies and M.W. Roberts, Chem. Commun. (1998) 1793.
[50] A.F. Carley, P.R. Davies, D. Edwards and M. Parsons, in preparation.
[51] J. Hinze, R.F. Curl and Jr., J. Am. Chem. Soc. 86 (1964) 5068.
[52] E.C. Tuazon, R. Atkinson, S.M. Aschmann and J. Arey, Res. Chem. Intermediates 20 (1994) 303.
[53] M. Bronstrup, D. Schroder, I. Kretzschmar, C.A. Schalley and H. Schwarz, Eur. J. Inorg. Chem. (1998) 1529.

Available online at www.sciencedirect.com
SCIENCE DIRECT®
Surface Science 573 (2004) 284–290
SURFACE SCIENCE
www.elsevier.com/locate/susc

# Aromatic interactions in the close packing of phenyl-imides at Cu(1 1 0) surfaces

Philip R. Davies *, Dyfan Edwards, Darran Richards

*School of Chemistry, Cardiff University, P.O. Box 912, Cardiff CF10 3TB, United Kingdom*

Received 9 July 2004; accepted for publication 29 September 2004
Available online 13 October 2004

**Abstract**

The oxidation of aniline at Cu(1 1 0) surfaces at 290 K has been studied by XPS and STM. A single chemisorbed product, assigned to a phenyl imide ($C_6H_5N(a)$), is formed together with water which desorbs. Reaction with preadsorbed oxygen results in a maximum surface concentration of phenyl imide of $2.8 \times 10^{14}$ mol cm$^{-2}$ and a surface dominated by domains of three structures described by $\begin{pmatrix} 4 & 0 \\ 2 & 2 \end{pmatrix}$, $\begin{pmatrix} 4 & 0 \\ -1 & 2 \end{pmatrix}$ and $\begin{pmatrix} 4 & 0 \\ 1 & 2 \end{pmatrix}$ unit meshes. However, concentrations of phenyl imide of up to $3.3 \times 10^{14}$ mol cm$^{-2}$ were obtained from the coadsorption of aniline and dioxygen (300:1 mixture) resulting in a highly ordered biphasic structure with $\begin{pmatrix} 3 & 0 \\ -1 & 2 \end{pmatrix}$ and $\begin{pmatrix} 3 & 0 \\ 1 & 2 \end{pmatrix}$ domains. Comparison of the STM and XPS data shows that only half the phenyl imides at the surface are imaged. Pi-stacking of the phenyl rings is proposed to account for this observation.


*Keywords:* X-ray photoelectron spectroscopy; Scanning tunneling microscopy; Chemisorption; Surface structure, morphology, roughness, and topography; Copper; Aromatics; Low index single crystal surfaces

## 1. Introduction

In this communication we report the first structural information at a molecularly resolved level of the reactive chemisorption of aniline with oxygen at Cu(1 1 0) surfaces at 290 K. Amine-surface interactions play an important role in applications ranging from corrosion inhibition [1–3] and adhesion [4–6] to heterogeneous catalysis [7–9]. We have previously studied the interactions of ammonia [10–13] and pyridine [14,15] with clean and oxidized surfaces; aniline makes an interesting

* Corresponding author. Tel.: +029 2087 4072; fax: +029 2087 4030.
*E-mail address:* daviespr@cf.ac.uk (P.R. Davies).

0039-6028/$ - see front matter © 2004 Elsevier B.V. All rights reserved.
doi:10.1016/j.susc.2004.09.039

Table 1
A comparison of the basicity of aniline with other amines in the gas phase and in solution

| Molecule | pKb [16] | Gas phase basicity [17]/kJ mol$^{-1}$ |
|---|---|---|
| Pyridine | 8.75 | 898.1 |
| Aniline | 9.37 | 850.6 |
| Ammonia | 4.75 | 819.0 |

alternative model because of the associated phenyl ring and differing basicity from that of either ammonia or pyridine, Table 1.

Previous studies of aniline surface chemistry have concentrated on adsorption at clean metal [18–25] or clean silicon surfaces [26,27] using temperature programmed desorption (TPD) and vibrational spectroscopy (HREELS). It has been reported that the molecule dissociates at clean Cu(1 1 0) surfaces to give an amide (PhNH(a)) in which the phenyl ring lies approximately parallel to the surface [28,29]. The aim of the present work was to investigate whether the reaction of the amine group with oxygen was affected by the differing basicity of aniline from pyridine and ammonia and the steric hindrance of the phenyl ring.

## 2. Experimental

Experiments were conducted using a combined variable temperature STM/XPS instrument with a base pressure of $2 \times 10^{-10}$ mbar and described in detail elsewhere [30]. All XP spectra were recorded with a pass energy of 50 eV resulting in typical peak halfwidths of ≈1.8 eV. Spectra were obtained by the combination of 10–20 individual scans over a 25 eV wide region, with a total acquisition time of between 10 min (I(3d) and Cu(2p) spectra) and 20 min (C(1s) spectra). The spectra were calibrated to the clean Cu($2p_{3/2}$) peak at 932.7 eV. XPS data were acquired using commercial software (EIS, Omicron Vacuum Physik) and analysed using software developed in-house.

The calculation of the surface concentration of adsorbates from photoelectron data was discussed in detail by Carley and Roberts [31]; the subshell photoionisation cross sections tabulated by Scofield [32] being used in Eq. (1), a modification of that proposed by Madey et al. [33]:

$$\sigma_a = \frac{I_a \mu_s E_a N \rho \lambda \cos\phi}{I_s \mu_a E_s M} \quad (1)$$

where $\sigma_a$ is the concentration of adsorbate; $\mu_a/\mu_s$ is the modified [34] Scofield photoionisation cross sections, $\rho$ is the density of substrate, $E_a/E_s$ is the kinetic energy of photoelectrons, $\lambda$ is the mean free path of electrons within the substrate, $\phi$ is the angle of collection with respect to the sample normal; $M$ is the relative atomic mass of the substrate. The accuracy of this approach has been confirmed in many systems [30,35–37]. We estimate the error in surface concentration of the oxygen to be $\pm 1.5 \times 10^{13}$ cm$^{-2}$, and slightly greater in the case of carbon and nitrogen which have weaker signals. STM tunnelling conditions, (i.e. sample bias ($V_S$) and tunnelling current ($I_T$)), are given in the figure legends. STM images were analysed using WSxM© [38].

The 7 × 7 mm sample (Metal Crystals Ltd.) was 0.5 mm thick and polished mechanically down to 0.25 μm. Cleaning involved cycles of $Ar^+$ sputtering (0.75 keV, 20 μA cm$^{-2}$ for 20 min) and annealing for 60 min at 700 K. This procedure resulted in flat terraces approximately 10–20 nm wide. Sample cleanliness was checked by XPS. Gases were dosed via a leak valve at pressures of between $10^{-9}$ and $5 \times 10^{-7}$ mbar. The aniline (Aldrich, 99.5%) was subjected to several freeze pump thaw cycles using a dry ice/acetone slush and its purity was monitored with in situ mass spectrometry. Oxygen (Argo Ltd., 99.998%) was used as received.

## 3. Results

### 3.1. Reactive chemisorption of aniline at partially oxidised surfaces

The extent of aniline adsorption at clean Cu(1 1 0) surfaces at 290 K is limited [39] but a facile reaction occurs in the presence of *preadsorbed* oxygen, generating water, which desorbs, and an adsorbed product which the XP spectra show has a $C_6N_1$ stoichiometry Fig. 1(i). The initial oxygen concentration of $1.3 \times 10^{14}$ cm$^{-2}$ is reduced to zero after 10 L [1] exposure to aniline which results in a

[1] 1 L = 1 Langmuir = $10^{-6}$ Torr s.

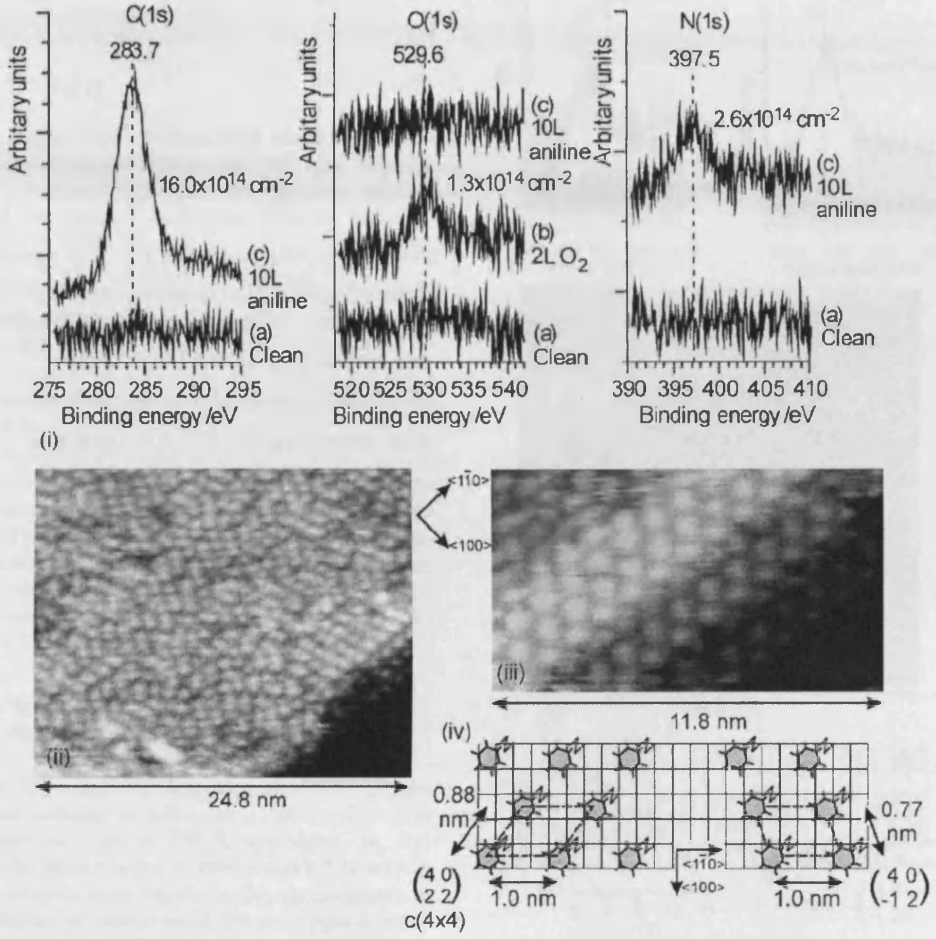


Fig. 1. The chemisorptive replacement of oxygen by aniline at a Cu(1 1 0) surface at 293 K. (i) XP spectra of the C(1s), O(1s) and N(1s) regions: (a) clean surface, (b) after exposure to 2L $O_2$ (g); (c) after exposure to 10 L aniline. (ii) STM image of phenyl imide in (i)(c), $V_S = 1.26$ V; $I_T = 3.66$ nA; (iii) Close up of phenyl imide domain structure near a step edge, $V_S = 1.27$ V; $I_T = 3.65$ nA. (iv) Model of the phenyl imide structures observed in the STM images.

final nitrogen concentration of $2.6 \times 10^{14}$ $cm^{-2}$. The overall reaction stoichiometry is therefore 2 aniline: 1 oxygen, suggesting the formation of a chemisorbed phenyl amide, (PhNH(a)), through Eqs. (2) and (3). However, vibrational spectroscopy has established in the case of ammonia that despite a similar 2:1 stoichiometry, reaction with oxygen gives an imide (NH(a)). An assignment to an imide would be supported in the present case by the N(1s) binding energy of 397.5 eV. The 2:1 reaction stoichiometry would imply the formation of the imide through steps (2), (3) and (5).

$$PhNH_2(g) + O(a) \rightarrow PhNH(a) + OH(a) \quad (2)$$

$$PhNH_2(g) + OH(a) \rightarrow PhNH(a) + H_2O(g) \quad (3)$$

$$PhNH_2(g) + O(a) \rightarrow PhN(a) + H_2O(g) \quad (4)$$

$$PhNH(a) \rightarrow PhN(a) + H(a) \quad (5)$$

$$2H(a) \rightarrow H_2(g) \quad (6)$$

A molecularly resolved STM image of the surface after reaction is shown in Fig. 1(ii). The surface is covered with ~0.7 nm diameter features which are present in several different domains, including a $\begin{pmatrix} 4 & 0 \\ 2 & 2 \end{pmatrix}$ structure (c(4 × 4) in Wood's notation) shown in close up in Fig. 1(iii). The other domains are less clearly resolved but correspond to $\begin{pmatrix} 4 & 0 \\ -1 & 2 \end{pmatrix}$ and $\begin{pmatrix} 4 & 0 \\ 1 & 2 \end{pmatrix}$ structures. These are mirror images of each other and closely related to the $\begin{pmatrix} 4 & 0 \\ 2 & 2 \end{pmatrix}$ structure. Fig. 1(iv) shows possible models for the observed structures, assuming that the nitrogen is adsorbed in a bridge site as in the case of NH(a) [12]. An important observation is that the saturation coverage of all three of these structures, assuming one molecule per unit cell, is 0.125, corresponding to $1.4 \times 10^{14}$ molecules $cm^{-2}$. We return to this point below.

### *3.2. The coadsorption of aniline and dioxygen at clean Cu(110) surfaces*

XP C(1s) and N(1s) spectra of a clean copper surface exposed to 200 L of a 300:1 aniline and dioxygen mixture at 290 K are shown in Fig. 2(i). The total oxygen exposure was 0.7 L, which, in equivalent experiments in this spectrometer in the absence of aniline, results in an oxygen concentration of $\sim 1 \times 10^{14}$ $cm^{-2}$. However, no oxygen is observed by either XPS or STM. Instead, single peaks are present in the C(1s) and N(1s) spectra with binding energies of 284 and 397.8 eV respectively and surface concentrations in a 6:1 C:N ratio. These data suggest that a similar phenylimide product to that formed from preadsorbed oxygen is present but the total imide concentration ($3.3 \times 10^{14}$ $molcm^{-2}$) is significantly greater.

An STM image of the surface after coadsorption is shown in Fig. 2(ii). There have been changes in step structure during reaction with average terrace lengths reduced from ca. 15 nm at the clean surface to 3 nm and steps no longer bunching in twos and threes but occurring singularly with heights of 0.13 nm, Fig. 2(iii).

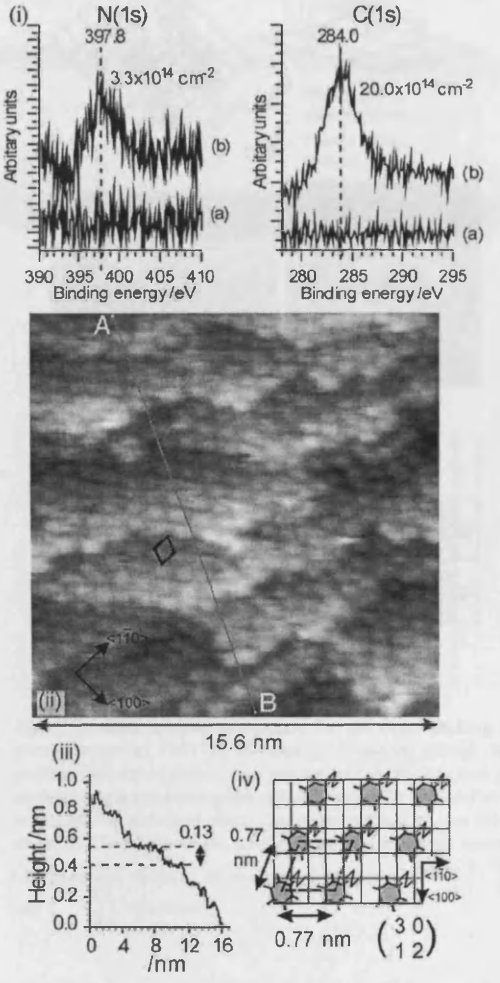


Fig. 2. The coadsorption of aniline and dioxygen at a Cu(110) surface at 290 K. (i) XP spectra of the C(1s) and N(1s) regions. (a) clean, (b) after 200L of a 300:1 aniline/dioxygen mixture. (ii) STM image recorded after exposure to aniline/dioxygen mixture, $V_S = 0.58$ V, $I_T = 2.89$ nA. (iii) Line profile along line AB showing short terraces and single atomic steps. (iv) Schematic of one domain of the close packed phenyl imide adlayer formed from coadsorbing aniline and dioxygen.

All of the terraces are uniformly covered with similar features to those assigned above to phenyl imide but arranged in a $\begin{pmatrix} 3 & 0 \\ 1 & 2 \end{pmatrix}$ or $\begin{pmatrix} 3 & 0 \\ -1 & 2 \end{pmatrix}$ structure (Fig. 2(iv)). Assuming one molecule per unit cell this corresponds to a maximum imide concentration of $1.7 \times 10^{14}$ mol cm$^{-2}$. The height corrugations between features are 0.05 nm, but this low value may reflect the difficulty of the tip imaging between such close packed molecules rather than a true height.

## 4. Discussion

Aniline reacts with oxygen at Cu(110) surfaces readily at 290 K with no sign in the STM of any intermediate $(3 \times 1)$ structures such as those seen with pyridine [14] and some other amines [40], hinting that the stability of the $(3 \times 1)$ intermediate correlates with the gas phase basicity. The results also highlight the utility of the coadsorption methodology which yields more densely packed and better ordered phenyl-imide adlayers than reaction with preadsorbed oxygen. What is particularly interesting about the aniline/oxygen system however is the close packing of the phenyl imide product which forms a monolayer with a surface concentration, calculated from the XPS data, as high as $3.3 \times 10^{14}$ mol cm$^{-2}$. This corresponds to a *maximum* intermolecular spacing of 0.55 nm, (assuming a square unit cell) when the approximate van der Waals radius for the molecule is 0.6 nm [41]. In comparison, the smaller imide (NH(a)) [35] and the phenoxy species [41] form $c(2 \times 4)$ and $c(4 \times 2)$ structures at Cu(110) surfaces respectively, with maximum concentrations of only $2.6 \times 10^{14}$ mol cm$^{-2}$.

In contrast to the XPS results, the STM images of the adsorbed phenyl imide show a structure with a maximum surface concentration of $1.6 \times 10^{14}$ mol cm$^{-2}$, half of that determined by XPS, and a nearest neighbour spacing of 0.76 nm. Fig. 3 shows two alternative models to account for the high packing density and "missing" phenyl groups in the STM image. In Fig. 3(i) the phenyl rings are stacked in an edge-to-face T-shaped structure, with alternate phenyl rings

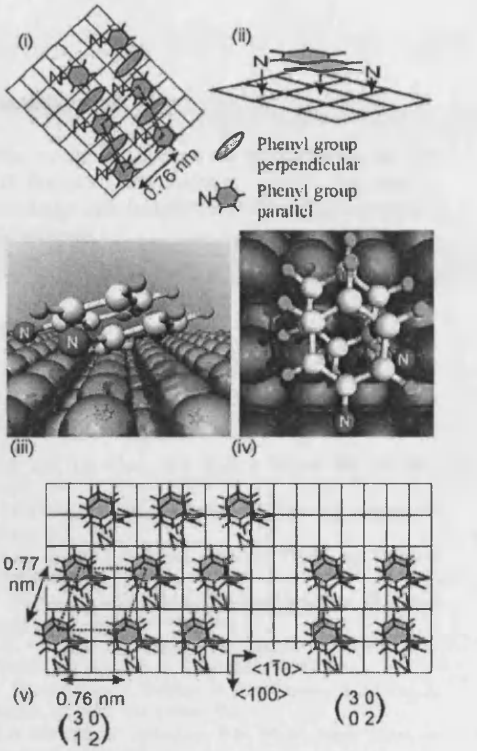


Fig. 3. Possible models to account for the close packing of phenyl imides at Cu(110) surfaces. (i) T-shaped phenyl ring packing with mixed phenyl ring orientations (ii) Face to face pi-stacking of phenyl-imide pairs. (iii) Side view of a ball and stick model of the adsorbed phenyl imide pairs showing the tilted rings. (iv) Top view of the phenyl-imide ball and stick model. (v) Schematic diagram of the phenyl imide pairs in $\begin{pmatrix} 3 & 0 \\ 1 & 2 \end{pmatrix}$ and $\begin{pmatrix} 3 & 0 \\ 0 & 2 \end{pmatrix}$ structures.

orientated perpendicular to the surface so that STM imaging of the phenyl groups parallel to the surface would be hindered by the large height corrugation. The reduction in heat of adsorption that results from the perpendicular orientation of half the phenyl rings in this model, would be compensated for by the formation of the T-shaped complex known to be a favourable structure for close packed aromatic systems [42]. However, the almost circular shape of the phenyl imides in the STM images would suggest facile rotation of

the rings about the axis perpendicular to the surface for this model: this seems unlikely at such high surface densities. An alternative, Fig. 3(ii), is a form of pi-stacking in which the phenyl groups are parallel to each other and partly overlap. Fig. 3(iii) and (iv) show a more detailed model of a possible complex with the lower phenyl ring situated above a hollow site and the nitrogen atom in the short bridge site. The phenyl ring of the second molecule is parallel to the first, 0.15 nm above it and rotated by 65°, placing the nitrogen group above another short bridge site.

By tilting the two phenyl rings at approximately 15 20° to the surface plane around an axis which does not include either nitrogen atom, it is possible to bring the nitrogen of the upper ring to a similar height to that of the lower molecule thus making it possible for both nitrogens to be coordinated to the surface. Surface vibrational spectroscopy indicates that the phenyl ring is orientated close to parallel to the surface [28,29] but to date, these studies have concerned aniline reactions only with clean surfaces where the surface concentration of phenyl imide may not be high enough to force the formation of the pi-stacked complex.

There are many other similar arrangements possible for the phenyl-imide complex, for example with the nitrogen atoms in different short bridge sites; without further experimental (or theoretical) information a definitive structure cannot be determined. However, the model presented here has the advantage of a compact structure which would be consistent with the 0.7 nm diameter of the features observed in the STM and also offers a explanation for the absence of the $\begin{pmatrix} 4 & 0 \\ 0 & 2 \end{pmatrix}$ and $\begin{pmatrix} 3 & 0 \\ 0 & 2 \end{pmatrix}$ structures from the surface, since these structures would result in the overlap of a nitrogen and a hydrogen at a bridge site, Fig. 3(v).

Pi-stacking of aromatic groups is employed in the construction of 3-d supramolecular structures from large molecules such as porphyrins [43] and has been reported for smaller molecules deposited from solution [44,45]. The present results suggest that pi-pi interactions can also play a role in the close packing of aromatic groups in a monolayer deposited from the gas phase where solvent interactions are absent.

**Acknowledgments**

This work was supported by EPSRC and The Royal Society. The authors would also like to acknowledge the insightful and helpful comments of the referees.

**References**

[1] E. Lazarova, G. Petkova, R. Raicheff, G. Neykov, J. Appl. Electrochem. 32 (2002) 1355.
[2] K.F. Khaled, N. Hackerman, Electrochim. Acta 49 (2004) 485.
[3] T.B. Du, J.J. Chen, D.Z. Cao, J. Mater. Sci. 36 (2001) 3903.
[4] F. Gaillard, J.P. Joly, E. Peillex, M. Romand, J. Adhes. 72 (2000) 317.
[5] M.K. Harun, S.B. Lyon, J. Marsh, Prog. Org. Coat. 46 (2003) 21.
[6] J. Marsh, L. Minel, M.G. Barthes-Labrousse, D. Gorse, Appl. Surf. Sci. 133 (1998) 270.
[7] J.C. Penzien, C. Haessner, A. Jentys, K. Kohler, T.L. Muller, J.A. Lercher, J. Catal. 221 (2004) 302.
[8] C. Bronnimann, Z. Bodnar, R. Aeschimann, T. Mallat, A. Baiker, J. Catal. 161 (1996) 720.
[9] S.P. Griffiths, P. Johnston, P.B. Wells, Appl. Catal. A-Gen. 191 (2000) 193.
[10] P.R. Davies, N.G. Newton, Surf. Sci. 546 (2003) 149.
[11] A.F. Carley, P.R. Davies, K.R. Harikumar, R.V. Jones, G.U. Kulkarni, M.W. Roberts, Top. Catal. 14 (2001) 101.
[12] P.R. Davies, J.M. Keel, PCCP 1 (1999) 1383.
[13] A.F. Carley, P.R. Davies, M.W. Roberts, Chem. Commun. (1998) 1793.
[14] A.F. Carley, P.R. Davies, R.V. Jones, G.U. Kulkarni, M.W. Roberts, Chem. Commun. (1999) 687.
[15] P.R. Davies, N. Shukla, Surf. Sci. 322 (1995) 8.
[16] CRC Handbook of Chemistry and Physics; 59 ed.: R.C. Weast, Ed.; CRC Press Inc: Boca Raton, 1979; Vol. 59, p. F215.
[17] E.P. Hunter, S.G. Lias, J. Phys. Chem. Ref. Data 27 (1998) 413.
[18] D.M. Thornburg, R.J. Madix, Surf. Sci. 226 (1990) 61.
[19] T. Sasaki, T. Aruga, H. Kuroda, Y. Iwasawa, Surf. Sci. 276 (1992) 69.
[20] D.E. Gardin, G.A. Somorjai, J. Phys. Chem. 96 (1992) 9424.
[21] W. Erley, R. Xu, J.C. Hemminger, Surf. Sci. 389 (1997) 272.
[22] J.J. Chen, N. Winograd, Surf. Sci. 326 (1995) 285.
[23] J.J. Birtill, P. Ridley, S. Liddle, T.S. Nunney, R. Raval, Ind. Eng. Chem. Res. 40 (2001) 553.
[24] S.M. Barlow, S. Haq, R. Raval, Langmuir 17 (2001) 3292.
[25] X.P. Xu, C.M. Friend, J. Vac. Sci. Technol. A: Vac. Surf. Films 9 (1991) 1599.

[26] T. Bitzer, T. Alkunshalie, N.V. Richardson, Surf. Sci. 368 (1996) 202.
[27] R.M. Rummel, C. Ziegler, Surf. Sci. 418 (1998) 303.
[28] M.R. Ashton, T.S. Jones, N.V. Richardson, R.G. Mack, W.N. Unertl, J. Electron Spectrosc. Relat. Phenom. 54 (1990) 1133.
[29] R.V. Plank, N.J. Dinardo, J.M. Vohs, Surf. Sci. 340 (1995) L971.
[30] A.F. Carley, P.R. Davies, R.V. Jones, K.R. Harikumar, G.U. Kulkarni, M.W. Roberts, Surf. Sci. 447 (2000) 39.
[31] A.F. Carley, M.W. Roberts, Proc. R. Soc. London, Ser. A 363 (1978) 403.
[32] J.H. Scofield, J. Elec. Spec. Rel. Phen. 8 (1976) 129.
[33] T.E. Madey, J.T. Yates Jr., N.E. Erickson, Chem. Phys. Lett. 19 (1973) 487.
[34] R.F. Reilman, A. Msezane, S.T. Manson, J. Elec. Spec. Rel. Phen. 8 (1976) 389.
[35] A.F. Carley, P.R. Davies, R.V. Jones, K.R. Harikumar, G.U. Kulkarni, M.W. Roberts, Top. Catal. 11 (2000) 299.
[36] P.R. Davies, M.W. Roberts, J.C.S. Faraday Trans. 88 (1992) 361.
[37] G.U. Kulkarni, S. Laruelle, M.W. Roberts, J.C.S. Faraday Trans. 92 (1996) 4793.
[38] WSxM©. Available from <http://www.nanotec.es>.
[39] P.R. Davies, D. Edwards, D. Richards, J. Phys. Chem., accepted for publication.
[40] A.F. Carley, P.R. Davies, D. Edwards, M. Parsons, M.W. Roberts, in preparation.
[41] X.C. Guo, R.J. Madix, Surf. Sci. 341 (1995) L1065.
[42] C.A. Hunter, K.R. Lawson, J. Perkins, C.J. Urch, J. Chem. Soc.-Perkin Trans. 2 (2001) 651.
[43] A. Gesquiere, S. De Feyter, F.C. De Schryver, F. Schoonbeek, J. van Esch, R.M. Kellogg, B.L. Feringa, Nano Lett. 1 (2001) 201.
[44] L.S. Pinheiro, M.L.A. Temperini, Surf. Sci. 441 (1999) 45.
[45] L.S. Pinheiro, M.L.A. Temperini, Surf. Sci. 464 (2000) 176.